NEW STRATEGIES TO DELIVER DRUGS FOR THE LOCAL TREATMENT OF SEVERE PULMONARY DISEASES

A thesis submitted to attain the degree of

DOCTOR OF PHILOSOPHY

Presented to the Department of Pharmacy,
Graduate School of Pharmaceutical Science
The University of Naples Federico II

Presented by

GABRIELLA COSTABILE

APPROVED BY

Prof. Francesca Ungaro, PhD

Prof. Maria Valeria D'Auria, PhD

University of Naples Federico II, Naples, Italy

May, 2016

ABBREVIATION LIST

$3OC_{12}$-HSL	*N*-3-oxo-dodecanoyl-homoserine lactone
5-FC	5-fluorocytosine
AB	Ammonium bicarbonate
ABS	Absorbance
ABT	Air-blood tissue barrier
ALI	Air-liquid interface
AM	Artificial mucus
ANOVA	One way anallysis of variance
AT	Aztreonam
BAL	Bronchoalveolar lavage
BALC	Bronchoalveolar lavage cells pellets
CEN	Comitè Europeen de normalization
CF	Cystic Fibrosis
CFTR	Cystic fibrosis transmembrane regulator
COPD	Chronic obstructive pulmonary disease
COX-2	Cyclooxygenase-2
CTAB	Cetyltrimethyl ammonium bromide
DCs	Dendritic cells
Dec-ODN	Decoy oligonucleotide against NF-κB
DMSO	Dimethyl sulfoxide
DNA	Deoxyribonucleic acid
DOTAP	1,2-Dioleoyl-3-trimethylammoniumpropane
DPI	Dry powder inhaler
DPPC	Dipalmitoylphosphatidylcholine
DSC	Diferential scanning calorimetry
DSPC	1,2-Distearoyl-sn-glycero-3-phosphocholine
DTPA	Diethylenetriaminepentaaetic acid
ED	Emitted dose
EMA	European medicines agency
ENaC	Epithelial sodium channel
EPS	Extracellular polysaccharides
FDA	Food and drug administration
FDKP	Fumaryl diketopiperazine

FPF	Fine particle fraction
GRAS	Generally regarded as safe
GSD	Geometric standard deviation
HA	Hyaluronic acid
hNP	Hybrid nanoparticle
HPH	High pressure homogenization
IL	Interleukin
LCPS	Light counts *per* second
LDH	Lactate dehydrogenase
LOD	Limit of detection
LOQ	Limit of quantification
LPP	Large porous particle
LPS	Lipopolysaccharide
MARCO	Macrophage receptor with collagenous structure
MDDC	Monocyte-derived dendritic cells
MDM	Monocyte-derived macrophages
MEM	Minimum essential medium
MIC	Minimum inhibitory concentration
MMAD	Mass mean aerodynamic diameter
MOC	Micro-orifice collector
MOPS	3-(N.morpholino)propanesulfonic acid
MTT	3-(4,5-dimethylthiazol-2-yl)-2,5-diphenyltetrazolium bromide
NCL	Niclosamide
NF-κB	Nuclear factor κB
NGI	Next generation impactor
NLCs	Nanostructured lipid carriers
NP	Nanoparticle
NS	Nanosuspension
OD	Optical density
PADDOCC	Pharmaceutical aerosol deposition device on cell cultures
PCS	Photon correlation spectroscopy
PEG	Poly(ethyleneglycol)
PEI	Poly(ethylenimine)
Ph.Eur	Eropean pharmacopoeia 8th edition
PI	Polydispersity index
PLGA	Poly(lactic-co-glycolic) acid
pMDI	Pressurised metered dose inhalers

PCS	Photon correlation spectroscopy
PVA	Poly(vinyl alcohol)
QS	Quorum sensing
RDI	Redispersibility index
Rhod	Rhodamine
RP-HPLC	Reverse-phase high-performance liquid chromatography
SD	Standard deviation
S.E.M.	Standard error mean
SEM	Scanning electron microscopi
SILF	Simulated interstitial lung fluid
siRNA	Small interfering RNA
SLNs	Solid lipid nanoparticles
Tb	Tobramycin
TC_{50}	Toxic concentration at 50%
TCCC	Triple cell co-culture
TEM	Trasmission electron microscopi
TNF-α	Tumour necrosis factor α
VMT	Vibrating mesh technology

SUMMARY

The lungs are perhaps the most ancient route of drug delivery. As early as 1,500 BCE, the ancient Egyptians inhaled vapors to treat a variety of diseases. Unfortunately, the lungs were soon forgotten as a major route of drug delivery, and it only in 1950s serious consideration of the lungs was resurrected with the invention of the first metered dose inhaler. Today, researchers have made enormous strides in the development of precise pulmonary drug delivery technologies, both in terms of inhaler design and advances in particle engineering.

Although dated back of some years, the opportunity to selectively target a drug to lungs remains a fascinating option to strongly limit ubiquitous distribution of systemically, and often chronically, administered drugs used to treat severe pulmonary diseases. Indeed, a new direction in inhalation technology has begun to focus on severe and chronic lung diseases such as chronic obstructive pulmonary disease (COPD), cystic fibrosis (CF) and lung cancer. The main research focus is to combine the advanced, and often "nanotechnology-based", delivery strategies with the pulmonary route of administration. In this scenario, a number of advanced devices and drug delivery strategies are under development to increase the amount of drug reaching the target and its persistence in situ, to reduce dose frequency and time required for administration, as well as to allow combined therapy.

The use of specially designed formulations may be highly beneficial to overcome extracellular and cellular barriers imposed by the lung. This aspect is especially critical in severe lung diseases, such as CF, where submucosal glands and distal airways are obstructed by thick tenacious secretions, resulting in a failure of normal mucociliary clearance and defective air way defense mechanism against bacteria. Lung mucus may strongly limit the amount of drug reaching the target, such as lung epithelial cells, macrophages or bacterial cells. The way to the target is even more complicated for inhaled antimicrobial agents due to the biofilm-like mode of growth adopted by *Pseudomonas aeruginosa*, which chronically infects CF lung. Infact, the slow penetration and possible entrapment within the biofilm can strongly reduce drug availability in proximity of bacteria colonies.

Recent advances in materials, particle engineering techniques and inhalation devices make it possible to formulate inhalable nano- and micro-carriers for pulmonary delivery of drugs with improved ability to overcome lung barriers and potential to fulfill specific therapeutic needs. Although carrier-free formulations for inhalation are somewhat advisable due to their mild toxicological profile, biocompatible materials, such as approved surfactants, biodegradable polymers and lipids, may allow efficient protection and delivery of both antibiotics to bacteria growing in biofilm and gene material to airway epithelial cells. Of note, inhalable polymer particles can be produced through adequate combination of available particle technologies with helping or "functional" excipients so as to develop sustained-release and easy-to-use dry powders for inhalation. Indeed, it is evident from the literature that the interest in dry powders for inhalation is growing and they represent the challenge of the future of local therapy of severe lung diseases.

In this scenario, the general aim of this work is the design and development of advanced nano- and micro-carriers for pulmonary delivery of drugs potentially useful in the local treatment of CF-related chronic lung infection and inflammation. This objective has been pursued through the development of four different formulation strategies, driven by both technological and biological design rules. Through the adequate combination of the most appropriate materials and available technologies, inhalable formulations allowing repositioning of two distinct old drugs, namely niclosamide and flucytosine, for local therapy of lung infections have been successfully developed. Then, biodegradable large porous particles have been especially designed for combined and sustained release of two bioactive macromolecules, namely a decoy oligonucleotide and poly(ethylenimine) with antinflammatory and antimicrobial properties. Finally, novel hybrid lipid/polymer nanoparticles are proposed to face the current challenge of siRNA delivery on the human airway epithelial barrier.

The most appropriate formulation approach was selected taking into account the distinct physico-chemical profile of the drug under investigation (e.g., solubility, stability, molecular weight) and the peculiarities of CF lung. *In vitro/in vivo* studies represented a critical step before selection of the best formulation to candidate for

further development. Special attention was paid to the optimization of the lung deposition profile of the drug. Nevertheless, *in vitro* studies aimed to acquire knowledge on what happens after the particles have landed were considered crucial for formulation choice. An important challenge that has been taken in count is the toxicity of the selected materials to the lung cell/tissues and its biodistribution and persistence in the lung *in vivo*.

CHAPTER 1

1.1. PULMONARY DRUG DELIVERY: PRINCIPLES AND TECHNOLOGICAL CHALLENGES

The pulmonary route is, and has long been, a highly desired route for local and systemic administration of drugs to be used in the therapy of more or less severe diseases, not only local but also systemic. In fact, lungs are characterized by an enormous absorptive surface area (close to 100 m^2), a small aqueous volume at the absorptive surface and a highly permeable and vascularized epithelium, especially in the alveolar region, which leads to a rapid drug absorption and therapeutic effect.[1,2] Furthermore, the relatively low proteolytic activity in the alveolar area and the absence of first-pass metabolism minimize drug enzymatic degradation as compared to conventional route of administration. Nevertheless, the first application of pulmonary drug delivery was the treatment of local diseases and it remains the most widely attempted. Indeed, direct delivery into the human airways may allow to achieve high concentrations of the drug at the site of action, with fewer systemic side effects as compared to conventional routes of administration (i.e. parenteral, oral). An idea of the tremendous improvement in lung targeting with corresponding low systemic concentrations afforded by pulmonary drug delivery as compared to systemic administration is given in Fig.1.1.

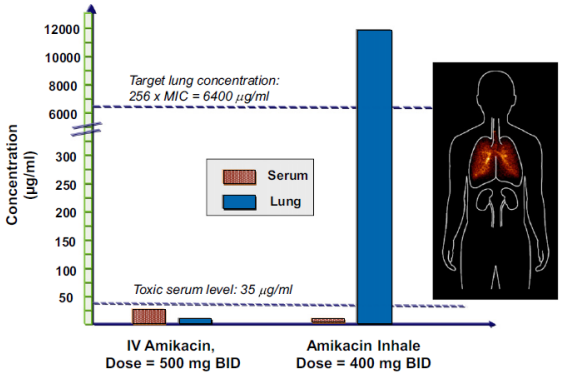

Figure 1.1. Comparison of mean serum and bronchial secretion concentrations of amikacin following intravenous administration of a 500 mg dose twice daily, and inhalation administration of a 400mg dose of Amikacin Inhale (Bayer) twice daily to pneumonia patients.[3]

Despite promising, clinical efficacy of inhaled drugs is primarily determined by the total and regional lung deposition of the drug. This result from the complex interaction of several factors, that are:

- lung anatomy and airways morphometry;
- aerodynamic behavior of the inhaled particle;
- breathing pattern of the patients;
- inhalation device;
- drug formulation.

Of note, the maximum therapeutic effect is achieved when the drug adequately deposits along the airways, remains *in situ* as long as possible and is able to overcome extracellular and cellular barriers. Indeed, the structural complexity of the lungs, the presence of lung lining fluids and macrophage uptake may strongly influence drug deposition and can reduce the absorbed dose down to the 10-20% with respect to the administered one.[4,5]

1.1.1. The complex structure of human lungs

Lung airways start with oronasal passages, followed by the larynx, trachea, main bronchi, bronchioles, all the way down to the gas-exchange tissue, that is the alveoli. Moving down to the lower airways, the number of airways in humans multiply mostly *via* dichotomous branching patterns. The airways bifurcate many times (i.e., bronchial generations) before the alveoli and with each bifurcation the airway dimensions become reduced. At the same time and as one proceeds further towards the alveolar region, multiple bifurcation patterns cause the overall lung volume to increase in non-linear fashion. The most commonly used anatomical model is the Weibel model[6] (Fig. 1.2). In this model, the ways of bifurcation are indicated, designating the trachea as the first airway (order 0) and presuming that each airway leads to two branches (regular dichotomy). The bronchial generations are adopted for the calculation of deposition fractions of inhaled aerosol particles.

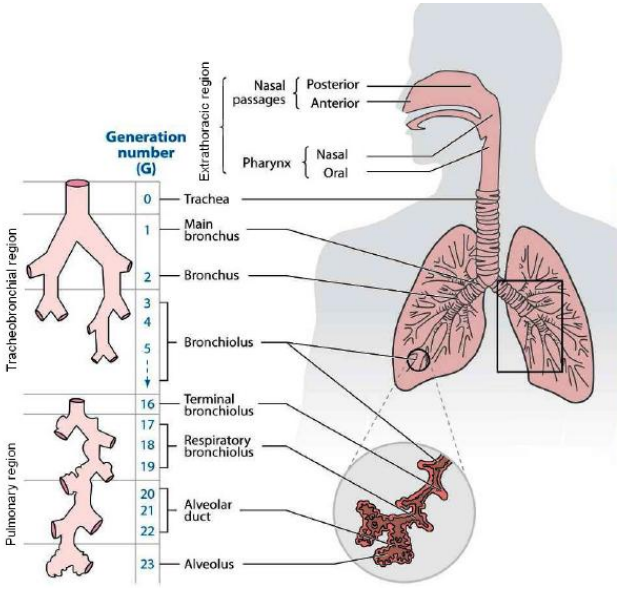

Figure 1.2. Human lung anatomical regions and airway generation model according to the International Commission for Radiological Protection (ICRP)[7] Tracheobronchial (generations 0-16) and pulmonary (generations 17-23) regions are the most important target of inhaled drug particles.

Besides the number of lung generations, the human respiratory tract can be divided into four anatomical regions. Nasal or oral pathways are known as extra-thoracic region, which serves as an important first stage filter for inhaled particles entering the lung. This region also contains associated lymph vessels and lymph nodes called bronchus-associated lymphoid tissue (BALT). Therefore, from the point of view of toxicology and human health, understanding the nature of airflow and particle transport in the human nasal-oral passages is also important. Nevertheless, the therapeutic effect of inhaled drugs is first dependent upon the dose of deposited drug and its distribution in the air conducting system within the thoracic region.

The bronchial region is the first part of the air conducting system within the thorax and consists of the trachea (assigned generation 0, Fig. 1.2), the main bronchi, and the intrapulmonary bronchi (usually grouped around generation 8). After the bronchial region, there is the bronchiolar region, which consists of the bronchioles (comprising generations 9 to 16 in Fig. 1.2). The branches of the last generation are called terminal bronchioles; whereas all airways beyond the terminal bronchioles

carry alveoli. The alveolar-interstitial region compartment comprises the respiratory tract system up to the terminal bronchioles that groups together generations 16 to 26 (Fig. 1.2) known as the respiratory bronchioles and the alveolar ducts. The gas-exchange region is represented by the alveolar sacs, which are closed at the peripheral end by a group of alveoli.

The pseudostratified epithelium of cells that constitutes the barrier to drug absorption at lung is markedly different and gradually thinner going from bronchial to the bronchiolar region (Fig. 1.3).

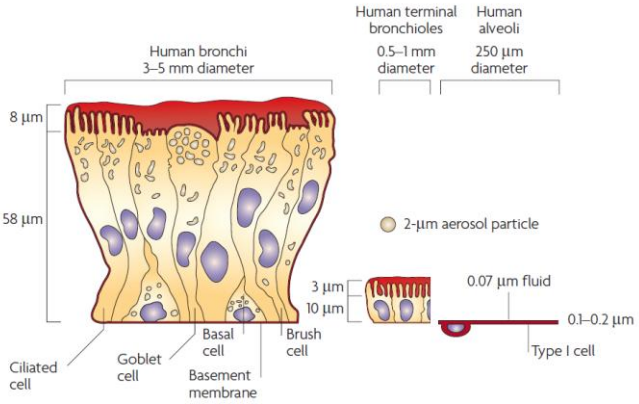

Figure 1.3. Schematic drawing of human airway epihtelium in the different regions of the lung. The cells are drawn at their relative sizes. The darker orange colour in the figure is the liquid layer, which gets thinner in thickness as the airways become smaller in diameter with a final thickness <0.1 µm in the alveoli [8].

The upper human airways have anatomical structures that efficiently serve as a filter for inhaled non-gaseous pollutants. In fact, the epithelium of the trachea primarily consists of ciliated cells ending with mucus-secreting goblet cells and specialized mucus-secreting glands that collectively form the *mucociliary escalator*. The synchronized beating patterns of cilia drives mucus and deposited foreign particles up to the larynx, where they are either swallowed or expectorated. The bronchioles are airways without cartilage and glands, where basal cells are rarely found. They are characterized by ciliated cells that clear secretory fluid towards the base of bronchial region.

According to its function, the epithelium in the conducting airways differs substantially from that in the peripheral lungs, which should provide a large and thin

surface facilitating gas exchange. Here, the epithelium is comprised of an extremely thin cell monolayer composed of two major cell types: alveolar type I and alveolar type II cells. Although type I cells only account for 10% of the alveolar cell number, they cover more than 90% of the surface in the peripheral lung; this is mainly due to their extremely outstretched morphology with protruding nuclei which facilitate the exchange of oxygen and carbon dioxide. Type II cells are more compact in shape and mainly serve as secretory cells for alveolar surfactant.[9]

1.1.2. Mechanisms and factors governing lung deposition

Understanding the mechanisms and factors determining aerosol deposition is of outmost importance to allow drug selective administration in specific regions of the lungs.

From a physical point of view, three primary mechanisms are responsible for the deposition of drug aerosols in the respiratory tract, that is *inertial impaction*, *gravitational sedimentation* and *Brownian diffusion*[10]. They may be supplemented by *electrostatic attractions* and *particle interception* (in case of elongated particles) and are likely affected by the turbulent air flow. Each deposition mechanism applies to a different particle size range and governs aerosol deposition in a peculiar region of the lungs.

Deposition *via* inertial impaction and sedimentation by the gravitational force primarily depend upon the *aerodynamic behaviour of the aerosol particles*. Particle aerodynamic diameter is defined according to the equation (1)

$$d_{ae} = d_v \sqrt{\frac{\rho}{\rho_0 X}} \qquad (1)$$

in which d_v represents the volume diameter, ρ is the density of the particle, while ρ_o is a density of control (1 g/ml) and X is the dynamic shape factor, which is 1 for a sphere. This parameter critically influences the deposition of the inhaled formulation in the upper airways, rather than the conducting airways and the alveolar region of the lungs[10,11] (Fig. 1.4).

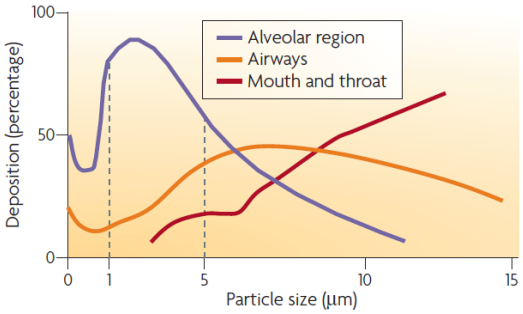

Figure 1.4. Effect of aerodynamic particle size on their regional deposition of inhaled particles along the human respiratory tract. Following a slow inhalation and a 5-second breath hold, larger particles deposit in the airways or mouth and throat, whereas smaller particles mainly deposit in the alveolar region. Particles <1 µm can be exhaled, thereby reducing deep-lung deposition[12].

Large particles (d_{ae}>10 µm) are mainly deposited by inertial impaction in the upper airways and at the bifurcations, where the airways and the airstream change direction (Fig 1.5). Indeed, particles become more and more inert with growing size, setting rate increases and their ability to follow the respiratory flow is reduced proportionally to the velocity of flow. If pharmaceutical aerosols penetrate the small conducting airways, the dominant mechanism leading to particle deposition is gravitational sedimentation, meaning that particles fall under gravity onto an airway wall (Fig.1.5). This process is again dependent upon aerodynamic particle size (1<d_{ae}<10 µm) and to the length of particle stay in the lungs. Both impaction and sedimentation result in deposition of particles larger than 3-5 µm in the smaller airways (i.e. bronchus, bronchioles) before reaching the alveoli. Differently, particles with a d_{ae} in the 1–2 µm range will likely deposit into the capillary-rich alveolar airspaces, which represent the target for systemic drug delivery through the lungs. Here, deposition is mainly influenced by Brownian diffusion, which dominates for particles with diameters less than 1 µm (Fig. 1.5). In particular, particles with an aerodynamic diameter between 0.1 and 1 µm are mostly exhaled, whereas ultrafine particles (lower than 100 nm) may paradoxically deposit in the respiratory tract taking advantage of their random Brownian motion[13] (Fig. 1.5).

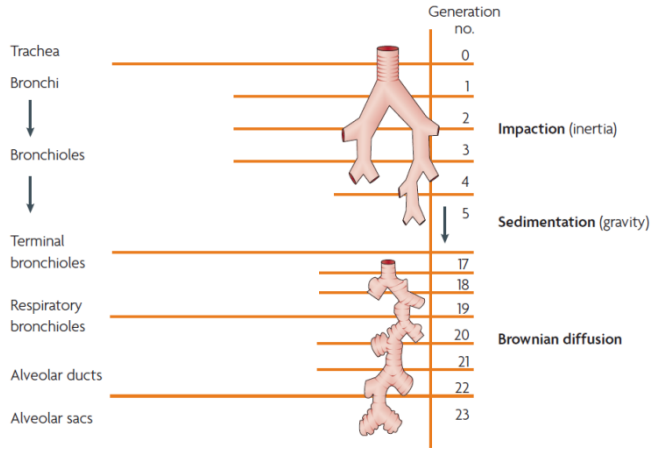

Figure 1.5. Mechanisms governing the deposition of inhaled particles along the different anatomical regions/airway generations of the human respiratory tract [12].

Alveolar deposition of small particles can be enhanced by improving the patient's inhalation technique. Indeed, *the mode of inhalation* is another critical factor determining lung deposition. Faster inspiratory flow rates increase inertial impaction of aerosols in the oropharynx and at bifurcations in the large central airways, thus reducing lung deposition in the peripheral airways[10] (Fig. 1.6). Nevertheless, dry powder inhalers (DPIs) represent and important exception to this rule, since lung deposition from dry powder devices paradoxically increases as inspiratory flow increases. Infact, maximal patient therapeutic effort may be needed to deaggregate the powder and to provide a large mass of particles with sufficiently small aerodynamic diameter to enter the lungs.[14] The penetration of aerosol particles into the lung periphery may be also enhanced by deep inhalation and breath holding increases time for small particles to diffuse and/or to settle by gravity and to deposit on the alveolar surface, resulting in improved alveolar deposition. In other words, the probability that a particle will be deposited in the lungs by diffusion increases with increasing residence time.

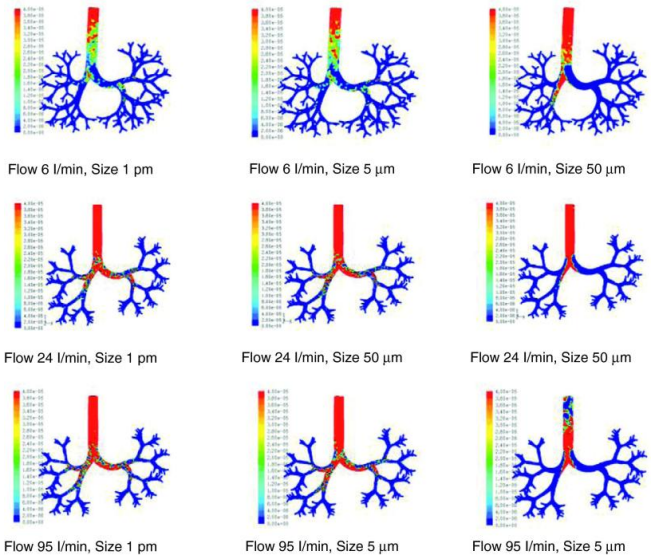

Figure 1.6. Results of the simulation with computational fluid dynamics (CFD) of particle behavior at different sizes (1pm, 5µm, and 50µm), which are dragged by flows of 6, 24, and 95 l/min. The red areas indicate a high density of trapped particles. As the size of the particle and flow increase, more particles tend to become trapped in more central regions of the airway due to impaction.[15]

1.1.3. Inhalation device

The increasing research interest towards inhaled therapeutics has recently led to tremendous innovations in designing inhalation devices able to ensure high aerosolization performance, consistent therapeutic efficacy and satisfactory patient adherence. Vibrating-mesh and software technologies have resulted in nebulisers that have remarkably accurate dosing and portability. Alternatively, advanced particle engineering techniques have made DPIs highly favourable for delivering also high-dose drugs, such as antibiotics. On the other hand, innovations are still needed to overcome the technical constrains in drug-propellant incompatibility and delivering high-dose drugs with pressurised metered dose inhalers (pMDIs).[16]

1.1.3.1 Nebulisers

Nebulisers have a long and complex history, and were defined in the 1870s as "*instruments for converting a liquid into a fine spray, especially for medical*

purposes". More than one century has passed and they are still widely employed, especially for pediatric and geriatric patients and for a more convenient delivery of high drug doses, as in case of chronic antibiotic therapies.[10] Indeed, design changes over the past decade have created different nebulizer categories, with different and always increasing performances in human therapy.[16,17]

The most common nebulizer type is the *jet nebuliser*, which generates aerosols from the liquid drug formulation (solution or suspension) using a source of compressed gas. The compressor entrains room air, compresses it to a higher pressure and emits the air at a given flow rate. The air enters the nebuliser chamber and passes through a small hole, a "venture", beyond which the air expands rapidly creating a negative pressure; this draws the medication up a feeding tube where it is atomised into particles. Larger particles will impact on the baffle within the nebuliser chamber and onto the walls of the chamber and be returned back to the well of the chamber to be re-nebulised. Smaller particles will be continuously released from the nebuliser chamber during both inspiration and expiration of the patient.

A large number of conventional compressor and nebuliser combinations are available and these combinations have different characteristics in terms of aerosol particle size, nebulisation time and mass of medication delivered. Optimisation of existing nebuliser technologies has focused on maximizing aerosol lung deposition with each breath.[16] This is the case of breath-enhanced (e.g., PARI LC® Plus) or breath-assisted (e.g., AeroEclipse®) jet nebuliser (Fig. 1.7). Breath-enhanced jet systems use a valve system to allow air to be drawn in during inhalation (Fig. 1.7A). During exhalation, the valve closes and the airflow through the chamber is decreased to that coming from the compressor only. This decreases the amount of particles released during expiration and, consequently, medication wastage.

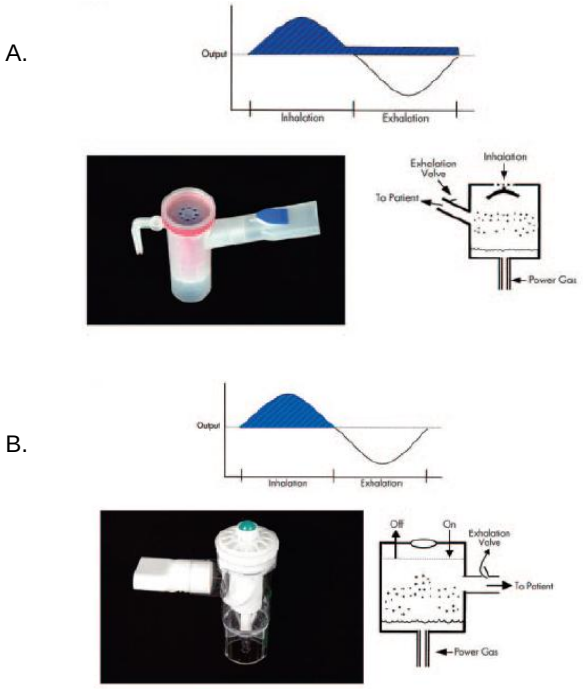

Figure 1.7. Advanced designs of jet nebulisers. A) Breath-enhanced nebuliser. B) Breath-actuated nebulizer. In each diagram, the device's aerosol output is indicated by the striped area. (From: Hess DR, Myers TR, Rau JL. A guide to aerosol delivery devices. Irving TX: American Association for Respiratory Care; 2007. Available from http://www.aarc.org/education/aerosol_devices/aerosol_delivery_guide.pdf.

Conventional jet nebulisation systems tend to be cheaper than the alternatives and are less prone to reliability or delivery problems (or both) due to poor cleaning and maintenance. They are, however, noisy and bulky and therefore less portable. They also produce variable particle sizes and have a larger residual volume as compared to alternative systems, so leading to more wastage of medication. These limitations have led to the development of a new class of nebulizers, using the principle of the vibrating mesh technology (VMT).

Vibrating mesh nebulizers aerosolise medication utilising a vibrating, perforated mesh to generate particles. This is achieved by using a piezoelectric element which either vibrates a transducer horn or which is annular and encircles the mesh causing

it to vibrate. Both methods result in medication pumping through the perforated mesh, when creates homogenous particles (Fig. 1.8).

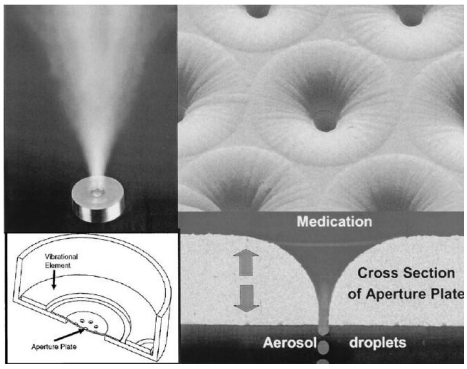

Figure 1.8. Aerosol generation through VMT technology. The aerosol generator uses a piezo element to vibrate an aperture plate (lower left) containing 1000 funnel-shaped orifices (magnified view, upper right) to create an electronic micropump (lower right), extruding aerosol droplets. Particle size is dictated by the diameter of the aperture.[18]

Advanced VMT systems are silent, portable (being small and battery powered), fast and produce more homogenously-sized particles as compared to conventional jet nebulizer systems. There are a number of currently available devices for clinical use, such as the Aeroneb Pro® and the Pari eFlow®, which have been especially designed to deliver medications more efficiently and quicker. Deposition of medication in CF patients, as measured by sputum levels, was found to be greater with VMT as compared to conventional Jet nebulizers when used over a longer period of time.[17]

Addressing many of the concerns associated with previous nebulisers types, the newest VMT nebulisers are expected to be more and more employed in the next future by patients, particularly in the domiciliary setting. Nevertheless, future studies are needed to definitively confirm the cost-effectiveness of these devices.

1.1.3.2. Dry powder inhalers (DPIs)

For long time, pMDIs have been the most commonly used inhalers for drug inhalation in the treatment of asthma and COPD. Nonetheless, pMDIs require the use of liquid drug formulations (mainly suspensions) in polluting propellants and

delivery efficiency strongly depends by the actuation-breath coordination of the user. As a viable alternative to pMDIs, DPIs have become accepted increasingly by both patients and formulators. Indeed, DPIs do not contain propellants and breath-actuated, or "passive", DPIs have completely eliminated the problem of actuation-breath coordination. Furthermore, lung deposition from DPIs is often higher and less variable than for pMDIs and novel DPIs have been especially designed to deliver large drug doses.[10]

The possibilities for dry powder dispersion were first explored in the '50s and in 1971 one of the first DPI, the Spinhaler®, became commercially available. Since then, DPIs evolved and diversified rapidly into a huge variety of different concepts (i.e., multi-unit, multi-dose reservoir, reusable single dose, single-use) with specific pros and cons for a large number of different inhaled drugs, with an increased awareness that DPIs may have potential for several new areas of interest for pulmonary administration (e.g., lung infections, vaccination, systemic diseases)[14] (Fig. 1.9).

Figure 1.9. DPI devices: (a) Turbuhaler™/Turbohaler™ , (b) Exubera®, (c) Podhaler™, (d) Turbospin, (e) Staccato®, (f) Cricket™, (g) Dreamboat™, (h) 3 M Taper DPI™, (i) MicroDose DPI (j), Twincer™, (K) ARCUS® inhaler (l) DPI — The University Of Western Ontario.[19]

DPIs are complex delivery systems which must meter a drug dose, transfer it into the inhaled air and, often, deaggregate the powder into respirable particles. As a consequence, the performance of breath-actuated DPIs strongly depends on the

correct balance between the inhaler device, the powder formulation and the airflow generated by the patient (Fig. 1.10).

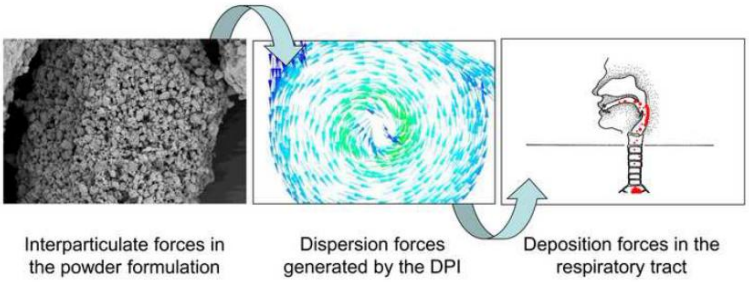

Figure 1.10. Desired balance for optimal DPI-based therapy between the interparticulate forces, the dispersion forces generated by the inhaler and the deposition forces in the respiratory tract during inhalation.[14]

From a formulation point of view, the handling, processing and inhalation of excipient-free dried drug particles are challenging. Indeed, particles in the micron size range are intrinsically cohesive and display poor flow properties. This makes difficult both to meter accurate masses of drug and to disperse them. To overcome this issue, the classical approach employed for dry powder formulations has been to blend micronized drug particles with large particles made of inert carriers. The excipient, that is lactose, and the drug will form an interactive and ordered mixture with improved flow properties, which is more easily metered and delivered from the device and deaggregate during dry powder inhalation.

To reduce excipient amount in dry powder formulations, comprising often more than 99% of the powder, novel strategies have been developed and investigated for drug inhalation *via* DPIs, including microparticles.[19] Working on size, shape and density of the particles, the first microparticles for inhalation have faced the market. Advanced products include PulmoSphere™ particles, hollow porous tobramycin-containing microparticles made of a dipalmitoylphosphatidylcholine derivative, the principal component of endogenous lung surfactants. Technosphere™ Insulin (MannKind Corp., Valencia, USA), based on the intermolecular self-assembly of fumaryl diketopiperazine (FDKP), forming a three-dimensional highly porous sphere, is also facing the market**.**

Nevertheless, the number and quantities of excipients approved for inhalation by Food and Drug Administration (FDA) and the European Medicines Agency (EMA)

is still very small. Some of them, along with those currently under investigation for inhalation are presented in Table 1.1.

Table 1.1. Summary of excipients used or with potential for use in dry powder formulations for pulmonary delivery. Modified from.[19]

Excipient	Function	Status
Amino acids (leucine, glycine, arginine)	Improved aerosolization properties Coating Buffering agent	Endogenous substances but no data on lung toxicity Proven in vitro safety in lung cell line Approved by FDA for injectables Approved DPI product: Exubera
Ammonium carbonate	Blowing agent	Promising excipent
Calcium chloride	Stabilising agent	Approved: TOBI® Podhaler
Chitosan and derivativess	Controlled release	Biocompatible and biodegradable Low or non-existent toxicity *in vitro* and *in vivo* FDA GRAS
Citric acid	Absorption enhancer	FDA GRAS Promising excipient Approved by FDA for injectables
Dextran	Particle matrix/ stabilising agent	Proven lung safety in animal studies FDA GRAS
FDKP (fumaryl diketopiperazine)	Carrier/particles matrix	Afrezza® (MannKind Corporation) under clinical trials
Glucose	Carrier	Approved in Bronchodual®
Hyaluronic acid	Controlled release	FDA approved for injectables, approved in Hyaneb® Promising excipient and biocompatible
Hydroxypropyl-β-cyclodestrin	Absorption enhancer/stabilising agent	Promising results FDA approved for injectables
Lactose	Carrier/coating	Approved (several products)
Lipids	Particle matrix /coating/surfactant/absorption enhancer	Approved in TOBI® Podhaler™ biocompatible and biodegradable Liposomal drugs in clinical trials Proven lung safety
Mannitol	Carrier/particle matrix/ stabilising agent	Approved in Exubera® and Bronchitol® FDA GRAS[a]
Magnesium stearate	Protection from moisture	Approved in SkyeProtect®, Seebri Breezhaler®, Foradil®, Certihaler®
Linear and branched PEG	Stabilising agent	Promising excipient FDA approved for inhalation
PLA, PGA, and PLGA	Particle matrix/stabilising agent	FDA approved for injectables Promising excipients for sustained release
Polaxamer	Surfactant/particle matrix	Good biocompatibility and proved lung safety
Sodium citrate	Buffering agent/stabilising agent	Approved: Exubera® FDA GRAS[a]
Sucrose/Threalose	Stabilising agent	Promising excipient for peptide and protein delivery FDA GRAS[a]

[a] FDA GRAS: FDA food substance generally recognised as safe.

1.2. OVERCOMING BARRIERS IN SEVERE LUNG DISEASES: THE CASE OF CYSTIC FIBROSIS

Acknowledging that efficient deposition of aerosol particles in the lungs is still a necessary condition for successful pulmonary drug delivery, it is not always sufficient. Indeed, there is an increasing need to understand and control what happens after a particle has landed. Nowadays it is clear that at the interface between inhaled materials and biological systems, the organic and synthetic worlds merge into a new science concerned with the safe and effective use of innovative inhalation technologies. After deposition at lung, the success of any inhalation therapy will strongly depend also upon: i) drug permeation through airway mucus; iii) drug interaction with the cell target; iv) macrophage clearance escape.[9] In the case of antimicrobials, the ability of the drug to penetrate bacterial biofilm is of great importance, too (Fig. 1.11).[3]

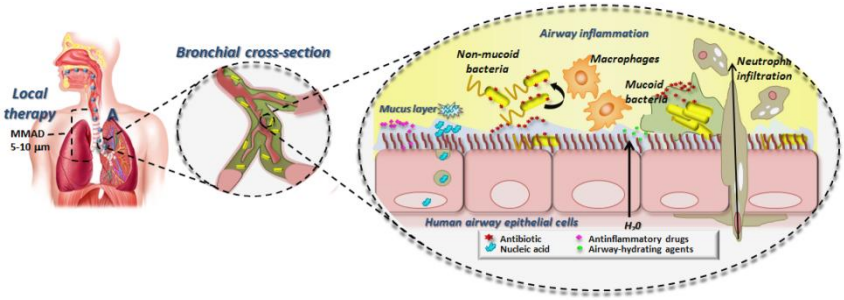

Figure 1.11. Anatomical/biological barriers imposed by diseases lung (i.e., chronically inflamed and infected) to the most widely investigated inhaled drugs. Once landed at lung, the intact drug should: permeate through the mucus barrier, escape macrophages, interact with the cell target (e.g., biofilm bacteria, airway epithelial cells). Enzyme-mediated degradation is also critical for labile drugs (e.g., nucleic acids). Modified from ref[20].

If the deposition and clearance of aerosol particles in the lungs has been under investigation for decades, the rate, the extent and the various mechanisms underlying the interactions between the aerosol particle and the biological environment (e.g., particle/mucus interactions, mucociliary clearance, uptake by macrophages/lung epithelial cells, translocation across the lung epithelium) are still unclear. A thorough understanding of the behavior of the inhaled drug in the lung

and its interaction with lung cellular/extracellular environment is, thus, considered crucial for a beneficial therapeutic outcome and should be properly taken into account when designing new inhalable medicines.

1.2.1. Lung cellular and extracellular barriers

The cellular elements of the air-blood barrier are diverse and complex. Besides epithelial cells, which show dramatic differences in morphology and function between the upper (airways) and lower (alveolar) regions of the respiratory tract, there are macrophages and other cells of the immune system. The non-cellular elements determine the diffusion, the solubility and the rate of dissolution of particulate matter in the lung lining fluids, as well as its agglomeration or disintegration, water uptake, adsorption of biomolecules. These, in turn, will likely affect particle interaction with the cellular elements of the lung barrier.

1.2.1.1. Non-Cellular barriers

The non-cellular barriers of the airways pose a major challenge for particle dissolution, diffusion and drug adsorption. In fact, after landing at lung, the inhaled particle maybe altered by surrounding environment and, in turn, this can modify its fate in term of diffusion, disaggregation, dissolution and clearance. However, the significance of such changes for particle clearance or translocation through the epithelium as well as the mechanisms of particle mobility and transport within the mucus blanket have not been fully elucidated, yet.

Compared to oral drug delivery, it is barely known if and to what extent the composition and the structure of the lining fluids in the lung play a role in drug dissolution and absorption. The two essential elements of the lung lining fluid are mucus and pulmonary surfactant, which vary in volume and thickness along the respiratory tract. The rather small total fluid volume in the lungs may be a challenge for new, often poorly soluble active pharmaceutical ingredients. Thus, insoluble drugs can quickly reach their saturation concentration and prevent further dissolution. Formulating drugs as nanoparticles (e.g., nanocrystals) increases the surface area to volume ratio, thereby increasing solubilization and dissolution rate.[21]

Other aspects that are not clear yet are physical, chemical or metabolic changes of the carriers and drug materials following deposition. Concerning physical and chemical changes, surface properties, agglomeration status, density and water content are fundamental, not merely for deposition but also for translocation and mobility of particles in mucus. Airway mucus is one of the more investigated non-cellular barrier affecting the fate in the lungs of any inhaled particles.[22,23] Indeed, the amount, the composition and the rheological properties of the mucus, its turn-over, along with wash-out of fluids that line the epithelia, determine the efficiency of the mucociliary clearance mechanism and are the main determinants of *in situ* permanence and extent of drug absorption.[24] In particular, the mucus layer is composed of highly cross-linked mucin chains, creating a dense porous structure, with thickness and porosity variable for lung area and pathological conditions.[12,25,26] Two major mechanisms may stop particles from readily diffuse through mucus gel, that are "size filtering" through the mucus meshes and "interaction filtering" (Fig. 1.12).

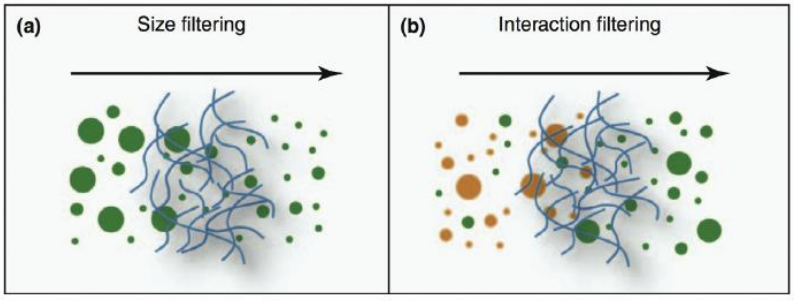

Figure.1.12. Mechanisms governing the diffusion of inhaled particles through the airway mucus layer.[22,23]

Infact, mucin, the principal mucus component, is a negatively-charged glycoprotein, due to the presence of sialic acids, able to establish interactions with a broad range of pharmaceutical molecules *via* hydrophobic, electrostatic, and hydrogen bonding interactions.[27] Thus, insoluble particles maybe trapped in the mucus gel layer and moved toward the pharynx (and ultimately to the gastrointestinal tract) by the upward movement of mucus generated by the cilia beating (i.e. mucociliary clearance).[22,23]

Just as the thickness of lung epithelium, the pulmonary fluid layer reduces in thickness and surface coverage, forming single droplets on top of the scarcely ciliated cells of the lower bronchii and an extremely thin layer of surfactant in the outermost branches of the lungs, that is alveoli. There, the surfactant film reduces the surface tension at the air–liquid interface, thus preventing alveoli collapse during expiration. Pulmonary surfactant is composed of approximately 90% lipids and 10% proteins by weight. The most represented lipid is dipalmitoylphosphatidylcholine (DPPC), whereas four different surfactant proteins are commonly associated with the lung surfactant, that are surfactant protein A, B, C and D. Upon contact with surfactant, larger sized particles are displaced from the airspace to the hypophase due to wetting forces, a phenomenon that probably also occurs with nano-sized particles. In the hypophase, the particles may interact with surfactant proteins or may be taken up by alveolar macrophages.[28]

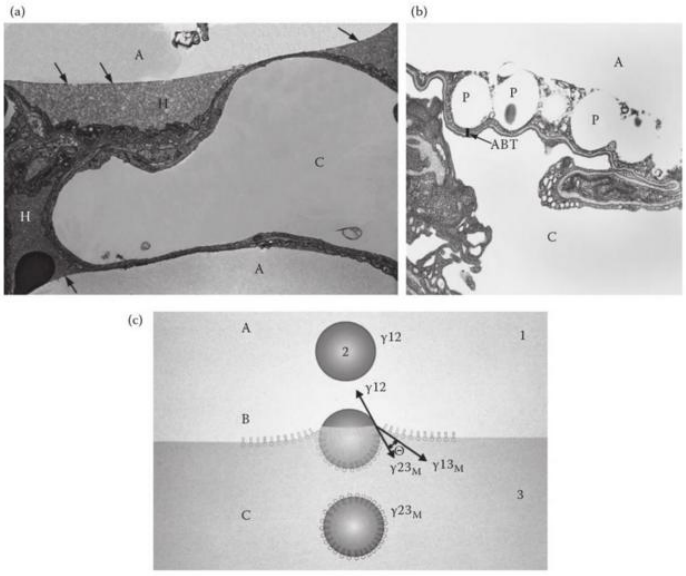

Figure 1.13. Particle-surfactant film interaction. (a) Electron micrograph of interalveolar septum of human lung showing aqueous hypophase (H) and surfactant (arrow). (b) Electron micrograph of 1-μm polystyrene particles depositedon the surface of alveolar wall after inhalation by hamster (P: particle; A: alveolar air; ABT: air-blood tissue barrier; C: capillary lumen). (c) Schematic drawing of the interaction of a particle with the surfactant film at the air-liquid interface (internal lung surface) and the subsequent displacement of the particle by surface forces exerted on it by surfactant, during which the particle might be coated with a film of surfactant or its components (1: air; 2: solid particle: 3: liquid and forces).[29]

Nevertheless, many literature findings suggest that, depending on their composition and size, inhaled particles may interfere with the function of pulmonary surfactant, thus hindering its physiological and essential role in the lung. This issue should be properly taken into account when designing novel nanoparticle-based inhalable drug formulations[29] (Fig. 1.13).

1.2.1.2. Lung epithelial barrier

The routes of drug absorption across the lung epithelium include passive and active transport mechanisms involving paracellular and transcellular transport, pore formation, vesicular transport, and drainage into the lymphatics depending on the drug and site of absorption. As described above, the composition and morphology of the lung epithelial cells reflect their different physiological functions and form a barrier that is so large as different. The drug solute will pass through a cellular barrier that varies from a monolayer of thick (about 60 mm) columnar cells in the bronchi to a monolayer of thin (0.2 mm) broad cells in the alveoli. Furthermore, the epithelial cells are attached to a basement membrane and below that, there is the lung interstitium, which contains a variety of cells, collagen, elastic fibers, interstitial fluid, and lymphatic vessels. If none of these tissues is considered a significant restrictor of the transport of drug solutes, there are also macrophages and other cells of the immune system, which play a role.

There is a great interest in fully understanding the mechanism of drug uptake by cells after deposition. The most important evidence is that only the nanosized fraction of particles with a diameter of 100 nm is able to penetrate with high efficiency through the air-blood tissue barrier. Without taking into account the possible alteration of the barrier properties of the epithelium in pathological conditions (e.g., lung inflammation), particle translocation through lung epithelium follows different passive and active mechanisms. Nevertheless, the greatest number of studies regard alveolar cells, while much less is known on the mechanism of drug absorption at bronchial/bronchiolar level, where the mucus blanket is considered determinant.

To improve drug accumulation at cell level, different formulation approaches can be pursued. By simply using carriers with adequate surface properties (charge, shielding cloud), one can regulate drug interaction with cells.[30] Along with facilitating cellular uptake of the macromolecule, the carrier has to promote its endosomal escape and release it at the final intracellular target.[31,32] This can be crucial in case of emerging nucleic acid-based therapeutics (DNA, siRNA and oligonucleotides), which should rely on adequately-engineered nanoparticulate systems, comprising not only biodegradable polymers able to compact, protect and sustain nucleic acid delivery *in situ*[33], but also a biomimetic shell containing agents able to facilitate endo-lysosomal escape (e.g., fusogenic peptides or lipids, endosome destabilizing polymers)[32,34]. Decoration of carrier surface with different functional motifs can be also attempted to build up actively-targeted constructs.[35]

In this context, advanced *in vitro* model play an important role to design and to develop effective novel carriers for inhaled therapy.[36] Well-established alveolar (A549) or bronchial (Calu-3, 16HBE14o-) models have been particularly useful in early stages of development of inhaled medicines and for toxicological studies. Meanwhile, advanced models may allow to better resemble what happens *in vivo*. When cultures at an air–liquid interface (ALI), cells are grown on membranes in Transwell supports and supplied with nutrients from the basal side. In this case, alveolar epithelial cells may secrete pulmonary surfactant while human bronchial epithelial cells may produce mucus. Furthermore, several exposure systems, such as the pharmaceutical aerosol deposition device on cell cultures (PADDOCC) or the VITROCELL®, may allow nowadays the direct aerosolization of the formulation on the cells, further affecting the results of transport studies (Fig. 1.14).

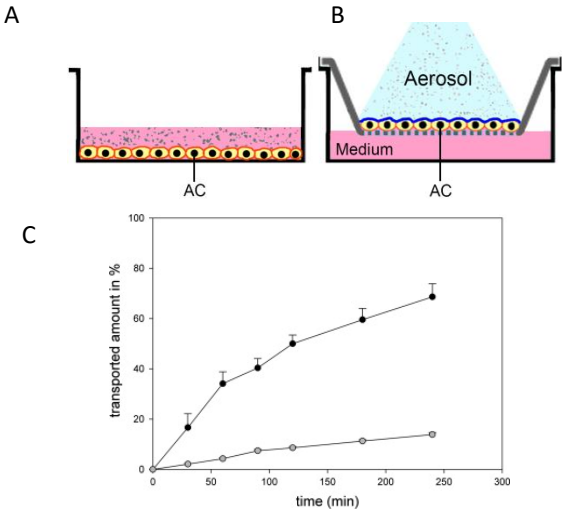

Figure 1.14. Schematic representation of different cell culture models for human airway epithelial cells (AC) and consequent exposure to inhaled drugs: A) AC grown at the bottom of well and exposed to the drug suspended/solubilized in the medium; B) AC cells grown on membranes at ALI and exposed to inhaled drugs applied as aerosols; C) transport of budesonide across filter-grown Calu-3 monolayers using the PADDOCC system (full circles) *versus* the dissolved drug using a conventional Transwell® setup (open circles).

Dual- or even triple-cell co-cultures particularly facilitated the investigation of particle translocation and clearance, especially with respect to the interplay between epithelial and immune cells (Fig. 1.15).[9,37] Although co-culture models are more physiologically relevant, they cannot depict all characteristics of the *in vivo* situation. Nevertheless, much progress in this area has been due to the efforts to improve such model systems. Potential interspecies incompatibilities in current co-culture models should be addressed in the future.[36]

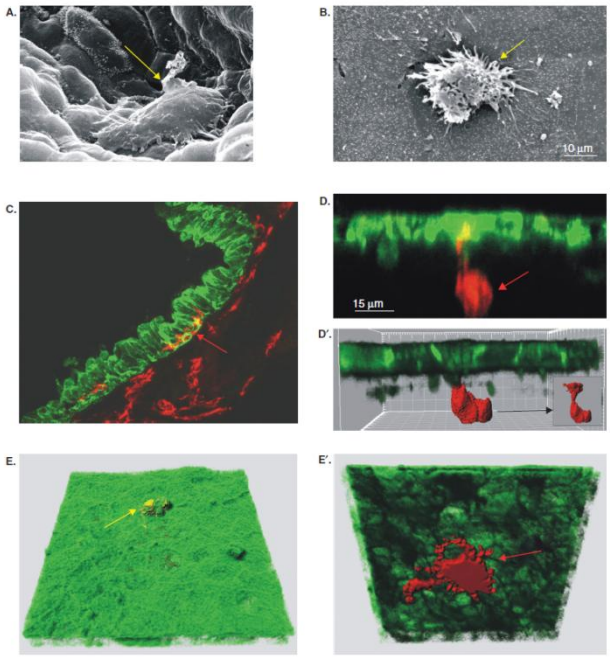

Figure 1.15. Triple cell co-culture model of airway epithelium. A. Scanning electron microscopic image of alveoli in human lung, a macrophage is on top of the epithelial cells (yellow arrow). B. Scanning electron micrograph of the triple cell co-culture system showing cells from top with a macrophage (yellow arrow) on the epithelial surface. C. Distribution of mouse dendritic cells (red) within the epithelium (green) shown by laser scanning microscopy. The red arrow points to intra-epithelial processes of dendritic cells. D, D′. In the triple cell co-culture model dendritic cells make processes through the membrane pores towards the apical side of the epithelium. E. A volume rendering from top of a laser scanning microscopy data set, showing macrophage (yellow arrow) on top of the epithelium. E′. When the same data set is shown upside down a dendritic cell (red arrow) can be seen at the bottom side.[38]

1.2.1.3. Macrophage-mediated clearance

Lung macrophages fulfill a crucial function in pulmonary immune reactions and the host defense system, and can be considered as the first line of defense against foreign material that reaches the lung environment. In particular, alveolar macrophages comprise more than 90% of the pulmonary immune cell population and are crucially involved in recovering the alveolar architecture and maintaining sterility in the peripheral lungs.[39] Once a particle is deposited in to the peripheral

lung it first contacts the alveolar lining fluid, and encounters the pulmonary surfactant system. Consequently, it will be displaced into the subphase where interaction with alveolar macrophages is most likely. If particles depositing in the tracheobronchial tree may be rapidly cleared by the mucociliary escalator, alveolar macrophages represent a unique cell population in the lung that promptly responds to any airborne irritant or microbe.[39] Particle–macrophage interactions and subsequent uptake can be promoted or reduced by optimizing size, shape, density, charge and hydrophilic/lipophilic character of particulate carriers.[40]

The size of particulate carrier systems significantly influences particle–macrophage interactions, as demonstrated in numerous studies. Particles with 1–5 μm size are taken up by alveolar macrophages at a greater extent compared with particles that are smaller or larger than 1–5 μm both *in vitro*[41] and in an *in vivo* setting.[42] Also the mechanism of particle uptake changes as a function of particle size. Inhaled particles in the micrometer range (1-5 μm) are taken up by alveolar macrophages mainly *via* active phagocytosis (or also macropinocytosis), whereas this is unlikely for nanosezed particles. Infact, particles with a mean size less than 500 nm are taken up sporadically and by non-specific mechanisms. Depending on their size, nanoparticles enter alveolar macrophages by pathways other than phagocytosis: while nanoparticles bigger than 0.2 μm are probably internalized *via* pinocytosis, smaller particles (less than 150 nm) can be internalized *via* calveolae (50-100 nm) or clathrin-mediated (100-120 nm) uptake.

Particle shape is another major factor affecting endocytic uptake and, thus, internalization of the inhaled particles by alveolar macrophages. In fact, the macrophage membrane undergoes structural changes in such a way that the membrane spreads around the particle and the progression of particle internalization is dependent on the contact angle between particle and macrophage membrane. It was successfully demonstrated that aspherical particles with aspect ratios greater than 20 were internalized at the greatest extent when the macrophage approached the particle at points with high curvature, whereas spherical particles were shown to be internalized from each side equally. Similarly, shape-switching PLGA elongated

particles were quickly engulfed by macrophages once the particles became spherical in shape[43] (Fig. 1.16).

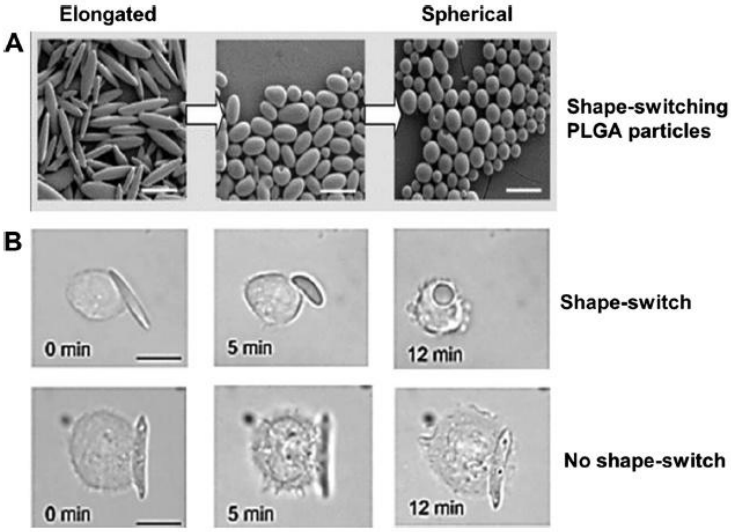

Figure 1.16. Morphology-dependent phagocytosis of poly lactic-co-glycolic acid (PLGA) particles by macrophages. (A) PLGA particles switching shape from elongated to spherical ones at pH 7.4. (B) Shape-switching PLGA elongated particles initially get attached to macrophages surface but not get internalized. Once the particles become spherical in shape, they are quickly engulfed by macrophages. (C) In the absence of shape-switching ability, particles are not internalized by macrophages.[43]

Besides the particle shape, the material and material properties may strongly affect particle uptake by alveolar macrophage. For example, increased mechanical robustness and overall stiffness of particles leads to increased phagocytosis. More importantly, the material composition of a particle can affect the adsorption of biomolecules with opsonin function, which is likely to influence the uptake by alveolar macrophages significantly. Furthermore, particle surface can be especially modified to enhance or avoid recognition by alveolar macrophages. For example, surface modification with DPPC, the major component of lung surfactant, was shown to reduce the macrophage uptake of PLGA microparticles by altering the cellular interactions occurring in the alveoli[44] (Fig. 1.17).

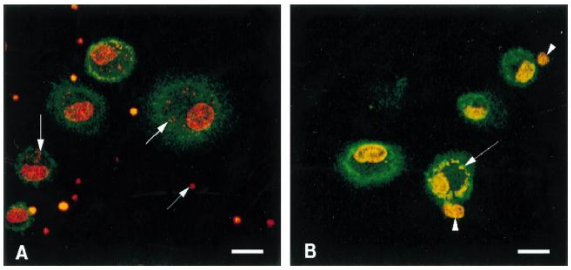

Figure 1.17 (A) Fluorescent confocal micrographs of rat alveolar macrophages (green) stained with FITC-phalloidin after a one hour exposure to peroxidase-containing PLGA particles (arrows). (B) Rat alveolar macrophages exposed to peroxidase-containing PLGA particles (arrow) modified with DPPC. Bar represents 10 microns.[44]

It should be underlined that uptake of a (nano-) particulate carrier system by AM can be a desired effect, especially in the case of infectious diseases such as tuberculosis, where the alveolar macrophage is the affected, and therefore, target cell. In this scenario, selective and controlled internalization of carrier systems loaded with anti-infective drugs by alveolar macrophages is under investigation for targeted antimicrobial therapy.

1.2.2. The CF lung disease

CF is a complex multisystem disease caused by the defect in a single gene.[45] The faulty gene was identified in 1989, and encodes an epithelial ion channel known as the CFTR, which regulates chloride ion and water movements.[46] Since CFTR is expressed throughout the body, CF disease affects multiple organs (i.e., lung, pancreas, gastrointestinal systems). Nevertheless, pulmonary disease is still the most important cause of CF morbidity and mortality.

In the lung, CFTR is detectable on the apical membrane of ciliated cells within the gland ducts and in the superficial epithelium of healthy individuals. The most widely accepted explanation for the clinical effects of CFTR deficiency in the lung is known as “the low volume hypothesis” (Fig. 1.18).[45-47]

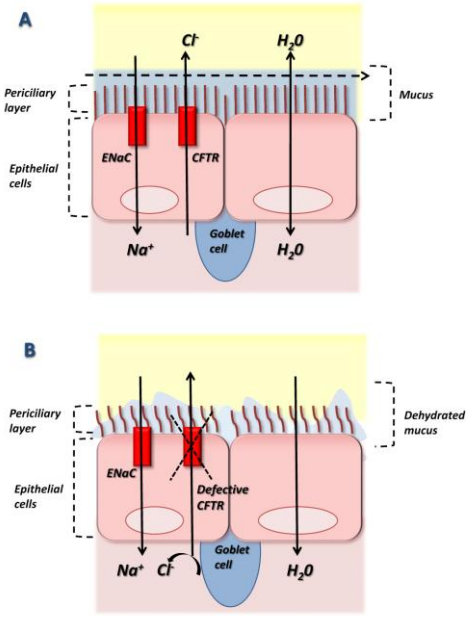

Figure 1.18 Proposed mechanism for the development of CF lung disease. In normal airways (A), hydration of lung lining fluids is controlled by Na+ absorption and Cl- secretion. In CF airways (B), the absence of CFTR leads to unregulated Na+ absorption and associated dehydration of the airway surface fluid layer with consequent poor mucociliary clearance.[20]

Since CFTR normally down-regulates ENaC in the lungs, the loss of CFTR function leads to ENaC over-activation. This results in depletion of airway surface liquid, which is essential to support ciliary stability and functioning, ciliary collapse and consequent decreased mucociliary transport. Retained secretions encourage bacterial adherence, chronic neutrophilic infection, and a vicious cycle of persistent/recurrent lung infection, chronic inflammation and tissue destruction. The hallmark of the condition is progressive and irreversible bronchiectasis and respiratory failure.

The dominant pathogen in CF airways is *Pseudomonas aeruginosa*, although other microrganisms (e.g., *Haemophilus influenza*, *Staphylococcus aureus*, *Burkholderia cepacia*) may play an important role in the pathogenesis of lung function decline[48]. While *H. influenza* and *S. aureus* colonize the lung early in life, sometimes causing recurrent infection, *P. aeruginosa* chronically infects 80% of CF patients by late adolescence.[45,49] *P. aeruginosa* possesses a large genetic diversity and a number of

features that contribute to its ability to persist in the environment, and to its pathogenicity. In the environment, it exists as a single motile bacteria, the so-called "non-mucoid form" of the organism. As colonization progresses, the cell density and the collective growth pattern of *P. aeruginosa* change, thus improving its capacity for survival.

In the "mucoid form", *P. aeruginosa* is able to form complex multicellular mucosa-attached aggregates (i.e., bacteria biofilm), which are more resistant than single bacteria to destruction by the innate immune system and become persistent.[50,51] Indeed, the production of an extracellular polysaccharide matrix has been shown to inhibit unopsonic phagocytosis of bacteria by resident monocytes and neutrophils both *in vitro* and *in vivo* and to increase bacterial adherence to the respiratory epithelia, thereby increasing *P. aeruginosa* rate of colonization within the respiratory tract.[50-52] In the aggregated biofilm mode, *P. aeruginosa* behaviour is regulated by the phenomenon of quorum sensing (QS), a cell-to-cell communication system involving small signaling molecules (N-acyl homoserine lactones, oligopeptides), which enables bacteria to express genes for different phenotypes, especially those responsible for their virulent behaviour.[53]

Lung infections become persistent in the first few years of life and contribute to the exaggerated, sustained, and prolonged inflammatory response responsible for much of the CF lung disease.[54] There is also evidence that inflammation is deregulated in CF airways, and may thus play a prominent role in early CF lung disease.[55] Although the direct relation of inflammation to the CFTR defect is still debated, intense neutrophil recruitment in the lung, activation of pro-inflammatory transcription factors and consequent production of inflammatory mediators by airway epithelial cells are critical determinants of chronic airway inflammation.[54]

Several transcription factors are activated in CF airway cells. Among them, numerous lines of evidence suggest that nuclear factor-κB (NF-κB) activation is a critical signal in evoking an inflammatory response in CF.[56] Whatever is the relation with NF-κB activation, elevated levels of pro-inflammatory cytokines (such as TNF-α, IL-6, IL-8, IL-1β) and reduced levels of anti-inflammatory cytokines (such as IL-10) have been typically found in the bronchoalveolar lavage and sputum of patients

with CF lung disease.[57] In addition, pro-inflammatory mediators contribute to the overproduction of mucus/mucins responsible for airway obstruction and mucociliary function failure.[58] These proteins are the main determinant of the rheological properties of mucus secretion, representing the major barrier to exogenous materials/drugs deposited in the lung[26]

1.2.3. Overbiobarriers in CF lung disease

Administration of drugs via the inhalation route is regarded with great interest in CF. As outlined in 2009 by the first European consensus on inhaled drugs for CF patients[59], the main advantages are generation of high drug levels in CF airways, limited systemic toxicity, fast onset of action, no drug inactivation before reaching the target organ, direct drug action on target site, and suitability for home therapy. Potential disadvantages include uncertainty about drug dose at the target site, local side effects (e.g., cough, hoarseness), variable systemic drug absorption and, last but not least, limited information on drug interactions in the lung. Indeed, the therapeutic effect of inhaled drugs in CF will dependent first upon the dose of deposited drug and, then, by its ability to overcome local non-cellular and cellular barriers, which can be completely altered in pathological conditions.

1.2.3.1. Airway narrowing and lung deposition

An exception to the general rules governing the deposition of any inhaled particle in the lungs may be caused by airway narrowing, change in lung function and mucus plugging typical of CF diseased lungs.[48,60] These factors can significantly influence the distribution of inhaled drugs and, as a consequence, their deposition pattern. In particular, pulmonary functional parameters indicating obstruction in CF patients were significantly correlated with aerosol bolus spreading and deposition.[61] Compared to healthy subjects, bronchial deposition is increased in CF at the expense of alveolar deposition most likely because of a decreased distance and increased turbulence at constricted sites caused by airway narrowing, which facilitate particle settlement or displacement on the airway wall.[60-62] Furthermore, also deposition patterns are more heterogeneous in the diseased lung than in the healthy lung. Thus, predicting the actual site of deposition in CF lung is difficult, since airway caliber

and anatomy as well as pharmacological treatments strongly differ among CF population as a function of disease stage and complications.

1.2.3.2. CF mucus

In case of severe lung diseases, such as CF, the overproduction of a viscous and highly complex mucus may further limit the amount of drug reaching the target.[34,63,64] CF sputum is characterized by a reduced amount of water (around 90% versus 95% typical of healthy individuals) and intact mucins (less than 20 g/L), with a contemporary increase of DNA and actin.[34,65] These high molecular weight biopolymers can cross-link, thereby forming DNA or actin gels, which drastically increase the viscoelasticity of CF mucus, creating a dense porous structure, likely acting as a sieve toward inhaled macromolecular drugs and colloidal drug carriers.[26] Additionally, mucus may establish adhesive interactions with drugs or particulate carriers hydrophobic, electrostatic, and hydrogen bonding interactions.[66] Since mucous plugs in CF patients are mainly composed of negatively charged mucins and DNA, positively charged aminoglycosides, such as tobramycin, may be bound to these compounds.[67,68] On the other hand, electrostatic repulsion can be envisaged in case of negatively-charged nucleic acid therapeutics.[34] Indeed, biopolymers in CF sputum form a network of bundled fibers with 100-1000 nm meshes, which can allow an easy diffusion of most nanosized gene carriers.[34,69]

In the light of these observations, to penetrate CF mucus, inhaled drug particles should be in theory small enough to avoid steric obstruction (i.e., “nano” is better than “micro”) and have a hydrophilic/neutral surface to avoid mucus interactions.[23,66]

1.2.3.3. Biofilm-forming bacteria

The main challenge of CF chronic infections remains the biofilm-like mode of growth adopted by *P. aeruginosa*, forming complex multicellular mucosa-attached aggregates (biofilm), characterized by massive production of alginates and other extracellular polysaccharides (EPS).[50,51] Bacteria growing in biofilm display high resistance levels to antimicrobials, due both to reduced penetration of the antibiotic molecules through the EPS layer and to modification in biofilm cell physiology.[52,70]

Indeed, the slow penetration and possible entrapment within the biofilm due to electrostatic interactions with the negatively-charged alginate matrix can strongly reduce drug availability in proximity of bacteria colonies (Fig. 1.19).

The efficacy of inhalable tobramycin is to date severely impaired by drug binding in CF airways, likely due to tobramycin/biofilm electrostatic interactions.[71,72] As a matter of fact, 300 mg of tobramycin inhalable solution (i.e., Tobi®, Bramitob®) or 112 mg of tobramycin DPI (i.e., Tobi® Podhaler™) twice a day are currently needed to achieve therapeutically active concentrations at the lung target. Particulate carriers with adequate size and surface properties may hide chemical properties of the free molecule (e.g., charge, degree of lipophilicity) and reduce its non-specific interactions with biofilm surrounding bacteria.[73-75] Furthermore, the increasing knowledge on a number of protein components/receptors which have been identified within biofilm[76] could be useful, at least in principle, to increase drug carrier selectivity through surface decoration.

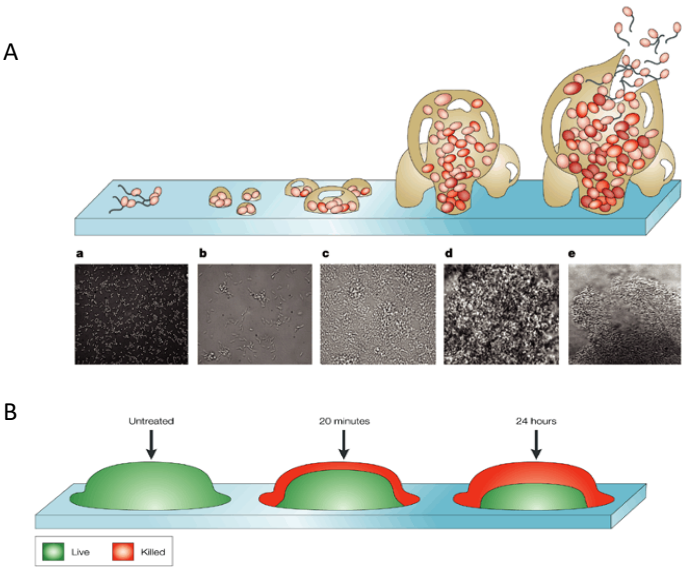

Figure 1.19. The five stages of P. aeruginosa biofilm development (A) and consequent resistance to antimicrobials (B). Treatment of biofilms with antibiotics often results in incomplete killing allowing unaffected bacteria to act as a nucleus for the spread of infection following the withdrawal of antibiotic therapy[77]

1.2.3.4. CF Airway epithelial cells

Although there is no literature evidence supporting their use in CF, surface exposure of a ligand (proteins, antibodies or immunoglobulin fragments) recognizing a receptor over-expressed in CF airway epithelial cells or in bacterial cells may further increase carrier selectivity by activating receptor-mediated transport mechanisms. For example, an increased expression of toll-like receptors 2 and 5 has been found at the apical surface of CF lung epithelium.[78] On the other hand, a potential target for inhalable gene carriers can be intercellular adhesion molecule-1 (ICAM-1, CD54), which is up-regulated in chronically inflamed airway epithelium[79], where CFTR is expressed predominantly. This hypothesis has been confirmed by very recent *in vivo* studies with receptor-targeted lipoplexes comprising a peptide motif (SERSMNF) displaying close similarity to the receptor binding proteins of two intracellular pathogens, rhinovirus and *Listeria monocytogenes*.[80]

1.2.3.5. Defective phagocytosis

Numerous evidences suggest a dysfunctional phagocytosis in CF patients, likely ascribed to an inherent defect in both airway neutrophils and macrophages.[81] Reduced expression of cell surface recognition receptors has been suggested as one mechanism for these observations. Recent studies have shown that macrophages from sputum of CF patients express reduced levels of the Macrophage Receptor with Collagenous structure (MARCO) and mannose receptors responsible of binding bacteria.[82] Efferocytosis -that is the "burying of dead cells" - by alveolar macrophages[83], seems also impaired in CF and is associated by the cleavage, mediated by neutrophil elastase, of the cell surface receptor for phosphatidylserine (one of the most important "eat me" signal of apoptotic cells).[84,85]

Whatever the mechanism is, new insights into the failure of phagocytes to clear pathogens, and likely inhaled materials, could provide a new tool for a proper design of the inhaled drug formulations, paving the way to more efficient therapeutic options for CF.

1.3. EMERGING PULMONARY DELIVERY STRATEGIES TO OVERCOME LUNG BARRIERS IN SEVERE LUNG DISEASES

As highlighted above, the number of excipients currently available (i.e., generally regarded as safe – GRAS – by FDA) for improving the technological properties of inhalable formulations is very limited.[86]

Although calling in question safety issues, which should be adequately addressed, the specific use of especially engineered lipid-based and polymer-based carriers may further help in reducing daily drug doses and number of administrations and overcoming extracellular and cellular barriers imposed by lung. Both micron-sized or nano-sized carriers can be selected on the basis of the specific goal. (Fig. 1.18).

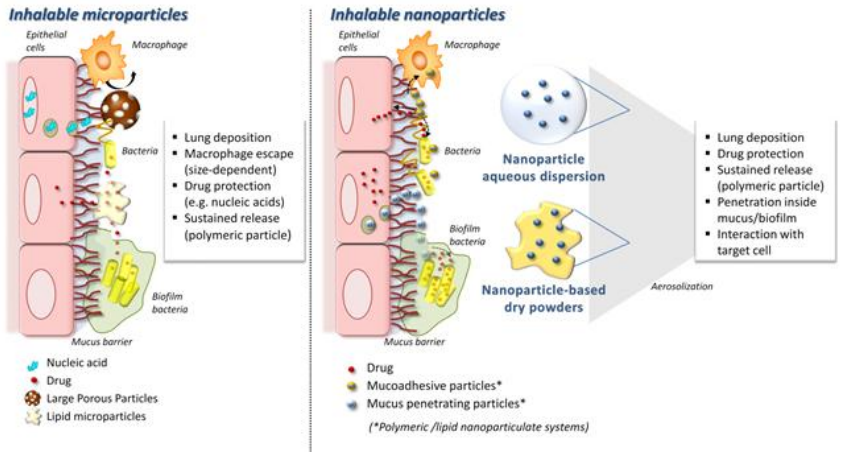

Figure 1.18. Inhalable engineered for overcoming anatomical and biological barriers imposed by diseased lung. The peculiar advantages of microparticulate and nanoparticulate systems are highlighted.[20]

1.3.1 Drug nanocrystals

Several new drug candidates emerging from drug discovery programmes are water insoluble and, therefore, poorly bioavailable. Estimates state that 40% of the drugs in the pipelines have solubility problems. There are many ways to solubilize poorly soluble drugs but often these methods are limited to drugs with certain properties in regard to their chemistry (e.g., solubility in certain organic media) or to their molecular size or conformation (e.g., molecules to be incorporated into the

cyclodextrin ring structure. Apart from that, the use of surfactants or co-solvents is also possible, but sometimes leads to increased side effects (eg, Cremophor EL (BASF, Ludwigshafen, Germany) and other disadvantages (eg, organic solvent residues). The micronization of drug powders to sizes between 1 and 10 μm has been also attempted to increase the surface area, and thus the dissolution velocity, but is not always sufficient to overcome drug bioavailability issues.

A consequent and recent step to improve the dissolution profile of poorly soluble drugs was to move from drug micronization to "nanonization", producing so-called drug nanocrystals.[21] Drug nanocrystals are particles made of 100% drug which can be used in form of colloidal dispersion, i.e. the nanocrystals are dispersed in a stabilizer-containing aqueous medium, producing a nanosuspension (NS). Although this approach has exploded recently, nanocrystals were invented in the 1990s when Elan Nanosystems (San Francisco, CA, USA) to enhance drug oral bioavailability. The first product came into the market in the 2000s (Emend®).[87]

The main advantages of drug nanocrystals are reported in figure 1.19. The smartness of nanocrystal technologies is that it can be universally applied to pratically any drug. The nanocrystal can be performed by two basic approaches: *Bottom-up technologies* building particles up from the molecular state (e.g. precipitation) or *top-down technologies* by breaking larger non micron-sized particles down (e.g. wet milling, high pressure homogenization). Top-down technologies are more widely used than bottom-up technologies because of the yield, good control over the processing parameters and avoidance of the organic solvent removal typical in precipitation processes.

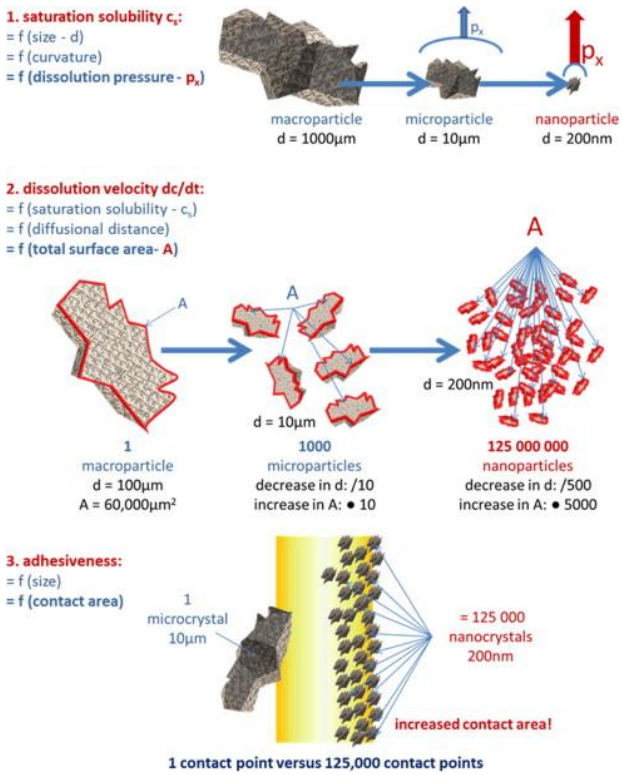

Figure 1.19 Main features of nanocrystals: increased saturation solubility due to increased dissolution pressure of strongly curved small nanocrystals (upper), increased dissolution velocity due to increased surface area (middle), and increased adhesiveness of nanomaterial due to increased contact area of small *versus* large particles (at identical total particle mass).[21]

NS are a valid alterative to dry powders to deliver poorly soluble drugs at lung level. Infact, their pulmonary administration can be simply performed by aerosolizing the aqueous NS by the most appropriate nebulizer.[88] When the aerosol droplets deposit in the lung, as fine particles, nanocrystals are expected to spread more evenly on the lung surface, especially when stabilized with appropriate surfactants.[89-91]

Despite their advantages, the stability of NSs is a critical aspect that defines the safety and efficacy of the drug product. Nanosizing results in the creation of additional surface area and/or interfaces that lead to a change in free energy and become thermodynamically unstable while tending to minimize the free energy.[92] In addition to physical stability, chemical stability of the active content in suspension is affected in some cases by hydrolysis of the compound. The last important concern is

the biological stability, especially in case of pulmonary delivery. Surfactants are commonly used to minimize the free energy, therefore selection of appropriate stabilizer for NS is a challenging task.[88] Nevertheless, the correct choice of surfactant does not completely solve the biological and chemical stability issues.

Conversion of the NS to a solid form becomes essential if stable NS is unatainable, solid dosage form are convinient also with renard to the market. Methods that are commonly used for conversion of NS include spray drying and freeze drying (lyophilization) pelletization and granulation. Spray drying and lyophilization are the most common processes and in particolar spray dryng is preferred by the pharmaceutical industry becouse it is faster and consumes less energy. In conclusion the method depends on the effectiveness in preserving particle size after processing.

1.3.2 Lipid-based carriers

The urgent need to increase concentration of the drug at the lung target in antimicrobial respiratory therapies and the promising results obtained by DSPC microparticles (i.e., PulmoSphere™) have prompted researchers and pharmaceutical industries to investigate the potential of lipid particles for the delivery of different antibiotic molecules. Indeed, the most commonly employed lipid materials in drug carriers development, such as phospholipids and cholesterol, are well tolerated since they constitute a significant portion of the naturally occurring pulmonary surfactant pool.[93,94] Furthermore, the hydrophobic nature of lipids, especially of neutral lipids, reduces the absorption of the ubiquitous vapour onto particles during inhalation, limiting aggregation and adhesion phenomena.[86]

Among lipid-based carriers of interest in inhalation therapy, both research and industry attention has been focused on novel liposome-based formulations for antibiotic and combined therapies and lipoplexes as non-viral vectors for gene therapy. More recent is the history of solid lipid particles both micro and nano particles, which are still in early development for pulmonary delivery (Fig. 1.20).

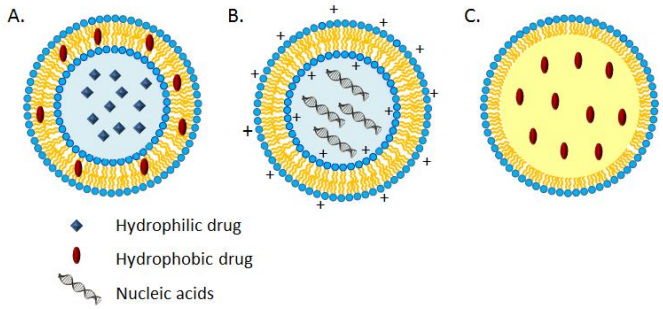

Figure 1.20. Schemmatic respresentation of some of the most investigated lipid carriers for pulmonary delivery: A) liposomes; B) cationic lipid-based carriers (lipoplexes); C) solid lipid particles (both microparticles and nanoparticles).

Liposome-encapsulated drugs represent very promising drug delivery systems for lung targeting.[93-95] In case of extracellular pathogens, such as *P. aeruginosa* in CF, the major advantages of liposomal antibiotics are: i) overcoming bacterial drug resistance ii) protection of the drug from antibiotic-inactivating enzymes (like β-lactamases) iii) tuning interactions between antibiotic and lung lining fluids (mucus and biofilm).[20,94]

From a technological standpoint, *liposomes* have a great design versatility since single lipid blocks can be assembled, resulting in tuned physicochemical properties and, consequently, adequate interactions with mucus, biofilm matrix and bacterial cell surface.[95,96] Of course, attention should be paid to the effect of liposome composition on carrier stability, drug entrapment efficiency and release. Indeed, the use of inhaled liposomal antibiotics as therapeutic agents is still challenged by their well-established physical and chemical instability in aqueous dispersions for long-term storage, often causing vesicle aggregation, drug leakage, phospholipid hydrolysis and/or oxidation.[95-97] Nevertheless, advanced clinical studies are ongoing on two neutral liposomal formulations for antibiotic inhalation, that are Arikace™ and Lipoquin™ (ARD-3100). Furthermore, many methods available for stabilization of liposomes and, possibly, achievement of DPI liposomal formulations (e.g., lyophilization, spray-drying and supercritical fluid technology) are currently being investigated.[97-99]

As compared to bare liposomes, lipid cationic nanocarriers (or *lipoplexes*) are mostly investigated to condense and deliver intracellularly negatively charged DNA and short nucleic acid derivatives.[100,101] They are commonly composed of cationic lipids, such as 1,2-Dioleoyl-3-trimethylammoniumpropane (DOTAP). Although direct delivery at lung should limit systemic side effects of lipoplexes, the toxicity of the carrier, usually dose-related, appears still critical for *in vivo* translation of cationic lipid-based particles.[101,102] Indeed, the major issue related to their use is the potential for inducing dose-dependent cellular toxicity and, when complexed with DNA, triggering undesired macrophage-mediated pro-inflammatory cytokine production.

Solid lipid nanoparticles (SLNs) are also being explored as a viable alternative to liposomes for drug and gene delivery to the lung SLNs have evolved in solid lipid particles, known as Nanostructured Lipid Carriers (NLCs), made of a blend of a solid lipid and an oil consisting in a semi-crystal structure with more flexibility and able to better accommodate drugs.[103] NLCs have the same advantages of SLNs, that is controlled drug release, improved chemical stability of encapsulated drug molecules and simple and non-expensive production, also on a large scale, as compared to liposomes.

1.3.3 Polymer-based carriers

Although it can be dated back to 90's[42], the concept of using polymer particles for pulmonary delivery has evolved during time and is experiencing growing research interest in recent years, also for CF.[20,104,105] A fundamental feature of polymer systems, which is only partly shared by liposomal carriers, relies on their ability to exert a prolonged drug release. This is crucial to reduce the number of administrations and increase patient adherence to complex therapeutic regimens required by chronic lung diseases, such as CF[106]. Polymer particles have also the potential: i) to increase drug stability in the bottle and *in vivo*; ii) to co-deliver different molecules with complementary functionalities; iii) to promote cell uptake of delivered drug cargo. Indeed, various systemic and cellular barriers imposed to nucleic acid therapeutics, including nucleases, cell membrane, endosomal

compartment and nuclear membrane, maybe successfully circumvented by adequately designed polymer carriers. Nevertheless, to be successful, design of inhalable NPs should take into account well-defined rules to overcome limitations associated to pulmonary route of administration, providing adequate composition, size, and surface modification along with respirability (Fig. 1.21).

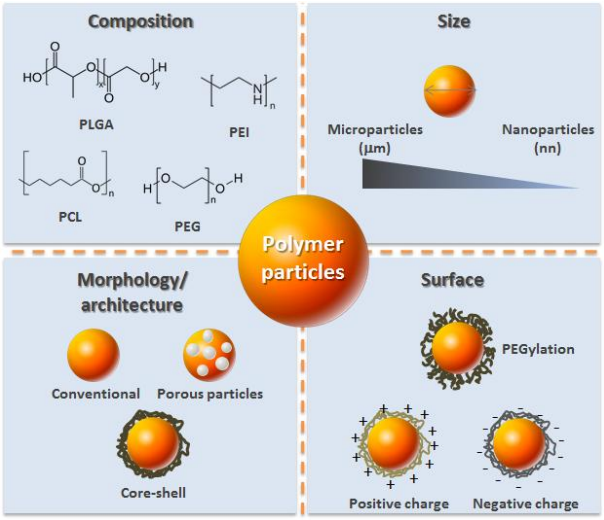

Figure 1.21 Overview of the main design rules dictating the development of efficient polymeric particles for inhalation.

Among polymers currently under investigation, synthetic biodegradable polymers represent the most promising class of materials for pulmonary delivery, as evidenced by increasing literature data, fulfilling also important safety concerns. Amid them, poly(lactic-co-glycolic acid) copolymers (PLGA) have generated tremendous research interest due to their excellent biocompatibility as well as the possibility to tailor their biodegradability by varying monomer composition (lactide/glycolide ratio), molecular weight and chemical structure (i.e. capped and uncapped end-groups).[104] PLGAs characterized by very different *in vivo* life-times, ranging from 3 weeks to over a year, are available and approved for human use. Among all commercially available PLGA types, those characterized by a rapid *in vitro* degradation are undoubtedly preferred for inhalation and have shown no toxicity on

both healthy[107-109] and CF human airway epithelial cells.[110,111] Drug encapsulation within PLGA copolymers is regarded also as a powerful mean to achieve its sustained release for long time-frames and, in the case of labile drugs, effectively protect the molecule from *in vivo* degradation occurring at the administration site.[112]
To increase the availability of the delivered drug at the lung target, engineered inhalable PLGA particles have been developed through the addition of specific.[104]At nanosize level, particle surface modification with helper hydrophilic polymers (e.g., PEG, poloxamer, chitosan, polyvinyl alcohol) has been found useful to modulate carrier interactions with lung cellular and extracellular barriers.[66,109,113]
Excipients playing a dual role in the formulation can be preferred in the production of PLGA microparticles, especially if one of their effects is to widen and/or enhance the biological activity of the inhaled drug. Poly(ethylenimine) (PEI), used as non-viral gene transfer agent since 90's, could represent an interesting polymer candidate for inhaled drugs in CF due to its proved synergic antimicrobial properties with several antibiotics directed against *P. Aeruginosa.*[114]
Amongst the parameters that can be adjusted to achieve inhalable microparticles, mass density and size have drawn researchers' attention to limit loss of drug due to particle aggregation in the inhaler and macrophage-mediated clearance of the particles from the lungs.[8] The idea is that conventional polymer particles achieved by micronization (i.e., 1–3 μm) are poorly flowable, prone to aggregation and can be rapidly phagocytosed in the deep lung by alveolar macrophages. On the contrary, large porous particles (LPP) with low mass density (<0.4 g/cm^3) and high geometric diameter (>5 μm) can be used to enhance both particle aerosolization behaviour and residence time in the lung.[42]
In the attempt to find out novel anti-inflammatory therapies for CF, the first example of dry powders for oligonucleotide inhalation, consisting in biodegradable LPP based on PLGA for prolonged delivery of a decoy oligonucleotide to nuclear factor-κB (dec-ODN), have been recently developed (Fig. 1.22).[110,111,115] Of note, intratracheal insufflation of dec-ODN LPP by means of a low-scale DPI in rats challenged with LPS from *P. Aeruginosa* resulted in the inhibition of

bronchoalveolar neutrophil infiltration as well as the reduction of IL-8 and MUC2 mRNA levels induced by LPS as compared to naked dec-ODN.[115]

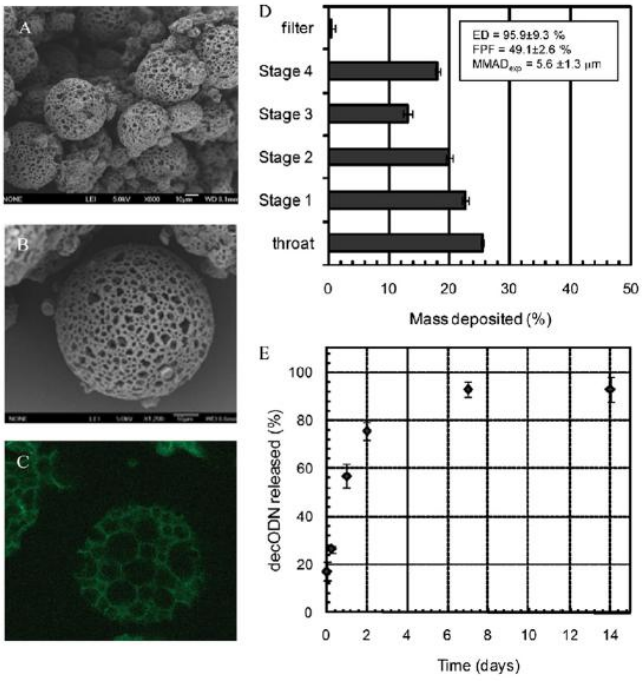

Figure 1.22. Bulk, aerodynamic and release properties of PLGA LPP for prolonged delivery of a decoy oligonucleotide to nuclear factor-κB in the lung.[115]

In the current era of nanotechnology, increasing research efforts have been devoted also to engineer PLGA nanoparticles (NPs) for pulmonary drug delivery.[105] Actually, nanoparticulate systems can be considered of choice for drug targeting to specific airway tissues/cells as well as to overcome lung extracellular barriers. While polymer particles with a mean size around 500 nm may be blocked by the mucus layer, NPs smaller than 200 nm are expected to diffuse more easily through mucus.

To tune NP interaction with the lung microenvironment, hydrophilic polymers, both mucoadhesive (e.g., chitosan, hyaluronic acid) and mucoinert (PEG) have been employed to impart the desired surface properties.[109,116] Despite promising, the effect of hydrophilic polymers in modulating PLGA NP/mucus interactions is still

unclear and debated. It has been recently observed that PLGA NPs of 200–500 nm modified at surface with non-adhesive PEG, the so-called MPP, may deeply penetrate human mucus secretions.[116] In case of CF lung disease, the use of non-adhesive PEGylated PLGA NPs could represent also a promising approach to avoid interactions, responsible of the loss in activity, between the drug and the biofilm produced by bacteria, such as *P. Aeruginosa*, in chronic lung infections.[74] Nevertheless, surface modifications of PLGA NPs may have also a significant impact on their interaction with the target cell. For example, the uptake of PLGA NPs into macrophages may be significantly reduced upon PEGylation.[40] Overcoming cell membrane to reach intracellular targets is also mandatory, in case of emerging nucleic-acid therapeutics (i.e., oligonucleotides, siRNA, DNA).[32]

One particular strategy to modulate the surface of PLGA NPs, and hence also influence their behavior at the nano–bio interface, is by depositing a stabilized phospholipid layer onto the hydrophobic NP core. As for liposomes, this lipid layer can be also employed to anchor amphiphilic PEGylated lipids to the surface of the particles and/or conjugate targeting moieties[117] (Fig. 1.23).

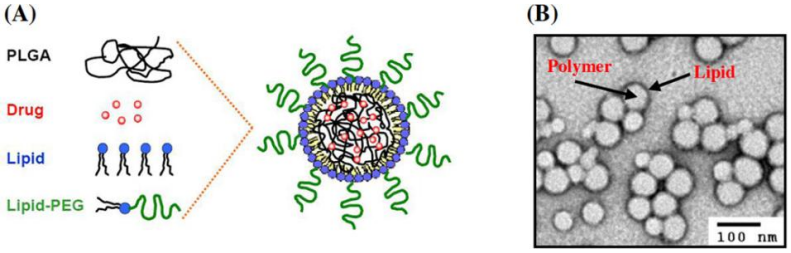

Figure 1.23. Schematic illustration of a ipid-polymer hybrid NP comprising bare and PEGylated phospholipids (A) and corresponding morphology observed by transmission electron microscopy (TEM).[118]

Lipid–PLGA hybrid nanoparticles with core–shell morphology have been especially designed for siRNA delivery.[117] In particular, siRNA was efficiently entrapped in PLGA NPs with the aid of a positively charged lipid, that is DOTAP. The gene knock-down level *in vitro* was positively correlated to the weight ratio of DOTAP in the NPs, which were successfully transformed in dry powders for inhalation by spray-drying in mannitol.[108,119] Nevertheless, toxicity may be an issue when using non-natural lipids. Fostered by these limitations, a growing interest exists in the

implementation of bio-inspired and bio-mimetic materials. In particular, recent progresses in nanotechnologies and emerging knowledge on the properties of the nano-bio interface have paved the way toward core–shell lipid–polymer hybrid NPs, where the synthetic polymeric core is surrounded with a phospholipid bilayer of natural origin.[120]

References

1. Labiris, N. R.; Dolovich, M. B. Pulmonary drug delivery. Part I: physiological factors affecting therapeutic effectiveness of aerosolized medications. *Br. J. Clin. Pharmacol.* **2003,** *56* (6), 588-599.
2. Patton, J. S.; Fishburn, C. S.; Weers, J. G. The lungs as a portal of entry for systemic drug delivery. *Proc. Am. Thorac. Soc.* **2004,** *1* (4), 338-344.
3. Weers, J. Inhaled antimicrobial therapy - barriers to effective treatment. *Adv. Drug Deliv. Rev.* **2015,** *85*, 24-43.
4. Brand, P.; Schulte, M.; Wencker, M.; Herpich, C. H.; Klein, G.; Hanna, K.; Meyer, T. Lung deposition of inhaled alpha1-proteinase inhibitor in cystic fibrosis and alpha1-antitrypsin deficiency. *Eur. Respir. J.* **2009,** *34* (2), 354-360.
5. Dolovich, M. B.; Dhand, R. Aerosol drug delivery: developments in device design and clinical use. *Lancet* **2011,** *377* (9770), 1032-1045.
6. Weibel, E. R. A retrospective of lung morphometry: from 1963 to present. *Am. J. Physiol Lung Cell Mol. Physiol* **2013,** *305* (6), L405-L408.
7. Hussain, M.; Madl, P.; Khan, A. Lung deposition predictions of airborne particles and the emergence of contemporary diseases Part-I. *theHealth* **2011,** *2* (2), 51-59.
8. Patton, J. S.; Byron, P. R. Inhaling medicines: delivering drugs to the body through the lungs. *Nat. Rev. Drug Discov.* **2007,** *6* (1), 67-74.
9. Ruge, C. A.; Kirch, J.; Lehr, C. M. Pulmonary drug delivery: from generating aerosols to overcoming biological barriers-therapeutic possibilities and technological challenges. *Lancet Respir. Med.* **2013,** *1* (5), 402-413.
10. Newman, S.; Anderson, P.; Byron, P.; Dalby, R.; Peart, J. *Respiratory Drug Delivery: Essential Theory & Practice;* RDD Online: Richmond (VA), 2009.
11. Carvalho, T. C.; Peters, J. I.; Williams, R. O., III Influence of particle size on regional lung deposition--what evidence is there? *Int. J. Pharm.* **2011,** *406* (1-2), 1-10.
12. Patton, J. S.; Byron, P. R. Inhaling medicines: delivering drugs to the body through the lungs. *Nat. Rev. Drug Discov.* **2007,** *6* (1), 67-74.
13. Heyder, J. Deposition of inhaled particles in the human respiratory tract and consequences for regional targeting in respiratory drug delivery. *Proc. Am. Thorac. Soc.* **2004,** *1* (4), 315-320.
14. Hoppentocht, M.; Hagedoorn, P.; Frijlink, H. W.; de Boer, A. H. Technological and practical challenges of dry powder inhalers and formulations. *Adv. Drug Deliv. Rev.* **2014,** *75*, 18-31.
15. Fernandez, T. A.; Casan, C. P. Deposition of inhaled particles in the lungs. *Arch. Bronconeumol.* **2012,** *48* (7), 240-246.
16. Zhou, Q. T.; Tang, P.; Leung, S. S.; Chan, J. G.; Chan, H. K. Emerging inhalation aerosol devices and strategies: Where are we headed? *Adv. Drug Deliv. Rev.* **2014,** (14), 10.

17. Daniels, T.; Mills, N.; Whitaker, P. Nebuliser systems for drug delivery in cystic fibrosis. *Cochrane. Database. Syst. Rev.* **2013,** *4:CD007639. doi: 10.1002/14651858.CD007639.pub2.*, CD007639.

18. Kesser, K. C.; Geller, D. E. New aerosol delivery devices for cystic fibrosis. *Respir. Care.* **2009,** *54* (6), 754-767.

19. Healy, A. M.; Amaro, M. I.; Paluch, K. J.; Tajber, L. Dry powders for oral inhalation free of lactose carrier particles. *Adv. Drug Deliv. Rev.* **2014,** *75*, 32-52.

20. d'Angelo, I.; Conte, C.; La Rotonda, M. I.; Miro, A.; Quaglia, F.; Ungaro, F. Improving the efficacy of inhaled drugs in cystic fibrosis: challenges and emerging drug delivery strategies. *Adv. Drug Deliv. Rev.* **2014,** *75*, 92-111.

21. Muller, R. H.; Gohla, S.; Keck, C. M. State of the art of nanocrystals--special features, production, nanotoxicology aspects and intracellular delivery. *Eur. J. Pharm. Biopharm.* **2011,** *78* (1), 1-9.

22. Cone, R. A. Barrier properties of mucus. *Adv. Drug Deliv. Rev.* **2009,** *61* (2), 75-85.

23. Sigurdsson, H. H.; Kirch, J.; Lehr, C. M. Mucus as a barrier to lipophilic drugs. *Int. J. Pharm.* **2013,** *453* (1), 56-64.

24. Sanders, N.; Rudolph, C.; Braeckmans, K.; De Smedt, S. C.; Demeester, J. Extracellular barriers in respiratory gene therapy. *Adv. Drug Deliv. Rev.* **2009,** *61* (2), 115-127.

25. Widdicombe, J. G. Airway liquid: a barrier to drug diffusion? *European Respiratory Journal* **1997,** *10* (10), 2194-2197.

26. Lai, S. K.; Wang, Y. Y.; Wirtz, D.; Hanes, J. Micro- and macrorheology of mucus. *Adv. Drug Deliv. Rev.* **2009,** *61* (2), 86-100.

27. King, M. Effect of particle on mucus and mucociliary clearance. In *Particle-Lung Interactions, Second Edition*, Gehr, P., Muhlfeld, C., Rothen-Rutishauser, B., Blank, F., Eds.; CRC Press: 2010; pp 521-531.

28. Muhlfeld, C.; Rothen-Rutishauser, B.; Blank, F.; Vanhecke, D.; Ochs, M.; Gehr, P. Interactions of nanoparticles with pulmonary structures and cellular responses. *Am. J. Physiol Lung Cell Mol. Physiol* **2008,** *294* (5), L817-L829.

29. Gehr, P.; Tsuda, A. Interaction with lung surface. In *Nanoparticles in the Lung: Environmental Exposure and Drug Delivery*, Tsuda, A., Gehr, P., Eds.; CRC Press: 2014; pp 21-46.

30. Hillaireau, H.; Couvreur, P. Nanocarriers' entry into the cell: relevance to drug delivery. *Cell Mol. Life Sci.* **2009,** *66* (17), 2873-2896.

31. Merkel, O. M.; Kissel, T. Nonviral Pulmonary Delivery of siRNA. *Acc. Chem. Res.* **2011**.

32. Lam, J. K.; Liang, W.; Chan, H. K. Pulmonary delivery of therapeutic siRNA. *Adv. Drug Deliv. Rev.* **2011**.

33. Elsabahy, M.; Nazarali, A.; Foldvari, M. Non-viral nucleic acid delivery: key challenges and future directions. *Curr. Drug Deliv.* **2011,** *8* (3), 235-244.

34. Sanders, N.; Rudolph, C.; Braeckmans, K.; De Smedt, S. C.; Demeester, J. Extracellular barriers in respiratory gene therapy. *Adv. Drug Deliv. Rev.* **2009,** *61* (2), 115-127.

35. Ma, N.; Ma, C.; Li, C.; Wang, T.; Tang, Y.; Wang, H.; Moul, X.; Chen, Z.; Hel, N. Influence of nanoparticle shape, size, and surface functionalization on cellular uptake. *J. Nanosci. Nanotechnol.* **2013,** *13* (10), 6485-6498.

36. de Souza, C. C.; Daum, N.; Lehr, C. M. Carrier interactions with the biological barriers of the lung: advanced in vitro models and challenges for pulmonary drug delivery. *Adv. Drug Deliv. Rev.* **2014,** *75*, 129-140.

37. Schneider, M.; Loretz, B.; Windbergs, M.; Schneider-Daum, N.; Schaefer, U. F.; Lehr, C. M. Biological barriers--Advanced drug delivery, in vitro modelling, and their implications for infection research. *Eur. J. Pharm. Biopharm.* **2015,** *95* (Pt A), 1-2.

38. Rothen-Rutishauser, B.; Blank, F.; Muhlfeld, C.; Gehr, P. In vitro models of the human epithelial airway barrier to study the toxic potential of particulate matter. *Expert. Opin. Drug Metab Toxicol.* **2008,** *4* (8), 1075-1089.

39. Hussell, T.; Bell, T. J. Alveolar macrophages: plasticity in a tissue-specific context. *Nat. Rev. Immunol.* **2014,** *14* (2), 81-93.

40. Patel, B.; Gupta, N.; Ahsan, F. Particle engineering to enhance or lessen particle uptake by alveolar macrophages and to influence the therapeutic outcome. *European Journal of Pharmaceutics and Biopharmaceutics* **2015,** *89*, 163-174.

41. Hirota, K.; Hasegawa, T.; Hinata, H.; Ito, F.; Inagawa, H.; Kochi, C.; Soma, G.; Makino, K.; Terada, H. Optimum conditions for efficient phagocytosis of rifampicin-loaded PLGA microspheres by alveolar macrophages. *J. Control Release.* **2007,** *119* (1), 69-76.

42. Edwards, D. A.; Hanes, J.; Caponetti, G.; Hrkach, J.; Ben-Jebria, A.; Eskew, M. L.; Mintzes, J.; Deaver, D.; Lotan, N.; Langer, R. Large porous particles for pulmonary drug delivery. *Science.* **1997,** *%20;276* (5320), 1868-1871.

43. Yoo, J. W.; Mitragotri, S. Polymer particles that switch shape in response to a stimulus. *Proc. Natl. Acad. Sci. U. S. A* **2010,** *107* (25), 11205-11210.

44. Evora, C.; Soriano, I.; Rogers, R. A.; Shakesheff, K. N.; Hanes, J.; Langer, R. Relating the phagocytosis of microparticles by alveolar macrophages to surface chemistry: the effect of 1,2-dipalmitoylphosphatidylcholine. *J. Control Release.* **1998,** *51* (2-3), 143-152.

45. O'Sullivan, B. P.; Freedman, S. D. Cystic fibrosis. *Lancet.* **2009,** *373* (9678), 1891-1904.

46. Horsley, A. Genetics and Pathophysiology. In *Cystic Fibrosis*, Horsley, A., Cunningham, S., Innes, J. A., Eds.; Oxford University Press: New York (USA), 2010; pp 1-16.

47. Ratjen, F. A. Cystic fibrosis: pathogenesis and future treatment strategies. *Respir. Care.* **2009,** *54* (5), 595-605.

48. Gaspar, M. C.; Couet, W.; Olivier, J. C.; Pais, A. A.; Sousa, J. J. Pseudomonas aeruginosa infection in cystic fibrosis lung disease and new perspectives of treatment: a review. *Eur. J. Clin. Microbiol. Infect. Dis.* **2013,** *32* (10), 1231-1252.

49. Doring, G.; Worlitzsch, D. Microbiology of CF lung disease. In *Cystic Fibrosis*, Horsley, A., Cunningham, S., Innes, J. A., Eds.; Oxford University Press: New York, USA, 2010; pp 31-44.

50. Moreau-Marquis, S.; Stanton, B. A.; O'Toole, G. A. Pseudomonas aeruginosa biofilm formation in the cystic fibrosis airway. *Pulm. Pharmacol. Ther.* **2008,** *21* (4), 595-599.

51. Hoiby, N.; Ciofu, O.; Bjarnsholt, T. Pseudomonas aeruginosa biofilms in cystic fibrosis. *Future. Microbiol.* **2010,** *5* (11), 1663-1674.

52. Oglesby-Sherrouse, A. G.; Djapgne, L.; Nguyen, A. T.; Vasil, A. I.; Vasil, M. L. The complex interplay of iron, biofilm formation, and mucoidy affecting antimicrobial resistance of Pseudomonas aeruginosa. *Pathog. Dis.* **2014,** 10-632X.

53. Jakobsen, T. H.; Bjarnsholt, T.; Jensen, P. O.; Givskov, M.; Hoiby, N. Targeting quorum sensing in Pseudomonas aeruginosa biofilms: current and emerging inhibitors. *Future. Microbiol.* **2013,** *8* (7), 901-921.

54. Cohen-Cymberknoh, M.; Kerem, E.; Ferkol, T.; Elizur, A. Airway inflammation in cystic fibrosis: molecular mechanisms and clinical implications. *Thorax.* **2013,** *68* (12), 1157-1162.

55. Khan, T. Z.; Wagener, J. S.; Bost, T.; Martinez, J.; Accurso, F. J.; Riches, D. W. Early pulmonary inflammation in infants with cystic fibrosis. *Am. J. Respir. Crit Care Med.* **1995,** *151* (4), 1075-1082.

56. Cabrini, G.; Bezzerri, V.; Mancini, I.; Nicolis, E.; Dechecchi, M. C.; Tamanini, A.; Lampronti, I.; Piccagli, L.; Bianchi, N.; Borgatti, M.; Gambari, R. Targeting transcription factor activity as a strategy to inhibit pro-inflammatory genes involved in cystic fibrosis: decoy oligonucleotides and low-molecular weight compounds. *Curr. Med. Chem.* **2010,** *17* (35), 4392-4404.

57. Hartl, D.; Gaggar, A.; Bruscia, E.; Hector, A.; Marcos, V.; Jung, A.; Greene, C.; McElvaney, G.; Mall, M.; Doring, G. Innate immunity in cystic fibrosis lung disease. *J. Cyst. Fibros.* **2012,** *11* (5), 363-382.

58. Rose, M. C.; Voynow, J. A. Respiratory tract mucin genes and mucin glycoproteins in health and disease. *Physiol Rev.* **2006,** *86* (1), 245-278.

59. Heijerman, H.; Westerman, E.; Conway, S.; Touw, D.; Doring, G. Inhaled medication and inhalation devices for lung disease in patients with cystic fibrosis: A European consensus. *J. Cyst. Fibros.* **2009,** *8* (5), 295-315.

60. Darquenne, C. Aerosol deposition in health and disease. *J. Aerosol Med. Pulm. Drug Deliv.* **2012,** *25* (3), 140-147.

61. Anderson, P. J.; Blanchard, J. D.; Brain, J. D.; Feldman, H. A.; McNamara, J. J.; Heyder, J. Effect of cystic fibrosis on inhaled aerosol boluses. *Am. Rev. Respir. Dis.* **1989,** *140* (5), 1317-1324.

62. Labiris, N. R.; Dolovich, M. B. Pulmonary drug delivery. Part I: physiological factors affecting therapeutic effectiveness of aerosolized medications. *Br. J. Clin. Pharmacol.* **2003,** *56* (6), 588-599.

63. Lai, S. K.; Wang, Y. Y.; Hanes, J. Mucus-penetrating nanoparticles for drug and gene delivery to mucosal tissues. *Adv. Drug Deliv. Rev.* **2009,** *61* (2), 158-171.

64. Ibrahim, B. M.; Tsifansky, M. D.; Yang, Y.; Yeo, Y. Challenges and advances in the development of inhalable drug formulations for cystic fibrosis lung disease. *Expert Opin. Drug Deliv.* **2011,** *8* (4), 451-466.

65. Rubin, B. K. Mucus, phlegm, and sputum in cystic fibrosis. *Respir. Care.* **2009,** *54* (6), 726-732.

66. Ensign, L. M.; Schneider, C.; Suk, J. S.; Cone, R.; Hanes, J. Mucus penetrating nanoparticles: biophysical tool and method of drug and gene delivery. *Adv. Mater.* **2012,** *24* (28), 3887-3894.

67. Ramphal, R.; Lhermitte, M.; Filliat, M.; Roussel, P. The binding of anti-pseudomonal antibiotics to macromolecules from cystic fibrosis sputum. *J. Antimicrob. Chemother.* **1988,** *22* (4), 483-490.

68. Hunt, B. E.; Weber, A.; Berger, A.; Ramsey, B.; Smith, A. L. Macromolecular mechanisms of sputum inhibition of tobramycin activity. *Antimicrob. Agents Chemother.* **1995,** *39* (1), 34-39.

69. Ibrahim, B. M.; Park, S.; Han, B.; Yeo, Y. A strategy to deliver genes to cystic fibrosis lungs: a battle with environment. *J. Control Release.* **2011,** *155* (2), 289-295.

70. Rybtke, M. T.; Jensen, P. O.; Hoiby, N.; Givskov, M.; Tolker-Nielsen, T.; Bjarnsholt, T. The implication of Pseudomonas aeruginosa biofilms in infections. *Inflamm. Allergy Drug Targets.* **2011,** *10* (2), 141-157.

71. Tseng, B. S.; Zhang, W.; Harrison, J. J.; Quach, T. P.; Song, J. L.; Penterman, J.; Singh, P. K.; Chopp, D. L.; Packman, A. I.; Parsek, M. R. The extracellular matrix protects Pseudomonas aeruginosa biofilms by limiting the penetration of tobramycin. *Environ. Microbiol.* **2013,** *15* (10), 2865-2878.

72. Messiaen, A. S.; Nelis, H.; Coenye, T. Investigating the role of matrix components in protection of Burkholderia cepacia complex biofilms against tobramycin. *J. Cyst. Fibros.* **2014,** *13* (1), 56-62.

73. Meers, P.; Neville, M.; Malinin, V.; Scotto, A. W.; Sardaryan, G.; Kurumunda, R.; Mackinson, C.; James, G.; Fisher, S.; Perkins, W. R. Biofilm penetration, triggered release and in vivo activity of inhaled liposomal amikacin in chronic Pseudomonas aeruginosa lung infections. *J. Antimicrob. Chemother.* **2008,** *61* (4), 859-868.

74. Forier, K.; Messiaen, A. S.; Raemdonck, K.; Deschout, H.; Rejman, J.; De, B. F.; Nelis, H.; De Smedt, S. C.; Demeester, J.; Coenye, T.; Braeckmans, K. Transport of nanoparticles in cystic fibrosis sputum and bacterial biofilms by single-particle tracking microscopy. *Nanomedicine. (Lond).* **2013,** *8* (6), 935-949.

75. Messiaen, A. S.; Forier, K.; Nelis, H.; Braeckmans, K.; Coenye, T. Transport of Nanoparticles and Tobramycin-loaded Liposomes in Burkholderia cepacia Complex Biofilms. *PLoS. One.* **2013,** *8* (11), e79220.

76. Sharma, G.; Rao, S.; Bansal, A.; Dang, S.; Gupta, S.; Gabrani, R. Pseudomonas aeruginosa biofilm: Potential therapeutic targets. *Biologicals.* **2014,** *42* (1), 1-7.

77. Davies, D. Understanding biofilm resistance to antibacterial agents. *Nat. Rev. Drug Discov.* **2003,** *2* (2), 114-122.

78. Cohen, T. S.; Prince, A. Cystic fibrosis: a mucosal immunodeficiency syndrome. *Nat. Med.* **2012,** *18* (4), 509-519.

79. Chan, S. C.; Shum, D. K.; Tipoe, G. L.; Mak, J. C.; Leung, E. T.; Ip, M. S. Upregulation of ICAM-1 expression in bronchial epithelial cells by airway secretions in bronchiectasis. *Respir. Med.* **2008,** *102* (2), 287-298.

80. Manunta, M. D.; McAnulty, R. J.; Tagalakis, A. D.; Bottoms, S. E.; Campbell, F.; Hailes, H. C.; Tabor, A. B.; Laurent, G. J.; O'Callaghan, C.; Hart, S. L. Nebulisation of receptor-targeted nanocomplexes for gene delivery to the airway epithelium. *PLoS. One.* **2011,** *6* (10), e26768.

81. Donnelly, L. E.; Barnes, P. J. Defective phagocytosis in airways disease. *Chest.* **2012,** *141* (4), 1055-1062.

82. Wright, A. K.; Rao, S.; Range, S.; Eder, C.; Hofer, T. P.; Frankenberger, M.; Kobzik, L.; Brightling, C.; Grigg, J.; Ziegler-Heitbrock, L. Pivotal Advance: Expansion of small sputum macrophages in CF: failure to express MARCO and mannose receptors. *J. Leukoc. Biol.* **2009,** *86* (3), 479-489.

83. McCubbrey, A. L.; Curtis, J. L. Efferocytosis and lung disease. *Chest.* **2013,** *143* (6), 1750-1757.

84. Vandivier, R. W.; Fadok, V. A.; Ogden, C. A.; Hoffmann, P. R.; Brain, J. D.; Accurso, F. J.; Fisher, J. H.; Greene, K. E.; Henson, P. M. Impaired clearance of apoptotic cells from cystic fibrosis airways. *Chest.* **2002,** *121* (3 Suppl), 89S.

85. Vandivier, R. W.; Fadok, V. A.; Hoffmann, P. R.; Bratton, D. L.; Penvari, C.; Brown, K. K.; Brain, J. D.; Accurso, F. J.; Henson, P. M. Elastase-mediated phosphatidylserine receptor cleavage impairs apoptotic cell clearance in cystic fibrosis and bronchiectasis. *J. Clin. Invest.* **2002,** *109* (5), 661-670.

86. Pilcer, G.; Amighi, K. Formulation strategy and use of excipients in pulmonary drug delivery. *Int. J. Pharm.* **2010,** *392* (1-2), 1-19.

87. Muller, R. H.; Keck, C. M. Twenty years of drug nanocrystals: where are we, and where do we go? *Eur. J. Pharm. Biopharm.* **2012,** *80* (1), 1-3.

88. Shegokar, R.; Muller, R. H. Nanocrystals: industrially feasible multifunctional formulation technology for poorly soluble actives. *Int. J. Pharm.* **2010,** *399* (1-2), 129-139.

89. Jacobs, C.; Muller, R. H. Production and characterization of a budesonide nanosuspension for pulmonary administration. *Pharm. Res.* **2002,** *19* (2), 189-194.

90. Chiang, P. C.; Hu, Y.; Blom, J. D.; Thompson, D. C. Evaluating the suitability of using rat models for preclinical efficacy and side effects with inhaled corticosteroids nanosuspension formulations. *Nanoscale. Res. Lett.* **2010,** *5* (6), 1010-1019.

91. Rundfeldt, C.; Steckel, H.; Scherliess, H.; Wyska, E.; Wlaz, P. Inhalable highly concentrated itraconazole nanosuspension for the treatment of bronchopulmonary aspergillosis. *Eur. J. Pharm. Biopharm.* **2013,** *83* (1), 44-53.

92. Rabinow, B. E. Nanosuspensions in drug delivery. *Nat. Rev. Drug Discov.* **2004,** *3* (9), 785-796.

93. Jaafar-Maalej, C.; Elaissari, A.; Fessi, H. Lipid-based carriers: manufacturing and applications for pulmonary route. *Expert Opin. Drug Deliv.* **2012,** *9* (9), 1111-1127.

94. Cipolla, D.; Gonda, I.; Chan, H. K. Liposomal formulations for inhalation. *Ther. Deliv.* **2013,** *4* (8), 1047-1072.

95. Allen, T. M.; Cullis, P. R. Liposomal drug delivery systems: from concept to clinical applications. *Adv. Drug Deliv. Rev.* **2013,** *65* (1), 36-48.

96. Antimisiaris, S. G.; Kallinteri, P.; Fatouros, D. G. Liposomes and Drug Delivery. In *Pharmaceutical Manufacturing Handbook*, John Wiley & Sons, Inc.: 2008; pp 443-533.

97. Chen, C.; Han, D.; Cai, C.; Tang, X. An overview of liposome lyophilization and its future potential. *J. Control Release.* **2010,** *%19;142* (3), 299-311.

98. Misra, A.; Jinturkar, K.; Patel, D.; Lalani, J.; Chougule, M. Recent advances in liposomal dry powder formulations: preparation and evaluation. *Expert Opin. Drug Deliv.* **2009,** *6* (1), 71-89.

99. Willis, L.; Hayes, D., Jr.; Mansour, H. M. Therapeutic liposomal dry powder inhalation aerosols for targeted lung delivery. *Lung.* **2012,** *190* (3), 251-262.

100. Alton, E. W.; Boyd, A. C.; Cheng, S. H.; Cunningham, S.; Davies, J. C.; Gill, D. R.; Griesenbach, U.; Higgins, T.; Hyde, S. C.; Innes, J. A.; Murray, G. D.; Porteous, D. J. A randomised, double-blind, placebo-controlled phase IIB clinical trial of repeated application of gene therapy in patients with cystic fibrosis. *Thorax.* **2013,** *68* (11), 1075-1077.

101. Dass, C. R. Lipoplex-mediated delivery of nucleic acids: factors affecting in vivo transfection. *J. Mol. Med. (Berl).* **2004,** *82* (9), 579-591.

102. Lv, H.; Zhang, S.; Wang, B.; Cui, S.; Yan, J. Toxicity of cationic lipids and cationic polymers in gene delivery. *J. Control Release* **2006,** *114* (1), 100-109.

103. Weber, S.; Zimmer, A.; Pardeike, J. Solid Lipid Nanoparticles (SLN) and Nanostructured Lipid Carriers (NLC) for pulmonary application: A review of the state of the art. *Eur. J. Pharm. Biopharm.* **2013,** (13), 10.

104. Ungaro, F.; d'Angelo, I.; Miro, A.; La Rotonda, M. I.; Quaglia, F. Engineered PLGA nano- and micro-carriers for pulmonary delivery: challenges and promises. *J. Pharm. Pharmacol.* **2012,** *64* (9), 1217-1235.

105. d'Angelo, I.; Conte, C.; Miro, A.; Quaglia, F.; Ungaro, F. Pulmonary drug delivery: a role for polymeric nanoparticles? *Curr. Top. Med. Chem.* **2015,** *15* (4), 386-400.

106. Geller, D. E.; Madge, S. Technological and behavioral strategies to reduce treatment burden and improve adherence to inhaled antibiotics in cystic fibrosis. *Respir. Med.* **2011,** *105 Suppl 2:S24-31. doi: 10.1016/S0954-6111* (11)70024-5.), -5.

107. Coowanitwong, I.; Arya, V.; Kulvanich, P.; Hochhaus, G. Slow release formulations of inhaled rifampin. *AAPS. J.* **2008,** *10* (2), 342-348.

108. Jensen, D. K.; Jensen, L. B.; Koocheki, S.; Bengtson, L.; Cun, D.; Nielsen, H. M.; Foged, C. Design of an inhalable dry powder formulation of DOTAP-modified PLGA nanoparticles loaded with siRNA. *J. Control Release.* **2011**.

109. Ungaro, F.; d'Angelo, I.; Coletta, C.; d'Emmanuele, d., V; Sorrentino, R.; Perfetto, B.; Tufano, M. A.; Miro, A.; La Rotonda, M. I.; Quaglia, F. Dry powders based on PLGA nanoparticles for pulmonary delivery of antibiotics: modulation of encapsulation efficiency, release rate and lung deposition pattern by hydrophilic polymers. *J. Control Release.* **2012,** *157* (1), 149-159.

110. De Stefano, D.; Ungaro, F.; Giovino, C.; Polimeno, A.; Quaglia, F.; Carnuccio, R. Sustained inhibition of IL-6 and IL-8 expression by decoy ODN to NF-kappaB delivered through respirable large porous particles in LPS-stimulated cystic fibrosis bronchial cells. *J. Gene Med.* **2011,** *13* (4), 200-208.

111. Ungaro, F.; De, S. D.; Giovino, C.; Masuccio, A.; Miro, A.; Sorrentino, R.; Carnuccio, R.; Quaglia, F. PEI-Engineered Respirable Particles Delivering a Decoy Oligonucleotide to NF-kappaB: Inhibiting MUC2 Expression in LPS-Stimulated Airway Epithelial Cells. *PLoS. One.* **2012,** *7* (10), e46457.

112. De Rosa, G.; La Rotonda, M. I.; Quaglia, F.; Ungaro, F. Use of Additives in the Design of Poly(Lactide-Co-Glycolide) Microspheres for Drug Delivery. In *Handbook of Particulate Drug Delivery*, Ravi Kumar, M. N. V., Ed.; American Scientific Publisher: Stevenson Ranch (CA), 2008; pp 61-91.

113. Mura, S.; Hillaireau, H.; Nicolas, J.; Kerdine-Romer, S.; Le, D. B.; Delomenie, C.; Nicolas, V.; Pallardy, M.; Tsapis, N.; Fattal, E. Biodegradable nanoparticles meet the bronchial airway barrier: how surface properties affect their interaction with mucus and epithelial cells. *Biomacromolecules.* **2011,** *12* (11), 4136-4143.

114. Khalil, H.; Chen, T.; Riffon, R.; Wang, R.; Wang, Z. Synergy between polyethylenimine and different families of antibiotics against a resistant clinical isolate of Pseudomonas aeruginosa. *Antimicrob. Agents Chemother.* **2008,** *52* (5), 1635-1641.

115. De Stefano, D.; Coletta, C.; Bianca, R.; Falcone, L.; d'Angelo, I.; Ungaro, F.; Quaglia, F.; Carnuccio, R.; Sorrentino, R. A decoy oligonucleotide to NF-kappaB delivered through inhalable particles prevents LPS-induced rat airway inflammation. *Am. J. Respir. Cell Mol. Biol.* **2013,** *49* (2), 288-295.

116. Tang, B. C.; Dawson, M.; Lai, S. K.; Wang, Y. Y.; Suk, J. S.; Yang, M.; Zeitlin, P.; Boyle, M. P.; Fu, J.; Hanes, J. Biodegradable polymer nanoparticles that rapidly penetrate the human mucus barrier. *Proc. Natl. Acad. Sci. U. S. A.* **2009,** *106* (46), 19268-19273.

117. Raemdonck, K.; Braeckmans, K.; Demeester, J.; De Smedt, S. C. Merging the best of both worlds: hybrid lipid-enveloped matrix nanocomposites in drug delivery. *Chem. Soc. Rev.* **2014,** *43* (1), 444-472.

118. Zhang, L.; Chan, J. M.; Gu, F. X.; Rhee, J. W.; Wang, A. Z.; Radovic-Moreno, A. F.; Alexis, F.; Langer, R.; Farokhzad, O. C. Self-assembled lipid--polymer hybrid nanoparticles: a robust drug delivery platform. *ACS Nano* **2008,** *2* (8), 1696-1702.

119. Colombo, S.; Cun, D.; Remaut, K.; Bunker, M.; Zhang, J.; Martin-Bertelsen, B.; Yaghmur, A.; Braeckmans, K.; Nielsen, H. M.; Foged, C. Mechanistic profiling of

the siRNA delivery dynamics of lipid-polymer hybrid nanoparticles. *J. Control Release* **2015,** *201*, 22-31.

120. De, B. L.; Braeckmans, K.; Stuart, M. C.; Demeester, J.; De Smedt, S. C.; Raemdonck, K. Bio-inspired pulmonary surfactant-modified nanogels: A promising siRNA delivery system. *J. Control Release* **2015,** *206*, 177-186.

CHAPTER 2

TOWARDS REPOSITIONING NICLOSAMIDE FOR ANTI-VIRULENCE THERAPY OF PSEUDOMONAS AERUGINOSA LUNG INFECTIONS: DEVELOPMENT OF INHALABLE FORMULATIONS THROUGH NANOSUSPENSION TECHNOLOGY

G. Costabile[1], I. d'Angelo[2], G. Rampioni[3], R. Bondì[3], B. Pompili[4], F. Ascenzioni[4], E. Mitidieri[1], R. d'Emmanuele di Villa Bianca[1], R. Sorrentino[1], A. Miro[1], F. Quaglia[1], F. Imperi[4], L. Leoni[3], F. Ungaro[1]

[1]*Department of Pharmacy, University of Naples Federico II, Via Domenico Montesano 49, 80131 Naples, Italy*
[2]*Di.S.T.A.Bi.F., Second University of Naples, Via Vivaldi 43, 81100 Caserta, Italy*
[3]*Department of Sciences, University Roma Tre, Viale Marconi, 446, 00146 Rome, Italy*
[4]*Department of Biology and Biotechnology "Charles Darwin", Sapienza University of Rome, Via deiSardi 70, 00185 Rome, Italy*

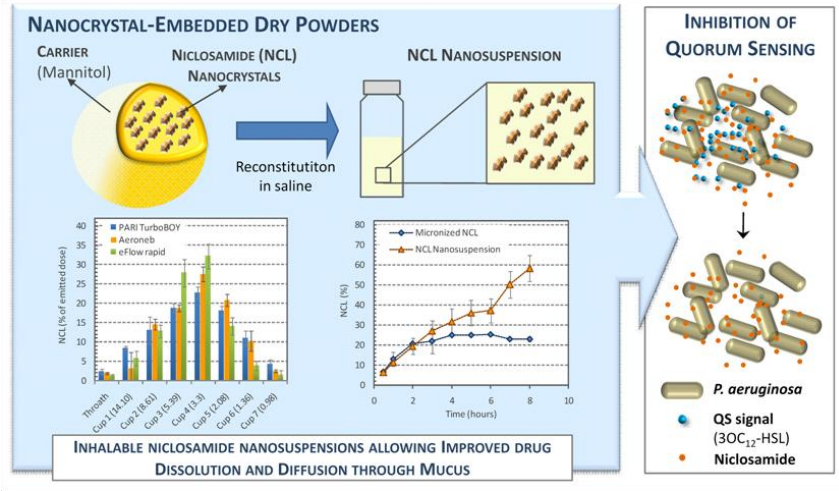

***Molecular Pharmaceutics,* 12(8):2604-17, 2015.**

ABSTRACT

Inhaled anti-virulence drugs are currently considered a promising therapeutic option to treat *Pseudomonas aeruginosa* lung infections in cystic fibrosis (CF). We have recently shown that the anthelmintic drug niclosamide (NCL) has strong quorum sensing (QS) inhibiting activity against *P. aeruginosa* and could be repurposed as an anti-virulence drug. In this work, we developed dry powders containing NCL nanoparticles that can be reconstituted in saline solution to produce inhalable nanosuspensions. NCL nanoparticles were produced by high-pressure homogenization (HPH) using polysorbate 20 or polysorbate 80 as stabilizers. After 20 cycles of HPH, all formulations showed similar properties in the form of needle-shape nanocrystals with a hydrodynamic diameter of approximately 450 nm and a zeta potential of -20 mV. Nanosuspensions stabilized with polysorbate 80 at 10% w/w to NCL (T80_10) showed an optimal solubility profile in simulated interstitial lung fluid. T80_10 was successfully dried into mannitol-based dry powder by spray drying. Dry powder (T80_10 DP) was reconstituted in saline solution and showed optimal *in vitro* aerosol performance. Both T80_10 and T80_10 DP were able to inhibit *P. aeruginosa* QS at NCL concentrations of 2.5-10 μM. NCL, and these formulations did not significantly affect the viability of CF bronchial epithelial cells *in vitro* at microbiologically active concentrations (i.e., ≤10 μM). *In vivo* acute toxicity studies in rats confirmed the no observable toxicity of the NCL T80_10 DP formulation upon intra-tracheal administration at a concentration 100-fold higher than the anti-QS activity concentration. These preliminary results suggest that NCL repurposed in the form of inhalable nanosuspensions has great potential for the local treatment of *P. aeruginosa* lung infections as in the case of CF patients.

2.1 INTRODUCTION

Cystic fibrosis (CF) is an autosomal disease caused by a defect in a single gene encoding the CF transmembrane conductance regulator (CFTR).[1] This condition predisposes CF patients to recurrent/persistent bacterial lung infections, which are the primary cause of bronchiectasis, respiratory failure and consequent death in CF patients.[1-3] The dominant pathogen in CF airways is *Pseudomonas aeruginosa*, though other microorganisms may play a role in lung function decline.[4] Although lung infections can be controlled to some extent by early, aggressive antibiotic treatments, 60–70% of CF patients become chronically infected by *P. aeruginosa* by the age of 20. Current treatment involves life-long daily inhaled antibiotic therapies.[5] Anti-virulence drugs, i.e., agents that inhibit the production of disease-causing virulence factors but are neither bacteriostatic nor bactericidal, are considered promising therapeutic options for the treatment of *P. aeruginosa* infections in CF, either alone or in combination with antibiotics. These drugs are expected to prevent the establishment of the chronic infection and to reduce its severity by inhibiting bacterial processes essential for virulence and pathogenicity, rather than targeting bacterial growth. The main advantages of anti-virulence drugs over conventional antibiotics are that they are unlikely to drive the spread of resistant strains and that they have a reduced impact on the resident microbiota.[6,7]

The pathogenic potential of *P. aeruginosa* relies on the coordinated expression of a large array of virulence factors[8], the majority of which are positively controlled by an intercellular communication process called quorum sensing (QS). *P. aeruginosa* QS is based on the production, secretion and perception of different signal molecules; *N*-3-oxo-dodecanoyl-homoserine lactone ($3OC_{12}$-HSL) is considered the major QS signal produced by *P. aeruginosa*.[9] When the $3OC_{12}$-HSL signal molecule reaches a threshold concentration, it binds to the LasR transcriptional regulator, triggering the expression of hundreds of genes, including genes for the production of a large number of virulence factors and for biofilm formation.[9] Numerous studies support the role of QS in *P. aeruginosa* infection and highlight its importance as a candidate for novel virulence-targeted drugs (reviewed in[10]). Therefore, the search

for QS inhibitors to be used as lead compounds for the development of "non-antibiotic" drugs against *P. aeruginosa* has become a field of intensive research.[11,12] Despite the huge efforts made to date in the field of anti-QS research, clinical applications remain out of reach, mainly due to the unfavorable pharmacological properties of the majority of the QS inhibitors identified so far.[12] A potential shortcut is the use of a drug repurposing approach for the identification of QS inhibitory compounds with low toxicity and already approved for use in humans. This strategy recently led to the identification of the anthelmintic drug niclosamide (NCL) as a strong inhibitor of the $3OC_{12}$-HSL-dependent QS system in *P. aeruginosa*. Preliminary experiments suggested that NCL interferes with the LasR-dependent signaling pathway rather than with the synthesis of $3OC_{12}$-HSL. As a consequence of LasR-dependent signaling inhibition, NCL strongly reduced virulence factor production, impaired biofilm development, and attenuated *P. aeruginosa* pathogenicity in the *Galleria mellonella* model of acute infection.[13]

The potential therapeutic value of NCL has been clearly demonstrated, and thus, an adequate inhalable formulation for the proposed clinical application is needed. Pulmonary administration represents an ideal route to treat respiratory infections typical of CF lung disease.[14,15] Important determinants of the clinical outcomes of the inhaled drug are the lung dose as well as the ability of the drug to overcome extracellular and cellular barriers.[16] From a technological point of view, the major obstacles related to the pulmonary administration of NCL are the achievement of appropriate particle size distribution and the potential poor dissolution properties in lung lining fluids[17] due to its low aqueous solubility.

Among the available formulation options for reducing the particle size of poorly soluble active molecules, pulmonary delivery of "nanosuspensions" can be considered. Nanosuspensions are colloidal dispersions of drug nanocrystals stabilized by surfactants,[18] which can also increase drug interactions with biological substrates.[19,20] An aqueous nanosuspension can be delivered through commercially available nebulizers to generate an aerosol with a 1-5 µm droplet size suitable to achieve the desired distribution in the lung.[21-23] A number of smart, efficient and

portable nebulizers, such as adaptive aerosol delivery nebulizers with vibrating mesh technology (VMT), are available to CF patients.[24]

The aim of this work was to develop inhalable NCL formulations for anti-virulence therapy against *P. aeruginosa* lung infections. To this end, different NCL nanosuspensions have been produced, and optimized formulations have been selected on the basis of morphology, size, zeta potential, and solubility profile in different media. A strategy to improve long-term stability of the formulations is proposed. *In vitro* aerosol performance, QS inhibitory activity and cytotoxicity in CF human airway epithelial cells of optimized NCL formulations have been investigated. Finally, the *in vivo* acute lung toxicity of the most promising NCL formulation was tested in rats following intra-tracheal administration

.

2.2 EXPERIMENTAL METHODS

2.2.1 Materials

NCL, polysorbates (Tween® 80 and Tween® 20), diethylenetriaminepentaacetic acid (DTPA), dimethyl sulfoxide (DMSO), 3-(*N*-morpholino)propanesulfonic acid (MOPS), *N*-3-oxo-dodecanoyl-homoserine lactone ($3OC_{12}$-HSL), egg yolk emulsion, RPMI amino acid solution, type II mucin from porcine stomach, calcium chloride dihydrate, magnesium chloride, potassium chloride, potassium phosphate dibasic, sodium acetate, sodium bicarbonate, sodium chloride, sodium citrate dehydrate, sodium phosphate dibasic, sodium sulfate, and 3-(4,5-dimethylthiazol-2-yl)-2,5-diphenyltetrazolium bromide (MTT) were obtained from Sigma-Aldrich (Italy). Mannitol (Pearlitol®C160) was a kind gift of Roquette Italia S.p.a. (Italy). Tryptone and yeast extract were obtained from Acumedia (Neogen Corporation, MI, USA). Analytical grade methanol was supplied by Carlo Erba (Italy). Distilled water filtered through 0.22 μm cellulose filters (Phenex® RC, Phenomenex, USA) was employed throughout the study.

2.2.2 Niclosamide quantitation

The amount of NCL in solution was determined by UV-vis spectrophotometry using a Shimadzu 1204 spectrophotometer (Shimadzu, Italy) fitted out with a 0.1-cm quartz cell (Hellma® Italia, Italy). The absorbance (ABS) of NCL samples was measured at 331 nm. A calibration curve was obtained by plotting ABS *versus* the concentration of NCL standard solutions in methanol. The linearity of the response was verified over a concentration range of 0.2–20 μg/mL (r^2= 0.999). The limit of detection (LOD) (estimated as 3 times the background noise) was 0.22 μg/L. The limit of quantitation (LOQ) (estimated as 10 times the background noise) was 0.53 μg/L. In each case, the presence in the samples of interfering substances that could affect the UV-vis spectrum of NCL was accounted for with the appropriate blank. All blank media had negligible absorption at 331 nm.

2.2.3 Development of niclosamide nanosuspensions

2.2.3.1 Production of NCL nanosuspensions

NCL nanosuspensions were prepared by high-pressure homogenization (HPH) using two different polysorbates as stabilizers (i.e., Tween 20 and Tween 80). Four nanosuspensions were developed: T20_10 and T20_20, which contained Tween 20 at 10% or 20% w/w NCL, respectively, and T80_10 and T80_20, which contained Tween 80 at 10% or 20% w/w NCL, respectively (Table 2.1).

Table 2.1. Composition of NCL nanosuspensions.

	NCL (w/v)	Polysorbate 80 (w/w to NCL)	Polysorbate 20 (w/w to NCL)
T80_10	1%	10%	-
T80_20	1%	20%	-
T20_10	1%	-	10%
T20_20	1%	-	20%

Before processing, NCL raw material (mean volume diameter approximately 18 μm) was pre-milled for 10 min in a colloid mill (Model IG/.W2/E, Giuliani, Italia) equipped with a 20 mL agate jar and balls. After milling, an appropriate amount of micronized NCL (Micro NCL) (1% w/v) was dispersed in 100 mL of a stabilizer solution in water. The dispersion was pre-mixed using a high-speed homogenizer (Ystral, Heidolph, Germany) operating at 19000 rpm (tool 10F) for 15 minutes and then subjected to a predetermined number of HPH cycles (10, 15 and 20 cycles) at 1800 bar in a PandaPlus 2000 high-pressure homogenizer from NiroSoavi (Parma, Italy). To optimize process parameters, the size of NCL crystals was monitoredthroughout the HPH process by laser light scattering (Coulter LS 100Q, USA) upon dilution of the samples in water to a suitable scattering intensity.

The amount of NCL solubilized was determined just after production. Briefly, the nanosuspension was centrifuged at 11000 g for 30 min at 25°C (Hettich Zentrifugen, Universal 16R). After centrifugation, the supernatant was withdrawn, filtered

through 0.45 µm cellulose filters (Phenex® RC, Phenomenex, USA) and analyzed for NCL content.

2.2.3.2 Size and morphology of NCL nanocrystals

To select the process parameters, the size of the NCL nanocrystals was determined just after processing by laser light scattering (Coulter LS 100Q, USA) upon dilution of the samples in water to a suitable scattering intensity. The size of NCL raw material and Micro NCL was determined for comparison. Results are expressed as volume diameter (d_{10}, d_{50} and d_{90}) ± standard deviation (SD) of values collected from three different batches (n=6).

The hydrodynamic diameter (HD), the polydispersity index (PI) and the zeta potential of the final nanosuspensions were determined by photon correlation spectroscopy (PCS) with a Malvern Zetasizer Nano ZS (Malvern Instruments, UK). Results are expressed as mean value±standard deviation (SD) of triplicate measurements on different batches (n =6). Particle shape and external morphology were analyzed by Scanning Electron Microscopy (SEM) (Leica S440, Germany) upon air drying 10 µL of nanosuspensions on paper filters for 24 hours. Dried samples were stuck on a metal stub and coated with gold under vacuum for 120 s.

2.2.3.3 Stability of NCL nanosuspensions

After production, nanosuspensions were stored in BD Falcon™ polypropylene conical tubes at 4°C (up to 3 months) and 25°C (for 1 month) in the dark. The stability over time was assessed in terms of morphology (SEM), size and PI (PCS).

The change in NCL content over time was also assessed upon storage in BD Falcon™ polypropylene conical tubes at 4°C and 25°C for 1 month in the dark. Experiments were run in triplicate for each time point, and the results were reported as NCL content (µg/mL) ± standard deviation.

2.2.3.4 In vitro dissolution studies

Dissolution profiles of NCL nanosuspensions were determined in simulated interstitial lung fluid (SILF) by the USP paddle method using a Sotax (ModelAT7, Switzerland) dissolution system at 37°C. SILF was prepared following the preparation instructions dictated by Marques et al. [25] Briefly, 1 L of SILF contains

0.095 g magnesium chloride, 6.019 g of sodium chloride, 0.298 g of potassium chloride, 0.126 g of sodium phosphate dibasic, 0.063 g of sodium sulfate, 0.368 g calcium chloride dihydrate, 0.574 g of sodium acetate, 2.604 g of sodium bicarbonate and 0.097 g of sodium citrate dihydrate.

For the experiment, 1 mL of nanosuspension was added to 500 mL of SILF in the dissolution vessel and stirred at 100 rpm. At predetermined time intervals, 2 mL of the dissolution medium was withdrawn, and the same volume of fresh SILF was added. NCL concentration was measured by spectrophotometric analysis as described above. The dissolution profile of Micro NCL was evaluated as a control.

2.2.4 Development of nanocrystal-embedded dry powders

Dry powders containing nanosuspensions stabilized with polysorbate 80 at 10% w/w to NCL (T80_10 DP) were produced either by lyophilization or spray drying for processing into a solid dosage form with long-term stability. Freeze-drying was first attempted the nanosuspension was pre-frozen at either -20°C or -80 °C. To improve dry powder properties, mannitol at different NCL/mannitol ratios by weight was added as cryoprotectant to the nanosuspension before freeze-drying. Samples were then dried for 24 hours by a Modulyo freeze-drier (Edwards, UK) operating at 0.01 atm and -60°C.

Briefly, nanosuspensions were processed in a Mini Spray Dryer Büchi 190 (Flawil, Switzerland) equipped with a high-performance cyclone for the recovery of small powder amounts. Formulations at different NCL/mannitol ratios (1:2; 1:5; 1:10 w/w) were individually spray-dried with the following process parameters: feed rate 3 mL/min; aspirator setting 20; spray-flow 600 mL/h; inlet temperature 140°C (resulting outlet temperature = 70°C). A 0.5 mm nozzle was used throughout the experiments. Powders were collected and stored at 22°C in a glass vacuum desiccators until use.

The mean geometric diameter and size distribution of spray-dried powders were determined by laser light scattering (Coulter LS 100Q, USA) of a powder suspension in methanol. Size is expressed as volume mean diameter± SD of values

collected from three batches. SEM analysis of dried samples was performed as described for NCL nanosuspensions.

To evaluate the redispersibility of NCL nanosuspensions after the solidification process (after lyophilization and spraydrying), particle size analysis of the reconstituted liquid dispersion was performed through both laser light scattering (Coulter LS 100Q, USA) and PCS (Zetasizer Nano ZS, Malvern Instruments, UK) analysis. Results are reported as the redispersibility index (RDI), defined as

$$RDI = \frac{D}{D_0}$$

where D_0 represents the size of the nanosuspension prior to drying, and D represents the corresponding value post-rehydration of the dried sample in water.

Thermoanalytical tests were carried out to study the melting behavior of NCL within the spray-dried powders by differential scanning calorimetry (DSC). The DSC instrument (Q20, TA Instruments, U.S.A.) was calibrated with a pure indium standard. The samples (approximately 5 mg) were placed in hermetically sealed aluminum pans, equilibrated at 25°C and heated to 300°C at 10°C/min. Measurements were carried out under an inert nitrogen atmosphere, purged at a flow rate of 50 mL/min. The melting temperatures (T_m, °C) were obtained from the corresponding thermograms by peak integration.

2.2.5 *In vitro* dissolution in simulated CF mucus

To better recapitulate *in vivo* conditions, the release of NCL from artificial CF mucus to SILF from T80_10 nanosuspension and the corresponding dry powder T80_10 DP was followed *in vitro* by membrane dialysis. For comparison, the release kinetics of Micro NCL in the same conditions were analyzed. Briefly, the artificial mucus was prepared by adding 250 µL of sterile egg yolk emulsion, 250 mg of mucin, 0.295 mg DTPA, 250 mg NaCl, 110 mg KCl and 1 mL of RPMI to 50 mL of water. The dispersion was stirred until a homogenous mixture was obtained.

T80_10 nanosuspension (0.1 mL) or a corresponding amount of T80_10 DP was added to 0.3 mL of donor medium (artificial mucus or PBS) and placed in a dialysis

membrane bag (MWCO: 5000 Da, Spectra/Por®). The sample was placed into 5 mL of external medium and kept at 37°C. At scheduled time intervals, 1 mL of the external medium was withdrawn and analyzed for NCL content by spectrophotometric analysis as described above. The medium was replaced by the same amount of fresh medium. At the end of each release experiment, the amount of residual NCL in the dialysis bag was assessed upon dissolution in methanol. Experiments were run in triplicate for each time point of release kinetics.

2.2.6 *In vitro* aerosol performance

The aerosolization properties of NCL nanosuspensions were tested *in vitro* after delivery from different commercial nebulizers. The deposition pattern of the T80_10 formulation was investigated using a Next Generation Impactor (NGI) (Copley Scientific, UK) according to the *Comité Européen de Normalization* (CEN) standard methodology for nebulizer systems[26], with sampling at 15 L/min and insertion of a filter in micro-orifice collector (MOC).

For each test, 2 mL of fresh T80_10 nanosuspension or reconstituted T80_10DP spray-dried powder was transferred to the reservoir of the nebulizer, which was connected to the induction port of the NGI. The nebulizer was operated at 15 L/min, and the aerosol was drawn through the impactor until dryness. The amount of NCL deposited on the seven NGI collection cups was quantitatively recovered by dissolution in 2 mL of methanol. The amount of NCL deposited in the induction port and remaining inside the nebulizer chamber was also determined by washing with an appropriate amount of methanol. The results achieved with different nebulizer systems were compared; the tested systems were PARI TurboBOY®(PARI GmbH, Germany), eFlow®*rapid* (PARI GmbH, Germany) and Aeroneb® Go (Aerogen, Ireland). Three determinations were made for each nebulizer.

The emitted dose (ED) was measured as the difference between the total amount of NCL initially placed and the amount remaining in the nebulizer chamber. Upon emission, the experimental mass median aerodynamic diameter (MMAD) and the geometric standard deviation (GSD) were calculated according to the European Pharmacopeia deriving a plot of cumulative mass of particle retained in each

collection cup (expressed as percent of total mass recovered in the impactor) *versus* the cut-off diameter of the respective stage. The MMAD of the particles was determined from the same graph as the particle size at which the line crosses the 50% mark, and the GSD was defined as

$$GSD = (Size\ X/Size\ Y)^{1/2}$$

where size X was the particle size at which the line crosses the 84% mark and size Y the size at which it crosses the 16% mark.

The fine particle fraction (FPF) was calculated taking into account the actual amount of NCL deposited on stage 3 through 7 (MMAD < 5.39 μm) compared to the initial amount loaded into the nebulizer chamber; that is the nominal dose of NCL, according to the following equation:

$$FPF = \frac{\text{NCL amount on cup 3 through 7}}{\text{NCL amount loaded into the device}} \text{ x } 100$$

The respirable fraction (RF) was defined as:

$$RF = \frac{\text{NCL amount on cup 3 through 7}}{\text{NCL total amount deposited in the NGI}} \text{ x } 100$$

2.2.7 Measurements of QS inhibitory activity in *P. aeruginosa*

The QS inhibitory activity of the formulations T80_10, T80_10 DP and raw NCL dissolved in DMSO was compared by using the whole cell biosensor PA14-R3[27] in the presence of 3 μM synthetic $3OC_{12}$-HSL, as previously described[13]. The biosensor PA14-R3 was routinely grown in Luria-Bertani broth (LB; 10 g/L tryptone, 5 g/L yeast extract, 10 g/L NaCl).

T80_10 and T80_10 DP were diluted/resuspended in sterile distilled water to obtain stock nanosuspensions containing NCL at 15 mM. Raw NCL was dissolved in DMSO to obtain a 10 mM stock solution.[13] As negative controls, DMSO and stock solutions containing T80 alone or in combination with mannitol dissolved in water

were used. Serial dilutions of NCL in DMSO, T80_10, and T80_10 DP and negative controls were prepared in sterile distilled water and incubated at 37°C for 16 hours. The assay was initiated by mixing 100 µL of each NCL dilution and an equal volume of the biosensor mix in microtiter wells. The biosensor mix contained the biosensor strain PA14-R3, LB (2-fold concentrated), 100 mM MOPS (pH 7.0) and 6 µM $3OC_{12}$-HSL. The starting ABS at 600 nanometers (A_{600}) of the biosensor mix was 0.09.

After incubation of the microtiter plates for 6 h at 37°C, A_{600} and light counts per second (LCPS) were measured in a Wallac 1420 Victor3V multilabel plate reader (PerkinElmer).

2.2.8 Cytotoxicity assay

The CF bronchial epithelial cell line CFBE41o (F508del/F508del)[28] was maintained in MEM with 20 mM L-glutamine, 100 units/mL penicillin, 100 µg/mL streptomycin and 10% fetal bovine serum (FBS). When confluent, CFBE41o cells were trypsinized and seeded in 96-well microtiter plates at 30000 cells per well (in 200 µL final volume). Twenty-four hours after seeding, cells were washed three times with culture medium without any additive (FBS or antibiotics), and 200 µL of culture medium with or without different amounts of NCL formulations or their corresponding controls were added to each well. After 3 h of incubation at 37°C, the cell culture medium was discarded, and each well was washed with 200 µL of Hank's balanced buffer solution (HBSS). Cells were then incubated for 3 h at 37°C in the presence of 200 µL of 0.5 mg/mL MTT in HBSS. The MTT solution was then discarded, 100 µL of DMSO was added to each well, and ABS at 570 nm (A_{570}) was read using an ELISA microtiter plate reader.[29]

2.2.9 *In vivo* acute lung toxicity

2.2.9.1 Animals and treatment

Male Wistar rats (weighing between 200 to 220 g; Charles River, Lecco, Italy) were kept at a temperature of 23±2°C, relative humidity range 40-70% and 12 h light/dark cycles. Standard chow and drinking water were provided *ad libitum*. A period of 7 days was allowed for the acclimatization of the rats before any experimental

manipulation. Experimental procedure was performed following the specific guidelines of the Italian (N. 116/1992) and the European Council law (N.86/609/CEE) for animal care. All the procedures were also approved by the Animal Ethics Committee of the University of Naples "Federico II" (Italy).

Rats were anesthetized using ketamine (100 mg/kg, i.p.) and xylazine (5 mg/kg, i.p.), and the depth of anesthesia was continuously controlled. Rats were then placed ventral side up on a surgical table provided with a temperature-controlled pad to maintain physiological temperature. To avoid breathing problems, rats were placed on a slanted board (30° from the vertical). Rats were divided into different groups and treated with PBS (50 µL, SHAM group) or NCL T80_10 DP (10, 30 and 100 µg/50 µL/rat). All the solutions were intra-tracheally administered by a MicroSprayer® (model IA-1B, PennCentury, USA). The cannula of the tracheal dispositive was inserted directly into the trachea through the mouth.[30] Twenty-four hours after *in vivo* administration, the rats were anesthetized by urethane (25% i.p; 10 ml/kg), and after euthanization, bronchoalveolar lavage (BAL) and the lungs were obtained for cell counts, BAL fluid (BALF) protein evaluation and western blot analysis.

2.2.9.2 Cell count in bronchoalveolar lavage

The trachea was cannulated with a polyethylene tube (1 mm inner diameter) to perform BAL as previously reported[30]. Briefly, the lungs were sequentially washed by flushing with 4 mL of sterile, ice-cold PBS three times for each animal. The first PBS recovery was immediately placed on ice and then centrifuged at 500 g for 10 min at 4°C. The resulting cell pellets (BALC) were pooled with the other two and re-suspended in 1 mL of PBS. BALC suspensions (100 µL) were stained with Turk solution (0.1% w/v crystal violet in 3% v/v glacial acetic acid) causing hemolysis of the red blood cells and staining of the nuclei of white blood cells. Neutrophil and macrophage cell count was determined microscopically using a Neubauer hemacytometer chamber, according to standard morphology criteria. The first BALF recovered after centrifugation was stored and used for total protein evaluation. The total volume of BALF recovered from each animal was also evaluated.

2.2.9.3 Protein evaluation in BALF

Total protein concentration in BALF was determined by Bio-Rad Protein assay and calculated against a calibration curve of bovine serum albumin (BSA) (0.05-0.5 mg/mL) (Sigma-Aldrich, USA). Briefly, 10 µL of each standard and sample solution *plus* 200 µL of Dye Reagent (1:4) were dispensed into a single well using a 96-well plate. The optical absorbance of the solution at 595 nm was measured.

2.2.9.4 Lung Western blot analysis

Western blots were performed as previously described[31]. Briefly, frozen lung was homogenized in modified RIPA buffer (50 mM Tris-HCl pH 8.0, 150 mM NaCl, 0.5% sodium deoxycholate, 0.1% sodium dodecyl sulfate, 1 mM EDTA, 1% Igepal, 1× inhibitor) (Roche Applied Science, Italy) and protease inhibitor cocktail (Sigma-Aldrich, USA). Protein concentration was determined by the Bradford assay using BSA as a standard (Sigma-Aldrich, USA). Denatured proteins (50 µg) were separated on 10% sodium dodecyl sulfate polyacrylamide gels and transferred to a polyvinylidene fluoride membrane. The membranes were blocked by incubation in PBS containing 0.1% v/v Tween 20 and 5% non-fat dried milk for 1 h at room temperature and then incubated overnight at 4°C with mouse monoclonal antibody for cyclooxygenase-2 (COX-2, 1:2000; BD Bioscience, Erembodegem, Belgium) or rabbit polyclonal antibody for inducible nitric oxide synthase (iNOS, 1:500; Novus Biologicals Europe, Cambridge, UK). Membranes were extensively washed in PBS containing 0.1% v/v Tween-20 prior to incubation with horseradish peroxidase-conjugated secondary antibody for 2 h at room temperature. Following incubation, membranes were washed and developed using an ImageQuant-400 (GE Healthcare, USA). The target protein band intensity was normalized over the intensity of the housekeeping GADPH (1:5000, Sigma-Aldrich, Milan, Italy).

2.2.9.5 Statistical analysis

The significance of differences was determined with the software GraphPad InStat, using One-Way Analysis of Variance (ANOVA) followed by the Tukey-Kramer multiple comparison test. *In vivo* data were analyzed by One-Way ANOVA followed by Bonferroni post hoc test. A p value <0.05 was considered significant.

2.3. RESULTS

2.3.1. Development of niclosamide nanosuspensions

Formulation development studies were carried out to select the most appropriate stabilizer and homogenization parameters for nanosuspensions. Two different surfactants, polysorbate 20 and polysorbate 80, were chosen as stabilizers and used at different ratios by weight to NCL (Table 1). In each case, NCL raw material was micronized through a colloid mill (Micro NCL) before dispersion in polysorbate to prevent blocking of the homogenizer gap during HPH. After 2 cycles of milling for 10 minutes, the mean volume diameter of Micro NCL powders was 8.78 ± 0.92 µm. The particle size distribution after a different number of homogenization cycles was evaluated by laser light scattering, and volume diameter values (i.e., d_{10}, d_{50} and d_{90}) decreased significantly with increasing HPH cycle. (Fig. 2.1).

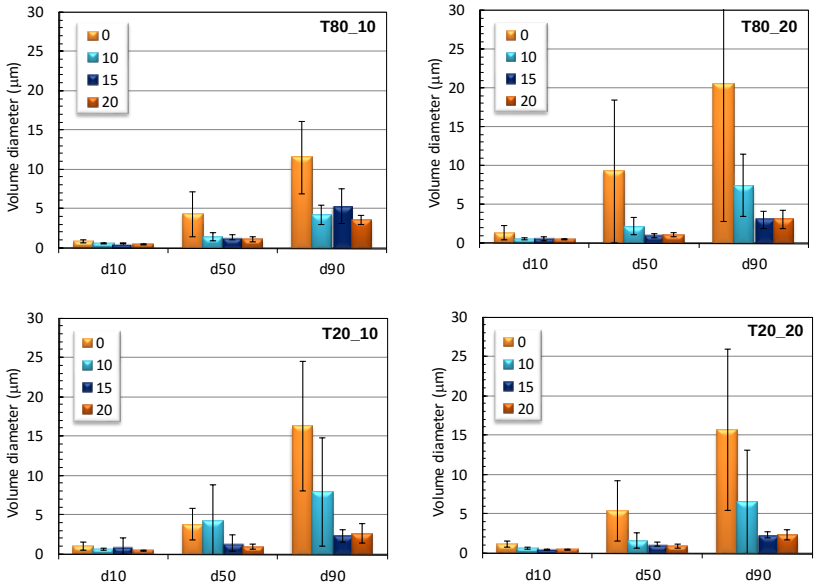

Figure 2.1. Effect of the number of homogenization cycles (0, 10, 15, 20) on the size distribution of NCL nanosuspensions.

As apparent from the error bars, highly variable values were achieved just upon dispersion of Micro NCL in polysorbate aqueous solution. On the contrary, a fine

and stable nanosuspension that was unaltered in terms of size, PI and zeta potential upon dilution in isotonic saline was obtained after 20 cycles of HPH (Fig. 2.2).

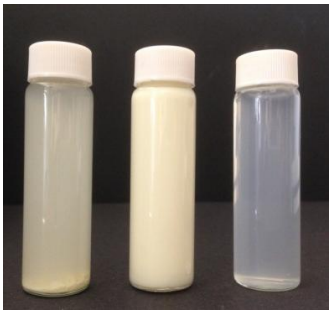

Figure 2.2. Visual appearance of (A) dispersion of micronized NCL in polysorbate 80; (B) T80_10 nanosuspension; (C) T80_10 nanosuspension upon 1:20 dilution in isotonic saline.

No significant differences were observed in the values of d_{10}, d_{50} and d_{90}, which fell within the range of 0.5-3.0 μm (Table 2.2).

Table 2.2. Overall properties of NCL nanosuspensions.

	Volume diameter* (μm ± SD)			**HD** (nm ± SD)**	**Polydispersity index (PI ± SD)**	**ζ-potential (mV ± SD)**	**NCL content (μg/mL ± SD)**
	d10	**d50**	**d90**				
T80_10	0.490 ±0.038	0.951 ±0.292	2.835 ±0.958	417.8 ± 66.4	0.360 ± 0.054	-23.1 ± 6.08	10.2 ± 0.17
T80_20	0.514 ±0.051	1.058 ±0.303	3.059 ±1.241	427.8 ± 27.2	0.337 ± 0.041	-22.8 ± 3.60	18.4 ± 0.068
T20_10	0.482 ±0.031	0.920 ±0.246	2.760 ±0.918	483.2 ± 57.9	0.367 ± 0.031	-19.2 ± 2.60	4.53 ± 0.11
T20_20	0.486 ±0.051	0.914 ±0.343	2.652 ±1.103	428.2 ± 75.7	0.346 ± 0.065	-20.4 ± 2.50	7.03 ± 0.051

*Volume diameter as determined by laser light scattering.
**Hydrodynamic diameter evaluated by PCS analysis.

Bulk analysis of the particle morphology performed through SEM revealed significant differences in the morphologies of the raw material, Micro NCL and NCL nanosuspensions (Fig. 2.3). The raw NCL sample comprised coarse and large particles with a limited amount of needle-like NCL crystals. The size of NCL raw material was reduced after colloid milling (Micro NCL in Fig. 2.3), although the sample appeared to still contain differently sized and shaped particles. A

homogeneous population of needle-like particles was observed in the case of polysorbate-stabilized NCL nanosuspensions with some aggregates in the case of T20_10 and T20_20.

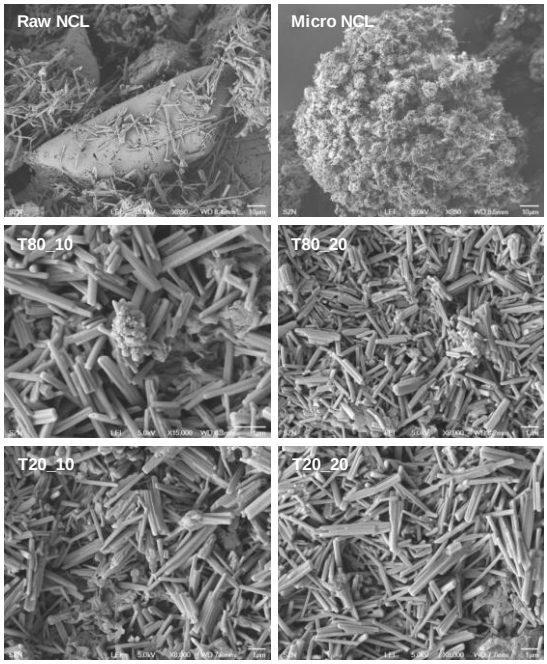

Figure 2.3. SEM images of NCL nanosuspensions just after production (magnification 8000/15000x). SEM micrographs of raw and milled NCL at 850x magnification are reported for comparison. Field is representative of the sample.

Complementary TEM analysis were performed on 10 μl of nanosuspensions, which were applied to a carbon-coated copper grid, air dried and stained with phosphotungstic acid (2%, w/v). As can be seen in Fig. 2.4, all formulations showed typical needle-shape nanocrystals and no surfactant-based micelles were apparent in the background.

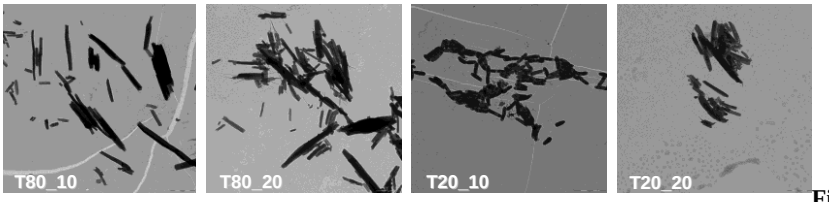

Figure 2.4. TEM photographs of NCL nanosuspensions just after production. Field is representative of the sample.

The mean HD, PI and ζ-potential of the nanocrystals are reported in Table 2.2. As determined by PCS analysis, HD was always approximately 450 nm with an approximate PI value of 0.35, which may help the diffusion of the nanosized NCL through the network of bundled fibers with 100-1000 nm meshes characteristic of CF sputum[16]. On the other hand, a negative ζ-potential around -20 mV was achieved in each case, which may promote electrostatic repulsions between the particles and negatively charged airway mucus and/or biofilm bacteria in the lung.[16]

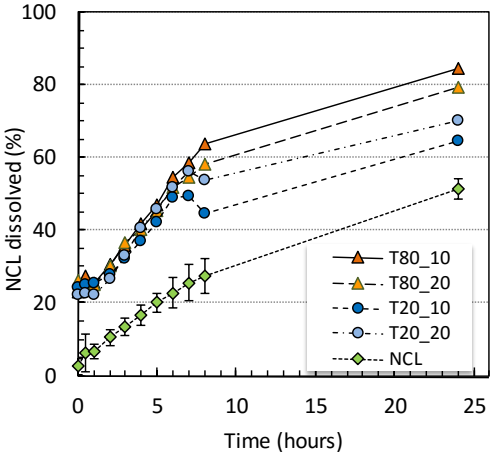

The dissolution profiles of NCL formulations in SILF are reported in Fig. 2.5.

Figure 2.5. *In vitro* dissolution profile of NCL nanosuspensions in SILF at 37°C. The dissolution profile of NCL after colloid milling (Micro NCL) is reported for comparison.

Micro NCL exhibited the lowest dissolution rate and an incomplete dissolution profile, with only 50% of NCL dissolved in 24 hours. The same percent amount was dissolved from NCL nanosuspensions after only 5 hours, with T80_10 and T80_20 allowing the dissolution of almost 100% of the initial NCL amount in 24 hours.

2.3.2. Stability of nanosuspensions upon storage

Nanosuspensions were stored at room temperature and 4°C for the stability over time studies (Fig. 2.6).

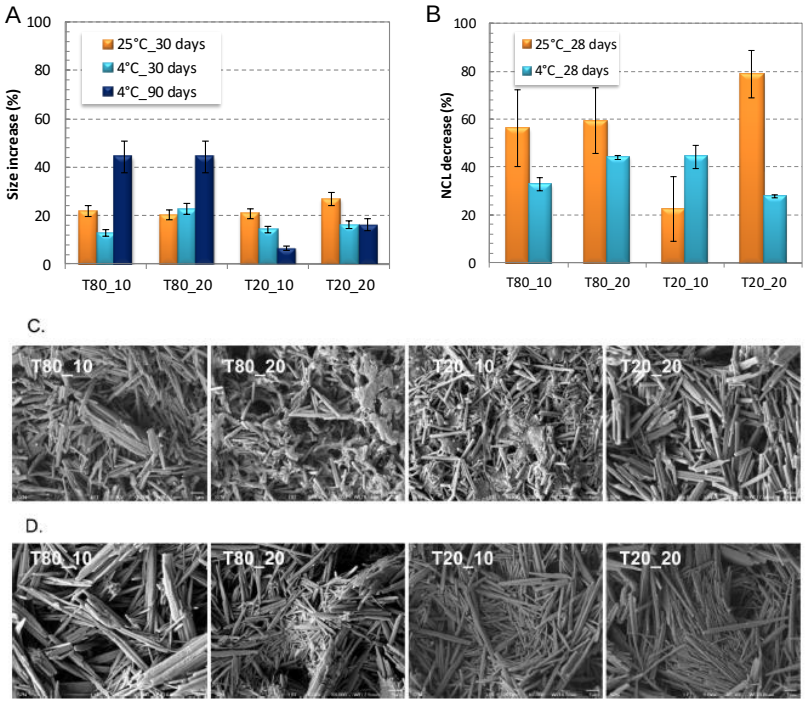

Figure 2.6. Physical stability of NCL nanosuspensions at room temperature (25 ± 2°C) and 4°C over time: (A) Percent increase of hydrodynamic diameter; (B) percent decrease of NCL content in supernatant; (C) SEM images of NCL nanosuspensions after storage for 30 days at room temperature; (D) SEM images of NCL nanosuspensions after storage for 90 days at 4 °C (field is representative of the sample).

In each case, a 25% increase in the particle hydrodynamic diameter compared to the original value was observed after 1 month of storage at room temperature (Fig. 2.6A). Apart from the T80_10 and T20_20 formulations, the increase in size was not always related to an increase of the PI value (Fig. 2.7)

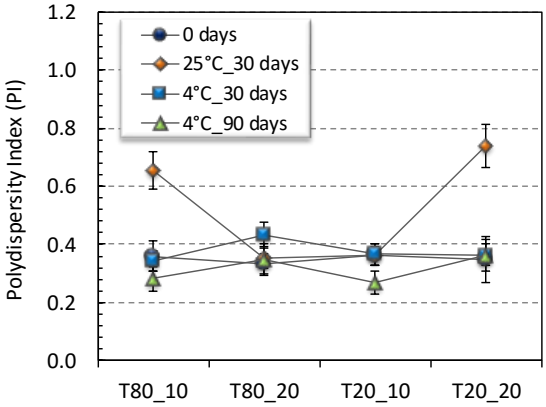

.

Figure 2.7. PI values of NCL nanosuspensions upon storage at room temperature (25 ± 2°C) and 4°.

Nevertheless, the occurrence of nanocrystal aggregation upon storage at room temperature was evident from SEM analysis of T80_20 and T20_10 formulations (Fig. 2.6C). Upon storage at 4°C for 1 month, a 13-14% increase of size was observed for T80_10 and T20_10 formulations, whereas it was slightly higher for T80_20 (22.6%) and T20_20 (16.2%) nanosuspensions (Fig. 2.6A). The size of nanocrystals was less stable after 3 months of storage (Fig. 2.6A), and a great increase in nanocrystal length was evident from SEM analysis of the stored samples (Fig. 2.6A). Again, the variations in particle size were not related to a variation in the PI value, which was almost constant at 4°C for up to 3 months (Fig. 2.7). Nevertheless, a progressive decrease in the amount of solubilized NCL was observed up to 1 month, both at 25°C and 4°C (Fig. 2.6B).

2.3.3. Development of nanocrystal-embedded dry powders

To improve the long-term stability of the optimized T80_10 nanosuspension, nanocrystal-embedded dry powders were produced through either lyophilization or spray drying using mannitol as a stabilizer. When the nanocrystals underwent the lyophilization process, massive particle aggregation was observed, independently of the freezing procedure or the presence of mannitol as a cryoprotectant (Fig. 2.8).

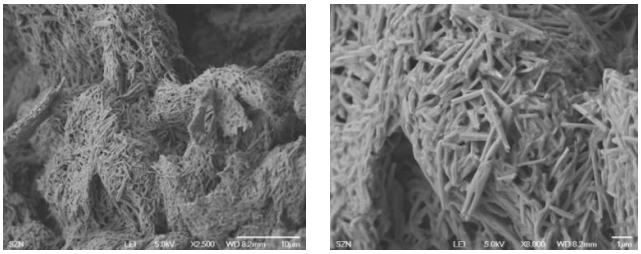

Figure 2.8. SEM photographs of T80_10 nanosuspensions upon freeze-drying without cryoprotectant at different magnifications. Field is representative of the sample.

To overcome this issue, dry powders containing different amounts of mannitol were produced by spray drying. The RDI of the spray-dried powder was decreased by increasing the amount of stabilizer in the nanosuspension up to a minimum value of 1.35 when the NCL/mannitol ratio by weight was 1:10. At this NCL/mannitol ratio, a homogeneous population of mannitol-based spherical particles, named T80_10 DP, was achieved (Fig.2.9).

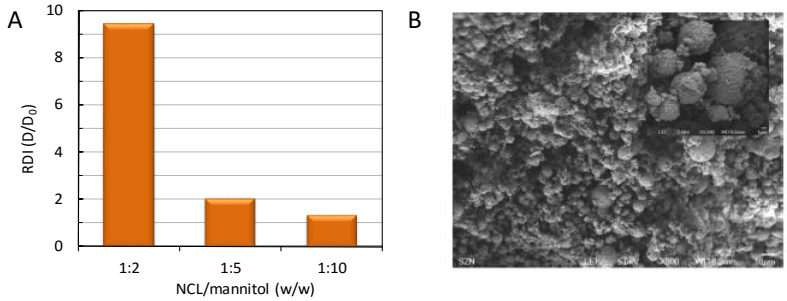

Figure 2.9. Nanocrystal-embedded dry powders produced by spray drying: A) RDI of spray-dried powders prepared at different NCL/mannitol ratios by weight (optimal value at 1:10 w/w); B) SEM images of optimized powders (T80_10 DP) at different magnifications (fields are representative of the sample).

The presence of some NCL nanocrystals on the particle surface was evident by SEM and confirmed by DSC studies (Fig. 2.10).

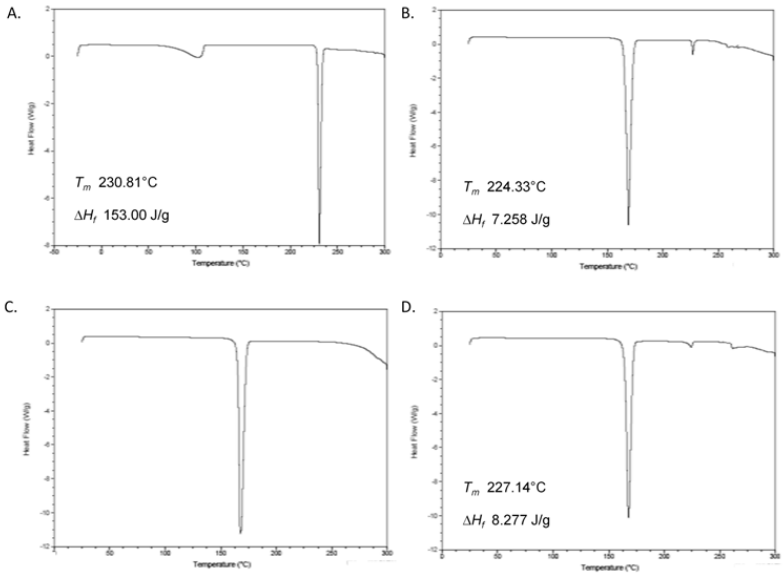

Figure 2.10. DSC thermograms and corresponding values of NCL melting temperature (T_m) and heat of fusion (ΔH_f): A) raw NCL; B) T80_10 DP. Thermograms of mannitol (C) and mannitol/raw NCL physical mixture (D) are reported as control.

DSC thermograms of raw NCL displayed a dehydration endothermic peak at approximately 100°C and a sharp endothermic melting peak at approximately 230°C, typical of the NCL monohydrate crystal forms[32]. The corresponding ΔH_f was 153 ± 2 J/g. T80_10 DP exhibited two endothermic peaks at 168°C and 224°C, ascribable to the melting of mannitol and NCL crystals, respectively, in the T80_10 DP powders. Upon peak integration, ΔH_f associated to NCL melting was 7.3 ± 0.1 J/g, a value comparable to that calculated from the simple physical mixture of mannitol and NCL at the same ratio by weight (i.e., 8.3± 0.2 J/g). In both cases, a shift of the endothermic peak to a lower value (from 230°C to 224°C) and a corresponding reduction of ΔH_f was observed compared to the NCL raw material, indicating a partial interaction with mannitol and consequent amorphization of NCL. Results of *in vitro* release studies of NCL performed by membrane dialysis from simulated CF mucus to SILF are reported in Figure 2.10 as the percentage of NCL

diffused over time. No pronounced difference in the percentage of NCL diffused after 8 h was observed between T80_10 DP (58.1 ± 6.5%) and T80_10 (63.3 ± 8.0%). In contrast, the diffusion rate of Micro NCL slowed down significantly, and after 8 h, only 22.9 ± 1.3% of the amount of NCL initially dispersed in mucus was found in the external medium.

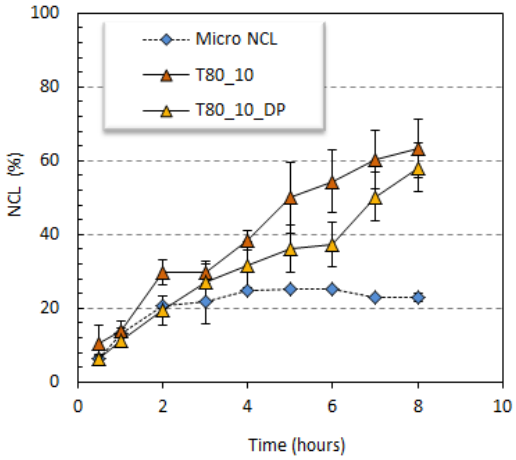

Figure 2.10. *In vitro* release profile of NCL from T80_10 and T80_10 DP from artificial CF mucus to SILF at 37°C. Data are presented as mean ± standard deviation (*n*=3).

2.3.4 *In vitro* aerosol performance of optimized formulations

In vitro aerosol performance of the T80_10 nanosuspension before and after spray drying (T80_10 DP) was assessed through NGI. According to the new regulatory guidelines, both USP and Ph.Eur. recognize the suitability of the NGI for nebulizer characterization when used at 15 L/min, excluding the pre-separator and placing an internal filter below the MOC[26].

In this configuration, the seven NGI stages produce cutoff diameters in the range of 14.1-0.98 μm, while the last five stages have cutoff diameters between 5.39 and 0.98 μm. Figure 2.11A and Figure 2.12A describe the cumulative droplet size distribution of the emitted dose of T80_10 nanosuspension and T80_10 DP after reconstitution in saline, respectively, from PARI TurboBOY®, eFlow®rapid and Aeroneb® Go.

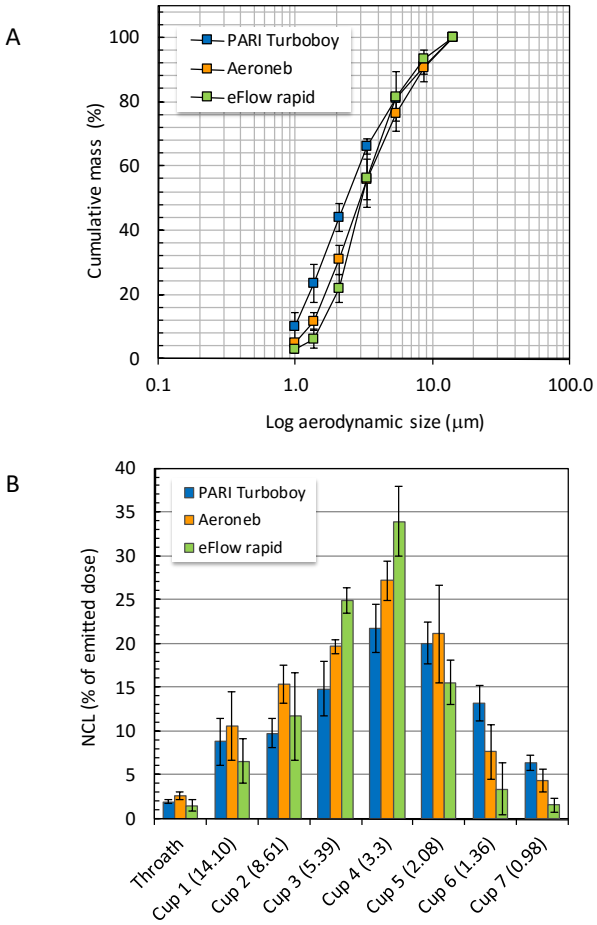

Figure 2.11. *In vitro* aerosol performance of T80_10 nanosuspensions: A. Cumulative mass recovered as a function of the cut-off diameter; B. NGI deposition pattern. The formulation was delivered through PARI TurboBOY® (PARI GmbH, Germany), eFlow® rapid (PARI GmbH, Germany) and Aeroneb® Go (Aerogen, Ireland) nebulizers. Data are presented as mean ± standard deviation (*n*=3).

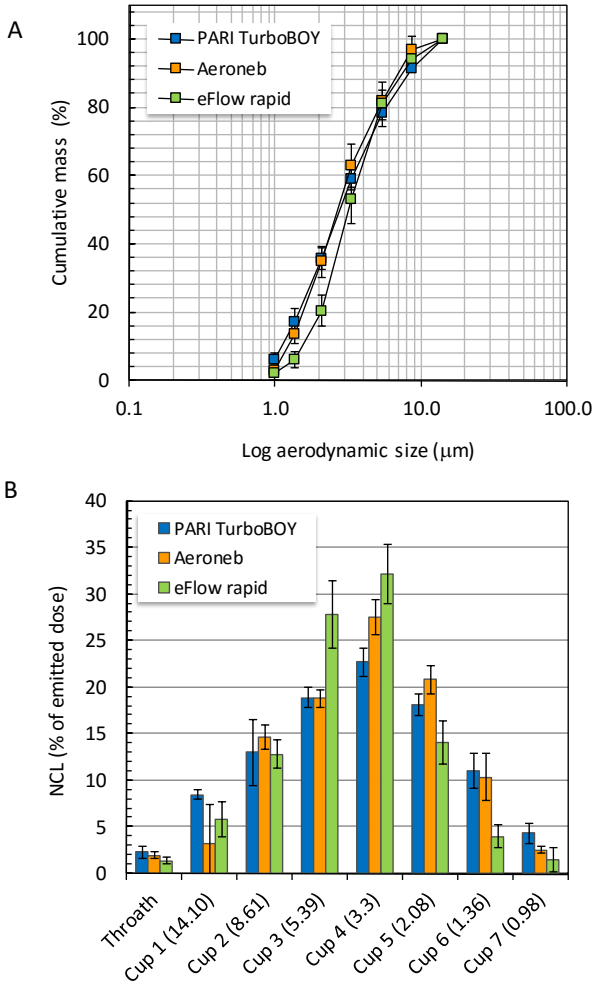

Figure 2.12. *In vitro* aerosol performance of T80_10 DP dry powders for inhalation suspension: A. Cumulative mass recovered as a function of the cut-off diameter; B. NGI deposition pattern. The formulation was delivered through PARI TurboBOY® (PARI GmbH, Germany), eFlow® rapid (PARI GmbH, Germany) and Aeroneb® Go (Aerogen, Ireland) after reconstitution in an appropriate amount of isotonic saline. Data are presented as mean ± standard deviation (*n*=3).

In each case, the best fit line was from logarithmic linear regression (r^2 = 0.96). The calculated values of MMAD are reported in Table 2.3. T80_10 showed an experimental MMAD of approximately 3 μm, independent of the nebulizer employed, whereas an increase of MMAD up to 5 μm was observed for the T80_10

DP dry powder for inhalation solution upon delivery from the eFlow® rapid system. Of note, the GSD of the lognormal distribution was always higher than 1 with values falling within the range of 2.34-2.68 and 2.18-2.49 for T80_10 and T80_10 DP, respectively (Table 2.3).

Table 2.3. Fine particle characteristics of the aerosol clouds generated upon delivery of T80_10 liquid nanosuspension and T80_10 DP powder for inhalation solution through different nebulizer systems.

	PARI® TurboBOY™		***Aeroneb® Pro***		***eFlow® rapid***	
	T80_10	**T80_10 DP**	**T80_10**	**T80_10 DP**	**T80_10**	**T80_10 DP**
MMAD (μm ± SD)	2.64 ± 0.20	3.01 ± 0.18	3.22 ± 0.19	2.98 ± 0.26	3.17 ± 0.12	5.05 ± 0.40
GSD (± SD)	2.68 ± 0.22	2.49 ± 0.074	2.41 ± 0.030	2.35 ± 0.020	2.34 ± 0.094	2.18 ± 0.012
FPF* (% ±SD)	49.0 ± 7.1	27.5 ± 3.9	53.6 ± 0.81	37.4 ± 1.5	30.1 ± 7.8	24.2 ± 2.7
RF* (% ±SD)	76.1 ± 4.7	74.8 ± 3.6	73.6 ± 9.0	79.8 ± 5.4	79.2 ± 9.0	79.3 ± 3.1

*FPF was calculated on the nominal NCL dose, whereas the RF refers to the emitted dose of NCL.

The deposition pattern of NCL throughout the NGI cups upon nebulization of T80_10 formulations showed a peak at 3.3 μm with 25-35% of the emitted dose recovered from Cup 4 independent of the nebulizer system (Figure 2.11B). In each case, less than 2.5% of the emitted NCL dose was deposited in the throat. Of note, 55-60% of the particles were < 3.3 μm, and 75-80% of the particles were < 5.39 μm. Again, no significant difference in the deposition pattern was observed when T80_10 DP dry powder for inhalation solution was nebulized (Figure 2.11B). When calculated on the actual amount of NCL deposited on NGI cups with a cut-off diameter of less than 5.39 μm (cups 3-7), FPF values of T80_10 nanosuspensions ranged from 30.1 to 53.6% (Table 2.3). The lowest value was achieved upon particle aerosolization through the eFlow® rapid system, whereas similar FPF (≈50%) were calculated for PARI TurboBOY® and Aeroneb® Go. In each case, the FPF values

decreased for T80_10 DP compared to the T80_10 fresh nanosuspension with a maximum value of 37.4% when using the Aeroneb® Go device. The differences in the FPF values were reflected by a different percent of NCL remaining inside the device chamber upon aerosolization. The amount of NCL remaining inside the nebulizer upon delivery through the NGI was quantitatively recovered and determined by dissolution in 2 ml of methanol (Figure 2.13).

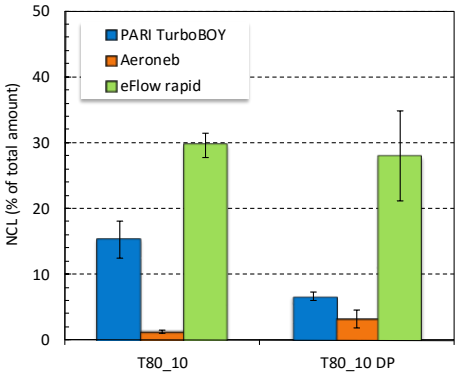

Figure 2.13. Amount of NCL remaining inside the nebulizer upon delivery through the NGI. Data are presented as percent of NCL total amount loaded inside nebulizer chamber ± standard deviation (*n*=3).

2.3.5 QS inhibitory activity in *Pseudomonas aeruginosa*

The ability of the NCL formulations T80_10 and T80_10 DP and of the NCL raw powder dissolved in DMSO to inhibit $3OC_{12}$-HSL-dependent QS in *P. aeruginosa* was compared by using the whole cell biosensor PA14-R3. This biosensor is a *P. aeruginosa* engineered strain that emits bioluminescence in response to $3OC_{12}$-HSL-dependent QS signaling[27]. A preliminary control experiment was carried out in order to test the effect of increasing concentrations of DMSO, T80 and T80 *plus* mannitol on the PA14-R3 response. The results showed that PA14-R3 bioluminescence emission was not affected by these substances at the concentrations used in our experimental setting (data not shown).

In accordance with previous studies[13], 1.25 µM NCL in DMSO was able to inhibit the biosensor response at approximately 60% with respect to the untreated control.

Interestingly, the QS inhibitory effect of the NCL formulated as T80_10 was comparable to that of NCL at any concentration tested. However, the NCL formulated as T80_10 DP was less active than the other NCL formulations, showing inhibitory activity similar to T80_10, and unformulated NCL showed inhibitory activity at concentrations in the range of 2.5 - 10 µM (Fig. 2.14).

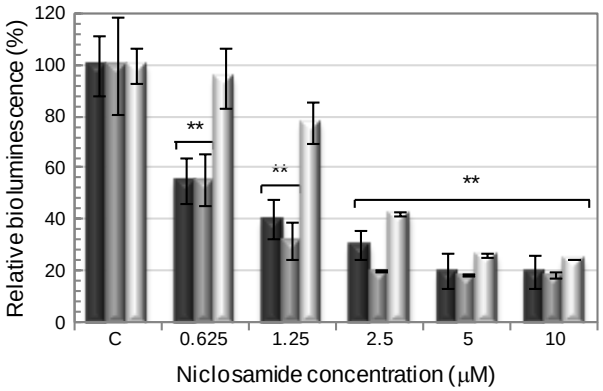

Figure 2.14. QS inhibitory activity of NCL formulations. The NCL-dependent inhibition of the *P. aeruginosa* QS response was measured as inhibition of luminescence emission by the PA14-R3 biosensor. Black bars, NCL in DMSO; dark grey bars, T80_10; light grey bars, T80_10 DP. Bioluminescence was normalized to the cell density of the bacterial culture (relative bioluminescence, $LCPS/A_{600}$) and expressed as a percentage relative to controls (indicated as C), corresponding to DMSO for the raw powder, T80for T80_10, and T80 plus mannitol for T80_10 DP at the same concentrations as in the samples containing 10 µM NCL. Values are the mean (± standard deviation) of three independent experiments. Asterisks indicate statistically significant differences ($p< 0.01$; ANOVA) with respect to the corresponding controls.

2.3.6 Cytotoxicity to CF bronchial epithelial cells

The cytotoxicity of the different NCL formulations against a CF bronchial epithelial cell line (CFBE41o) was assessed using the MTT assay. As shown in Figure 10, NCL did not significantly affect cell viability at any concentration tested (1-1000 µM), although slight toxicity was observed at 1000 µM. However, the reduction in cell viability was comparable to that obtained for the corresponding control (5% DMSO), thus hampering the evaluation of NCL cytotoxicity at very high concentrations. On the other hand, NCL nanosuspensions showed significant reductions of CFBE41o viability at concentrations corresponding to 100 µM

(T80_10) and 1000 µM NCL (both formulations), while the corresponding controls did not cause significant toxicity (Fig. 2.15).

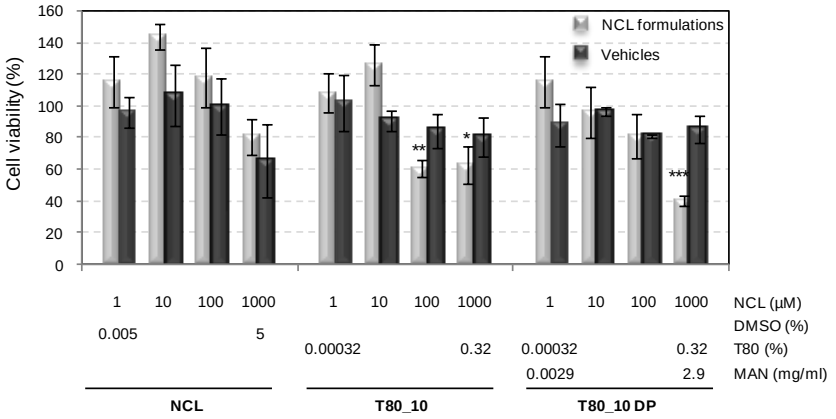

Figure 2.15. Cytotoxicity of NCL formulations to CFBE cells. Cell viability was assessed after 3-h incubation in the presence of NCL dissolved in DMSO, T80_10 or T80_10 DP at 1, 10, 100 or 1000 µM NCL concentrations (grey histograms) or their relative vehicles at the corresponding concentrations (black histograms; only the highest and lowest concentrations of each vehicle are indicated in the figure). Results are expressed as percentage of cell viability with respect to untreated controls (100%). Data are the mean ± standard deviation of 3 experiments performed in duplicate. Asterisks indicate statistically significant reduction in cell viability with respect to untreated controls (*, $p< 0.05$; **, $p< 0.01$; ***, $p< 0.001$) . Abbreviations: T80, Tween 80; MAN, mannitol.

Of note, the toxic concentration at 50% (TC_{50}) was only reached for T80_10DP (corresponding to 600 µM; data not shown), suggesting that the overall toxicity of NCL is quite low. Moreover, this assay clearly demonstrated that, at microbiologically-active concentrations (≤ 10 µM, see Fig. 2.14), NCL and its formulations do not significantly affect the viability of CF bronchial epithelial cells *in vitro*.

2.3.7 Lung acute toxicity in rats

Acute toxicity and pulmonary injury in rats at 24 h after intra-tracheal administration of NCL T80_10 DP were evaluated. To this end, the cellular infiltrate into rat airways after treatment was investigated. There was no significant difference in the volume of BALF recovered from each animal and within each treated group (data not shown). In addition, lung accumulation of macrophages (A) and neutrophils (B)

are reported in Figure 11. Of note, NCL doses of 10 and 30 µg/rat contained in T80_10DP did not cause differences in lung accumulation of both cells when compared to sham operated animals. On the other hand, a significant increase of cell number at 24 h ($p<0.001$) was observed with the NCL dose of 100 µg/rat compared to sham group (Fig. 2.16A and B). Total protein amount measured in each BALF, evaluated as an index of lung damage, revealed no significant differences in the samples from rats treated with the formulation at the equivalent NCL dose of 100 µg/rat (Fig. 2.17 A). To evaluate tissue injury and toxicity of NCL-loaded T80_10 DP, we also measured iNOS and COX-2 enzyme expression in lung homogenates at 24 h; these are considered to be markers of the inflammatory process. No iNOS expression was observed in lung homogenates from all animals of each group (data not shown). As reported in Fig. 2.17 (panel B), no significant difference was observed in COX-2 protein expression 24 h after treatment at all doses used.

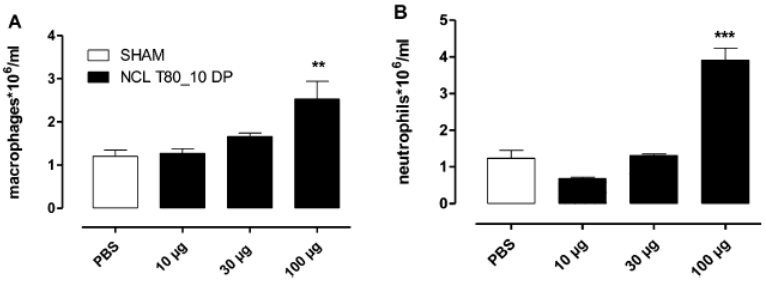

Figure 2.16. A. Macrophage in BAL 24 h after treatments. Sham (PBS 50 µL) and NCL T80_10 DP (10, 30 or 100 µg/50 µL/rat). B. Neutrophils in BAL 24 h after treatments. Sham (PBS 50 µL) and NCL T80_10 DP (10, 30 or 100 µg/50 µL/rat). The results are expressed as mean ± S.E.M. (n = 4 rats *per* group at each dose). ***p*< 0.01 and ****p*< 0.001 *versus* SHAM/PBS group.

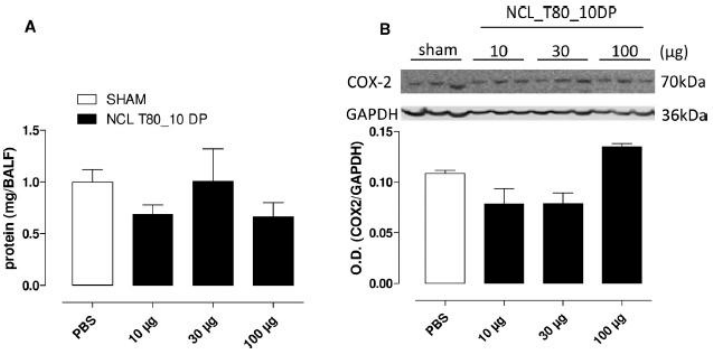

Figure 2.17. (A) Protein evaluation in BALF 24 h after treatment with PBS (50 µL) or NCL T80_10 DP (10, 30, or 100 µg/50 µL/rat). (B) COX-2 Western blot analysis reported as optical densitometric (O.D.) evaluation in lung homogenate 24 h after treatment with PBS (50 µL) or NCL T80_10 DP (10, 30, or 100 µg/50 µL/rat). Densitometric data are normalized to GAPDH and expressed as the mean ± standard error of the mean of three experiments.

2.4. DISCUSSION

Repurposing commercially available drugs for new therapeutic applications is an approach that has been used frequently in recent years. Approximately one out of four drugs/biologics that were approved in 2014 consisted of new formulations, new combinations or new therapeutic applications of existing drugs.[35] Nevertheless, the success of drug repositioning depends not only on the existing knowledge but also on available information from specific drug- and disease-oriented studies allowing for the selection and determination of the most appropriate repurposing approach.[33,34] Along these lines, in this work, nanocrystal-embedded dry powders generated into inhalable nanosuspensions by dilution in saline are proposed for repositioning of the poorly soluble anthelmintic drug NCL as an inhaled anti-virulence agent against *P. aeruginosa*, the dominant pathogen in the airways of CF patients.

NCL nanocrystals were produced through high-pressure homogenization, an industrially scalable process. To formulate NCL nanosuspensions for lung delivery, polysorbate 20 and polysorbate 80, two excipients already employed in marketed inhaled drugs[36], were chosen as stabilizers of the dispersion and tested at different concentrations. Preliminary technological studies were crucial to assess optimal HPH processing parameters, with particular regard to the number of homogenization cycles required to achieve consistent nanocrystal size distributions, a key parameter that drives the performance of nanosuspensions.[20] In accordance with the Noyes-Whitney theory, the greater surface to volume ratio of NCL nanocrystals compared to the micronized material is expected to increase the dissolution rate of the active ingredient by raising its saturation solubility and dissolution rate.[19] In fact, the dissolution profile of NCL in simulated lung fluids was strongly influenced by nanosizing with T80_10 nanosuspensions showing a significantly increased dissolution velocity compared to micronized NCL.

Because nanosizing results in the creation of new interfaces and in a positive Gibbs free energy change, nanosuspensions are also thermodynamically unstable systems with a tendency toward crystal growth or agglomeration.[37] Particle size growth is

largely responsible for agglomeration, and this was particularly evident upon storage of the nanosuspensions at 25°C. Since lower levels of nanoparticles agglomeration are expected upon decreasing the temperature (i.e., lower kinetic energy) of the system[37], suspension stability was expected to be improved at lower temperatures; however, aggregation and nanocrystal growth was observed after 3 months of storage at 4°C. Many reports have indicated that an increase in the intrinsic solubility of a drug mediated by a surfactant, including polysorbate 80, would lead to Ostwald ripening, when small crystals dissolve and redeposit onto larger crystals.[37] This effect typically results in an increase in the length of needle-shaped nanocrystals achieved by HPH during storage. On the other hand, a solution-mediated transformation of NCL nanocrystals upon exposure to water, with consequent transformation to round needles typical of NCL monohydrate, could not be excluded on the basis of DSC analysis[32,38]. Of note, this phenomenon is regarded as the greatest challenge in formulating physically stable and pharmaceutically acceptable NCL suspensions, since it generates a cement-like sediment during storage.[32,39]

In light of the observed suspension instability, NCL nanosuspensions were further processed to achieve a dry powder with long-term stability that could be reconstituted before use. The attention was focused on the T80_10 formulation, which not only showed the best solubility profile but also a lower amount of surfactant compared to T80_20. In principle, a nanosuspension can be processed into a solid dosage form using a well-established unit operation, such as freeze drying.[40] Nevertheless, polysorbate 80 is a liquid at room temperature, and therefore, nanocrystal adhesion and aggregation is very likely during drying[41] and could not be prevented using mannitol. As a viable alternative, nanocrystal-embedded dry powders were produced by spray drying in mannitol. This can be regarded as a "multifunctional" excipient, since it may prevent particle agglomeration in the dried state[42], improve the solubility profile of drug nanocrystals[43] and loosen CF mucus[44], potentially enhancing drug penetration.[45] Indeed, release data highlighted how NCL dissolution may be strongly reduced in a mucin-rich environment that more closely

resembles *in vivo* conditions, while the formulation facilitated diffusion of NCL through artificial CF mucus.

In each case, the aerodynamic assessment of fine particles upon delivery from several nebulizers that are among the most widely employed in clinical practice confirmed that the developed formulation has a great potential to improve the lung deposition of NCL. Higher FPF and lower MMAD values were achieved compared to commercial liquid suspensions for inhalation tested in similar conditions.[23] The best performances were achieved with the PARI® TurboBOY™, a conventional system relying on a compressor combined with a jet nebulizer, and the Aeroneb® Pro, which is a VMT nebulizer. As recently reported for inhalable itraconazole nanosuspensions[46], the ParieFlow® Rapid vibrating mesh nebulizer maybe less suited for nanosuspension aerosolization because higher amounts of residual dose within the nebulizer reservoir were observed for this device compared to the other devices tested. This is a well-established limitation of some VMT-based nebulizer systems, which may be overcome by modifying the priming dose of medication used.[24]

Assuming that the inhaled formulation successfully lands in the lung and cross the extracellular barriers, NCL has still to inhibit the $3OC_{12}$-HSL-dependent QS signaling system of *P. aeruginosa* to be effective. Our results demonstrate that the QS inhibitory activity of NCL formulated as T80_10 or T80_10 DPis was equivalent to that of the unformulated NCL pre-dissolved in DMSO. NCL formulations showed maximum anti-QS activity at NCL concentrations ≥ 5 µM, corresponding to ca. 80% inhibition of the *P. aeruginosa* QS response, although significant effects were also observed at 1-2.5 µM concentrations. These concentrations are 40-400-fold lower than the NCL concentrations that show toxicity to CF bronchial epithelial cells, suggesting that there is a wide therapeutic range that can be explored for repurposing NCL as an anti-*P. aeruginosa* drug in CF therapy. Notably, it has recently been shown that NCL also displays promising anticancer activities, and the potential of this drug as an anticancer agent has been demonstrated in several animal models (reviewed in[47]) Reports suggest that NCL had no significant toxicity to non-tumor cells *in vitro* and no obvious side effects in NCL-treated mice.[47] Moreover,

toxicity studies in different mammalian models suggested that NCL has no mutagenic, oncogenic or embryotoxic activity, even after long-term treatment (reviewed in[48]). In the present study, *in vivo* toxicity studies in rodents support the safety of NCL upon local pulmonary administration because no toxicity was observed after intratracheal administration of a single dose of 30 µg, roughly 100 times the maximum concentration that showed *in vitro* anti-QS activity. Local toxicity/inflammatory activity, such as lung accumulation of macrophages/neutrophils not related to COX-2 and iNOS expression, was observed only after intratracheal administration of a single dose of 100 µg of NCL, which is approximately 400-fold higher than the anti-QS activity concentrations.

2.5. CONCLUSION

In this work, NCL nanocrystals formulated as a dry powder for reconstitution using excipients approved for lung delivery in order to be delivered as a nebulized aerosol from a liquid dispersion were successfully produced through a 2-step process involving industrially scalable techniques (i.e., high-pressure homogenization and spray drying). The use of appropriate surfactant types and concentrations allowed the production of nanocrystals with suitable properties for pulmonary delivery. NCL nanoparticles were successfully spray dried and suspended in a solution containing mannitol. NCL nanosuspensions, prepared from reconstitutions of spray-dried particles in saline solution, were effectively delivered through nebulizers commonly used to deliver antibiotics to CF patients. The ability of nanosuspensions to inhibit *P. aeruginosa* QS at NCL concentrations that do not significantly affect the viability of CF bronchial epithelial cells was demonstrated *in vitro*. Finally, *in vivo* data confirmed the absence of acute toxicity effects of NCL nanosuspensions at the proposed therapeutic doses.

Overall, the presented experimental evidence provides the rationale for further development of NCL, an anti-virulence drug, as an alternative CF therapy and prompts the investigation of the anti-*P. aeruginosa* activity of the inhalable NCL formulations here developed in animal models of pulmonary infection. Repurposing a known drug, such as NCL, for inhalation to treat lung infections in CF patients may also result in considerable reduction in the cost of product development compared to developing new chemical entities.

References

1. Horsley, A.; Cunningham, S.; Innes, J. A. *Cystic Fibrosis;* Oxford University Press: New York (USA), 2010.

2. O'Sullivan, B. P.; Freedman, S. D. Cystic fibrosis. *Lancet.***2009,***373* (9678), 1891-1904.

3. Ratjen, F. A. Cystic fibrosis: pathogenesis and future treatment strategies. *Respir. Care.***2009,***54* (5), 595-605.

4. Doring, G.; Worlitzsch, D. Microbiology of CF lung disease. In *Cystic Fibrosis*, Horsley, A., Cunningham, S., Innes, J. A., Eds.; Oxford University Press: New York, USA, 2010; pp 31-44.

5. Rogers, G. B.; Hoffman, L. R.; Doring, G. Novel concepts in evaluating antimicrobial therapy for bacterial lung infections in patients with cystic fibrosis. *J. Cyst. Fibros.***2011,***10* (6), 387-400.

6. Rasko, D. A.; Sperandio, V. Anti-virulence strategies to combat bacteria-mediated disease. *Nat. Rev. Drug Discov.***2010,***9* (2), 117-128.

7. Allen, R. C.; Popat, R.; Diggle, S. P.; Brown, S. P. Targeting virulence: can we make evolution-proof drugs? *Nat. Rev. Microbiol.***2014,***12* (4), 300-308.

8. Lee, D. G.; Urbach, J. M.; Wu, G.; Liberati, N. T.; Feinbaum, R. L.; Miyata, S.; Diggins, L. T.; He, J.; Saucier, M.; Deziel, E.; Friedman, L.; Li, L.; Grills, G.; Montgomery, K.; Kucherlapati, R.; Rahme, L. G.; Ausubel, F. M. Genomic analysis reveals that Pseudomonas aeruginosa virulence is combinatorial. *Genome Biol.***2006,***7* (10), R90.

9. Williams, P.; Camara, M. Quorum sensing and environmental adaptation in Pseudomonas aeruginosa: a tale of regulatory networks and multifunctional signal molecules. *Curr. Opin. Microbiol.***2009,***12* (2), 182-191.

10. Schuster, M.; Sexton, D. J.; Diggle, S. P.; Greenberg, E. P. Acyl-homoserine lactone quorum sensing: from evolution to application. *Annu. Rev. Microbiol.***2013,***67:43-63. doi: 10.1146/annurev-micro-092412-155635. Epub;%2013 May 15.*, 43-63.

11. LaSarre, B.; Federle, M. J. Exploiting quorum sensing to confuse bacterial pathogens. *Microbiol. Mol. Biol. Rev.***2013,***77* (1), 73-111.

12. Rampioni, G.; Leoni, L.; Williams, P. The art of antibacterial warfare: Deception through interference with quorum sensing-mediated communication. *Bioorg. Chem.***2014,***55:60-8. doi: 10.1016/j.bioorg.2014.04.005. Epub;%2014 Apr 21.*, 60-68.

13. Imperi, F.; Massai, F.; Ramachandran, P. C.; Longo, F.; Zennaro, E.; Rampioni, G.; Visca, P.; Leoni, L. New life for an old drug: the anthelmintic drug niclosamide inhibits Pseudomonas aeruginosa quorum sensing. *Antimicrob. Agents Chemother.***2013,***57* (2), 996-1005.

14. Heijerman, H.; Westerman, E.; Conway, S.; Touw, D.; Doring, G. Inhaled medication and inhalation devices for lung disease in patients with cystic fibrosis: A European consensus. *J. Cyst. Fibros.***2009,***8* (5), 295-315.

15. Gaspar, M. C.; Couet, W.; Olivier, J. C.; Pais, A. A.; Sousa, J. J. Pseudomonas aeruginosa infection in cystic fibrosis lung disease and new perspectives of treatment: a review. *Eur. J. Clin. Microbiol. Infect. Dis.***2013,***32* (10), 1231-1252.

16. d'Angelo, I.; Conte, C.; La Rotonda, M. I.; Miro, A.; Quaglia, F.; Ungaro, F. Improving the efficacy of inhaled drugs in cystic fibrosis: Challenges and emerging drug delivery strategies. *Adv. Drug Deliv. Rev.***2014,***75C*, 92-111.

17. Devarakonda, B.; Hill, R. A.; Liebenberg, W.; Brits, M.; de Villiers, M. M. Comparison of the aqueous solubilization of practically insoluble niclosamide by polyamidoamine (PAMAM) dendrimers and cyclodextrins. *Int. J. Pharm.***2005,***304* (1-2), 193-209.

18. Rabinow, B. E. Nanosuspensions in drug delivery. *Nat. Rev. Drug Discov.***2004,***3* (9), 785-796.

19. Muller, R. H.; Gohla, S.; Keck, C. M. State of the art of nanocrystals--special features, production, nanotoxicology aspects and intracellular delivery. *Eur. J. Pharm. Biopharm.***2011,***78* (1), 1-9.

20. Chavhan, S. S.; Petkar, K. C.; Sawant, K. K. Nanosuspensions in drug delivery: recent advances, patent scenarios, and commercialization aspects. *Crit Rev. Ther. Drug Carrier Syst.***2011,***28* (5), 447-488.

21. Jacobs, C.; Muller, R. H. Production and characterization of a budesonide nanosuspension for pulmonary administration. *Pharm. Res.***2002,***19* (2), 189-194.

22. Chiang, P. C.; Hu, Y.; Blom, J. D.; Thompson, D. C. Evaluating the suitability of using rat models for preclinical efficacy and side effects with inhaled corticosteroids nanosuspension formulations. *Nanoscale. Res. Lett.***2010,***5* (6), 1010-1019.

23. Britland, S.; Finter, W.; Chrystyn, H.; Eagland, D.; Abdelrahim, M. E. Droplet aerodynamics, cellular uptake, and efficacy of a nebulizable corticosteroid nanosuspension are superior to a micronized dosage form. *Biotechnol. Prog.***2012,***28* (5), 1152-1159.

24. Daniels, T.; Mills, N.; Whitaker, P. Nebuliser systems for drug delivery in cystic fibrosis. *Cochrane. Database. Syst. Rev.***2013,***4:CD007639.*

25. Marques, M. R. C.; Loebenberg, R.; Almukainzi, M. Simulated Biological Fluids with Possible Application in Dissolution Testing. *Dissolution Technologies***2011,***18* (3), 15-28.

26. Marple, V. A.; Olson, B. A.; Santhanakrishnan, K.; Roberts, D. L.; Mitchell, J. P.; Hudson-Curtis, B. L. Next generation pharmaceutical impactor: a new impactor for pharmaceutical inhaler testing. Part III. extension of archival calibration to 15 L/min. *J. Aerosol Med.***2004,***17* (4), 335-343.

27. Massai, F.; Imperi, F.; Quattrucci, S.; Zennaro, E.; Visca, P.; Leoni, L. A multitask biosensor for micro-volumetric detection of N-3-oxo-dodecanoyl-homoserine lactone quorum sensing signal. *Biosens. Bioelectron.***2011,***26* (8), 3444-3449.

28. Gruenert, D. C.; Willems, M.; Cassiman, J. J.; Frizzell, R. A. Established cell lines used in cystic fibrosis research. *J. Cyst. Fibros.***2004,***3 Suppl 2*, 191-196.

29. Lanone, S.; Rogerieux, F.; Geys, J.; Dupont, A.; Maillot-Marechal, E.; Boczkowski, J.; Lacroix, G.; Hoet, P. Comparative toxicity of 24 manufactured nanoparticles in human alveolar epithelial and macrophage cell lines. *Part Fibre. Toxicol.***2009,***6*, 14.

30. De Stefano, D.; Coletta, C.; Bianca, R.; Falcone, L.; d'Angelo, I.; Ungaro, F.; Quaglia, F.; Carnuccio, R.; Sorrentino, R. A decoy oligonucleotide to NF-kappaB delivered through inhaleable particles prevents LPS-induced rat airway inflammation. *Am. J. Respir. Cell Mol. Biol.***2013,***49* (2), 288-295.

31. d'Emmanuele, d., V; Mitidieri, E.; Donnarumma, E.; Tramontano, T.; Brancaleone, V.; Cirino, G.; Bucci, M.; Sorrentino, R. Hydrogen sulfide is involved in dexamethasone-induced hypertension in rat. *Nitric. Oxide.***2014,** (14), 10.

32. van Tonder, E. C.; Maleka, T. S.; Liebenberg, W.; Song, M.; Wurster, D. E.; de Villiers, M. M. Preparation and physicochemical properties of niclosamide anhydrate and two monohydrates. *Int. J. Pharm.***2004,***269* (2), 417-432.

33. Cipolla, D.; Gonda, I. Formulation technology to repurpose drugs for inhalation delivery. *Drug Discovery Today***2011,***8* (3-4), 123-130.

34. Law, G. L.; Tisoncik-Go, J.; Korth, M. J.; Katze, M. G. Drug repurposing: a better approach for infectious disease drug discovery? *Curr. Opin. Immunol.***2013,***25* (5), 588-592.

35. Graul, A. I.; Cruces, E.; Stringer, M. The year's new drugs & biologics, 2014: Part I. *Drugs Today (Barc.)***2015,***51* (1), 37-87.

36. Pilcer, G.; Amighi, K. Formulation strategy and use of excipients in pulmonary drug delivery. *Int. J. Pharm.***2010,***392* (1-2), 1-19.

37. Wang, Y.; Zheng, Y.; Zhang, L.; Wang, Q.; Zhang, D. Stability of nanosuspensions in drug delivery. *J. Control Release***2013,***172* (3), 1126-1141.

38. de Villiers, M. M.; Mahlatji, M. D.; Malan, S. F.; van Tonder, E. C.; Liebenberg, W. Physical transformation of niclosamide solvates in pharmaceutical suspensions determined by DSC and TG analysis. *Pharmazie.***2004,***59* (7), 534-540.

39. de Villiers, M. M.; Mahlatji, M. D.; van Tonder, E. C.; Malan, S. F.; Lotter, A. P.; Liebenberg, W. Comparison of the physical and chemical stability of niclosamide crystal forms in aqueous versus nonaqueous suspensions. *Drug Dev. Ind. Pharm.***2004,***30* (6), 581-592.

40. Van, E. B.; Van Den Mooter, G.; Augustijns, P. Top-down production of drug nanocrystals: nanosuspension stabilization, miniaturization and transformation into solid products. *Int. J. Pharm.***2008,***364* (1), 64-75.

41. Teeranachaideekul, V.; Junyaprasert, V. B.; Souto, E. B.; Muller, R. H. Development of ascorbyl palmitate nanocrystals applying the nanosuspension technology. *Int. J. Pharm.***2008,***354* (1-2), 227-234.

42. Yamasaki, K.; Kwok, P. C.; Fukushige, K.; Prud'homme, R. K.; Chan, H. K. Enhanced dissolution of inhaleable cyclosporine nano-matrix particles with mannitol as matrix former. *Int. J. Pharm.***2011,***420* (1), 34-42.

43. Hecq, J.; Deleers, M.; Fanara, D.; Vranckx, H.; Amighi, K. Preparation and characterization of nanocrystals for solubility and dissolution rate enhancement of nifedipine. *Int. J. Pharm.***2005,***299* (1-2), 167-177.

44. Burness, C. B.; Keating, G. M. Mannitol dry powder for inhalation: in patients with cystic fibrosis. *Drugs***2012,***72* (10), 1411-1421.

45. Yang, Y.; Tsifansky, M. D.; Shin, S.; Lin, Q.; Yeo, Y. Mannitol-guided delivery of Ciprofloxacin in artificial cystic fibrosis mucus model. *Biotechnol. Bioeng.***2011,***108* (6), 1441-1449.

46. Rundfeldt, C.; Steckel, H.; Scherliess, H.; Wyska, E.; Wlaz, P. Inhaleable highly concentrated itraconazole nanosuspension for the treatment of bronchopulmonary aspergillosis. *Eur. J. Pharm. Biopharm.***2013,***83* (1), 44-53.

47. Li, Y.; Li, P. K.; Roberts, M. J.; Arend, R. C.; Samant, R. S.; Buchsbaum, D. J. Multi-targeted therapy of cancer by niclosamide: A new application for an old drug. *Cancer Lett.***2014,***349* (1), 8-14.

48. Andrews, P.; Thyssen, J.; Lorke, D. The biology and toxicology of molluscicides, Bayluscide. *Pharmacol. Ther.***1982,***19* (2), 245-295.

CHAPTER 3

DEVELOPMENT OF INHALABLE HYALURONAN/MANNITOL COMPOSITE DRY POWDERS TO REPOSITION FLUCYTOSINE FOR LOCAL THERAPY OF LUNG INFECTIONS

G. Costabile[1], I. d'Angelo[2], E. Mitidieri[3], R. d'Emmanuele di Villa Bianca[3], A. Miro[1], F. Imperi[4], L. Leoni[5], P. Visca[5], F. Quaglia[1], R. Sorrentino[3], F. Ungaro[1]

[1]Drug Delivery Labs, Department of Pharmacy, University of Naples Federico II, Via Domenico Montesano 49, 80131 Naples, Italy
[2] Di.S.T.A.Bi.F., Second University of Naples, Via Vivaldi 43, 81100 Caserta, Italy
[3] Pharmacology Labs, Department of Pharmacy, University of Naples Federico II, Via Domenico Montesano 49, 80131 Naples, Italy
[4] Department of Biology and Biotechnology "Charles Darwin", Sapienza University of Rome, Via dei Sardi 70, 00185 Rome, Italy
[5] Department of Sciences, University Roma Tre, Viale Marconi, 446, 00146 Rome, Italy

ABSTRACT

Flucytosine (5-fluorocytosine, 5-FC) is a fluorinated analogue of cytosine that is currently approved for the treatment of fungal infections and has been recently showed a very promising anti-virulence activity against *Pseudomonas aeruginosa*. In this work, we propose novel inhalable hyaluronic acid (HA)/mannitol composite dry powders for repositioning of 5-FC in the local treatment of CF lung infections. Dry powders were produced in one step by spray-drying. Formulation composition and process conditions were selected after in depth development studies aimed to achieve HA/mannitol particles loaded with 5-FC characterized by optimal properties for aerosolization and a convenient release profile in simulated lung fluids. The developed microparticles were effectively delivered from breath-activated dry powder inhalers (DPI) already available to CF patients, although the aerodynamic assessment of fine particles suggested that they well fit to a low-resistance DPI. The ability of optimised formulations to inhibit the growth of *Candida Albicans* and pyoverdine production in *Pseudomonas aeruginosa* at 5-FC concentrations ($\geq$ 3.9 μM and $\geq$ 1.2 μM, respectively) that do not affect the viability of bronchial epithelial cells, both normal and CF, was demonstrated *in vitro*. Finally, a pharmacokinetic comparison between the dry powder formulation here developed and 5-FC in solution after intra-tracheal delivery in rats was performed. *In vivo* results clearly demonstrated that, when formulated as HA/mannitol dry powders, 5-FC is able to reach a significant concentration in both broncoalveolar fluid and lung tissue and it can be sustained over time as compared to 5-FC solution. Taken all together, our data demonstrate for the first time the feasibility to develop effective 5-FC formulations for pulmonary delivery. Furthermore, results highlight that it is possible, by an appropriate formulation design, to modify the biodistribution of the drug at lung, where microorganisms, causing severe local infections and worsening the pathological status of the CF pulmonary disease, are located.

3.1. INTRODUCTION

Flucytosine (5-fluorocytosine, 5-FC) is a fluorinated analogue of cytosine that is currently used for the treatment of fungal infections caused by *Candida* and *Cryptococcus*, mainly in combination with other antimycotic agents.[1] Recently, a drug repurposing approach revealed that 5-FC is also able to reduce the virulence of the bacterium *Pseudomonas aeruginosa*[2], one of the most dreaded opportunistic pathogens in hospitals and the main cause of chronic lung infection and mortality in individuals with cystic fibrosis (CF)[3]. Systemic administration of 5-FC almost completely prevented *P. aeruginosa* lethality in a mouse model of pulmonary infection[2], highlighting the potential of this drug for antivirulence therapy of *P. aeruginosa* CF lung infections. On the other hand, although the prevalence and importance of fungi in the CF lung is still unclear, recent evidences suggest that chronic respiratory colonization of *Candida albicans* may be associated with worsening of CF lung disease.[4]

Pulmonary administration represents an ideal way to locally treat lung infections and recent technological advances have fostered the development of inhaled CF antimicrobial therapies.[5,6] In particular, novel particle engineering techniques, make portable and easily handled dry powder inhalers (DPIs) very appealing for drug inhalation in CF as demonstrated by recent approval of tobramycin and colistin DPIs.[7-9] Nevertheless, the clinical outcomes strongly depend on the concentration and persistency of the drug at the lung target. The maximum therapeutic effect is achieved when the drug adequately deposits along the airways, remains in situ as long as possible and is able to overcome non-cellular (i.e., mucus, biofilm) and cellular (i.e., lung epithelia, bacteria) barriers imposed by CF lung.[10] Thus, in order to translate the systemic treatment to an efficient inhalable administration approach *in vivo*, the old medication needs to be re-formulated taking into account its physico-chemical properties and the peculiarities of CF patients.[10,11]

Generating inhalable particles by spray-drying offers several advantages, the first of which relies in the possibility to produce dry powders of drug and carrier excipients in a one-step continuous particle processing operation.[12,13] Furthermore, it is possible to select adequate process conditions so as to achieve particles with optimal

properties for aerosolization.[13-15] Indeed, through the incorporation of selected excipients, it is possible to achieve spray-dried powders with enhanced dispersibility[15,16], improved stability upon storage[17] and modified drug release profile.[15] Furthermore, tuning drug distribution at lung and its pharmacokinetic profile upon pulmonary delivery is feasible thorough appropriately engineered spray-dried powders.[18-20]

Among materials currently under investigation for inhalation, an increasing knowledge has been acquired on the potential of hyaluronic acid (HA) not only as carrier but also as bioactive agent in the treatment of lung diseases.[21,22] In particular, inhaled HA at high molecular weight (~1,000 KDa) has been proven to have anti-inflammatory activity and to prevent bronchoconstriction induced in asthmatics by direct and indirect challenges.[21,22] Indeed, aerosolized HA is currently employed in CF patients to improve tolerability of hypertonic saline.[23,24] Nevertheless, only limited attempts have been made until now to produce HA-based spray-dried powders for inhalation.[25-27]

The aim of this work was the development of HA-based dry powders for lung delivery of 5-FC to be used in the local treatment of lung infections. Formulation composition and process conditions were selected after in depth development studies aimed to achieve HA particles with optimal properties for aerosolization. Optimised HA/mannitol microparticles loaded with 5-FC were produced by spray drying and characterized for 5-FC release in simulated lung fluids as well as for *in vitro* aerosolization properties upon delivery from DPIs commonly used in CF patients. *In vitro* antifungal and antivirulence properties, as well as toxicity towards human bronchial epithelial cells, both normal and CF, were determined. Finally, a pharmacokinetic comparison between the dry powder formulation here developed and 5-FC in solution after intra-tracheal delivery in rats was performed, highlighting the potential of the developed formulation for *in vivo* delivery of 5-FC at lung..

3.2. MATERIALS AND METHODS

3.2.1. Materials

5-fluorocytosine (5-FC), hyaluronic acid sodium salt (HA; 0.6-1.1 MDa), egg yolk emulsion, RPMI amino acid solution, type II mucin from porcine stomach, gelatin from bovin skin type B, rhodamine B, calcium chloride dihydrate, cetyltrimethyl ammonium bromide (CTAB), magnesium chloride, potassium chloride, potassium phosphate dibasic, sodium acetate, sodium bicarbonate, sodium chloride, sodium citrate dihydrate, sodium phosphate dibasic, sodium sulfate, Triton™ X-100 solution (10%) and 3-(4,5-dimethylthiazol-2-yl)-2,5-diphenyltetrazolium bromide (MTT) were obtained from Sigma-Aldrich (Italy). Mannitol (Pearlitol®C160) was a kind gift of Roquette Italia S.p.a. (Italy). HPLC grade acetonitrile was supplied by Carlo Erba (Italy). Distilled water filtered through 0.22 μm cellulose filters (Phenex® RC, Phenomenex, USA) was employed throughout the study.

3.2.2. Hyaluronic acid analysis

Hyaluronic acid (HA) was quantified by turbidimetric measurement upon complexation with CT.[28] Briefly, 2 mg of HA were accurately weighted, transferred into a flask and dissolved under stirring at 37°C for 15 min in 10 ml of acetate buffer at pH 6.0 (0.2 M sodium acetate, 0.15 M sodium chloride; adjusted to pH 6.0 by acetic acid). This stock solution was stable for at least a week when stored at 4°C. Working standard solutions of HA were freshly prepared by further dilution in acetate buffer at pH 6.0. One milliliter of working standard solutions of HA was added to 2 ml of a 1 g/ml CTAB solution in 2% (w/v) aqueous sodium hydroxide. The absorbance of HA samples was measured at 350 nm using a Shimadzu 1204 spectrophotometer (Shimadzu, Italy) fitted out with a 0.1-cm quartz cell (Hellma® Italia, Italy). All measurements were performed in triplicate at room temperature against a reagent blank. The linearity of the response was verified over the concentration range 4.0–200 μg/ml ($r^2 \geq 0.99$).

3.2.3. 5-FC quantitative analysis

The amount of 5-FC in solution was determined by UV-vis spectrophotometry. Briefly, the absorbance (ABS) of 5-FC samples was measured at the maximum absorption wavelength (275 or 285 nm) with a Shimadzu 1204 spectrophotometer (Shimadzu, Italy) fitted out with a 0.1-cm quartz cell (Hellma® Italia, Italy). Calibration curves were obtained by plotting ABS *versus* the concentration of 5-FC standard solutions in the different sample media, that is aqueous formic acid at pH 2 (1 % v/v), phosphate buffer at pH 7.2 (PBS) and simulated interstitial lung fluids (SILF). In each case, the linearity of the response was verified over a concentration range of 0.2–20 μg/mL (r^2= 0.999). The presence in the samples of interfering substances that could affect the UV-vis spectrum of 5-FC was accounted for with the appropriate blank. All blank media had negligible absorption at the maximum 5-FC absorption wavelength.

3.2.4. Production of microparticles

Blank HA (Hya) or HA/mannitol (HyaMan) microparticles were produced by spray drying. Briefly, HA was dissolved in a water/ethanol mixture (80:20 v/v) at 0.1 or 0.25 % w/v. When needed, mannitol was added to the mixture at theoretical HA:mannitol ratio of 1:1 or 1:2 w/w. Ammonium bicarbonate (AB) at 15 % (w/v) was also tested as porogen in blank formulations. Formulations were processed in a Mini Spray Dryer BüchiB290 (Flawil, Switzerland) equipped with a high-performance cyclone for the recovery of small powder amounts. Different formulations were individually spray-dried with the following process parameters: feed rate 3 ml/min; aspirator setting 20; spray-flow 600 Nl/h; inlet temperature 110°C (resulting outlet temperature = 75°C). A 0.5 mm nozzle was used throughout the experiments. Powders were collected and stored at 4°C until use.

HA/mannitol microparticles at a 5-FC theoretical loading of 10 % (i.e., 10 mg of 5-FC *per* 100 mg of dry powder) were produced in optimized formulation conditions. Briefly, HA concentration was fixed at 0.25 % w/v and mannitol was added to the water/ethanol mixture at a HA/mannitol ratio by weight of 1:2. Three different

formulations were produced by varying solvent composition (water/ethanol 80:20 or 70:30 v/v) and the feed rate of the spray-drying (1.8 and 3 ml/min).

3.2.5. Characterization of microparticles

Particle morphology was analyzed by scanning electron microscopy (SEM) (Leica S440, Germany). The mean geometric diameter and size distribution of microparticles were determined by laser light scattering (Coulter LS 100Q, USA) on a particle suspension in methanol containing polysorbate 80 (10% w/v) as dispersing agent. Size is expressed as volume mean diameter ± standard deviation of values collected from three different batches.

Powder tapped density was evaluated according to European Pharmacopoeia 8th Edition (Ph.Eur.).Briefly, a known weight of particles was transferred to a 10 (±0.05) ml graduated cylinder and the initial volume recorded. The cylinder was then mechanically tapped 1250 times up to volume plateau by a tapped density tester (Mod. IG/4, Giuliani, Italy). The tapped density of the powder (ρ) was expressed as the ratio between sample weight and the volume occupied after 1250 tappings (g/ml) ± standard deviation of values collected from three different batches.

The actual amount of HA *per* mg of HA/mannitol microparticles was also determined. Briefly, 5 mg of microparticles were dissolved in 10 ml of acetate buffer at pH 6.0 under stirring at 37°C and the HA content of the sample was determined by spectrophotometric analysis as reported above. Results are expressed as HA/Mannitol actual ratio by weight (HA/Man) ± standard deviation of values collected from three different batches.

Actual 5-FC loading of HA/mannitol microparticles was determined by dissolving 2 mg of dry powders under stirring in 1 ml of aqueous formic acid at pH 2 (1 % v/v). Aqueous samples were analyzed for 5-FC content by spectrophotometry as described above. Results are expressed as mg of 5-FC *per* mg of dry powders ± standard deviation of values collected from three different batches.

3.2.6. *In vitro* aerosolization properties

The aerosolization properties of the dry powders were tested *in vitro* after delivery from breath-activated reusable DPIs working with single unit capsule containing the dry powder using a Next Generation Impactor (NGI) (Copley Scientific, UK) according to Ph.Eur. 8th Ed. Depending on the dry powder, three devices with different resistances to the airflow were tested: the low-resistance DPI RS01 (Plastiape, Italy); the medium-resistance DPI Turbospin® (PH&T Pharma, Italy); the high-resistance DPI HandiHaler® (Boehringer Ingheleim, Germany). For each test, a hard gelatin capsule (size 2, Capsugel, USA) was filled with about 20 mg of the powder and placed in the DPI. The capsule was then pierced and the liberated powder drawn through the NGI operated at 60 or 90 L/min. The emitted dose (ED) was calculated by accurately weighing the capsule before and after DPI actuation.

The powder deposited on the seven NGI collection cups was quantitatively recovered by dissolution in an appropriate amount (2 or 8 ml for low-diameter or high-diameter collection cups, respectively) of aqueous solvent (acetate buffer at pH 6 or formic acid at pH 2 for HA and 5-FC quantitation, respectively). The powder deposited in the induction port and in the micro-orifice collector was also recovered by washing with 10 ml of solvent. The experimental mass median aerodynamic diameter (MMADexp) and the geometric standard deviation (GSD) were calculated according to Ph.Eur. deriving a plot of cumulative mass of powder retained in each collection cup (expressed as percent of total mass recovered in the impactor) *versus* cut-off diameter of the respective stage. The FPF was calculated by interpolation from the plot as the percentage of powder emitted from the inhaler with an aerodynamic diameter less than 5 μm. The $MMAD_{exp}$ of the particles was determined from the same graph as the particle size at which the line crosses the 50% mark and the GSD was defined as

$$GSD = (Size\ X/Size\ Y)^{1/2}$$

where size X was the particle size at which the line crosses the 84% mark and size Y the size at which it crosses the 16% mark.

3.2.7. *In vitro* assessment of fluorescent particle interactions with simulated CF mucus

Fluorescent HA/mannitol microparticles containing 0.1 % of rhodamine B (Rhod/HyaMan2) were produced by spray-drying in the same formulation conditions selected for 5-FC loading to assess particle behavior in an artificial CF mucus model as previously reported[29]. Artificial mucus (AM) was prepared by adding 250 μL of sterile egg yolk emulsion, 250 mg of mucin, 0.295 mg DTPA, 250 mg NaCl, 110 mg KCl and 1 mL of RPMI to 50 mL of water. The dispersion was stirred until a homogenous mixture was obtained. For the experiment, 1 ml of a gelatin solution in hot water (10% w/v)was placed in each well of a 24-well plate, hardened at room temperature and stored at 4°C until use. Before use, 1 ml of AM was placed on the hardened gelatin gel. Then, 3 mg of microparticles were uniformly distributed on the AM layer and maintained at room temperature. At regular time frames, the well plate was visually inspected and the microparticle-containing AM was withdrawn, centrifuged at 6,000 rcf and 4°C for 15 min (MIKRO 120, Hettich Zentrifugen, Germany) and the amount of rhodamine dissolved in mucus was evaluated by spectrofluorimetric analysis at $\lambda_{ex}/\lambda_{em}$ 553/577 nm (RF 1501 Spectrofluorometer, Shimadzu, Italy). Results are reported as percentage of rhodamine penetrated through AM (total amount of rhodamine in microparticles-amount of rhodamine in AM/total amount of rhodamine in microparticles x 100) ± standard deviation of values collected from three different batches.

3.2.8. *In vitro* 5-FC release in simulated lung fluids

The release of 5-FC from optimized HyaMan_FC microparticles was followed *in vitro* by membrane dialysis in AM and simulated interstitial lung fluid (SILF) as previously reported.[17] SILF was prepared following the preparation instructions dictated by Marques et al.[30]. Briefly, 1 L of SILF contains 0.095 g magnesium chloride, 6.019 g of sodium chloride, 0.298 g of potassium chloride, 0.126 g of sodium phosphate dibasic, 0.063 g of sodium sulfate, 0.368 g calcium chloride

dihydrate, 0.574 g of sodium acetate, 2.604 g of sodium bicarbonate and 0.097 g of sodium citrate dihydrate.

HyaMan_FC dry powders (2 mg) were added to 0.3 mL of donor medium (artificial mucus or PBS) and placed in a dialysis membrane bag (MWCO: 5000 Da, Spectra/Por®). The membrane was dropped into 5 mL of SILF and kept at 37°C. At scheduled time intervals, 1 mL of SILF was withdrawn and analyzed for 5-FC content by spectrophotometric analysis as described above. The medium was replaced by the same amount of fresh medium. At the end of each release experiment, the amount of residual 5-FCin the dialysis bag was assessed upon dissolution in 5 ml of aqueous formic acid at pH 2 (1 % v/v). Experiments were run in triplicate for each time point of release kinetics.

3.2.9. *In vitro* antifungal activity

For biological studies *in vitro* (§ 2.9, 2.10 and 2.11), stock solutions of HyaMan_FC#3 in sterile water was prepared at 6.33 mg/ml concentration (corresponding to 5 mM 5-FC). The minimum inhibitory concentration (MIC) of the 5-FC formulation for *Candida albicans* (ATCC 60193) was first determined using the broth microdilution method as previously described.[31] Briefly, about 10^4 *C. albicans* cells were inoculated in RPMI 1640 medium supplemented with 2 mM L-glutamine and buffered with 165 mM MOPS (pH 7.2) in the presence or absence of increasing concentrations of HyaMan_FC#3 or the same amount of 5-FC in saline and blank HyaMan as control, in 96-well tissue culture plates (200 µl final volume in each well). After 24 h of growth at 35°C under static conditions, ABS at 600 nm (A_{600}) was measured in a Victor plate reader (Wallac), and the 5-FC MICs were calculated as the lowest concentration of each formulation causing at least 50% reduction in A_{600} with respect to untreated controls.[32]

3.2.10. *In vitro* pyoverdine inhibitory activity

The anti-pyoverdine activity of different 5-FC formulations was assessed as previously described[2]. Briefly, the *P. aeruginosa* reference strain PAO1 (ATCC 15692) was cultured for 10 h at 37°C in the iron-depleted trypticase soy broth

dialysate medium (TSBD[33] supplemented with 50 μM $FeCl_3$, and then refreshed 1:1000 in fresh TSBD in the presence or absence of increasing concentrations of 5-FC in saline, HyaMan_FC#3 or HyaMan as control. After 14 h of growth, pyoverdine production was quantified by normalizing the ABS at 405 nm (A_{405}) in cell-free culture supernatants appropriately diluted in 100 mM Tris-HCl (pH 8) by the cell density of the corresponding bacterial cultures, determined as A_{600}.[34]

3.2.11. Cytotoxicity assay

16HBE14o- (wt/wt CFTR; normal human bronchial epithelial cells) and CFBE41o- (F508del/F508del; cystic fibrosis bronchial epithelial cells, homozygous for the ΔF508 mutation) cells[35] were maintained in MEM medium with 20 mM L-glutamine, 100 units/mL penicillin, 100 μg/mL streptomycin and 10% fetal bovine serum (FBS). When confluent, cells were trypsinized and seeded in 96-well microtiter plates at 30,000 cells per well (in 200 μL final volume). Twenty-four h after seeding, cells were washed three times with culture medium without any additive (FBS or antibiotics), and 200 μL of culture medium with or without different amounts of 5-FC formulations, or their corresponding controls, were added to each well. After 3 or 24 h of incubation at 37°C, cell culture medium was discarded and each well was washed with 200 μL of Hanks balanced buffer solution (HBSS). Cells were then incubated for 3 h at 37°C in the presence of 200 μL of 0.5 mg/mL MTT in HBSS. MTT solution was then discarded, 100 μL of DMSO were added to each well, and ABS at 570 nm (A_{570}) was read using an ELISA microtiter plate reader.[36]

3.2.12. *In vivo* biodistribution studies

3.2.12.1. Animals

Male Wistar rats (200-220 g; Charles River, Lecco, Italy) were used. All the experimental procedures were performed following the specific guidelines of the Italian and the European Council law for animal care. These procedures were also approved by the Animal Ethics Committee of the University of Naples "Federico II" (Italy).

3.2.12.2. Experimental procedures

*R*ats were anesthetized using ketamine (80-100mg/kg, i.p.) and xilazine (10mg/kg, i.p.) and the depth of anesthesia was continuously controlled. The animals were divided into different groups and treated with PBS (100 µL, SHAM group), HyaMan_FC#3 dry powders(2.5 mg/rat) or an aqueous solution containing an equivalent amount of 5-FC (200µg/100µl). The formulations were intra-tracheally administered by using a mini DPI (Model DP-4, Penncentury, USA)or a Microsprayer® (Model 1A-1B, PennCentury, USA), for dry powder and solution respectively. The cannula of the tracheal dispositive was inserted directly into the trachea through the mouth. At 5, 30 or 180 min after treatment and under anesthesia, the carotid artery was cannulated for blood collection. Thus after euthanization, bronchoalveolar lavage (BAL) and lungs were obtained. Briefly, the trachea was cannulated with a polyethylene tube (1 mm inner diameter) to perform BAL as previously reported.[17] Lungs were washed (three times) by flashing sterile ice cold PBS. The BAL was centrifuged to separate cells (BALC) from fluid (BALF), while blood was withdrawn in glass tube and left for 24h at 4°C to obtain serum. BALC and lungs were homogenized in PBS containing Triton 0.1%.

3.2.12.3. Sample treatment and analysis

BALC, BALF, lung homogenate and serum were processed for 5-FC quantitation by RP-HPLC. Briefly, biological samples were incubated 1 h under stirring with acetonitrile (1:1 v/v for BALC and BALF, 1:2 v/v for homogenates and serum) for protein precipitation. The resulting dispersion was centrifuged at 18,000 rcf for 5 min(MIKRO 120, HettichZentrifugen, Germany) and the surnatant filtered through 0.45 mm cellulose filters (Phenex®, Phenomenex, USA) for RP-HPLC analysis. The same biological matrices were also analysed to assess the presence of 5-FU, the active metabolite of the 5-FC. In each case, the presence in the samples of interfering substances was accounted for with the analysis of biological samples derived from the SHAM group.

A SHAM group was also used to determine the recovery yield of the extraction procedure. After spiking with known amounts of 5-FC or 5-FU (0.020-1.0 µg), the

biological samples from SHAM animals underwent the same extraction procedure used for BALC, BALF, lung homogenates and serum derived from treated groups and were successively analyzed by RP-HPLC. In each case, data were corrected for recovery yields, which were always higher than 80%.

The amount of 5-FC and its metabolite 5-FU in biological samples was determined by reverse-phase High-Performance Liquid Chromatography (RP-HPLC). The HPLC system consisted of a LC-10ADvp liquid chromatograph, a SIL-10ADvp auto-injector, a SPD-10Avp UV–Vis detector and a C-R6 integrator from Shimadzu (Japan). The quantitative analysis was performed by RP-HPLC on a Synergy Hydro column (250 × 4.6 mm, 100 Å) (Phenomenex, USA). The mobile phase was aqueous formic acid (1% v/v). The flow rate was 1 ml/min and the detection wavelength 285 nm. In these conditions the retention times of 5-FC and its metabolite 5-FU were 3.5 min and 6.5 min, respectively. Calibration curves were obtained by plotting peak area *versus* the concentration of 5-FC or 5-FU standard solutions in water. The linearity of the response was verified over the 5-FC concentration range of 0.2-20 μg/ml and 5-FU concentration range 0.25-25μg/ml ($r^2 \geq 0.99$).

The limit of detection (LOD) (estimated as 3 times the background noise) of 5-FC and 5-FU were 0.067 and 0.14 μg/ml, respectively. The limit of quantitation (QOD) of 5-FC and 5-FU (estimated as 10 times the background noise) were 0.22 and 0.45 μg/ml, respectively.

3.2.13. Statistical analysis

The significance of differences was determined with the software GraphPad InStat using one-way ANOVA followed by the Tukey−Kramer multiple comparison test. A p value < 0.05 was considered significant.

3.3. RESULTS

3.3.1. Design and development of 5-FC HA/mannitol dry powders for inhalation

In depth formulation studies were devoted to the development of HA-mannitol dry powders for inhalation. As first step, several HA formulations, differing for the concentration of HA, presence and concentration of AB as porogen agent, were individually spray dried and fully characterized (Hya formulations in Table 3.1).

Table 3.1. Composition of unloaded Hya and HyaMan spray-dried formulations.

Formulation[1]	HA (% w/v)	AB (% w/v)	HA/mannitol theoretical ratio (w/w)
Hya0.1	0.1	-	-
$Hya0.1_{AB15}$	0.1	15	-
$Hya0.1_{AB50}$	0.1	50	-
Hya	0.25	-	-
Hya_{AB15}	0.25	15	-
Hya_{AB50}	0.25	50	-
HyaMan1	0.25	-	1:1
$HyaMan1_{AB15}$	0.25	15	1:2
HyaMan2	0.25	-	1:1
$HyaMan2_{AB15}$	0.25	15	1:2

1. The acronyms used are composed by character strings indicating: presence and concentration of HA (Hya 0.1 or Hya), presence of mannitol and its weight ratio with HA (Man1 or Man2), presence and concentration of AB (AB15 or AB50) within the formulation.

As shown in Fig. 3.1, HA concentration in the spray-drying feeding solvent affected the morphology of the particles, which were less cohesive and collapsed when 0.25 % (w/v) HA was spray-dried. This effect was particularly evident when AB was added to the formulation as porogen.

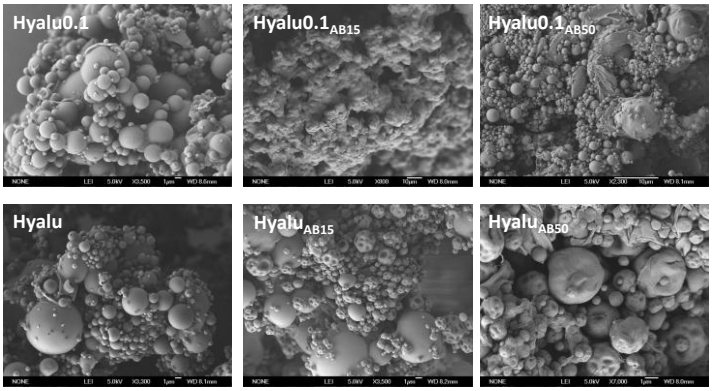

Figure 3.1. SEM micrographs of HA-based microparticles produced in different formulation conditions. Field is representative of the formulation.

Increasing the concentration of HA from 0.1% (w/v) to 0.25% (w/v) caused an increase of the production yield from 17% to 25%. Nevertheless, the percentage of dry powders delivered from a mini-DPI was always very low, ranging from 9% to 20%, suggesting very poor aerosolization properties for dry powders merely based on HA.

In order to improve particle properties of the HA dry powders achieved by spray-drying 0.25% (w/v) HA in water/ethanol 80:20 (v/v), mannitol was tested as second component. Different HA/mannitol formulations were spray-dried and fully characterized (HyaMan; Table 3.1). SEM images of HyaMan dry powders are reported in Fig.3.2.

While mannitol crystals are still evident on HyaMan1 and HyaMan$_{AB15}$ surface, more regular microparticles were achieved at a HA/mannitol ratio by weight of 1:2. Bulk and flow properties of the formulations are reported in Table 3.2.

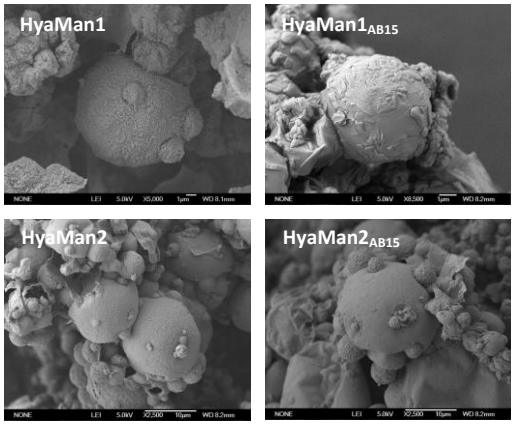

Figure 3.2. SEM micrographs of HA/mannitol microparticles. Field is representative of the formulation.

Table 3.2. Overall properties of blank HyaMan dry powders.

Formulation	Mean yield (%)	Actaul HA/Man ratio (w/w)	Volume mean diameter (d)[1] (μm ± SD[2])	Tapped density (ρ) (g/ml ± SD[2])	Emitted dose[3] (%± SD[2])
Hya		-	20.8 ± 2.0	0.045 ± 0.006	22.2 ± 5.3
HyaMan1	44.6	1.2 ± 0.19	19.4 ± 1.0	0.074 ± 0.008	85.3 ± 7.4
$HyaMan1_{AB15}$	48.9	1.7 ± 0.38	21.7± 6.2	0.050 ± 0.008	96.6 ± 2.3
HyaMan2	47.0	0.54 ± 0.10	18.7 ± 3.5	0.100 ± 0.009	100.2 ± 6.4
$HyaMan2_{AB15}$	47.6	0.53 ± 0.04	15.4± 5.7	0.097 ± 0.008	90.0 ± 1.5

1. Mean geometric diameter as determined by laser diffraction.
2. Standard deviation of values calculated on three different batches.
3. Percentage of dry powder delivered from a breath-activated medium-resistance DPI (Turbospin) operated at 60 L/min.

As expected, the production yield significantly increased, up to 45-49%. Despite their high geometric diameter, always around 20 μm, all particle formulations displayed very low tapped density values, ranging between 0.045 and 0.1 g/ml, suggesting a hollow structure, suitable for lung delivery. In each case, the theoretical HA/mannitol ratio by weight was maintained after spray-drying. Nevertheless,

differences were apparent in particle aerosol performance upon delivery from a medium-resistance breath-activated, reusable DPI, that is Turbospin® (PH&T Pharma, Milano, Italy). Results confirmed very poor aerosolization properties of HA particles, with an emitted dose (ED) as low as 22.2 ± 5.3 % of the initial amount loaded into the DPI (Table 2). The addition of mannitol to the formulation resulted in a significant increase of ED, with a maximum value, around 100%, for HyaMan2 microparticles. No actual advantage was observed when AB was added to the initial formulation (Table 3.2). On the basis of these encouraging *in vitro* aerosolization properties, HyaMan2 formulation was selected as carrier for 5-FC.

5-FC was added to the formulation before spray drying at a theoretical loading of 10% by weight and the effect of the solvent and spray-drying conditions on the overall properties of dry powders was investigated. In each case, microparticles with a tapped density value around 0.3 g/ml and an actual 5-FC loading close to the theoretical one were achieved with good yields (≥ 40%). Differences were apparent among volume mean diameters, strictly depending on the formulation conditions (Table 3.3).

The aerosolization properties of dry powders containing 5-FC were tested *in vitro* after delivery from Turbospin® DPI with a Next Generation Impactor (NGI) (Copley Scientific, UK) according to Ph.Eur. 8th Ed. The calculated values of fine particle fraction (FPF) (i.e., fraction of particles with an aerodynamic diameter lower than 5 μm) and experimental mass mean aerodyanamic diameter ($MMAD_{exp}$) are reported in Fig. 3.3. Of note, 5-FC loaded HA/Mannitol microparticles achieved by spray drying at lower flow rates (HyaMan_FC#3) showed the lowest $MMAD_{exp}$ value and the highest FPF. HyaMan_FC#3 dry powder was thus selected to investigate the *in vitro* and *in vivo* potential of the system for local antimicrobial therapy in CF.

Table 3.3. Composition, bulk and flow properties of HyaMan dry powders loaded with 5-FC.[1]

	HyaMan_FC#1	HyaMan_FC#2	HyaMan_FC#3
Feedrate[2] (ml/min)	3.0	3.0	1.8
Feed solvent (water/ethanol, v/v)	80:20	70:30	80:20
Volume mean diameter (μm ± SD)	10.3 ± 5.0	21.3 ± 4.4	15.1 ± 3.8
Tapped density (g/ml ± SD)	0.273 ± 0.023	0.295 ± 0.016	0.302 ± 0.015
Actualloading[3] (mg ± SD)	0.095 ± 0.035	0.102 ± 0.005	0.108 ± 0.007

1. All formulations were prepared at 0.25 % w/v of HA and 0.5 % w/v of mannitol in the feed solvent.
2. Corresponding to a pump rate of 10% and 6% when using a standard silicone tubing of 2/4.
3. Milligrams of 5-FC per mg of dry powder. The theoretical loading is 0.1 mg *per* 1 mg of dry powders.

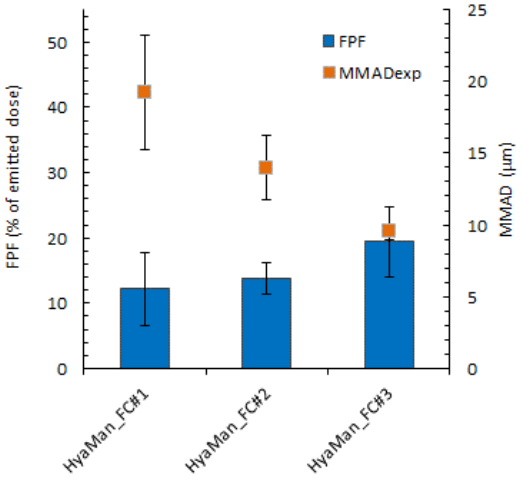

Figure 3.3. Effect of spray-drying conditions on the aerosolization properties of HA/mannitol microparticles loaded with 5-FC upon delivery from a medium-resistance DPI (Turbospin®). FPF = Fine particle fraction; $MMAD_{exp}$ = experimental mass mean aerodynamic diameter. Data are the mean ± SD of values calculated on three different batches.

3.3.2. *In vitro* aerosolization and release properties of optimized HyaMan_FC dry powders

The aerosol performance of HyaMan_FC#3 upon delivery from a low-resistance DPI [namely, RS01 (Plastiape, Italy)] was also investigated and results compared with those achieved with Turbospin®. As can be seen in Fig. 3.4, the NGI deposition pattern of HyaMan_FC#3 dry powder varied as a function of the flow rate (i.e., 60 and 90 L/min) and of the DPI resistance. At 60 L/min flow rate, less than 20% of the emitted 5-FC dose was deposited from cup 3 to MOC (i.e., MMAD<4.46 μm) with both DPIs tested. The remaining drug fraction was almost totally recovered in the throat/cup 1 when using Turbospin®, while it was found mostly in cup 1 (i.e., MMAD>8.06 μm) when using RS01(Fig. 3.4A).

At 90 L/min flow rate (Fig. 3.4B), the amount of 5-FC found in the throat when using both Turbospin® and RS01 lowered down to the benefit of cup 1 (>65 % of the emitted dose for Turbospin®). Nevertheless, a percentage as low as 15 % of the emitted dose was recovered from cup 2 to MOC (i.e., MMAD<6.48 μm) after delivery from Turbospin®. Furthermore, results achieved with Turbospin® were much less reproducible, making difficult to determine the actual values of MMAD and GSD.

The overall deposition pattern of the dry powder significantly improved when using RS01 at 90 L/min flow rate (Fig. 3.4B). The dry powder was delivered from RS01 at 90 L/min with maximum efficiency and homogeneously distributed thorough the seven stage down to MOC ,with more than 40 % of the emitted dose depositing from cup 2 to MOC (i.e., MMAD<6.48 μm) and about 25 % from cup 3 to MOC (i.e., MMAD<3.61 μm). The FPF at 90 L/min was 2-fold higher than that calculated at 60 L/min and $MMAD_{exp}$ was reduced by half accordingly (Fig. 3.4C).

A

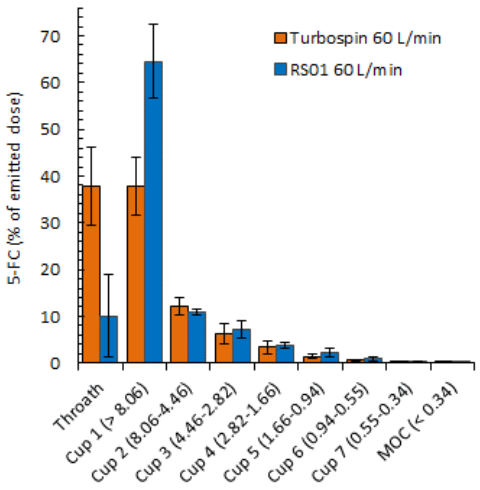

B

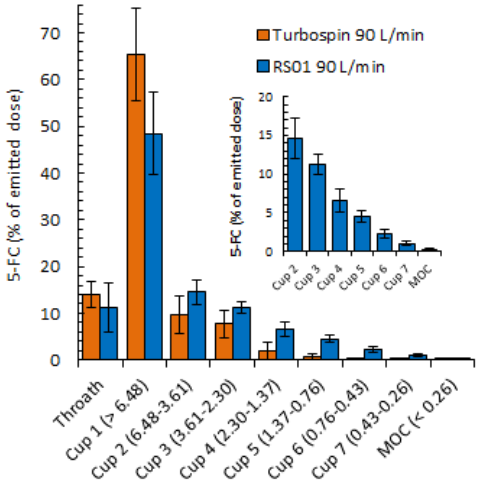

C

	60 L/min		90 L/min	
	Turbospin	**RS01**	**Turbospin**	**RS01**
$MMAD_{exp}$ (μm ± SD)	9.5 ± 0.55	13.8 ± 0.86	>20	6.9 ± 1.1
GSD (± SD)	2.1 ± 0.04	2.2 ± 0.06	ND	2.2 ± 0.03

Figure 3.4. NGI deposition pattern of optimized HyaMan_FC dry powder (HyaMan_FC #3). The formulation was delivered at 60 (A) and 90 (B) L/min through the low-resistance DPI RS01 or the medium-resistance DPI Turbospin®. The corresponding values of MMADexp and GSD are reported in panel C. Data are the mean ± SD of values calculated on three different batches

3.3.3 *In vitro* behavior of optimized HA/mannitol dry powders in simulated lung fluids

In vitro release of 5-FC from HyaMan_FC #3 dry powder was assessed in simulated interstitial lung fluids (SILF). As shown in Fig. 3.5, 5-FC was rapidly released from HA microparticles even if the release profile was slightly affected by the presence of simulated CF mucus, which slowed down 5-FC release in SILF.

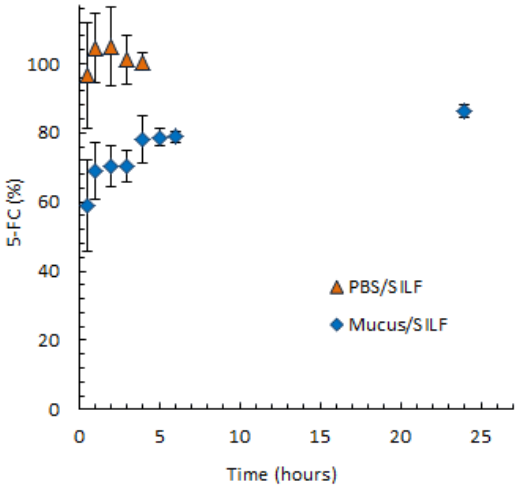

Figure 3.5. Release profile of 5-FC from optimized HyaMan_FC dry powder (HyaMan_FC#3) evaluated by membrane dialysis from either PBS at pH 7.2 or artificial CF mucus to simulated interstitial lung fluid (SILF). Data are presented as mean ± standard deviation (n=3).

The effect of mucus on HA/mannitol microparticles dissolution and drug diffusion was further investigated *in vitro* on an artificial CF mucus model. As can be seen in Fig. 3.6, fluorescent Rhod/HyaMan2 microparticles did not dissolve instantaneously in simulated CF mucus, and the released rhodamine B slowly diffused inside it within 24 h with the same kinetics observed for 5-FC.

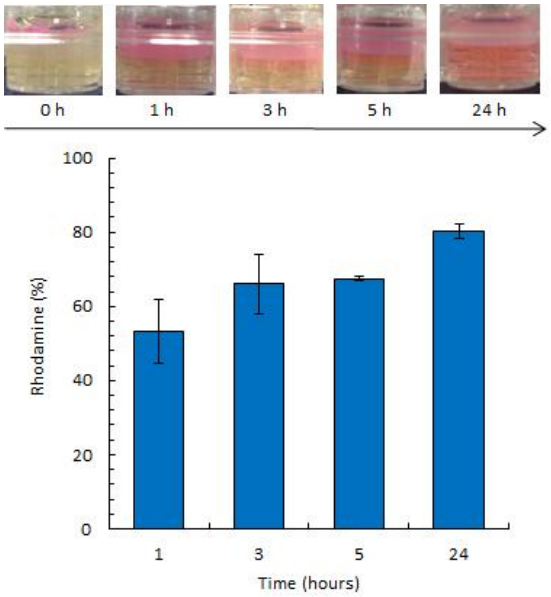

Figure 3.6. Visual inspection of fluorescent Rhod/HyaMan2 dry powder behaviour in an artificial mucus layer and corresponding percent amount of rhodamine permeated in the gelatin layer during time. Data are presented as mean ± standard deviation (n=3).

3.3.4. Antifungal, antivirulence and cytotoxic properties of HyaMan_FC#3 dry powders

Taking into account that 5-FC is currently employed in the clinic as antifungal agent, we first tested *in vitro* activity of HyaMan_FC#3 dry powders against *C. albicans*. Of note, 5-FC in saline and HyaMan_FC#3 had comparable antifungal activity, with a MIC value of 3.9 µM 5-FC (corresponding to 0.5 µg/ml). HyaMan did not inhibit *C. albicans* growth even at the highest concentration tested (635 µg/ml; data not shown).

5-FC was previously reported to reduce the virulence of *P. aeruginosa* by inhibiting the production of the siderophore pyoverdine, without affecting bacterial cells viability [3]. Thus, the anti-pyoverdine activities of 5-FC in saline and HyaMan_FC#3 on *P. aeruginosa* cells were compared. As shown in Figure 3.7, both HyaMan_FC#3 and 5-FC in saline inhibited pyoverdine production in *P. aeruginosa* at comparable levels (5-FC concentrations ≥ 1.2 µM). Conversely, the HyaMan vehicle without 5-FC had no effect on pyoverdine production.

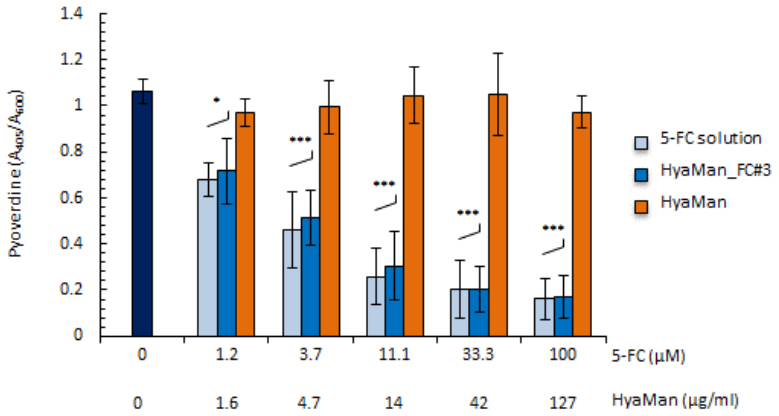

Figure 3.7. Pyoverdine production by *P. aeruginosa* PAO1 after 14-h growth in the iron-poor medium TSBD in the presence of increasing concentrations of 5-FC in saline (5-FC solution), 5-FC dry powders (HyaMan_FC#3), or the corresponding concentrations of blank HyaMan dry powders. Values are the mean (±SD) of three independent experiments. Asterisks indicate statistically significant differences with respect to the untreated control (* $p<0.05$, *** $p<0.01$; ANOVA) .

Finally, the cytotoxicity of the different 5-FC formulations was assessed on normal and CF bronchial epithelial cell lines (16HBE14o- and CFBE41o-, respectively), after 3- and 24-h treatments. After 3 h, 5-FC did not show any effect on viability of both cell lines, irrespective of the formulation or the concentration tested (Fig. 3.8A). After a 24-h treatment, a significant reduction in cell viability of 16HBE14o- cells and, to a lesser extent, of CFBE41o- cells was only observed for HyaMan_FC#3 at the highest concentration tested (corresponding to 1 mM 5-FC), and for the corresponding concentration of the HyaMan vehicle alone (Fig. 3.8B). In contrast, 5-FC in saline did not show any toxicity on both cell lines even at 1 mM (Fig. 3.8B), strongly suggesting that the *in vitro* cytotoxicity of HyaMan_FC#3 at the highest dosage after 24-h treatment is related to the very high amount of HA and mannitol excipients in the cell culture medium (1.27 mg/ml).

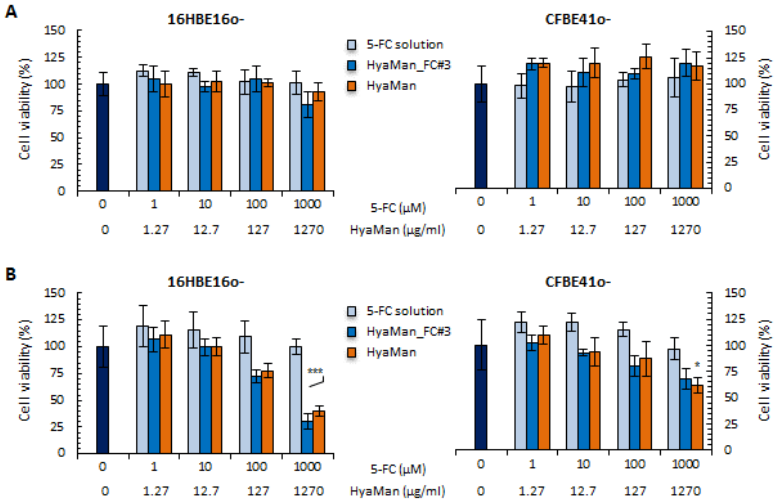

Figure 3.8. Cytotoxicity of 5-FC formulations to 16HBE16o- and CFBE41o- cells. Cell viability was assessed after (A) 3-h or (B) 24-h incubation in the presence of 5-FC in saline (5-FC solution), 5-FC dry powders (HyaMan_FC#3), or the corresponding concentrations of blank HyaMan dry powders. Results are expressed as percentage of cell viability with respect to untreated controls (100%) (blue bar), and represent the average (±SD) of three independent experiments performed in duplicate. Asterisks indicate statistically significant differences with respect to untreated controls (* $p < 0.05$, *** $p < 0.001$; ANOVA).

3.3.5. *In vivo* 5-FC biodistribution upon intratracheal insufflation of HyaMan_FC

The fate of 5-FC upon intra-tracheal insufflation of HyaMan_FC#3 dry powder in rats was investigated over time and results compared with those achieved upon intra-tracheal aerosolization of a 5-FC solution at the equivalent dose loaded in the dry powder formulation. The amount of 5-FC was determined in BALC, BALF, lung homogenates and serum by solvent extraction and subsequent RP-HPLC analysis. To determine the recovery yield of the extraction procedure, biological samples deriving from SHAM group spiked with known amounts of 5-FC or 5-FU were also analyzed.

As shown in Fig. 3.9A, the concentration of 5-FC in BALF was 2-fold higher in case of HyaMan_FC#3 dry powder as compared to 5-FC solution (11.3 ± 0.68 μg/ml and 5.81 ± 0.44 μg/ml for HyaMan_FC and 5-FC solution, respectively; $p<0.001$).

Furthermore, 30 min after the administration of HyaMan_FC #3, a 12-fold higher amount of 5-FC was found in BALF as compared to 5-FC solution (14.1 ± 0.59 μg/ml and 1.16 ± 0.04 μg/ml for HyaMan_FC#3 and 5-FC solution, respectively; $p<0.001$). Indeed, at 30 min the concentration of 5-FC after administration of the solution significantly dropped if compared to that at 5 min ($p<0.005$). A detectable and higher amount of 5-FC was still observed after 180 min after HyaMan_FC#3 administration as compared to 5-FC solution (Fig. 3.9A).

A different profile was observed in the lung homogenate immediately after the administration compared to the BALF data (Fig. 3.9B). In fact, after 5 min from HyaMan_FC#3 dry powder administration, 5-FC values were significantly lower compared to 5-FC solution ($p<0.01$); meanwhile, a major accumulation of the drug in the lung was observed at 30 min by using HyaMan_FC #3 formulation compared to the 5-FC solution ($p<0.01$). In fact 5-FC concentration was 4.44 ± 0.49 μg/g, a value more than 2-fold higher than that obtained with the 5-FC solution (1.91 ± 0.60 μg/g). A detectable but low amount of 5-FC in the lung was still observed 180 min after the administration of both HyaMan_FC#3 dry powder and 5-FC solution (Fig. 3.9B). Of note, the different distribution at lung did not significantly affected the blood concentration profile of 5-FC (Fig. 3.9C). In fact, no significant variation in 5-FC serum concentration between 5-FC solution and HyaMan_FC#3 dry powder was observed at any time interval (5, 30 or 180 min) from administration. In both cases, the amount of 5-FC in serum was significantly reduced after 180 min ($p<0.001$).

Finally, no significantly different amounts of 5-FC were found in BALC 5 min after administration of 5-FC solution and HyaMan_FC#3 dry powder (0.26 ± 0.079 and 0.20 ± 0.076 μg, respectively), while 5-FC was not detected in BALC samples at longer time intervals (30 and 180 min; data not shown).

In each case, we evaluated the possibility that an amount of 5-FC could be converted into 5-FU in the lung. Of note, after treatment with both HyaMan_FC#3 dry powder and 5-FC solution, no detectable amounts 5-FU was found in BALF, BALC, lung and serum samples (i.e., 5-FU<0.14 μg/ml).

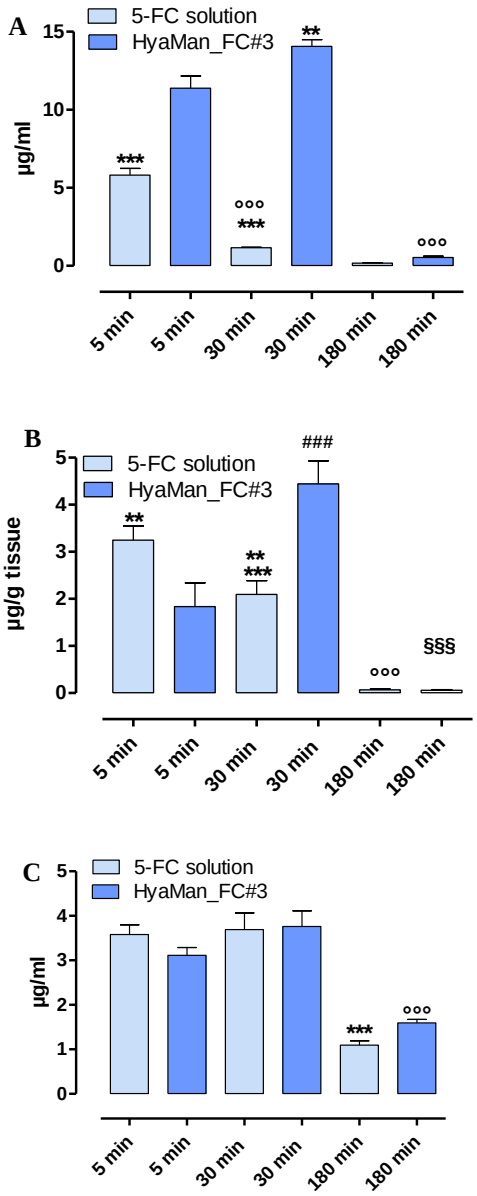

Figura 3.9. 5-FC amounts in rat BALF (A), lung (B) and serum (C) at different time intervals after intra-tracheal administration of HyaMan_FC#3 dry powder and of 5-FC solution by means of a low-scale DPI for rats. The results are expressed as mean ± S.E.M. (n=3).

3.4. DISCUSSION

Nowadays, pulmonary drug delivery is at cutting edge for local treatment of severe lung disease, such as CF. Particular research efforts have been directed towards development of dry powders for inhalation, due to a number of advantages over conventional liquid formulations.[8,10] Nevertheless, the development of inhalable dry powders runs into the need of safe materials for inhalation, which are currently very limited in number, and adequate engineering techniques, which should ensure effective deposition of the drug at the desired region of the lung and for the proper time interval.[37] Inspired by the recent encouraging findings on HA and mannitol for inhalation[21,24,38], in this work we have designed and developed novel inhalable composite HA/mannitol dry powders for local delivery of the antimycotic and antivirulence drug 5-FC in the treatment of lung infections.

Despite the huge number of engineering techniques currently under investigation to develop inhalable formulations, spray-drying remains an easy and scalable approach to produce more or less complex drug delivery systems.[12,13,39] Nevertheless, producing inhalable dry powders is straightforward in principle but complex in reality. Throughout the formulation studies, we run up into special difficulties to achieve pure HA aerosol particles within the respirable range. When used alone, the forces generated within the DPI were insufficient to aerosolize HA microparticles, with an emitted dose as low as 22%, likely as a result of poor HA particle flow properties. This issue is generally solved through the addition of a coarse material to produce free-flowing polymer particles/carrier blends.[40] Here, we decided to incorporate the excipient, that is mannitol, inside the spray-dried formulation, thus producing HA/mannitol composite microparticles with enhanced dispersibility, which could be delivered by a medium-resistance DPI with 100% efficiency.

In optimized formulation conditions, HA/mannitol composite microparticles could load 5-FC with high efficiency. In line with literature data[15], spray-drying offered the possibility to tune particle aerodynamic features through the selection of adequate processing conditions. In particular, two parameters were found to affect the properties of 5-FC-loaded HA/mannitol composite microparticles, that are feed

rate and feed solvent. Particles produced at the lowest feed rate and the highest percentage of ethanol inside the feeding solution, namely HyaMan_FC#3, displayed the lowest $MMAD_{exp}$ and the highest FPF. These formulations were, thus, selected for further investigations. Conceiving HyaMan_FC#3 for lung delivery, our focus was the thoroughly investigation of the aerodynamic behavior of the particles and their interaction with lung lining fluids.

For the successful development of any inhalation therapy based on DPIs, the correct drug–device combinations is crucial.[41] Thus, we become interested in testing the aerosolization properties of the developed dry powders delivered from DPIs characterized by distinct intrinsic resistances at the inspiratory flow and comparing their performance at different flow rates. As expected, the performance of the medium-resistance DPI, namely Turbospin, worsened by increasing the flow rate, while RS01 performance worked better at 90 L/min, useful to draw 4.0 L of air at a pressure drop of 4 kPa through the inhaler according to Pharmacopoeia. The deposition profiles and the fine particle characteristics of HyaMan_FC#3 in the different experimental conditions strongly suggested that the developed dry powders well fit to a low-resistance DPI. In fact, a poorer deposition profile of HyaMan_FC#3 was observed when using a high-resistance DPI (i.e., Handihaler, 39 L/min) as compared to both Turbospin and RS01 (data not shown).

Once the inhaled particles will deposit in the lung, the delivered drug has still to interact with local bacteria/fungi to be effective. The experimental conditions realized in the *in vitro* release studies well reproduced those occurring *in vivo*, taking into account that the inhaled particle will impact in the mucus layer, where microbial colonization will take place. Furthermore, the behavior of HyaMan_FC#3 upon contact with mucus was examined closely by further diffusion studies in the artificial CF mucus model. Combined results demonstrated the ability of the carrier system to assist 5-FC diffusion through airway mucus. A similar effect was already reported for mannitol-based dry powders, likely as a consequence of its osmotic properties.[42] At the same time, *in vitro* biological studies confirmed the activity of 5-FC against both *C. albicans* and *P. aeruginosa* at similar concentrations, which were not cytotoxic *in vitro* towards both normal and CF human bronchial epithelial cells.

Despite promising *in vitro* results, the therapeutic efficacy of the inhaled drugs *in vivo* will be definitively determined by the total lung deposition as well as the ability to overcome clearance mechanisms operating *in situ*. Thus, it was very interesting to compare the biodistribution of HyaMan_FC#3 dry powder *versus* 5-FC saline solution over 3 h after intra-tracheal administration in rats. The results obtained *in vivo* clearly demonstrated that, when adequately formulated, 5-FC is able to reach a significant concentration in the lung and this concentration may be sustained over time. In particular, optimized HyaMan_FC #3 dry powder offers the possibility to control local 5-FC concentration, increasing the drug level not only in the lung lining fluids but also into the lungs along time. Indeed, the clearance rate from the lungs may exert a major influence on the pharmacokinetic profile of the administered drug and this can depend on the physicochemical properties of both the drug and the carrier.[43,44] Of note, when the drug was administered as dry powder, a notable increase of 5-FC in the lung over time was observed, suggesting a slower 5-FC clearance as compared to the liquid formulation. Meanwhile, the very limited amount of 5-FC (~0.1% of the administered dose) within the cellular fraction of the BAL (i.e., BALC) 5 minutes after administration likely demonstrate that locally resident macrophages, and possibly neutrophils, do not phagocytosize HA/mannitol microparticles of this size and composition suggesting different clearance mechanisms.

It is well established that after pulmonary administration a molecule may quickly reach the circulation system (within few minutes) and, of course, this is tightly related to drug chemical/physical characteristics. After oral administration, 5-FC is well absorbed, easily penetrates into body tissues and is excreted mainly by the kidneys *via* glomerular filtration. The half-life of 5-FC is very short (1–2 h) in patients with normal renal function.[45] For its pharmacokinetic characteristics, the pulmonary administration of 5-FC solution can be thus assimilated to the intravenous one. On the other hand, the developed HA/mannitol dry powder HyaMan_FC#3 significantly modifies the persistence of the drug in the lung and this may be useful to improve local treatment while limiting undesirable systemic side effects. Indeed, by an higher amount of 5-FC in the lung, no significant differences

in serum concentrations were observed between 5-FC solution and the dry powder formulation.

The antifungal/antibacterial activity of 5-FC is due to its intracellular conversion into the cytotoxic compound 5-FU by fungal and bacterial enzymes that are not present in mammalian cells.[45,46] However, the rat lungs are not bacteria-free, hence it is relevant that 5-FU was not detected in biological matrices after treatment with both HyaMan_FC#3 dry powders and 5-FC solution.

3.5. CONCLUSIONS

HA/mannitol composite dry powders for controlled release of 5-FC at lung have been successfully developed by spray-drying. The composition of the formulation along with processing conditions played a pivotal role in determining particle aerosolization profile. The aerodynamic behavior of optimized formulation could be further controlled by a correct device choice. Indeed, the developed dry powders were efficiently delivered from a low-resistance DPI already available to CF patients and assisted 5-FC dissolution in simulated CF lung mucus. *In vitro* studies confirmed the ability of released 5-FC to inhibit both the growth of *C. albicans* and the production of pyoverdine in *P. aeruginosa*, thus attenuating its pathogenicity. At bioactive concentrations, the developed formulations did not display any toxicity towards both normal and CF bronchial epithelial cells. Finally, a pharmacokinetic comparison between the dry powder formulation here developed and 5-FC in solution after intra-tracheal delivery in rats highlighted the potential of the developed formulation for local and controlled delivery of 5-FC.

Taken all together, our data demonstrate for the first time the feasibility to develop effective 5-FC formulations for pulmonary delivery by inhalation. Furthermore, results clearly show that it is possible, by an appropriate formulation design, to force the concentration of the drug at lung, where the microorganisms causing severe local infections or worsening the pathological status of pulmonary diseases are located.

References

1. Nett, J. E.; Andes, D. R. Antifungal Agents: Spectrum of Activity, Pharmacology, and Clinical Indications. *Infect. Dis Clin. North Am.* **2016,** *30* (1), 51-83.
2. Imperi, F.; Massai, F.; Facchini, M.; Frangipani, E.; Visaggio, D.; Leoni, L.; Bragonzi, A.; Visca, P. Repurposing the antimycotic drug flucytosine for suppression of Pseudomonas aeruginosa pathogenicity. *Proc. Natl. Acad. Sci. U. S. A* **2013,** *110* (18), 7458-7463.
3. Driscoll, J. A.; Brody, S. L.; Kollef, M. H. The epidemiology, pathogenesis and treatment of Pseudomonas aeruginosa infections. *Drugs* **2007,** *67* (3), 351-368.
4. Gileles-Hillel, A.; Shoseyov, D.; Polacheck, I.; Korem, M.; Kerem, E.; Cohen-Cymberknoh, M. Association of chronic Candida albicans respiratory infection with a more severe lung disease in patients with cystic fibrosis. *Pediatr. Pulmonol.* **2015,** *50* (11), 1082-1089.
5. Flume, P. A.; VanDevanter, D. R. Clinical applications of pulmonary delivery of antibiotics. *Adv. Drug Deliv. Rev.* **2015,** *85*, 1-6.
6. Langan, K. M.; Kotsimbos, T.; Peleg, A. Y. Managing Pseudomonas aeruginosa respiratory infections in cystic fibrosis. *Curr. Opin. Infect. Dis.* **2015,** *28* (6), 547-556.
7. Tiddens, H. A.; Bos, A. C.; Mouton, J. W.; Devadason, S.; Janssens, H. M. Inhaled antibiotics: dry or wet? *Eur. Respir. J.* **2014,** *44* (5), 1308-1318.
8. Uttley, L.; Tappenden, P. Dry powder inhalers in cystic fibrosis: same old drugs but different benefits? *Curr. Opin. Pulm. Med.* **2014,** *20* (6), 607-612.
9. Uttley, L.; Harnan, S.; Cantrell, A.; Taylor, C.; Walshaw, M.; Brownlee, K.; Tappenden, P. Systematic review of the dry powder inhalers colistimethate sodium and tobramycin in cystic fibrosis. *Eur. Respir. Rev.* **2013,** *22* (130), 476-486.
10. d'Angelo, I.; Conte, C.; La Rotonda, M. I.; Miro, A.; Quaglia, F.; Ungaro, F. Improving the efficacy of inhaled drugs in cystic fibrosis: challenges and emerging drug delivery strategies. *Adv. Drug Deliv. Rev.* **2014,** *75*, 92-111.
11. Klinger-Strobel, M.; Lautenschlager, C.; Fischer, D.; Mainz, J. G.; Bruns, T.; Tuchscherr, L.; Pletz, M. W.; Makarewicz, O. Aspects of pulmonary drug delivery strategies for infections in cystic fibrosis--where do we stand? *Expert. Opin. Drug Deliv.* **2015,** *12* (8), 1351-1374.
12. Pilcer, G.; Amighi, K. Formulation strategy and use of excipients in pulmonary drug delivery. *Int. J. Pharm.* **2010,** *392* (1-2), 1-19.
13. Seville, P. C.; Li, H. Y.; Learoyd, T. P. Spray-dried powders for pulmonary drug delivery. *Crit Rev. Ther. Drug Carrier Syst.* **2007,** *24* (4), 307-360.
14. Rabbani, N. R.; Seville, P. C. The influence of formulation components on the aerosolisation properties of spray-dried powders. *J. Control Release* **2005,** *110* (1), 130-140.
15. Xu, E. Y.; Guo, J.; Xu, Y.; Li, H. Y.; Seville, P. C. Influence of excipients on spray-dried powders for inhalation. *Powder Technology* **2014,** *256*, 217-223.

16. Minne, A.; Boireau, H.; Horta, M. J.; Vanbever, R. Optimization of the aerosolization properties of an inhalation dry powder based on selection of excipients. *Eur. J. Pharm. Biopharm.* **2008,** *70* (3), 839-844.

17. Costabile, G.; d'Angelo, I.; Rampioni, G.; Bondi, R.; Pompili, B.; Ascenzioni, F.; Mitidieri, E.; d'Emmanuele, d., V; Sorrentino, R.; Miro, A.; Quaglia, F.; Imperi, F.; Leoni, L.; Ungaro, F. Toward Repositioning Niclosamide for Antivirulence Therapy of Pseudomonas aeruginosa Lung Infections: Development of Inhalable Formulations through Nanosuspension Technology. *Mol. Pharm.* **2015,** *12* (8), 2604-2617.

18. Pham, D. D.; Gregoire, N.; Couet, W.; Gueutin, C.; Fattal, E.; Tsapis, N. Pulmonary delivery of pyrazinamide-loaded large porous particles. *Eur. J. Pharm. Biopharm.* **2015,** *94*, 241-250.

19. Cuvelier, B.; Eloy, P.; Loira-Pastoriza, C.; Ucakar, B.; Sanogo, A. A.; Dupont-Gillain, C.; Vanbever, R. Minimal amounts of dipalmitoylphosphatidylcholine improve aerosol performance of spray-dried temocillin powders for inhalation. *Int. J. Pharm.* **2015,** *495* (2), 981-990.

20. Garcia, C. L.; Sung, J.; Ibrahim, M.; Elbert, K.; Edwards, D.; Hickey, A. Pharmacokinetics of Inhaled Rifampicin Porous Particles for Tuberculosis Treatment: Insight into Rifampicin Absorption from the Lungs of Guinea Pigs. *Mol. Pharm.* **2015,** *12* (8), 2642-2650.

21. Allegra, L.; Della, P. S.; Petrigni, G. Hyaluronic acid : perspectives in lung diseases. *Handb. Exp. Pharmacol.* **2012,** (207), 385-401.

22. Cantor, J. O. Potential therapeutic applications of hyaluronan in the lung. *Int. J. Chron. Obstruct. Pulmon. Dis.* **2007,** *2* (3), 283-288.

23. Furnari, M. L.; Termini, L.; Traverso, G.; Barrale, S.; Bonaccorso, M. R.; Damiani, G.; Piparo, C. L.; Collura, M. Nebulized hypertonic saline containing hyaluronic acid improves tolerability in patients with cystic fibrosis and lung disease compared with nebulized hypertonic saline alone: a prospective, randomized, double-blind, controlled study. *Ther. Adv. Respir. Dis.* **2012,** *6* (6), 315-322.

24. Ros, M.; Casciaro, R.; Lucca, F.; Troiani, P.; Salonini, E.; Favilli, F.; Quattrucci, S.; Sher, D.; Assael, B. M. Hyaluronic acid improves the tolerability of hypertonic saline in the chronic treatment of cystic fibrosis patients: a multicenter, randomized, controlled clinical trial. *J. Aerosol Med. Pulm. Drug Deliv.* **2014,** *27* (2), 133-137.

25. Esposito, E.; Menegatti, E.; Cortesi, R. Hyaluronan-based microspheres as tools for drug delivery: a comparative study. *Int. J. Pharm.* **2005,** *288* (1), 35-49.

26. Pham, D. D.; Fattal, E.; Ghermani, N.; Guiblin, N.; Tsapis, N. Formulation of pyrazinamide-loaded large porous particles for the pulmonary route: avoiding crystal growth using excipients. *Int. J. Pharm.* **2013,** *454* (2), 668-677.

27. Sivadas, N.; O'Rourke, D.; Tobin, A.; Buckley, V.; Ramtoola, Z.; Kelly, J. G.; Hickey, A. J.; Cryan, S. A. A comparative study of a range of polymeric microspheres as potential carriers for the inhalation of proteins. *Int. J. Pharm.* **2008,** *358* (1-2), 159-167.

28. DI, F. N. Turbidimetric measurement of acid mucopolysaccharides and hyaluronidase activity. *J. Biol. Chem.* **1956,** *220* (1), 303-306.

29. Ungaro, F.; d'Angelo, I.; Coletta, C.; d'Emmanuele, d., V; Sorrentino, R.; Perfetto, B.; Tufano, M. A.; Miro, A.; La Rotonda, M. I.; Quaglia, F. Dry powders based on PLGA nanoparticles for pulmonary delivery of antibiotics: modulation of encapsulation efficiency, release rate and lung deposition pattern by hydrophilic polymers. *J. Control Release* **2012,** *157* (1), 149-159.

30. Marques, M. R. C.; Loebenberg, R.; Almukainzi, M. Simulated Biological Fluids with Possible Application in Dissolution Testing. *Dissolution Technologies* **2011,** *18* (3), 15-28.

31. Odds, F. C.; Vranckx, L.; Woestenborghs, F. Antifungal susceptibility testing of yeasts: evaluation of technical variables for test automation. *Antimicrob. Agents Chemother.* **1995,** *39* (9), 2051-2060.

32. Clinical and Laboratory Standards Institute M27-A3. Reference method for broth dilution antifungal susceptibility testing of yeasts - Approved standard, third edition. Clinical and Laboratory Standards Institute: 2008.

33. Ohman, D. E.; Sadoff, J. C.; Iglewski, B. H. Toxin A-deficient mutants of Pseudomonas aeruginosa PA103: isolation and characterization. *Infect. Immun.* **1980,** *28* (3), 899-908.

34. Ambrosi, C.; Tiburzi, F.; Imperi, F.; Putignani, L.; Visca, P. Involvement of AlgQ in transcriptional regulation of pyoverdine genes in Pseudomonas aeruginosa PAO1. *J. Bacteriol.* **2005,** *187* (15), 5097-5107.

35. Gruenert, D. C.; Willems, M.; Cassiman, J. J.; Frizzell, R. A. Established cell lines used in cystic fibrosis research. *J. Cyst. Fibros.* **2004,** *3 Suppl 2*, 191-196.

36. Lanone, S.; Rogerieux, F.; Geys, J.; Dupont, A.; Maillot-Marechal, E.; Boczkowski, J.; Lacroix, G.; Hoet, P. Comparative toxicity of 24 manufactured nanoparticles in human alveolar epithelial and macrophage cell lines. *Part Fibre. Toxicol.* **2009,** *6*, 14.

37. Yang, M. Y.; Chan, J. G.; Chan, H. K. Pulmonary drug delivery by powder aerosols. *J. Control Release* **2014,** *193*, 228-240.

38. Nolan, S. J.; Thornton, J.; Murray, C. S.; Dwyer, T. Inhaled mannitol for cystic fibrosis. *Cochrane. Database. Syst. Rev.* **2015,** *10*, CD008649.

39. Sosnik, A.; Seremeta, K. P. Advantages and challenges of the spray-drying technology for the production of pure drug particles and drug-loaded polymeric carriers. *Advances in Colloid and Interface Science* **2015,** *223*, 40-54.

40. Hwang, S. M.; Kim, D. D.; Chung, S. J.; Shim, C. K. Delivery of ofloxacin to the lung and alveolar macrophages via hyaluronan microspheres for the treatment of tuberculosis. *J. Control Release* **2008,** *129* (2), 100-106.

41. Hoppentocht, M.; Hagedoorn, P.; Frijlink, H. W.; de Boer, A. H. Technological and practical challenges of dry powder inhalers and formulations. *Adv. Drug Deliv. Rev.* **2014,** *75*, 18-31.

42. Yang, Y.; Tsifansky, M. D.; Shin, S.; Lin, Q.; Yeo, Y. Mannitol-guided delivery of Ciprofloxacin in artificial cystic fibrosis mucus model. *Biotechnol. Bioeng.* **2011,** *108* (6), 1441-1449.

43. Patton, J. S.; Brain, J. D.; Davies, L. A.; Fiegel, J.; Gumbleton, M.; Kim, K. J.; Sakagami, M.; Vanbever, R.; Ehrhardt, C. The particle has landed--characterizing the

fate of inhaled pharmaceuticals. *J. Aerosol Med. Pulm. Drug Deliv.* **2010,** *23 Suppl 2:S71-87.*, S71-S87.

44. Loira-Pastoriza, C.; Todoroff, J.; Vanbever, R. Delivery strategies for sustained drug release in the lungs. *Adv. Drug Deliv. Rev.* **2014,** *75:81-91. doi: 10.1016/j.addr.2014.05.017. Epub;%2014 Jun 8.*, 81-91.

45. Vermes, A.; Guchelaar, H. J.; Dankert, J. Flucytosine: a review of its pharmacology, clinical indications, pharmacokinetics, toxicity and drug interactions. *J. Antimicrob. Chemother.* **2000,** *46* (2), 171-179.

46. Vermes, A.; Kuijper, E. J.; Guchelaar, H. J.; Dankert, J. An in vitro study on the active conversion of flucytosine to fluorouracil by microorganisms in the human intestinal microflora. *Chemotherapy* **2003,** *49* (1-2), 17-23.

CHAPTER 4

LARGE POROUS PARTICLES FOR SUSTAINED RELEASE OF A DECOY OLIGONUCELOTIDE AND POLY(ETHYLENIMINE): POTENTIAL FOR COMBINED THERAPY OF CHRONIC *PSEUDOMONAS AERUGINOSA* LUNG INFECTIONS

I. d'Angelo[1], B. Perfetto[2], G. Costabile[3], V. Ambrosini[2], P. Caputo[2], A. Miro[3], R. d'Emmanuele di Villa Bianca[4], R. Sorrentino[4], G. Donnarumma[2], F. Quaglia[3], F. Ungaro[3]

1 *Di.S.T.A.Bi.F., Second University of Naples, Via Vivaldi 43, 81100 Caserta, Italy*

2 *Department of Experimental Medicine- Section of Microbiology, Second University of Naples, Via Santa Maria di Costantinopoli 16, 80138 Naples, Italy.*

3 *Drug Delivery Labs, Department of Pharmacy, University of Naples Federico II, Via Domenico Montesano 49, 80131 Naples, Italy*

4 *Pharmacology Labs, Department of Pharmacy, University of Naples Federico II, Via Domenico Montesano 49, 80131 Naples, Italy*

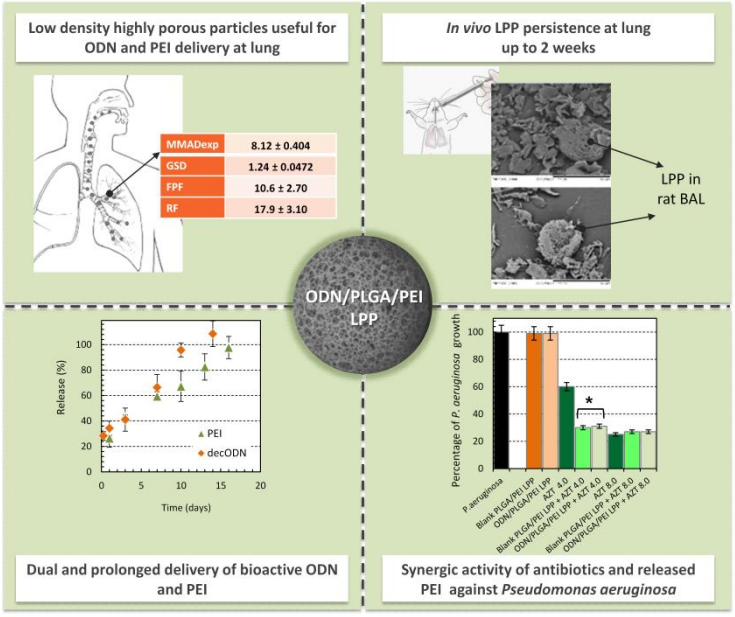

Biomacromolecules,March 22, 2016, Accepted

ABSTRACT

We have recently demonstrated that the specific inhibition of nuclear factor-κB by a decoy oligonucleotide (dec-ODN) delivered through inhalable large porous particles (LPP) made of poly(lactic-co-glycolic acid) (PLGA) may be highly beneficial for long-term treatment of lung inflammation. Nevertheless, besides chronic inflammation, multi-functional systems aimed to control also infection are required in chronic lung diseases, such as cystic fibrosis (CF). In this work, we tested the hypothesis that engineering PLGA-based LPP with branched poly(ethylenimine) (PEI) may improve LPP properties for pulmonary delivery of dec-ODN, with particular regard to the treatment of *Pseudomonas aeruginosa* lung infections. After getting insight into the role of PEI on the technological properties of PLGA-based LPP for delivery of dec-ODN, the putative synergistic effect of PEI free or PEI released from LPP on *in vitro* antimicrobial activity of tobramycin (Tb) and aztreonam (AZT) against *P. aeruginosa* was elucidated. Meanwhile, cytotoxicity studies on A549 cells were carried out. Results clearly demonstrate that the dry powders have promising aerosolization properties and afford a prolonged *in vitro* release of both dec-ODN and PEI. The encapsulation of PEI into LPP results in a 2-fold reduction of the minimum inhibitory concentration of AZT, while reducing the cytotoxic effect of PEI. Of note, the developed ODN/PLGA/PEI LPP persisted at lung at least for 14 days after intratracheal administration in rats where they can provide sustained and combined release of dec-ODN and PEI. dec-ODN will likely act as an anti-inflammatory drug, while PEI may enhance the therapeutic activity of inhaled antibiotics, which are commonly employed for the treatment of concomitant lung infections.

4.1. INTRODUCTION

Innovative oligonucleotide (ON)-based therapies are rather recent in the respiratory field but very intriguing in the light of their proved *in vitro* and *in vivo* potential, also in humans.[1-3] Different formulation approaches have been recently pursued to fulfil the requirements dictated by translation of ON-based inhalation therapy in humans.[3,4] Amid them, poly(lactic-co-glycolic) acid (PLGA) particles have generated considerable research interest due to their biodegradability and excellent biocompatibility[5]. Infact, ON encapsulation within PLGA microparticles can be regarded as a powerful mean to achieve its sustained release for long time-frames and to effectively protect the labile macromolecule from *in vivo* degradation occurring at the administration site.[6,7] Furthermore, PLGA microparticles may be engineered through the addition of specific excipients to proper deposit at lungs, to transport ONs in lung lining fluids and to enhance ON internalization in lung epithelial cells, where the target is located.[8]

Among excipients investigated to engineer PLGA microparticles for inhalation, those playing a dual role in the formulation should be preferred, especially if one of their effects is to widen and/or to enhance the biological activity of the inhaled drug.[8,9] This is the case of poly(ethylenimine) (PEI), which has been used as non-viral gene transfer agent since 90's[10-12] and has recently shown promise also for pulmonary delivery of ONs[13-15]. Due to high cationic charge density, PEI very efficiently condenses negatively-charged nucleic acid molecules into nanosized complexes, which provide escape from the harsh endosomal/lysosomal environment after internalization and allow a highly efficient transgene expression.[10-12]

We have recently tested PEI in the formulation of inhalable large porous particles (LPP) of PLGA for sustained delivery of a decoy oligonucleotide against NF-κB (dec-ODN) in cystic fibrosis (CF).[16] Indeed, PLGA-based LPP were demonstrated: i) to display promising aerodynamic properties for delivery from breath-actuated dry powder inhalers (DPI); ii) to exert a temporal control over dec-ODN released amount, while preserving its integrity; iii) to cause a persistent inhibition of the expression of important pro-inflammatory mediators as compared to naked dec-

ODN[16,17], also *in vivo*.[7] Nevertheless, engineering of PLGA-based LPP with PEI was demonstrated crucial to control mucin gene expression in mucoepidermoid lung epithelial cells, suggesting a potential active role of PEI in CF treatment.[16] Actually, besides chronic inflammation, multi-functional systems aimed to control also overproduction of the viscous airway mucus and lung infections is highly desirable in CF treatment.

Chronic *Pseudomonas aeruginosa* airway infections remain among the primary cause of mortality and morbidity in the CF population. Despite aggressive antibiotic therapy, *P. aeruginosa* is rarely eradicated owing to its level of intrinsic resistance to many drugs.[18] A major cause of resistance is the outer membrane of Gram-negative bacteria, which consists of an asymmetric double layer of polyanionic lipopolysaccharide (LPS) molecules (outer leaflet) and glycerophospholipids (inner leaflet). LPS molecules are electrostatically linked by bivalent cations (e.g. Mg^{2+} and Ca^{2+}), forming a strong structure that acts as an effective permeability barrier against hydrophobic antibiotics, detergent, dyes and macromolecules.[19] PEI may act as an effective permeabilizer of Gram-negative bacteria[20] and displays antibacterial properties ascribable to its polycationic structure, that comes from amino groups.[21,22] In fact, the bactericidal activity of PEI increases by increasing its polycationic character.[23] In particular, Gibney et al.[24] pointed out recently that it depends on both molecular weight and architecture of the macromolecule (i.e., linear or branched structure of polymer).

In this work, we test the hypothesis that engineering PLGA-based LPP with branched PEI may improve their carrier properties for pulmonary delivery of ONs, with particular regard to CF treatment. After getting an insight into the role of PEI on the technological properties of PLGA-based LPP for delivery of ONs, the synergistic effect of PEI free and PEI released from LPP on *in vitro* antimicrobial activity of tobramycin (Tb) and aztreonam (AZT) against P. *aeruginosa* is elucidated.

4.2. MATERIALS AND METHODS

4.2.1 Materials

Poly(D,L-lactide-co-glycolide) (50:50) (PLGA) (Resomer RG 504 H; Mw 41.9 kDa; inherent viscosity 0.5 dl/g) was purchased from Boehringer Ingelheim (Germany). Phosphorothioate oligodeoxynucleotide synthesis was performed by Tib Molbiol (Roche Diagnostics, Italy). Ammonium hydrogen carbonate, polyethylenimine (Mw 25 KDa; branched, PEI), polysorbate 80, polyvinylalcohol (PVA, Mowiol® 40−88), aztreonam (AZT) and tobramycin (Tb) were obtained from Sigma-Aldrich (Italy). Analytical grade sodium chloride, potassium chloride, sodium phosphate dibasic anhydrous, sodium bicarbonate, methylene chloride, were supplied by Carlo Erba (Italy).

A plain double-stranded decoy oligodeoxynucleotide to nuclear factor-kB (dec-ODN) was prepared by annealing sense and antisense phosphorothioate ONs *in vitro* in filtered water solution as previously reported [16]. The wild-type NF-kB consensus sequence used (dec-ODN) was: 5'−GAT CGA GGG GAC TTT CCC TAG C−3'; 3'−CTA GCT CCC CTG AAA GGG ATC G−5'.

4.2.2 Preparation of PEI-engineered LPP

PEI-engineered LPP were prepared in different formulation conditions by a modified double emulsion-solvent evaporation technique assisted by gas-foaming as previously reported.[16] Briefly, 0.25 ml of water containing ammonium bicarbonate (AB) as porogen (10-18 % w/v) and dec-ODN (0.140 nmol *per* mg of LPP) were poured into 2.5 ml of methylene chloride containing PLGA (15% w/v) in the presence of PEI (PEI:PLGA ratio 1:100−1:200 w/w). Emulsification was achieved using a high-speed homogenizer (Ystral, Heidolph, Germany) operating at 755 x*g* (tool 6G) for 3 minutes. Afterwards, the emulsion was added to 25 ml of aqueous PVA solution (0.5−1.0 % w/v) and homogenised 676 x*g* (tool 10F) for 2 minutes to produce the multiple emulsion ($w_1/o/w_2$). Solvent evaporation and subsequent particle hardening was achieved under magnetic stirring (MR 3001K, Heidolph, Germany) at room temperature. After 3 h, particles were collected, washed three

times with distilled water by centrifugation (Hettich Zentrifugen, Universal 16R) and freezed at -80°C. Samples were then dried for 36 h by a Modulyo freeze-drier (Edwards, UK) operating at 0.01 atm and -60°C.

LPP encapsulating dec-ODN at the theoretical loadings of 1.0 and 2.0 nmol *per* mg of LPP were also achieved by increasing PEI amount in the organic phase (PEI:PLGA ratio 1:50−1:100 w/w). LPP containing dec-ODN without PEI, blank LPP containing PEI (PEI:PLGA ratio 1:50, 1:100 or 1:200 w/w) without dec-ODN in the internal water phase were prepared as controls. Fluorescent LPP were prepared using Rhodamine-labeled PLGA (PLGA-Rhod) in the organic phase at 10 % w/w with respect to the total PLGA amount. PLGA-Rhod was synthesized according to a previously reported procedure.[25]

4.2.3 Characterization of PEI-engineered LPP

Particle shape and morphology were analysed by Scanning Electron Microscopy (SEM) (Leica S440, Germany). The samples were stuck on a metal stub and coated with gold under vacuum for 90−120 seconds.

The mean geometric diameter and size distribution of the particles were determined by laser light scattering (Coulter LS 100Q, USA) on a dispersion of freeze-dried particles in 0.2 % w/v aqueous PVA. Particle size is expressed as volume mean diameter ± standard deviation of values collected from three different batches.

Powder density was estimated by tapped density measurements according to Ph. Eur. 8th Ed. A known weight of particles (100 mg) was transferred to a 10 (±0.05) ml graduated cylinder and the initial volume recorded. The cylinder was then mechanically tapped 1250 times up to volume plateau, by mean of a tapped density tester (Mod. IG/4, Giuliani, Italy). Tapped density of particles (ρ) was expressed as the ratio between sample weight (g) and the volume occupied after 1250 tappings (ml).

To achieve information about LPP flow properties, the compressibility index or *Carr's Index* was estimated through the relative percent difference between bulk and tapped density as stated by US Pharmacopoeia:

$$\text{Carr's Index} = (1 - \rho_i/\rho)*100 \qquad (1)$$

where ρ and ρ_i are tapped and bulk density of the powder, respectively. On the basis of Carr's Index value, powder flow ability is defined as: 5−12%, excellent; 12−18%, good; 18−21%, fair; 21−25%, poor, fluid; 25−32%, poor, cohesive; 32−38%, very poor; >40%, extremely poor.

The theoretical mass mean aerodynamic diameter ($MMAD_t$) of the particles was also estimated on the basis of the definition:

$$MMAD_t = d\,(\rho/\rho_0 X)^{1/2} \qquad (2)$$

where d is the geometric mean diameter, ρ_0 is a reference density of 1 g/ml and *X* is the dynamic shape factor, which is 1 for a sphere. In the case of porous particles of approximately spherical shape:

$$\rho \approx \rho_s(1-\varepsilon) \qquad (3)$$

where ρ_s is the skeletal mass density of the particle as measured by pycnometry, ε is the particle porosity. An approximate bulk measure of ρ as defined by equation (3) is provided by tapped density.

Fluorescent LPP were further characterised by confocal laser scanning microscopy (CLSM) analysis carried out on a LSM 510 Zeiss confocal inverted microscope equipped with a Zeiss 20X/3 NA objective lens (Carl Zeiss, Germany). An argon laser (excitation = 541 nm; emission = 572 nm) was used.

The amounts of dec-ODN and PEI encapsulated within LPP were determined after particle degradation in 0.5 N NaOH. For dec-ODN, 10 mg of LPP were dissolved in 2 ml of 0.5 N NaOH under stirring at 37°C until a limpid solution was obtained. Dec-ODN content in the resulting solution was quantified by UV spectrophotometric analysis using a Shimadzu 1204 apparatus (Shimadzu, Milan, Italy) operating at 265 nm. The linearity of the response was verified over the concentration range 0.020–1.0 nmol/ml ($r^2 > 0.99$). Blank LPP were used as control to verify that no particle component interfered with dec-ODN quantification. The amount of PEI in the solution was contemporary quantified by UV spectrophotometric analysis at 285 nm after complexation with cupper(II) as previously reported.[26] Results are expressed as encapsulation efficiency (ratio of

actual and theoretical loadings × 100) ± standard deviation of values collected from three different batches.

4.2.4 *In vitro* release of dec-ODN and PEI from ODN/PLGA/PEI LPP

4.2.4.1 In vitro release of dec-ODN

In vitro release of dec-ODN from optimised PLGA/PEI LPP (ODN/PLGA/PEI) was monitored by membrane dialysis in phosphate buffer (120 mM NaCl, 2.7 mM KCl, 10 mM phosphate salts) (PBS) at 37°C. Prior to use, the pH was adjusted to 7.2 with 0.01 M HCl to better resemble *in vivo* conditions.[27] A known amount of dec-ODN-loaded LPP (5 mg) was suspended in 0.35 ml of PBS and placed in a dialysis membrane bag (MWCO: 50000 Da, Spectra/Por®). The sample was dropped into 5 ml of PBS (sink condition) and kept at 37°C. At scheduled time intervals, 1 ml of external medium was withdrawn and replaced by the same amount of fresh PBS. The withdrawn medium was analyzed for dec-ODN content by UV analysis as described above.

4.2.4.2 In vitro release of PEI

In vitro release of PEI from LPP was evaluated suspending a known amount of ODN/PLGA/PEI LPP (10 mg) in 1 ml of PBS at pH 7.2 and 37°C as described above for *in vitro* release of dec-ODN. The samples were incubated in a horizontal-shaking water bath at 40 rpm and 37°C (ShakeTempSW 22, Julabo Italia, Italy). At scheduled time intervals, the samples were centrifuged at 5000 x*g*, 4°C for 15 min (Hettich Zentrifugen, Universal 16R), 1 ml of release medium was withdrawn and replaced by the same amount of fresh PBS. The withdrawn medium was analyzed for PEI content by UV analysis after complexation with cupper(II) as described above for actual loading. As control, PEI release profile from blank PLGA/PEI LPP prepared in the absence of dec-ODN was determined.

Release kinetics are expressed as percentage of dec-ODN or PEI released *versus* time ± standard deviation of values collected from three different batches.

4.2.5 *In vitro* aerosolization properties of LPP

The aerosolization properties of optimised ODN/PLGA/PEI LPP were tested *in vitro* after delivery from Turbospin® (PH&T Pharma, Milano, Italy), a breath-activated, reusable medium resistance DPI working with single unit gelatin capsule containing the dry powder. The deposition pattern of the powder was investigated using a Next Generation Impactor (NGI) (Copley Scientific, UK) according to Ph. Eur. 8th Ed.

For each test, a hard gelatine capsule (size 2, Capsugel, USA) was filled with about 20 mg of the powder and placed in the Turbospin®. The capsule was then pierced and the liberated powder drawn through the impactor operated at 60 L/min for 4 s. The powder deposited on the seven NGI collection cups was quantitatively recovered by dissolution in an appropriate amount of dichloromethane. The powder deposited in the induction port and in the micro-orifice collector (MOC) was also recovered by washing with 10 ml of dichloromethane.

The emitted dose (ED) was calculated by accurately weighing the capsule before and after Turbospin® actuation. Upon emission, the experimental mass median aerodynamic diameter ($MMAD_{exp}$) and the geometric standard deviation (GSD) were calculated according to Ph.Eur. deriving a plot of cumulative mass of powder retained in each collection cup (expressed as percent of total mass recovered in the impactor) *versus* cut-off diameter of the respective stage. The $MMAD_{exp}$ of the particles was determined from the same graph as the particle size at which the line crosses the 50% mark and the GSD was defined as

$$GSD = (\text{Size X}/\text{Size Y})^{1/2}$$

where size X was the particle size at which the line crosses the 84% mark and size Y the size at which it crosses the 16% mark.

The fine particle fraction (FPF) was calculated taking into account the actual amount of LPP deposited on stage 3 through 7 (MMAD < 4.46 μm) as compared to the initial amount loaded into the nebulizer chamber, that is the nominal dose of NCL, according to the following equation:

$$FPF = \frac{\text{LPP amount on cup 3 through 7}}{\text{LPP amount loaded into the device}} \text{ x } 100$$

On the other hand, the respirable fraction (RF) was defined as:

$$RF = \frac{\text{LPP amount on cup 3 through 7}}{\text{LPP total amount deposited in the NGI}} \text{ x } 100$$

4.2.6 *In vitro* effect of PEI on antibiotic susceptibility of *P. aeruginosa*

4.2.6.1 Minimum inhibitory concentration of free antibiotics

The minimum inhibitory concentration (MIC) of free Tb and AZT was determined by the broth microdilution method in 96-well microplates (Falcon). The AZT- and Tb-sensitive *P. aeruginosa* strain used for the experiments was a clinical isolate at the Operating Unit Laboratory of Virology and Microbiology, Faculty of Medicine and Surgery, Second University of Naples (Italy). Briefly, *P. aeruginosa* was grown in Brain Heart Infusion (BHI) broth at 37 °C. The bacterial suspension to be used as the inoculum was diluted to yield an optical density (OD) around 1 at 600 nm (corresponding to about 1×10^{8} CFU/ml). Afterwards, the bacterial cell suspension was further diluted 100-folds to produce a bacterial cell suspension of 10×10^{5} CFU/ml.

Free AZT and Tb were serially diluted twofold in BHI broth to achieve final Tb concentrations ranging from 7.9 μg/ml to 0.95 μg/ml and AZT concentrations ranging from 32 to 0.25 μg/ml in a final volume of 200 μl (including 100 μl of bacterial suspension). The bacterial suspension alone was used as the positive control while the negative controls were the antibiotics at the highest concentrations and BHI broth alone. After 24 h of incubation the spectrophotometric absorbance was measured at 600 nm.

The MIC is defined as the lowest concentration of the tested antibiotic that inhibited the visible growth of the inoculum. The MIC endpoints were determined by reading the optical density (OD) of the plate at 600 nm with a Biophotometer 860 (Bio-Rad laboratories s.r.l., Italy) and confirmed by visual inspection. The lowest concentration that yields $OD \leq 0.1$ is determined as the MIC.

Results are expressed as percentage of *P. aeruginosa* growth ± standard deviation of values collected from three separate experiments performed in triplicate (n=9). *P. aeruginosa* alone has been considered as 100%.

4.2.6.2 Antibiotic susceptibility of P. aeruginosa in the presence of PEI

To test the susceptibility of *P. aeruginosa* to Tb and AZT in presence of PEI, either free or released from LPP, two set of experiments were set up.

Dose-response studies were first performed with free PEI in 96-well microplates. Briefly, 100 µl of free PEI were added to 100 µl of bacterial suspension (final *P. aeruginosa* concentration 5×10^5 CFU/ml) so as to achieve final PEI concentrations in the wells ranging from 5.0 to 40 µg/ml. After 1 h of incubation at 37°C, either Tb or AZT at MIC and sub-MIC concentrations were added to pre-treated *P. aeruginosa* and then incubated for 24 h to verify the inhibition of *P. aeruginosa* growth. Vehicle and PEI alone were added as control.

In case of released PEI, aqueous dispersions of blank PLGA/PEI LPP and ODN/PLGA/PEI LPP at 5 mg/ml were first incubated for 72 h at 37°C in PBS. The samples were then centrifuged at 3500 rpm for 15' and the supernatants were used for the study. In 96-well microplates, 100 µl of PEI-containing supernatants were added to 100 µl of *P. aeruginosa* inoculum (final bacteria concentration 5×10^5 CFU/ml). The inhibition of *P. aeruginosa* growth after further treatment with Tb and AZT was determined as described for free PEI. Blank PLGA LPP and ODN-loaded PLGA LPP (ODN/PLGA LPP), Tb (3.96 and 1.98 µg/ml), AZT (8 and 4 µg/ml) and *P. aeruginosa* alone were tested for comparison.

The inhibitory effects of the treatments were determined by reading the OD of the plate at 600 nm with a Biophotometer 860 (Bio-Rad laboratories s.r.l., Italy) and confirmed by visual inspection .

Results are expressed as percentage of *P. aeruginosa* growth ± standard deviation of values collected from three separate experiments performed in triplicate (n=9). *P. aeruginosa* alone has been considered as 100%.

4.2.7 Cytotoxicity studies on human alveolar basal epithelial cells

4.2.7.1 Cell culture and treatments

Human lung adenocarcinoma epithelial cells (A549) were grown in GIBCO™ F-12 K cell-culture medium (Invitrogen s.r.l., Italy) supplemented with 10% FBS, 1% glutamine and 1% penicillin/streptomycin at 37 °C and incubated at 90% humidity and 5% CO_2. The cells were allowed to grow until confluence and were trypsinized and seeded in plates (12 wells and/or 96 wells) for each experiment. Then, A549 cells ($1.5x10^5$ cells/well) were seeded in a final volume of 1 ml of DMEM supplemented with 10% FBS, 1% glutamine and 1% penicillin/ streptomycin at 37 °C and incubated at 90% humidity and 5% CO_2 for 24 h. Afterwards, the cells were treated for 24 h with different amounts of ODN/PLGA/PEI LPP (final concentration in the medium of 1.25, 2.5 and 5.0 mg/ml). Blank PLGA LPP, blank PLGA/PEI LPP and ODN-loaded PLGA LPP were used as control. Cytotoxicity of free PEI was tested in the concentration range 2.5 to 40 μg/ml. Tb and AZT have been also tested at the highest concentration employed on bacteria, respectively 7.9 and 32 μg/ml.

4.2.7.2 Trypan blue test

After 24 h of treatment, the cells were harvested and pooled in 1 ml of cell culture medium. The suspensions of treated or non-treated cells were diluted 1:1 v/v with a 0.4% sterile-filtered trypan blue solution (Sigma-Aldrich, Italy) for viable cell counting. Viable cells (uncoloured) compared to dead blue cells were counted on 10 μl of the trypan blue-cell suspension in four 1 x 1 mm squares of a Burker chamber under an optical microscope (Olympus CK40). The average number of cells *per* square was determined. For an accurate determination, the cell density was fixed between 20−50 cells/square overlying 1 mm^2. Results are expressed as percentage of cell vitality reduction ± standard deviation of values collected from three separate experiments performed in triplicate (n=9).

4.2.7.3 LDH release test

Lactate dehydrogenase (LDH) release in cell supernatants after 24 h of treatment was measured by a CytoTox 96® Non-Radioactive Cytotoxicity Assay (Promega, Italy) according to the manufacturer's instruction. Briefly, released LDH was measured with a 30-min coupled enzymatic assay, which results in the conversion of a tetrazolium salt (iodonitrotetrazolium chloride − INT) into a red formazan product. The spectrophotometric absorbance was measured at 490 nm. Results are expressed as percent increase of OD at 490 nm as compared to control ± standard deviation of values collected from three separate experiments performed in triplicate (n=9).

4.2.8 *In vivo* studies of LPP persistence at lung

4.2.8.1 Animals

Male Wistar rats (200−250 g, Charles River, Italy) were used for *in vivo* ODN/PLGA/PEI LPP persistence studies. Animals were housed in an environment with controlled temperature (21−24°C) and lighting (12:12 h light-darkness cycle). Standard chow and drinking water were provided *ad libitum*. A period of 7 days was allowed for acclimatisation of rats before any experimental manipulation was undertaken. Animals use was in accordance with the guidelines of Italian (N. 116/1992) and European Council law (N.86/609/CEE) for animal care. The experimental procedures were also approved by the Animal Ethics Committee of the University of Naples Federico II (Italy).

4.2.8.2 Lung administration of ODN/PLGA/PEI LPP

Animals were anesthetized using ketamine (100 mg/kg, i.p.) and xylazine (5 mg/kg, i.p.), and the depth of anaesthesia was continuously controlled. Rats were then placed ventral side up on a surgical table provided with a temperature-controlled pad to maintain physiological temperature. To avoid breathing problems, rats were placed on a slanted board (30° from the vertical). Rats were divided into different groups (n=4−6, for each group) and intratracheally administered with air (3 mL,

SHAM group) or about 2 mg of ODN/PLGA/PEI LPP by the low-scale DPI Model DP-4 (Penn-Century, USA). The cannula of the DPI was inserted directly into the trachea through the mouth. At predetermined time intervals (0, 3, 7 and 14 days), the rats were anesthetized by urethane (25% i.p.; 10 mL/kg), and after euthanization, bronchoalveolar lavage (BAL) was obtained for Scanning Electron Microscopy (SEM) analysis. As an index of the healthy status of the treated animals, rat body weights were recorded throughout the experiment.

4.2.8.3 SEM analysis of BAL

After euthanization, the trachea of rats was cannulated with a polyethylene tube (1 mm inner diameter) to perform BAL as previously reported.[28] Briefly, the lungs were sequentially washed by flushing with 4 mL of sterile, ice-cold PBS three times for each animal. The first PBS recovery was immediately placed on ice and then centrifuged at 1000 x*g* for 15 min at 25°C. The resulting pellet was suspended in 0.5 ml of aqueous formaldehyde (10% w/v). A small amount of each sample (20 μl) was transferred in a 24-well plate containing coverslips coated with pre-fibrillated collagen (100 μl of type I collagen *per* well were fibrillated at 37°C for 20 min). Samples were then dehydrated with 60%, 70%, 80% and 90% ethanol. Finally, coverslips were carefully taken out of the 24-well plates, dried overnight and coated with gold for SEM analysis (Leica S440 microscope, Germany)

4.3. RESULTS

4.3.1 Effect of the formulation conditions on the overall properties of PEI-engineered LPP

To investigate the role played by the excipients on the properties of LPP prepared by double emulsion (w_1/o/w_2) assisted by gas-foaming, preliminary formulation studies were carried out (table 4.1). In particular, three formulation variables were taken into account, that is the amount of AB in the internal aqueous phase (w_1), the PEI/PLGA ratio in the organic phase (o) and the PVA concentration in the external aqueous phase (w_2). Morphology, size and flow properties of the achieved formulations were compared with those of previously developed LPP_{PEI}.[16]

Table 4.1. Composition and overall properties of PLGA/PEI LPP containing dec-ODN[1] prepared by double emulsion ($w_1/o/w_2$) assisted by gas-foaming.

	LPP_{PEI}[2]	***$LPP_{PEI}200$***	***$LPP_{PEI}PVA$***	***$LPP_{PEI}15AB$***
AB in w_1 (w/v)	10 %	10 %	10 %	15 %
PEI/PLGA ratio (w/w)	1:100	1:200	1:100	1:100
PVA in w_2 (w/v)	0.5 %	0.5 %	1 %	0.5 %
Mean volume diameter[3] **(μm ± S.E.M.**[4]**)**	45.9 ± 3.3	34.6 ± 2.0	29.0 ± 2.5	43.4 ± 3.3
Tapped density (ρ) (g/ml ± S.E.M.[4]**)**	0.043 ± 0.004	0.011 ± 0.001	0.077 ± 0.001	0.029 ± 0.007
MMADt[6] **(μm ± S.E.M.**[4]**)**	3.6 ± 1.5	3.6 ± 1.0	8.0 ± 0.5	5.1 ± 0.6
Carr's index[7]	33.5 ± 0.78	9.9 ± 1.2	38.5 ± 0.011	23.7 ± 4.1

1. The theoretical loading was 0.140 nmoles of dec-ODN *per* mg of LPP.
2. Data from Ungaro *et al*. [16] are reported for comparison.
3. Mean geometric diameter as determined by laser diffraction.
4. Standard error mean of values calculated on three different batches (n=6).
5. Mass mean aerodynamic diameter estimated on the basis of the equation 2.
6. Powder flowability estimated on the basis of the equation 1.

As shown in Fig. 4.1, both the amount of PEI in the organic phase and AB in w_2 play a crucial role in determining the morphology of LPP. The reduction of PEI amount inside the formulation determined breaking and collapsing of LPP (Fig. 4.1, A1-A2), while a homogeneous population of highly porous particles was achieved in case of $LPP_{PEI}PVA$ (Fig. 4.1, B1-B2) and $LPP_{PEI}15AB$ (Fig. 4.1, C1-C2). In particular, LPP produced in the presence of 15% of AB in w_1 displayed numerous and regular pores homogeneously distributed through the particle surface (Fig. 4.1, B2).

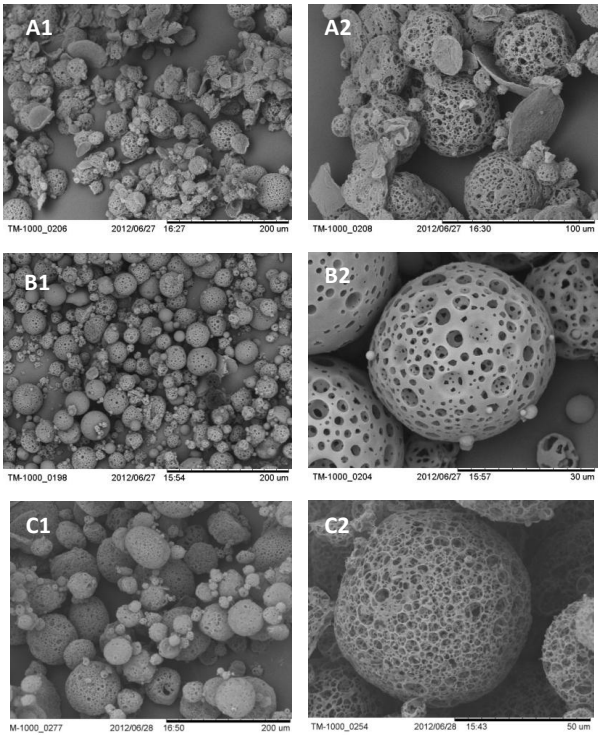

Figure 4.1. SEM micrographs at different magnification of dec-ODN loaded PEI-engineered LPP produced in different formulation conditions: $LPP_{PEI}200$ (A1-A2); $LPP_{PEI}PVA$ (B1-B2); $LPP_{PEI}15AB$ (C1-C2). Field is representative of the formulation.

Nevertheless, a slight increase the amount of AB up to 18 % in w_1 was detrimental for particle morphology (Fig. 4.2).

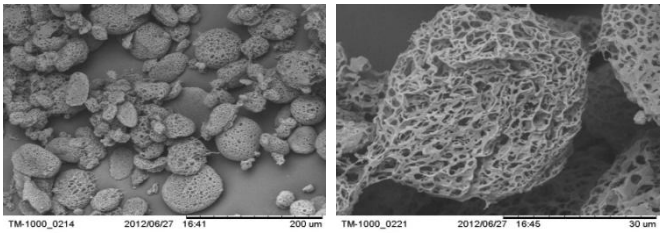

Figure 4.2. SEM micrographs at different magnification of dec-ODN loaded PEI-engineered LPP (PEI/PLGA 1:100 w/w) produced in the presence of 18% AB in the internal water phase. Field is representative of the formulation.

The developed LPP formulations displayed volume mean diameters falling approximately within the range 30−45 μm. A reduction of particle size was observed either by reducing PEI amount in the organic phase or increasing PVA concentration in w_2, with a minimum mean diameter value around 30 μm for $LPP_{PEI}PVA$ (Table 4.1). On the other hand, by the same amount of PEI in the organic phase, AB concentration in w_1 did not affect significantly the mean geometric diameter of the particles (45.9 ± 3.3 and 43.4 ± 3.3 μm for LPP_{PEI} and $LPP_{PEI}15AB$, respectively).

Flow properties and entrapment efficiency of the developed LPP are relevant parameters to select the proper formulation conditions. As far as LPP aerodynamic diameter and, consequently, aerosolization properties, are concerned, the right combination of three main parameters, that is LPP shape, geometric diameter and mass density should occur. Despite their highly irregular shape and morphology, $LPP_{PEI}200$ displayed the lowest values of tapped density and Carr's index. Meanwhile, a lower tapped density and a higher flowability was shown by $LPP_{PEI}15AB$ as compared to their counterpart prepared at 10% AB in w_1 (i.e., LPP_{PEI}) and those of $LPP_{PEI}PVA$. Nevertheless, formulation conditions affected also entrapment efficiency of PEI and dec-ODN (Fig. 4.3).

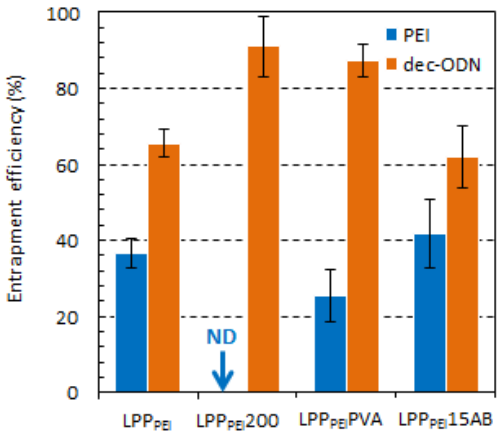

Figure 4.3. Effect of formulation conditions on the entrapment efficiency of PEI-engineered LPP. Data on previously developed LPP_{PEI} are reported for comparison[16]. No-Detectable (ND) amount of PEI was found in $LPP_{PEI}200$ particles.

While the amount of dec-ODN entrapped within LPP increased by increasing PVA concentration in w_2, PEI entrapment efficiency decreased as compared to both previously developed LPP_{PEI} [16] and $LPP_{PEI}15AB$. On the other hand, at the same amount of dec-ODN entrapped as compared to LPP_{PEI}, $LPP_{PEI}15AB$ allowed a slight increase of PEI entrapment efficiency from 36 to 42%.

Of note, no detectable amount of PEI was found in $LPP_{PEI}200$, although this did not result in a lower dec-ODN entrapment efficiency. The effect of the amount of PEI in LPP on dec-ODN entrapment efficiency was better elucidated by increasing the amount of dec-ODN inside the formulation. Results demonstrated that only a 2-fold increase of PEI in the organic phase allowed to entrap amount of dec-ODN ranging between 0.8 to 1.5 nmol *per* mg of LPP with very good efficiency (≈65%) (Fig. 4.4).

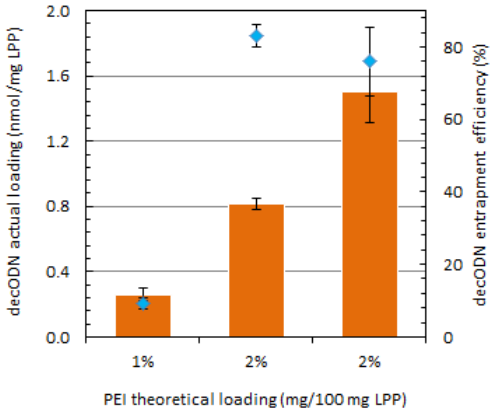

Figure 4.4. Dec-ODN actual loading and entrapment efficiency ofPEI-engineered LPP as a function of PEI theoretical loading.

4.3.2 Release features and aerosolization properties of optimized ODN/PLGA/PEI LPP

On the basis of the promising flow properties and entrapment efficiency, LPP_{PEI}15AB, from here on called ODN/PLGA/PEI LPP, were selected for further studies. *In vitro* release kinetics of dec-ODN and PEI from ODN/PLGA/PEI LPP were evaluated as described above. As reported in Fig. 4.5A, encapsulated dec-ODN was slowly released from LPP, with a typical two-stage release profile. After a burst effect around 30% in the first hours, LPP displayed a sustained release of the dec-ODN lasting about 15 days, with an approximately zero-order release kinetics. A very similar release profile was observed for PEI, which was slowly released from ODN/PLGA/PEI LPP for 15 days as well (Fig. 3.5B). Of note, the release rate of PEI from blank PLGA/PEI LPP prepared in the absence of dec-ODN slowed down as compared to ODN/PLGA/PEI LPP (Fig. 3.5B).

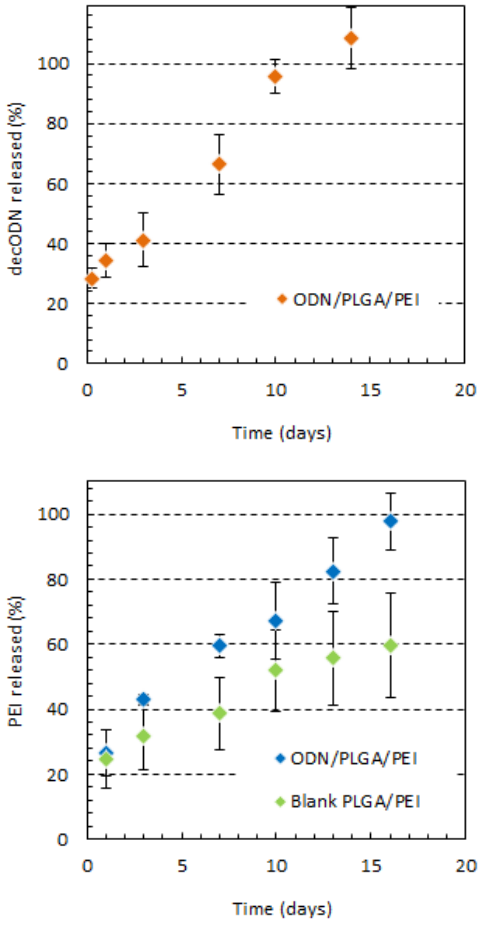

Figure 4.5. *In vitro* release kinetics of dec-ODN (A) and PEI (B) from ODN/PLGA/PEI LPP in PBS at pH 7.2 and 37°C. The release profile of PEI from blank PLGA/PEI LPP prepared without dec-ODN is reported for comparison in panel B.

In vitro aerosolization properties of ODN/PLGA/PEI LPP have been evaluated by NGI upon delivery from a low-resistance DPI. To this purpose, fluorescently-labeled ODN/PLGA/PEI LPP have been produced replacing 20% of the initial amount of PLGA with PLGA-Rhod. This allowed the achievement of fluorescent highly porous microparticles (Fig. 4.6A) characterized by the same properties of unlabeled ODN/PLGA/PEI LPP (data not shown). Of note, fluorescent ODN/PLGA/PEI LPP

distributed along all the NGI stages down to MOC. The dry powders displayed a $MMAD_{exp}$ around 8 μm, with a FPF and RF of 10.6 and 17.9 %, meaning that about 20% of the emitted dose has a MMAD lower than 5 μm (Fig. 4.6B).

A

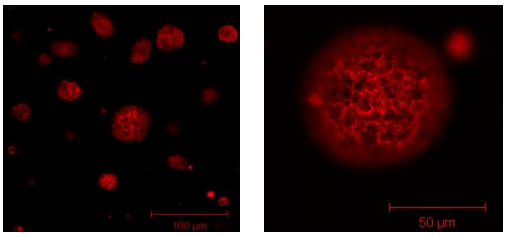

B

MMADexp (μm ± SD)	8.12 ± 0.404
Geometrical Standard Deviation (GSD) (± SD)	1.24 ± 0.0472
Fine particle fraction (FPF) (% ± SD)	10.6 ± 2.70
Respirable Fraction (RF) (% ± SD)	17.9 ± 3.10

Figure 4.6. Fluorescent ODN/PLGA/PEI LPP and their *in vitro* aerosolization properties: A) CLSM analysis (field is representative of the sample); **B)** Values of $MMAD_{exp}$, FPF (calculated on the nominal LPP dose) and RF (calculated on the emitted LPP dose) upon delivery from a medium-resistance DPI (Turbospin®)**.** Standard deviation (SD) is calculated on two different batches (n=6).

4.3.3 *In vivo* lung persistence of ODN/PLGA/PEI LPP

To allow a proof of concept of the ability of the developed LPP to deposit and to persist at lung *in vivo*, the developed ODN/PLGA/PEI LPP were intra-tracheally delivered in healthy rats and their fate in the lung upon delivery followed during time. As shown in Fig. 4.7, BAL analysis suggest the presence of a huge amount of LPP in the lung just after administration (time 0). Nevertheless, detectable amounts of LPP were found in the rat BAL for at least two weeks. Furthermore, body weight changes were monitored as a sensitive indication of the general health status of the treated animals. Of note, no significant differences in the body weight were found

between the treated and the sham group at each time interval (data not shown). Nevertheless, a significant increase in the body weight was observed at 7 and 14 days (* $p<0.05$ and *** $p<0.001$, respectively) as compared to time 0, in both treated and sham groups.

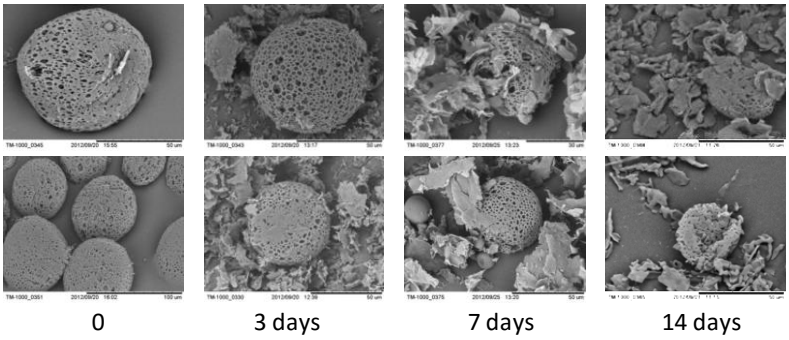

Figure 4.7. SEM micrographs of rat BAL samples collected at different time intervals upon intratracheal administration of ODN/PLGA/PEI LPP. Fields are representative of the sample.

4.3.4 Effect of PEI on antibiotic susceptibility of *P. aeruginosa*

Fig. 4.8 shows the effect of PEI alone and in association with either Tb or AZT on *P. aeruginosa* growth. In a preliminary set of experiments we tested Tb at concentrations ranging from 7.9 to 0.95 μg/ml and AZT concentrations ranging from 32 to 0.25 μg/ml (data not shown). The resulting MIC of Tb and AZT were 3.9 μg/ml and 8 μg/ml, respectively. In Fig. 4.8A we show that free PEI (2.5−40 μg/ml) did not affect *P. aeruginosa* growth and did not show any effect on Tb antimicrobial activity, at all concentration tested (ranging from 20 to 2.5 μg/ml) and similar results were obtained by using AZT at the concentration of 8 μg/ml. On the other hand, concentrations of 5, 10 and 20 μg/ml of PEI were able to reduce the MIC of AZT from 8 to 4 μg/ml (Fig. 4.8.B). The same concentrations of PEI were not able to further reduce the value of MIC in association with AZT ranging from 2 to 0.25 μg/ml (data not shown).

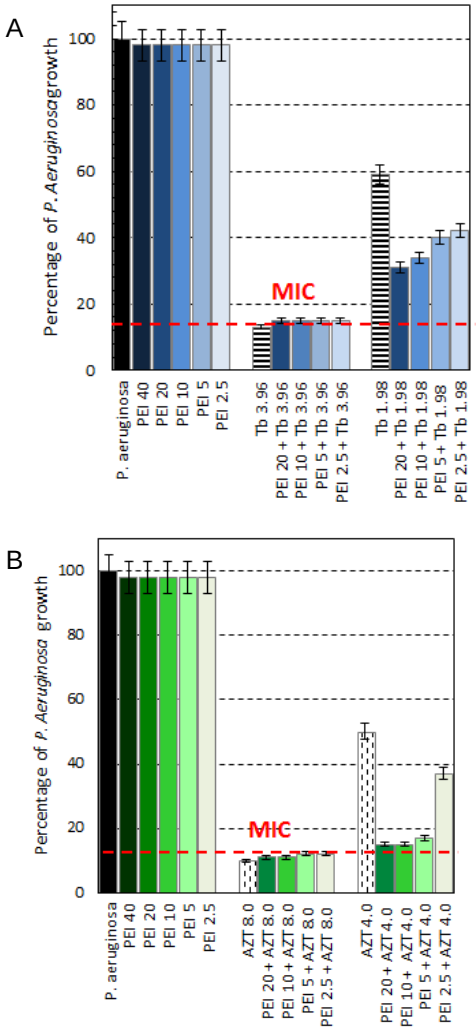

Figure 4.8. Effect of PEI (ranging from 40 to 2.5 μg/ml) on *P. aeruginosa* growth and on *P.aeruginosa* susceptibility *vs* Tb (3.96 and 1.98 μg/ml) (A) and *vs* AZT (8 and 4 μg/ml) (B). *P. aeruginosa* alone was used as control. The dotted lines represent the percentage of *P. aeruginosa* growth at MIC concentrations. Data are the mean values of three independent experiments, each performed in triplicates (n=9).

A parallel set of experiments was performed on PEI released from ODN/PLGA/PEI LPP and blank PLGA/PEI/LPP after 72 h of incubation at 37°C in association with Tb or AZT (Fig. 4.9). Of note, PEI released from LPP (5 mg/ml) did not reduce the MIC of Tb (Fig. 4.9A), while it was able to reduce the value of MIC for AZT from 8 μg/ml to 4 μg/ml (Fig. 4.9B).

4.3.5 Cytotoxicity of ODN/PLGA/PEI LPP towards A549 cells

The effect of ODN/PLGA/PEI LPP on A549 cells viability was investigated and compared with the same amount of free PEI. Blank PLGA LPP, blank PLGA/PEI LPP and PLGA LPP containing dec-ODN without PEI (ODN/PLGA) were also tested as controls. Fig. 4.10A shows the results of the trypan blue exclusion test. All the treatments performed with the LPP formulations did not significantly affect A549 cell viability, whereas free PEI at 10 μg/ml and 20 μg/ml determined a significant reduction in cell viability. On the other hand, no difference in cell viability was observed by using free PEI 5 μg/ml. The measurement of LDH activity confirmed the results showing a significant LDH release only in presence of free PEI concentrations (Fig. 4.10B). Tb and AZT did not show any cytotoxic effect on A549 cells at the concentration used (data not shown).

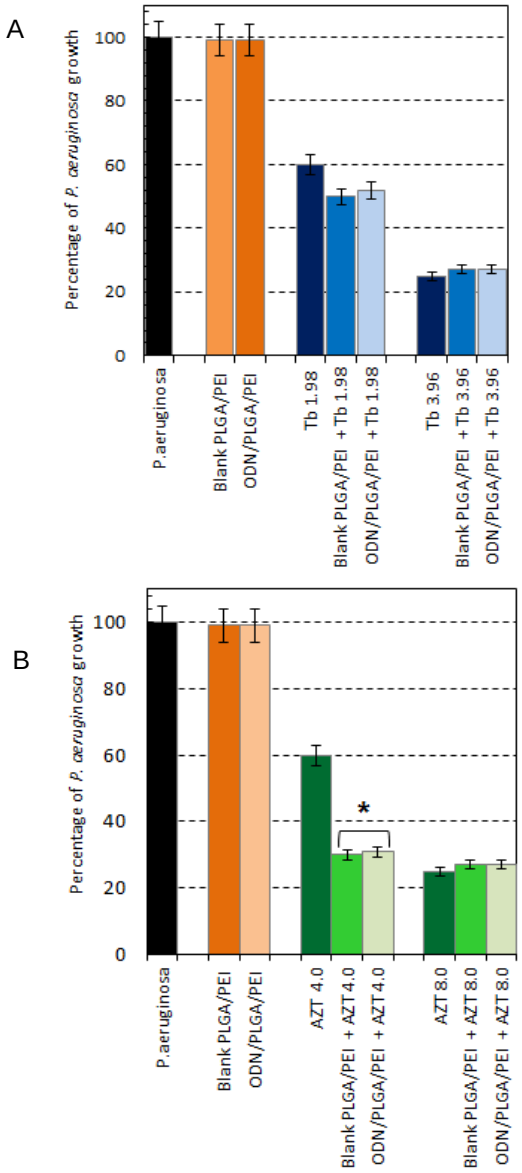

Figure 4.9. Effect of PEI released at 72 h from blank PLGA/PEI and ODN/PLGA/PEI LPP on *P. aeruginosa* growth and on *P.aeruginosa* susceptibility *vs* Tb (3.9 and 1.98 μg/ml) (A) and *vs* AZT (8 and 4 μg/ml) (B). *P. aeruginosa* alone was used as control. Data are the mean values of three independent experiments, each performed in triplicates (n=9).

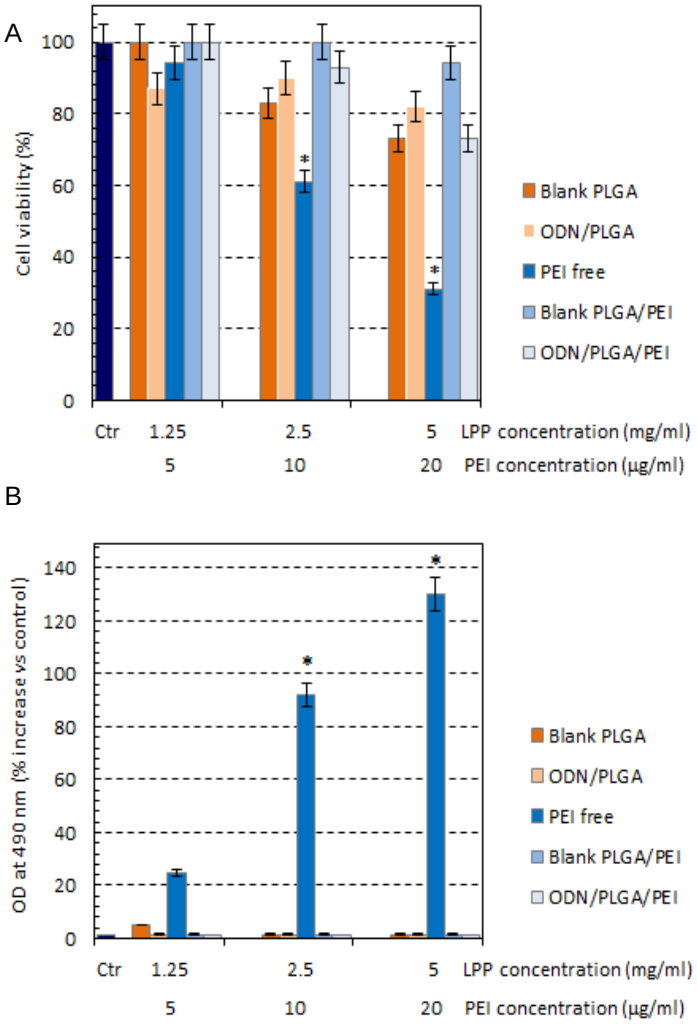

Figure 4.10. Cytotoxicity studies on A549 cells: A) percent reduction of cell viability upon 24 h incubation with ODN/PLGA/PEI LPP as compared to untreated control cells (Ctr, 100% viability) as determined by Trypan Blue test; B) LDH release at 24 h expressed as percent increase of OD at 490 nm as compared to untreated control cells (Ctr, <1%). Data are the mean values of three independent experiments, each performed in triplicates (n=9).

4.4. DISCUSSION

In order to limit inflammation and hyper-production of mucin in CF patients, a therapeutic strategy based on the specific inhibition of the nuclear transcription factor NF-κB by an oligonucleotide decoy, named dec-ODN, has been recently proposed.[29] Nevertheless, the structural complexity of this macromolecule as compared to conventional drugs demands for an efficient delivery system to allow dec-ODN to easily access and to remain at the target site, i.e. at lung. With this idea in mind, we have recently developed dry powders for dec-ODN inhalation consisting in LPP made of a biodegradable sustained-release polymer, that is PLGA.[7,16,17] This study tests the hypothesis that PEI could work as multifunctional excipient in PLGA-based LPP engineered for pulmonary drug delivery, from both a technological and a therapeutic point of view. On one hand, PEI could be of help in optimizing aerosolization properties due to its possible action on LPP porosity.[30,31] On the other hand, it may act as an adjuvant in the therapy of CF lung disease, due to its potential ability to permeabilize the membrane of Gram negative bacteria, such as *P. aeruginosa*.[20]

Conceiving LPP for sustained delivery of dec-ODN in the lung, the effect of the formulation conditions on the most relevant properties of PEI-engineered LPP for inhalation was first elucidated. Among aerosol drug delivery technologies, we selected dry powders, which should allow to overcome stability and bioavailability issues associated with conventional modes of ON aerosolization. Nevertheless, the use of DPIs encompasses the need of adequately engineered particles, which should possess optimal size, density and flow properties to be delivered from the DPI and to effectively deposit at lung.[32] Thus, the formulation studies were useful to select those LPP characterized by adequate bulk and flow properties for inhalation. Furthermore, the ability to entrap an adequate amount of dec-ODN and PEI was considered a key requisite. This was the case of LPP prepared at the highest PLGA/PEI ratio (i.e., 1:100) and porogen concentration (i.e., 15 % w/v).

Optimised ODN/PLGA/PEI LPP displayed promising *in vitro* aerosolization properties. The dry powder was delivered from a medium-resistance breath-actuated

DPI with a maximum efficiency. Around 20% of the recovered dose of ODN/PLGA/PEI LPP displayed $MMAD_{exp}$ lower than 5 μm, likely depositing in deep lung. In fact, a widespread deposition along bronchi and bronchioles is expected on the basis of distribution in rat lungs found for similar LPP with a $MMAD_{exp}$ lower than 10 μm.[33]

Once deposited in the lung, ODN/PLGA/PEI LPP are expected to serve as a local depot for the slow release of dec-ODN and PEI. To this purpose, two conditions should subsist: i) LPP persistence at lung; ii) sustained dual release of the entrapped dec-ODN and the antimicrobial polycation PEI. Concerning LPP clearance from the lung, although LPP are reported to escape uptake from pulmonary macrophages[34], mucociliary clearance, designed by evolution to eliminate inhaled and possibly noxious material from the airways, may considerably limits the benefits of sustained-release inhalation therapy.[35] Here, *in vivo* persistence studies performed after intratracheal administration of ODN/PLGA/PEI LPP clearly showed that the particles deposit at lung, by virtue of their aerosolization properties, and remain in situ at least for 2 weeks, supporting the ability of LPP to overcome macrophage-mediated clearance. Furthermore, the developed LPP allowed a sustained *in vitro* release of both dec-ODN and PEI lasting two weeks.

Of note, dec-ODN and PEI were released from LPP with very similar kinetics. In our previous papers, we demonstrated that it is possible to entrap ON and PEI in PLGA particles and release them in the form of complexes, thus improving ON uptake inside cells in vitro.[36,37] Here, dec-ODN/PEI interactions cannot be excluded and, consequently, their release in the form of complexes as well. Thus, ODN/PLGA/PEI LPP may serve as carrier for the combined and sustained release of dec-ODN and PEI. The first will likely act as an anti-inflammatory drug[7,16,17], the second could in principle enhance the therapeutic activity of inhaled antibiotics commonly employed for the treatment of concomitant *P. aeruginosa* lung infections. To prove this hypothesis, we tested antimicrobial activity of free PEI and its synergic effect with antibiotics commonly used in CF. Consensus guidelines recommend an early and aggressive treatment to eradicate acquired *P. aeruginosa* lung infections, although no specific protocol is preferred in CF patients. In the

setting of pulmonary exacerbation, the therapy frequently consists of β-lactams, such as AZT, and/or an aminoglycoside, such as Tb. In recent years, the evidence that the use of AZT solution for inhalation is associated with an increase in quality-adjusted life–years and improvement of clinical outcomes among patients with CF with extensive prior use of Tb solution for inhalation.[38,39] Our data showed that free PEI itself up to 40 μg/ml did not affect or interfere with the growth of *P. aeruginosa*. Nevertheless, PEI showed a synergic effect with AZT and not with Tb, with a consequent two-fold reduction of AZT MIC from 8 to 4 μg/ml. Similar results were achieved when PEI was released from LPP. It seems that PEI, similarly to other polyamines and polymyxin B nonapeptide, disorganizes the outer membrane of *P. aeruginosa* by intercalating in the LPS layer thus causing outer membrane permeabilization without significant liberation of LPS.[40,41] Although being a potent permeabilizer, PEI did not inhibit bacterial growth but, by virtue of its permeability-increasing properties, it may facilitate antibiotic delivery into cells, thus potentiating antibacterial effect. As previously reported, this synergic effect strictly depends on the chemical structure of the antibiotic and more benefits are expected for hydrophobic molecules, such as AZT, entering bacterial wall through passive diffusion.[19]

Unfortunately, PEI may act as a permeabilizer on all types of membranes. Thus, a great attention should be paid to PEI potential cytotoxicity towards lung epithelial cells, strictly dependent on its molecular weight.[10,42] It has been demonstrated that PEI exerts its cytotoxic effect by a two-phase mechanism.[43] In a first phase, PEI molecules bind to the plasma membrane proteoglycans resulting in membrane destabilization. This was found to generate significant release of LDH within the first hours, which continued in a time-dependent manner. On the other hand, significant activation of caspase-3 occurs 24 h post-treatment with PEI, suggesting that apoptosis represents phase II cytotoxicity.[43] LDH release test allowed us to confirm the destabilization of the cell membrane caused by PEI. On the other hand, trypan blue assay demonstrated that free PEI determines also late apoptosis/necrosis in A549 cells. Thus, cytotoxicity of free PEI would strongly hamper its use as synergic agent with antibiotics. Interestingly, PEI cytotoxicity was significantly

reduced once entrapped in the LPP developed here, presumably due to a slow and sustained PEI release. In perspective, LPP are expected to give synergic effects with specific antibiotic therapies without arising toxicity concerns.

4.5. **CONCLUSIONS**

Sustained drug delivery to the lungs is nowadays regarded as an effective strategy for local treatment of chronic lung diseases, such as CF, to achieve long-term maintenance of therapeutic drug concentrations, to reduce doses and dosing frequency and, last but not least, to improve patient adherence to the therapy. In this work, by acting on crucial formulation parameters, PLGA-based LPP have been successfully engineered for deposition and long-term persistence at lung in form of dry powders. The developed system affords slow dual release of a decoy ON against NF-kB with a well-established anti-inflammatory activity and PEI, displaying a synergic effect with one of the inhaled antibiotic currently used in CF, that is AZT. Meanwhile, cytotoxicity studies demonstrate the feasibility of PEI-based antimicrobial therapy only when slowly released from LPP, which allow to avoid PEI mediated epithelial cell damage. Taken all together, our data pave the way to the use of biodegradable PLGA LPP as sustained-release carriers for combined anti-inflammatory and antimicrobial therapy of CF lung disease.

REFERENCES

1. Durcan, N.; Murphy, C.; Cryan, S. A. Inhalable siRNA: potential as a therapeutic agent in the lungs. *Mol. Pharm.* **2008,** *5* (4), 559-566.
2. Ferrari, N.; Seguin, R.; Renzi, P. Oligonucleotides: a multi-targeted approach for the treatment of respiratory diseases. *Future. Med. Chem.* **2011,** *3* (13), 1647-1662.
3. Lam, J. K.; Liang, W.; Chan, H. K. Pulmonary delivery of therapeutic siRNA. *Adv. Drug Deliv. Rev.* **2011**.
4. Merkel, O. M.; Rubinstein, I.; Kissel, T. siRNA delivery to the lung: what's new? *Adv. Drug Deliv. Rev.* **2014,** *75*, 112-128.
5. Beck-Broichsitter, M.; Merkel, O. M.; Kissel, T. Controlled pulmonary drug and gene delivery using polymeric nano-carriers. *J. Control Release* **2012,** *161* (2), 214-224.
6. Mundargi, R. C.; Babu, V. R.; Rangaswamy, V.; Patel, P.; Aminabhavi, T. M. Nano/micro technologies for delivering macromolecular therapeutics using poly(D,L-lactide-co-glycolide) and its derivatives. *J. Control Release.* **2008,** *125* (3), 193-209. L.; d'Angelo, I
7. De Stefano, D.; Coletta, C.; Bianca, R.; Falcone,.; Ungaro, F.; Quaglia, F.; Carnuccio, R.; Sorrentino, R. A decoy oligonucleotide to NF-kappaB delivered through inhalable particles prevents LPS-induced rat airway inflammation. *Am. J. Respir. Cell Mol. Biol.* **2013,** *49* (2), 288-295.
8. Ungaro, F.; d'Angelo, I.; Miro, A.; La Rotonda, M. I.; Quaglia, F. Engineered PLGA nano- and micro-carriers for pulmonary delivery: challenges and promises. *J. Pharm. Pharmacol.* **2012,** *64* (9), 1217-1235.
9. d'Angelo, I.; Conte, C.; La Rotonda, M. I.; Miro, A.; Quaglia, F.; Ungaro, F. Improving the efficacy of inhaled drugs in cystic fibrosis: challenges and emerging drug delivery strategies. *Adv. Drug Deliv. Rev.* **2014,** *75*, 92-111.
10. Boussif, O.; Lezoualc'h, F.; Zanta, M. A.; Mergny, M. D.; Scherman, D.; Demeneix, B.; Behr, J. P. A versatile vector for gene and oligonucleotide transfer into cells in culture and in vivo: polyethylenimine. *Proc. Natl. Acad. Sci. U. S. A* **1995,** *92* (16), 7297-7301.
11. Lai, W. F. In vivo nucleic acid delivery with PEI and its derivatives: current status and perspectives. *Expert Rev. Med. Devices.* **2011,** *8* (2), 173-185.
12. Merkel, O. M.; Zheng, M.; Debus, H.; Kissel, T. Pulmonary gene delivery using polymeric nonviral vectors. *Bioconjug. Chem.* **2012,** *23* (1), 3-20.
13. Ferrari, S.; Pettenazzo, A.; Garbati, N.; Zacchello, F.; Behr, J. P.; Scarpa, M. Polyethylenimine shows properties of interest for cystic fibrosis gene therapy. *Biochim. Biophys. Acta.* **1999,** *1447* (2-3), 219-225.
14. Davies, L. A.; Hyde, S. C.; Nunez-Alonso, G.; Bazzani, R. P.; Harding-Smith, R.; Pringle, I. A.; Lawton, A. E.; Abdullah, S.; Roberts, T. C.; McCormick, D.; Sumner-Jones, S. G.; Gill, D. R. The use of CpG-free plasmids to mediate persistent gene expression following repeated aerosol delivery of pDNA/PEI complexes. *Biomaterials.* **2012,** *33* (22), 5618-5627.
15. Suk, J. S.; Kim, A. J.; Trehan, K.; Schneider, C. S.; Cebotaru, L.; Woodward, O. M.; Boylan, N. J.; Boyle, M. P.; Lai, S. K.; Guggino, W. B.; Hanes, J. Lung Gene Therapy

with Highly Compacted DNA Nanoparticles that Overcome the Mucus Barrier. *J. Control Release.* **2014,** (14), 10.

16. Ungaro, F.; De, S. D.; Giovino, C.; Masuccio, A.; Miro, A.; Sorrentino, R.; Carnuccio, R.; Quaglia, F. PEI-Engineered Respirable Particles Delivering a Decoy Oligonucleotide to NF-kappaB: Inhibiting MUC2 Expression in LPS-Stimulated Airway Epithelial Cells. *PLoS. One.* **2012,** *7* (10), e46457.

17. De Stefano, D.; Ungaro, F.; Giovino, C.; Polimeno, A.; Quaglia, F.; Carnuccio, R. Sustained inhibition of IL-6 and IL-8 expression by decoy ODN to NF-kappaB delivered through respirable large porous particles in LPS-stimulated cystic fibrosis bronchial cells. *J. Gene Med.* **2011,** *13* (4), 200-208.

18. Gaspar, M. C.; Couet, W.; Olivier, J. C.; Pais, A. A.; Sousa, J. J. Pseudomonas aeruginosa infection in cystic fibrosis lung disease and new perspectives of treatment: a review. *Eur. J. Clin. Microbiol. Infect. Dis.* **2013,** *32* (10), 1231-1252.

19. Khalil, H.; Chen, T.; Riffon, R.; Wang, R.; Wang, Z. Synergy between polyethylenimine and different families of antibiotics against a resistant clinical isolate of Pseudomonas aeruginosa. *Antimicrob. Agents Chemother.* **2008,** *52* (5), 1635-1641.

20. Helander, I. M.; Alakomi, H. L.; Latva-Kala, K.; Koski, P. Polyethyleneimine is an effective permeabilizer of gram-negative bacteria. *Microbiology* **1997,** *143 (Pt 10)*, 3193-3199.

21. Klibanov, A. M. Permanently microbicidal materials coating. *J. Mater. Chem.* **2007,** *17*, 2479-2482.

22. Lin, J.; Qiu, S.; Lewis, K.; Klibanov, A. M. Bactericidal properties of flat surfaces and nanoparticles derivatized with alkylated polyethylenimines. *Biotechnol. Prog.* **2002,** *18* (5), 1082-1086.

23. Murata, H.; Koepsel, R. R.; Matyjaszewski, K.; Russell, A. J. Permanent, non-leaching antibacterial surface--2: how high density cationic surfaces kill bacterial cells. *Biomaterials* **2007,** *28* (32), 4870-4879.

24. Gibney, K. A.; Sovadinova, I.; Lopez, A. I.; Urban, M.; Ridgway, Z.; Caputo, G. A.; Kuroda, K. Poly(ethylene imine)s as antimicrobial agents with selective activity. *Macromol. Biosci.* **2012,** *12* (9), 1279-1289.

25. Maiolino, S.; Moret, F.; Conte, C.; Fraix, A.; Tirino, P.; Ungaro, F.; Sortino, S.; Reddi, E.; Quaglia, F. Hyaluronan-decorated polymer nanoparticles targeting the CD44 receptor for the combined photo/chemo-therapy of cancer. *Nanoscale.* **2015,** *7* (13), 5643-5653.

26. Ungaro, F.; De, R. G.; Miro, A.; Quaglia, F. Spectrophotometric determination of polyethylenimine in the presence of an oligonucleotide for the characterization of controlled release formulations. *J. Pharm. Biomed. Anal.* **2003,** *31* (1), 143-149.

27. Pezzulo, A. A.; Tang, X. X.; Hoegger, M. J.; Alaiwa, M. H.; Ramachandran, S.; Moninger, T. O.; Karp, P. H.; Wohlford-Lenane, C. L.; Haagsman, H. P.; van, E. M.; Banfi, B.; Horswill, A. R.; Stoltz, D. A.; McCray, P. B., Jr.; Welsh, M. J.; Zabner, J. Reduced airway surface pH impairs bacterial killing in the porcine cystic fibrosis lung. *Nature.* **2012,** *487* (7405), 109-113.

28. Costabile, G.; d'Angelo, I.; Rampioni, G.; Bondi, R.; Pompili, B.; Ascenzioni, F.; Mitidieri, E.; d'Emmanuele, d., V; Sorrentino, R.; Miro, A.; Quaglia, F.; Imperi, F.; Leoni, L.; Ungaro, F. Toward Repositioning Niclosamide for Antivirulence Therapy of Pseudomonas aeruginosa Lung Infections: Development of Inhalable Formulations through Nanosuspension Technology. *Mol. Pharm.* **2015,** *12* (8), 2604-2617.

29. Cabrini, G.; Bezzerri, V.; Mancini, I.; Nicolis, E.; Dechecchi, M. C.; Tamanini, A.; Lampronti, I.; Piccagli, L.; Bianchi, N.; Borgatti, M.; Gambari, R. Targeting transcription factor activity as a strategy to inhibit pro-inflammatory genes involved in cystic fibrosis: decoy oligonucleotides and low-molecular weight compounds. *Curr. Med. Chem.* **2010,** *17* (35), 4392-4404.

30. Gupta, V.; Ahsan, F. Influence of PEI as a core modifying agent on PLGA microspheres of PGE(1), a pulmonary selective vasodilator. *Int. J. Pharm.* **2011,** *413* (1-2), 51-62.

31. Lee, Y. S.; Lim, K. S.; Oh, J. E.; Yoon, A. R.; Joo, W. S.; Kim, H. S.; Yun, C. O.; Kim, S. W. Development of porous PLGA/PEI1.8k biodegradable microspheres for the delivery of mesenchymal stem cells (MSCs). *J. Control Release* **2015,** *205*, 128-133.

32. Hoppentocht, M.; Hagedoorn, P.; Frijlink, H. W.; de Boer, A. H. Technological and practical challenges of dry powder inhalers and formulations. *Adv. Drug Deliv. Rev.* **2014,** *75*, 18-31.

33. Ungaro, F.; Giovino, C.; Coletta, C.; Sorrentino, R.; Miro, A.; Quaglia, F. Engineering gas-foamed large porous particles for efficient local delivery of macromolecules to the lung. *Eur. J. Pharm. Sci.* **2010,** *41* (1), 60-70.

34. Edwards, D. A.; Hanes, J.; Caponetti, G.; Hrkach, J.; Ben-Jebria, A.; Eskew, M. L.; Mintzes, J.; Deaver, D.; Lotan, N.; Langer, R. Large porous particles for pulmonary drug delivery. *Science* **1997,** *276* (5320), 1868-1871.

35. Henning, A.; Schneider, M.; Nafee, N.; Muijs, L.; Rytting, E.; Wang, X.; Kissel, T.; Grafahrend, D.; Klee, D.; Lehr, C. M. Influence of particle size and material properties on mucociliary clearance from the airways. *J. Aerosol Med. Pulm. Drug Deliv.* **2010,** *23* (4), 233-241.

36. De, R. G.; Quaglia, F.; Bochot, A.; Ungaro, F.; Fattal, E. Long-term release and improved intracellular penetration of oligonucleotide-polyethylenimine complexes entrapped in biodegradable microspheres. *Biomacromolecules.* **2003,** *4* (3), 529-536.

37. Ungaro, F.; De Rosa, G.; Quaglia, F.; Fattal, E.; La Rotonda, M. I. Controlled release of oligonucleotide/polyethyleneimine complexes from PLGA-based microspheres: potential of spray-drying technique. *Journal of Drug Delivery Science and Technology* **2005,** *15* (2), 137-143.

38. Hutchinson, D.; Barclay, M.; Prescott, W. A.; Brown, J. Inhaled aztreonam lysine: an evidence-based review. *Expert Opin. Pharmacother.* **2013,** *14* (15), 2115-2124.

39. Tiddens, H. A.; De, B. K.; Clancy, J. P.; Fayon, M.; H G M A; Bresnik, M.; Derchak, A.; Lewis, S. A.; Oermann, C. M. Open label study of inhaled aztreonam for Pseudomonas eradication in children with cystic fibrosis: The ALPINE study. *J. Cyst. Fibros.* **2015,** *14* (1), 111-119.

40. Kwon, D. H.; Lu, C. D. Polyamines increase antibiotic susceptibility in Pseudomonas aeruginosa. *Antimicrob. Agents Chemother.* **2006,** *50* (5), 1623-1627.

41. Vaara, M.; Porro, M. Group of peptides that act synergistically with hydrophobic antibiotics against gram-negative enteric bacteria. *Antimicrob. Agents Chemother.* **1996,** *40* (8), 1801-1805.

42. Vicennati, P.; Giuliano, A.; Ortaggi, G.; Masotti, A. Polyethylenimine in medicinal chemistry. *Curr. Med. Chem.* **2008,** *15* (27), 2826-2839.

43. Hunter, A. C.; Moghimi, S. M. Cationic carriers of genetic material and cell death: a mitochondrial tale. *Biochim. Biophys. Acta* **2010,** *1797* (6-7), 1203-1209.

CHAPTER 5

HYBRID LIPID/POLYMER NANOPARTICLES FOR PULMONARY DELIVERY OF siRNA: DEVELOPMENT AND FATE UPON *IN VITRO* DEPOSITION ON THE HUMAN EPITHELIAL AIRWAY BARRIER

G. Costabile[1], I. d'Angelo[2], E. Durantie[3], A. Miro[1], F. Quaglia[1], B. Rothen-Rutishauser[3], F. Ungaro[1]

[1] *Drug Delivery Labs, Department of Pharmacy, University of Naples Federico II, Via Domenico Montesano 49, 80131 Naples, Italy*
[2] *Di.S.T.A.Bi.F., Second University of Naples, Via Vivaldi 43, 81100 Caserta, Italy*
[3] *BioNanomaterials, Adolphe Merkle Institute, University of Fribourg, Ch. des Verdiers 4, 1700, Fribourg, Switzerland*.

ABSTRACT

In the last years, the down-regulation of genes directly involved in the pathogenesis of severe lung diseases, such as cystic fibrosis (CF), through siRNA delivery to the lung has gained tremendous research interest. Nevertheless, adequately engineered inhalable siRNA formulations are required to translate this approach *in vivo*. Here, we propose novel hybrid lipid/polymer hybrid nanoparticles (hNPs) for pulmonary siRNA delivery consisting of a poly(lactic-co-glycolic) acid (PLGA) core surrounded by a dipalmitoyl phosphatidylcholine (DPPC) shell. A preliminary formulation study allowed to select optimized muco-inert PLGA/DPPC hNPs, comprising or not poly(ethylenimine) (PEI) as third component, which displayed mean hydrodynamic diameters around 150 nm, low polydispersity index (~0.1) and negative zeta potential (about -25 mV). Stable hNP-based dry powders were produced by freeze-drying with mannitol. A combination of siRNA against α and β subunits of the ENaC channel was entrapped with high efficiency (75-95 %) in optimised hNPs. The fate and the effects of hNPs upon *in vitro* deposition on a triple cell co-culture model (TCCC) mimicking human epithelial airway barrier were assessed. Transmission electron microscopy analysis before and after aerosolization demonstrated hNP stability towards nebulization. Cell uptake studies confirmed the ability of fluorescently labelled hNPs to be internalized inside the epithelial airway barrier. As measured by LDH release 24 h after treatment, PLGA/DPPC hNPs did not exert any cytotoxic effect towards TCCC. Furthermore, TCCC exposure to PLGA/DPPC hNPs did not result in a significant increase of TNF-alpha release after 24 h, suggesting no acute pro-inflammatory effect. Overall, results demonstrate the great potential of PLGA/DPPC hNPs as carriers for siRNA delivery on the human epithelial airway barrier, prompting towards investigation of their therapeutic effectiveness in CF.

5.1. INTRODUCTION

RNA interference refers to the inhibition of gene expression by small, double-stranded RNA molecules (small interference RNA or siRNA) that direct the mRNA machinery to degrade a specific mRNA. siRNA therapeutics have many advantages in terms of clinical applications, the first of which is their virtual potential to specifically silence any gene underlying more or less complex pathologies.[1,2] In particular, severe lung diseases, such as lung cancer and cystic fibrosis (CF), nowadays represent a very important area of application for siRNA-based therapies.[3] Nevertheless, to harness the full potential of the siRNA strategy for severe lung diseases, an appropriately designed delivery system is mandatory.[4,5]

Naked siRNAs have a half-life of less than an hour in human plasma and are often unable to penetrate cellular membranes. In fact, cellular uptake and the escape from endo-lysosomes are critical steps before siRNA reaches the cytoplasm, where its target is located. Conceiving siRNA for local delivery by inhalation, the presence of high mucin, DNA and actin concentrations, making airway mucus a very complex barrier, should also be taken into account.[4,5] Thus, optimal inhalable formulations are required to: i) enhance siRNA stability; ii) overcome lung cellular and non-cellular barriers; iii) increase siRNA availability at the target level. Amid advanced drug delivery systems, the encapsulation of siRNA into colloidal carriers is considered a very promising formulation approach for inhaled treatment of severe lung diseases.[4,5]

The most studied nanocarriers for the delivery of siRNA are based on lipids and comprise either the entrapment of siRNA into liposomal vescicles or, more often, its complexation with positively charged lipids (i.e., lipoplexes).[4,6] Thanks to their ability to enhance cell uptake and their good tolerance in the pulmonary tract, these carriers gained tremendous interest for pulmonary delivery, both in the scientific and industrial environment.[7] Nevertheless, the application of lipid-based carriers is strongly limited by the low loading efficiencies, especially for hydrophilic drugs and, depending on their composition, by poor stability and drug release control *in vitro/in vivo*.[7,8]

Biodegradable polymeric nanoparticles (NPs) represent a viable alternative for pulmonary delivery of nucleic acid therapeutics,[9] since they may overcome most of the lipid carrier limitations. Among the polymers of interest for lung delivery of siRNA, poly(lactic-co-glycolic) acid (PLGA) seems very promising.[5,9] In fact, PLGA-based NPs may provide protection of the therapeutic cargo from enzymatic degradation, prolonged release (i.e., decreased number of administrations) and improved retention in the lungs.[10,11]

In the attempt to combine the most valuable properties of both lipid and polymeric nanocarriers, hybrid lipid–polymer nanoparticles (hNPs) are under investigation.[12,13] Along these lines, our aim was to design and optimize core-shell hNPs consisting of a PLGA core surrounded by a dipalmitoylphosphatidylcholine (DPPC) shell. hNPs have been further engineered with poly(ethylenimine) (PEI), introduced as a third component to assist siRNA entrapment in the hNPs and its cell uptake.[14] A preliminary formulation study allowed to select optimized muco-inert PLGA/DPPC hNPs containing or not PEI. To allow a proof of principle of their potential for siRNA delivery to the lung, selected formulations were loaded with therapeutic siRNA of interest for CF therapy, that is a combination of siRNA against α and β subunits of the sodium transepithelial channel (ENaC).[15,16] Finally, a thorough *in vitro* study allowed to assess the fate and the effect of hNPs upon aerosolization on a triple cell co-culture model (TCCC) grown at air-liquid interface (ALI) mimicking the human airway epithelial barrier.[17]

5.2. MATERIALS AND METHODS

5.2.1. Materials

Resomer® RG 502H (uncapped PLGA 50:50, inherent viscosity 0.16 - 0.24 dl/g) was purchased from Boehringer Ingelheim (Ingelheim, Germany). siRNA (siGENOME Human SCNN1A and SCNN1B) was purchased from Dharmacon (GE Healthcare). Rhodamine-labeled PLGA was synthesized as previously described[18]. 1,2-dipalmitoyl-sn-glycero-3- phosphocholine (DPPC) was a kind gift of Lipoid GmbH (Cam, Switzerland). Ph.Eur. grade lactose was used (NEW.FA.DEM., Italy) and mannitol (Pearlitol® C160) was kindly gifted by Roquette Italia S.p.a. (Italy). Egg yolk emulsion, phosphate buffer salts, polyvinyl alcohol (PVA, Mowiol® 40–88), porcin mucin, branched polyethylenimine (PEI; 25 KDa), potassium chloride, rhodamine B (Rhod-B), RPMI amino acid solution, type II mucin from porcin stomach, sodium chloride were purchased from Sigma Aldrich (USA). Methylene chloride and ethanol were supplied by Carlo Erba (Italy). All other reagents were of analytical grade or better.

5.2.2. Preparation of PLGA/DPPC hybrid nanoparticles

PLGA/DPPC hNPs were prepared by a modified emulsion/solvent diffusion technique. Briefly, a water in oil emulsion (w/o) was achieved adding 100 μl of water to 1 ml of methylene chloride solution containing PLGA (1% w/v) and DPPC at different DPPC/PLGA ratios (1:10; 1/20; 1:50; 1:100; 1:150), under vortex mixing (2400 min^{-1}, Heidolph, Germany). When needed, PEI was added to the internal water phase at the theoretical loading of 0.016 % (0.016 mg *per* 100 mg of hNPs). Just after mixing, the w/o emulsion was added to 12.5 ml of ethanol 96° under moderate magnetic stirring, leading to immediate precipitation of the polymer blend in the form of hNPs. The formulation was diluted with 12.5 ml of Milli-Q water under stirring for 10 min. Afterwards, residue organic solvent was removed by rotary evaporation under vacuum at 30ºC (Rotavapor®, Heidolph VV 2000, Germany). hNP colloidal dispersion was collected and adjusted to a final volume of 5 ml. Finally, hNPs were isolated by centrifugation at 7000 rcf for 20 minutes at 4°C

(Hettich Zentrifugen, Germany) and dispersed in ultrapure water. A table summarizing all blank PLGA/DPPC hNP formulations produced is reported (Table 1).

Table 5.1 Composition of blank PLGA/DPPC hNPs prepared by emulsion/solvent diffusion in the presence or not of PEI.

Formulation	PEI theoretical loading (mg/100 mg of hNP)	DPPC/PLGA ratio (w/w)
DPPC10	-	1/10
DPPC20	-	1/20
DPPC50	-	1/50
DPPC100	-	1/100
DPPC150	-	1/150
PEI/DPPC10	0.016	1/10
PEI/DPPC20	0.016	1/20
PEI/DPPC50	0.016	1/50
PEI/DPPC100	0.016	1/100
PEI/DPPC150	0.016	1/150

Fluorescently-labelled hNPs ($DPPC_{Rhod}$ and $PEI/DPPC_{Rhod}$) were prepared using rhodamine-labelled PLGA (PLGA-Rhod) in the organic phase at 10% w/w with respect to the total PLGA amount. siRNA-loaded hNPs were prepared at a theoretical loading of 1 nmol/100 mg of PLGA (N/P theoretical ratio of 10 in PEI-modified hNPs) by adding siRNA to the internal water phase.

Just after production, the hydrodynamic diameter, the polydispersity index (PI) and the zeta potential (ζ potential) of hNPs were determined by photon correlation spectroscopy (PCS) with a Malvern Zetasizer Nano ZS (Malvern Instruments, UK). Results are expressed as mean value ± standard deviation of triplicate measurements on different batches.

5.2.3. Freeze-drying studies

Optimized blank PLGA/DPPC hNPs (i.e., DPPC20 and PEI/DPPC20) underwent freeze-drying in the presence or not of appropriate cryoprotectants. In particular, a freeze-drying study was carried out on a 2 mg/ml aqueous dispersion of hNPs employing different types and concentrations of cryoprotectants (Table 2).

Table 5.2 Types and amounts of cryoprotectant used for the freeze-drying studies.

hNP formulation	Cryoprotectant	Cryoprotectant concentrantion (mg/ml)	hNP/Cryoprotectant ratio (w/w)
DPPC20	Trehalose	50	1/25
		100	1/50
	Lactose	50	1/25
		100	1/50
	Mannitol	50	1/25
		100	1/50
	Lactose/Mannitol blend (1:1 w/w)	50	1/25
		100	1/50
PEI/DPPC20	Trehalose	50	1/25
		100	1/50
	Lactose	50	1/25
		100	1/50
	Mannitol	50	1/25
		100	1/50
	Lactose/Mannitol blend (1:1 w/w)	50	1/25
		100	1/50

The obtained hNP dispersion was frozen at -80°C and freeze-dried for 24 h by a Modulyo freeze-drier (Edwards, UK) operating at 0.01 atm and -60°C. The dried particles were reconstituted with 1 ml of ultrapure water and the samples were analysed by PCS, as described above, in order to evaluate the particle size and PI after the freeze-drying process. Results were compared with those achieved on freshly prepared hNPs and hNPs freeze-dried in the absence of cryoprotectant.

Results are expressed as mean values ± standard deviation of triplicate measurements on different batches.

The effect of the cryoprotectant in the aqueous solution on hNP size and PI was excluded by the appropriate control.

5.2.4. *In vitro* assessment of hNP interactions with mucus

The mucoadhesive tendency of PLGA/DPPC hNPs was assessed by turbidimetric measurement of mucin/particle interactions as previously described.[19,20] Briefly, a saturated solution of type II mucin was prepared by centrifugation at 6000 rcf for 20 min of a 0.08% (w/v) mucin dispersion in water stirred overnight. For turbidimetric analysis, hNPs were dispersed in the mucin solution at a concentration of 1 mg/ml by vortexing for 1 min. The turbidity of the mucin/hNPs mixtures was measured by spectrophotometric analysis at 650 nm at time 0 and after incubation for 30 or 60 minutes at room temperature. Reference ABS of mucin and 1 mg/ml hNP dispersions in water were also evaluated. Experiments were run in triplicate and results are expressed as ABS at 650 nm ± standard deviation over time.

5.2.5. siRNA loading inside hNPs

siRNA actual loading was measured indirectly by quantitation of non-encapsulated siRNA. Briefly, just after production hNPs were collected by centrifugation (7000 rcf for 20 minutes at 4°C) and the supernatant was analysed for siRNA content by spectrofluorimetry (EnVision® Multilabel Plate Readers, PerkinElmer Inc., USA) using Quant-IT™ RiboGreen® reagent (Thermo Fisher Scientific) according to the manufacturer's instructions.

Results were reported as actual loading (nmol of encapsulated siRNA *per* mg of hNPs) and encapsulation efficiency (actual siRNA nmol/theoretical siRNA x 100) ± standard deviation of values collected from three different batches.

5.2.6. *In vitro* exposure of airway triple cell co-cultures to nanoparticles

All *in vitro* exposure experiments were conducted with a three dimensional triple cell co-culture model of the human epithelial airway barrier comprising human

bronchial epithelial cells (16HBE14o-), human blood monocyte-derived macrophages (MDM) and dendritic cells (MDDC).[17]

5.2.6.1. 16HBE14o- cell cultures

16HBE14o- cells were kindly provided by Dieter Gruenert (passage number P2.54; University California, San Francisco, CA, USA). Cells were maintained in minimum essential media (MEM) 1X medium (with Earle's Salts, 25 mM HEPES and without L-glutamine; Gibco BRL), supplemented with 1 % L-glutamine, 1 % penicillin/streptomycin and 10 % foetal calf serum. For experimental cultures, cells were seeded at a density of 0.5 x 106 cells/insert on transparent BD Falcon cell culture inserts (surface area of 0.9 cm2, pores with 3.0 μm diameter, PET membranes for 12-well plates). The cell culture inserts were pre-treated with 150 μL of a fibronectin coating solution containing 0.1 mg/mL bovine serum albumin (Sigma-Aldrich), 1 % Type I bovine collagen (BD Biosciences) and 1 % human fibronectin (BD Biosciences) in LHC Basal Medium (Sigma-Aldrich). Inserts were placed in BD Falcon tissue culture plates (12-well plates) with 1 mL medium in the upper and 2 mL in the lower chamber. The cells were kept at 37 °C in 5 % CO_2 humidified atmosphere for 7 days (medium changed after 3–4 days).

5.2.6.2. Triple cells co-culture (TCCC) system

To produce the TCCC *in vitro* model, 16HBE14o- cells cultures were supplemented on the apical side with MDM and on the baso-lateral side with MDDC derived from human blood as previously reported.[17,21] Briefly, 16HBE14o- were cultured as described above. At 7 days, the medium was removed from the upper and lower chamber, the inserts turned upside down and the bottom was abraded carefully with a cell scraper. The inserts were then incubated with 65 μL medium containing 83 x 10^4 MDDC/mL on the basal side for two hours. Afterwards, the non-adherent cells were removed, the inserts turned around again and placed in BD FalconTM tissue culture plates (12-well plates). In the lower chamber 1.5 mL of medium and at the apical side of the TCCC 500 μL medium containing 2.5 x 10^4 MDM/mL was added. Once again the systems were incubated for two hours to allow the macrophages to

attach, before non-adherent cells were washed away. The complete TCCC systems were kept with 1.5 mL of medium in the lower chamber and 0.5 mL in the upper chamber at 37 °C in 5 % CO2 humidified atmosphere for 24 h.
To establish the air-liquid interface (ALI), the medium in the upper chamber of the TCCC systems was removed 24 h prior to exposure in the Vitrocell® Cloud, while the medium in the lower chamber was replaced by 0.6 mL of fresh medium.

5.2.6.3. In vitro TCCC exposure to aerosolized nanoparticles

Cell exposure to hNPs at ALI was carried out with the Vitrocell® Cloud system (Vitrocell Systems GmbH, Germany). Briefly, the Vitrocell® Cloud consists of three main components: a droplet generator (nebulizer), an exposure chamber and a flow system with an incubation chamber providing temperature and humidity conditions suitable for cell cultivation. The aerosol is generated into the exposure chamber by a perforated vibrating membrane nebuliser (Aeroneb®Pro with a larger span of 2.5 to 6.0 μm VMD). Before each experiment, freeze-dried NPs were dispersed in 0.5 μM sodium chloride. For TCCC exposure to low hNP concentrations, 200 μL of a 0.5 mg/mL hNP dispersion were aerosolized (corresponding to a total hNP amount of 0.1 mg). In case of high hNP concentrations, TCCC were exposed to further 400 μL (2 x 200 μL) of a 0.9 mg/mL hNP dispersion (corresponding to a total hNP amount of 0.5 mg). TCCC exposed to sodium chloride and mannitol aqueous solutions in the absence of hNPs were used as control. Following the exposure in the chamber (for about 10 or 30 minutes, depending on the concentration of nebulized hNPs), the inserts were immediately placed in new BD Falcon tissue culture plates (12- well plates), with 0.6 ml of fresh medium in the bottom for cell uptake studies, cytotoxicity assay and evaluation of tumor necrosis factor α release.

5.2.7. Stability of hNPs upon aerosolization

In order to evaluate the stability of hNPs after nebulisation, transmission electron microscopy (TEM) analysis was performed on hNP samples before and after nebulization. To this purpose, TEM copper grid (Plano, Germany) were exposed in the

Vitrocell® Cloud system to different amounts of aerosolized blank DPPC, blank PEI/DPPC, siRNA/DPPC and siRNA-PEI/DPPC hNPs. After air drying, representative images of both the stock dispersions of hNPs before nebulization and the deposited samples were captured using a Tecnai F20 transmission electron microscope (FEI, Eindhoven, The Netherlands) equipped with an Ultra- Scan 1000XP 2 k CCD camera (Gatan Inc., Pleasanton, CA, USA).

5.2.8. Cell uptake studies

For cell uptake studies, the TCCC system was exposed to different concentrations of rhodamine-labeled hNPs, that is $DPPC_{Rhod}$ and $PEI/DPPC_{Rhod}$. After the post-incubation of 24 h, TCCC were fixed for 15 min with 3% paraformaldehyde in phosphate buffered saline (PBS) at room temperature. To permeabilise the cell membrane, cells were washed three times in PBS and subsequently treated with 0.2% Triton X-100 in PBS for 15 min. The actin cytoskeleton and the DNA of all cells were stained with phalloidin ALEXA (Molecular Probes, Life Technologies Europe B.V., Switzerland) in a 1:100 dilution and 4′,6- diamidin-2-phenylindol (DAPI) at 1 µg/mL in 0.3% Triton X-100 in PBS, respectively. For microscopy, membranes were embedded in Glycergel (DAKO Schweiz AG, Baar, Switzerland). Visualisation of the samples was conducted with an inverted Zeiss confocal laser scanning microscope 710 (LSM, Axio Observer.Z1). Representative images (z-stacks) were recorded at 5 independent fields of view for each sample.

Image processing was achieved with LAS AF Lite version (Leica software).

5.2.9. Cytotoxicity assay

To evaluate hNP cytotoxicity, the TCCC was exposed to different amounts of aerosolized siRNA/DPPC and siRNA-PEI/DPPC hNPs and corresponding blank hNPs. To exclude any effect of the cryoprotectant on cell viability, TCCC were also exposed to aqueous solutions of mannitol at the same concentrations of hNP dispersions.

After exposure, the release of the intracellular enzyme lactate dehydrogenase (LDH) by the TCCC, indicative of cell membrane damage, was assessed by the LDH

cytotoxicity detection kit (Roche Applied Science, Mannheim, Germany) according to the manufacturer's guidelines. The test was performed in triplicates and evaluated in comparison to the negative control, that is TCCC exposed to sodium chloride. As a positive control, co-cultures were treated with 100 µl of 0.2% Triton X-100 in H_2O on the apical side and incubated for 24 h at 37°C, 5% CO2.

5.2.10. Tumor necrosis factor α release

The potential hNP-mediated pro-inflammatory response was investigated by quantifying the release of the mediator tumor necrosis factor α (TNF-α). Again, the TCCC was exposed to different amounts of aerosolized siRNA/DPPC and siRNA-PEI/DPPC hNPs and corresponding blank hNPs. To exclude any effect of the cryoprotectant on cell viability, TCCC were also exposed to aqueous solutions of mannitol at the same concentrations of hNP dispersions. After exposure, TNF-α release in the medium was quantified by an ELISA kit (R&D Systems) according to the manufacturer's protocol.

5.2.11. Data analysis

Results are expressed as mean value ± standard error mean (S.E.M.) (n=3). The significance of differences was determined with the software Kaleidagraph using One-Way Analysis of Variance (ANOVA) followed by Bonferroni post-hoc test. A p value < 0.05 was considered significant.

5.3. RESULTS

5.3.1 Development of siRNA-loaded PLGA/DPPC hNPs

PLGA/DPPC hNPs were prepared by a modified emulsion/solvent diffusion technique, adding to the organic phase DPPC as surface-engineering excipient. Conceiving these systems for siRNA delivery, PEI, a well-established transfection agent for nucleic acid therapeutics, was added to the internal water phase as third component. An in depth formulation study was performed on blank hNPs to establish the optimal ratio between the three selected components, that are PLGA, DPPC and PEI. Overall properties of the developed blank hNPs are reported in Table 3.

Table 5.3 Overall properties of hNPs prepared by emulsion/ solvent diffusion technique at different DPPC/PLGA ratios.

Formulation	Hydrodinamic diameter (D_H) (nm ± SD)	Polydispersity index (PI) (mean ± SD)	Zeta Potential (mV ± SD)
DPPC10	151.3 ± 21.3	0.127 ± 0.079	-25.3 ± 0.5
DPPC20	149.7 ± 2.1	0.083 ± 0.006	-23.2 ± 2.4
DPPC50	135.4 ± 17.2	0.088 ± 0.008	-24.3 ±6.0
DPPC100	158.9 ± 7.1	0.082 ± 0.004	-28.4± 2.9
DPPC150	168.6 ± 7.1	0.124 ± 0.094	-15.7 ± 1.3
PEI/DPPC10	166.5 ± 13.9	0.128 ± 0.093	-26.1 ± 0.5
PEI/DPPC20	165.4 ± 9.1	0.102 ± 0.006	-31.7 ± 1.2
PEI/DPPC50	162.3 ± 13.9	0.124 ±0.041	-28.0 ± 0.7
PEI/DPPC100	150.9 ± 30.4	0.106 ± 0.027	-28.0 ± 0.3
PEI/DPPC150	146.4 ± 0.3	0.123 ± 0.027	-22.2 ± 2.7

Independent of the amount of lipid added to the organic phase and the presence of PEI in the internal water phase, the adopted formulation conditions lead to the formation of hNPs with a hydrodynamic diameter between 135 and 170 nm, monodisperse particle population (PI lower than 0.130) and negative ζ potentials (between -22 and -30 mV). Nevertheless, in each case a flocculation of the

exceeding amount of the lipid component was apparent after rotary evaporation of the diffusion solvent under vacuum. This phenomenon was particularly evident when high amounts of DPPC were added to the formulation, while it was limited up to DPPC/PLGA 1:20 ratio (w/w). These formulations, from here on named DPPC and PEI/DPPC, were thus selected for further studies.

Mucoadhesion studies were performed by measuring the turbidity at 650 nm (ABS) of DPPC and PEI/DPPC hNPs in mucin over time (Fig. 5.1). While the ABS of the reference mucin dispersion did not significantly deviate from zero (being within the range 0.040–0.045 arbitrary units), higher values of ABS were observed at each time-point upon addition of hNP dispersions. Nevertheless, no significant differences were observed between ABS of hNPs dispersed in water or in mucin (Fig. 5.1).

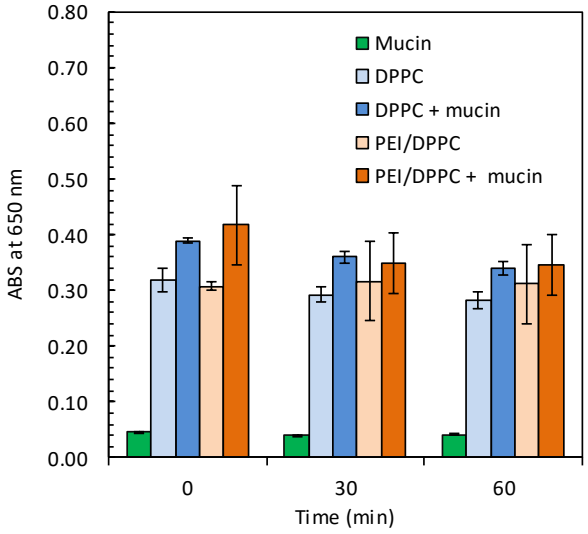

Figure 5.1. *In vitro* assessment of mucin interactions with optimized blank DPPC/PLGA hNPs. Data are expressed as turbidimetry (ABS at λ 650 nm) over time.

Both the formulations were chosen for the encapsulation of siRNA against ENaC at a theoretical loading of 1 nmol/100 mg of hNPs. The resulting siRNA-loaded hNPs were fully characterized in terms of hydrodynamic diameter, PI and ζ potential. As can be seen in Table 4, the addition of siRNA inside the formulation did not result in significant changes of hNP size and PI as compared to blank hNPs (DPPC20 and

PEI/DPPC20 in Table 5.3). siRNA-loaded hNPs with a hydrodynamic diameter around 140 nm and a low PI were produced with good yields (around 50%). siRNA was effectively entrapped inside PLGA/DPPC hNPs with a mean entrapment efficiency of 74.8%. Nevertheless, the addition of PEI inside the formulation allowed to increase siRNA actual loading from 1.35 nmol *per* mg of DPPC hNPs to 1.74 nmol *per* mg of PEI/DPPC hNPs.

Table 5.4. Overall properties of siRNA-loaded PLGA/DPPC hNPs prepared by emulsion/ solvent diffusion technique.

	siRNA-DPPC	**siRNA-PEI/DPPC**
Hydrodinamic diameter (nm ± SD)	141.4 ± 0.50	141.7 ± 1.8
PI (mean ± SD)	0.120 ± 0.018	0.114 ± 0.0050
ζ Potential (mV ± SD)	-29.1 ± 1.6	-29.9 ± 1.4
Yield of production (% ± SD)	52.0 ± 8.9	53.4 ± 2.5
siRNA actual loading [a] (% ± SD)	1.35 ± 0.02	1.74 ± 0.04
Entrapment efficiency (% ± SD)	74.8 ± 1.5	95.9 ± 2.2

[a]nmol of encapsulated siRNA *per* 100 mg of hNPs. The siRNA theoretical loading was 1 nmol/100 mg of hNPs.

5.3.2 Production of stable hNP-containing dry powders

To achieve long-term stable PLGA/DPPC hNP formulations, dry powders containing hNPs were produced by freeze-drying in the presence of a cryoprotectant. Different cryoprotectant types were tested and employed at different ratios by weight to the hNPs (Table 5.2). As can be seen in Fig. 5.2, the lowest variation in particle size and PI with respect to the control is observed for hNPs freeze-dried in presence of either trehalose or mannitol. No differences were observed changing the cryoprotectant amount used.

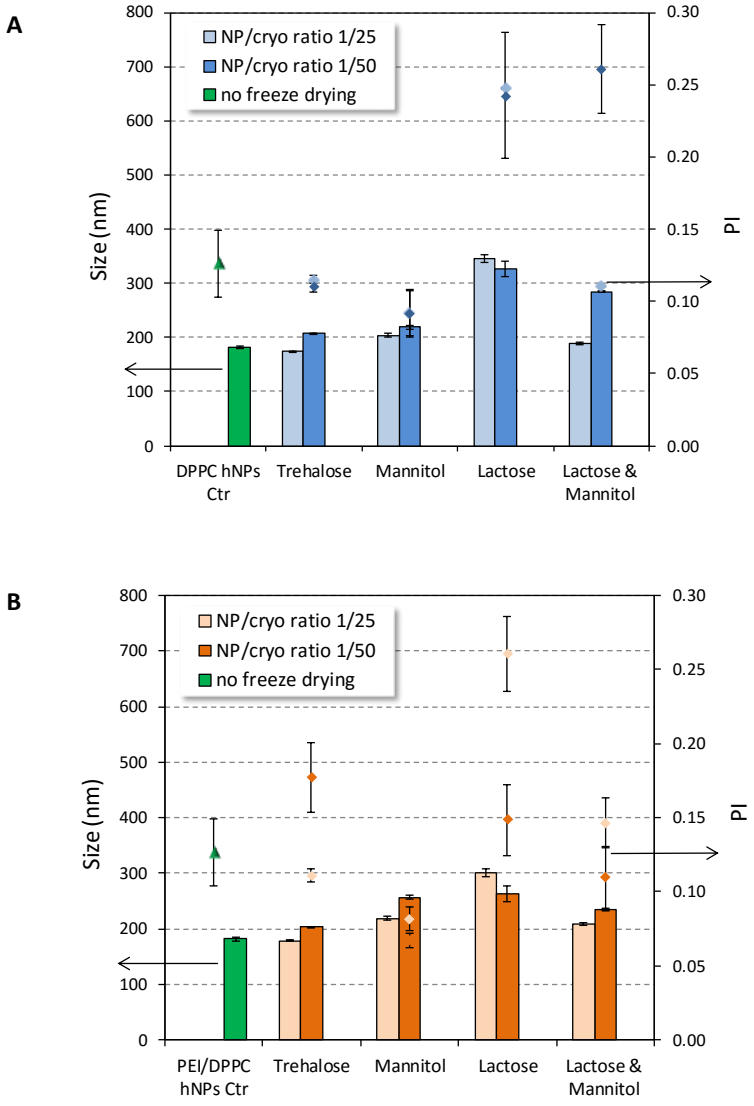

Figure 5.2. Size and PI of DPPC (A) and PEI/DPPC (B) hNPs after freeze-drying in the presence of different cryoprotectants. Measurements were performed after redispersion in water. Each cryoprotectant system (cryo) was employed at two different ratio by weight to hNPs.

Nevertheless, mannitol based dry powder were chosen for further experiments because of its approval for pulmonary delivery (i.e., Bronchitol) and the proved

osmotic beneficial properties on mucus viscosity in CF patients. All the *in vitro* experiments on TCCC were, thus, performed on freeze-dried hNPs, in presence of mannitol, after reconstitution in water at the appropriate concentration.

5.3.3 *In vitro* aerosolization of nanoparticles on TCCC

Optimized freeze-dried formulations underwent interaction studies with TCCC.
The stability of hNPs during the nebulisation process was confirmed by TEM analysis of freeze-dried hNPs in the presence of mannitol (1:25 NP/mannitol ratio) before and after nebulization in the Vitrocell® Cloud system (Fig. 5.3). From TEM images it is apparent that hNPs, according to data reported in literature,[22,23] display a typical core-shell structure characterized by a hydrophobic PLGA core and a DPPC shell. Of note, the core-shell structure of the hNPs was retained after the nebulization process, that did not cause any apparent modification of the hNP structure nor hNP aggregation (Fig. 5.3) at none of the tested concentrations (data not shown)

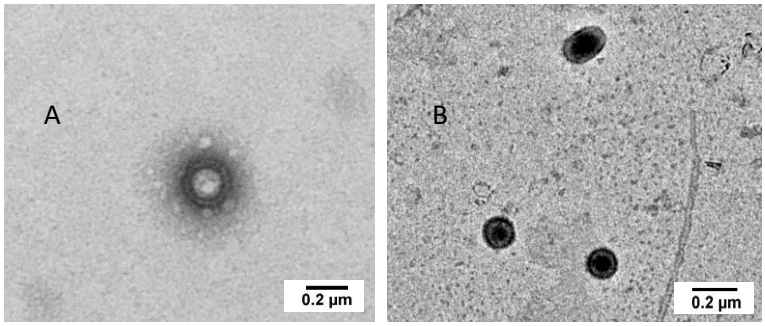

Figure 5.3. TEM images of reconstituted freeze-dried DPPC hNPs before (A) and after nebulization (B). Field is representative of the sample.

Morphological analysis was carried out by TEM also on optimised siRNA-loaded hNPs freeze-dried in the presence of mannitol (1:25 w/w NP/mannitol ratio) and results confirmed the core-shell structure observed in blank hNPs (Fig. 5.4).

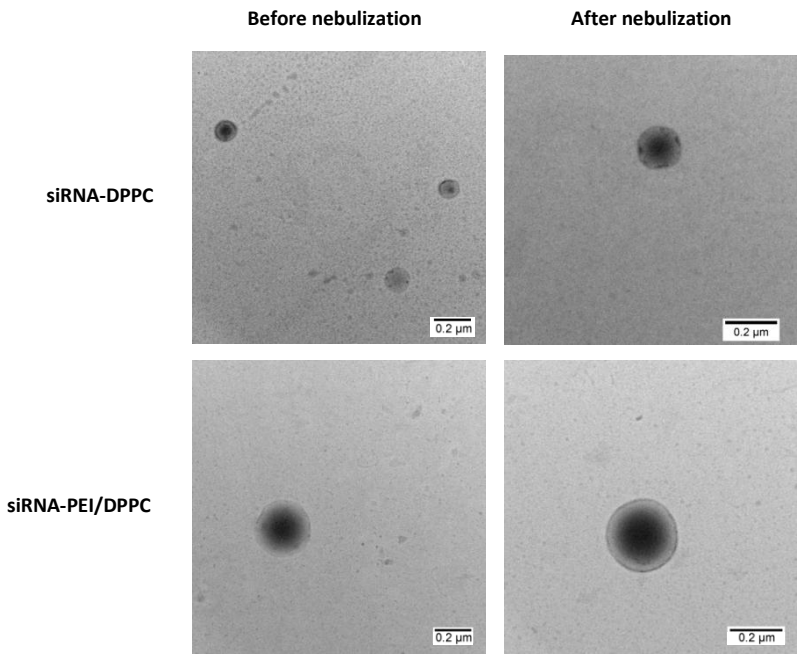

Figure 5.4. TEM images of reconstituted freeze-dried siRNA-loaded hNPs (siRNA-DPPC and siRNA-PEI/DPPC) before and after nebulization. Field is representative of the sample.

5.3.4 Uptake of aerosolized nanoparticles in TCCC

In order to run cell uptake studies, fluorescently labelled $DPPC_{Rhod}$ and $PEI/DPPC_{Rhod}$ hNPs were produced using PLGA-Rhod. Of note, the addition to the formulation of 10 % w/w PLGA-Rhod with respect to the total PLGA amount did not affected hNP properties as compared to non-fluorescent hNPs (data not shown). After 24 h of incubation in the presence of deposited $DPPC_{Rhod}$ and $PEI/DPPC_{Rhod}$, CLSM analysis of treated TCCC were performed (Figure 5). Results indicate that both $DPPC_{Rhod}$ and $PEI/DPPC_{Rhod}$ hNPs (labelled in red) can effectively penetrate into cells and are localized intracellularly (labelled in blue).

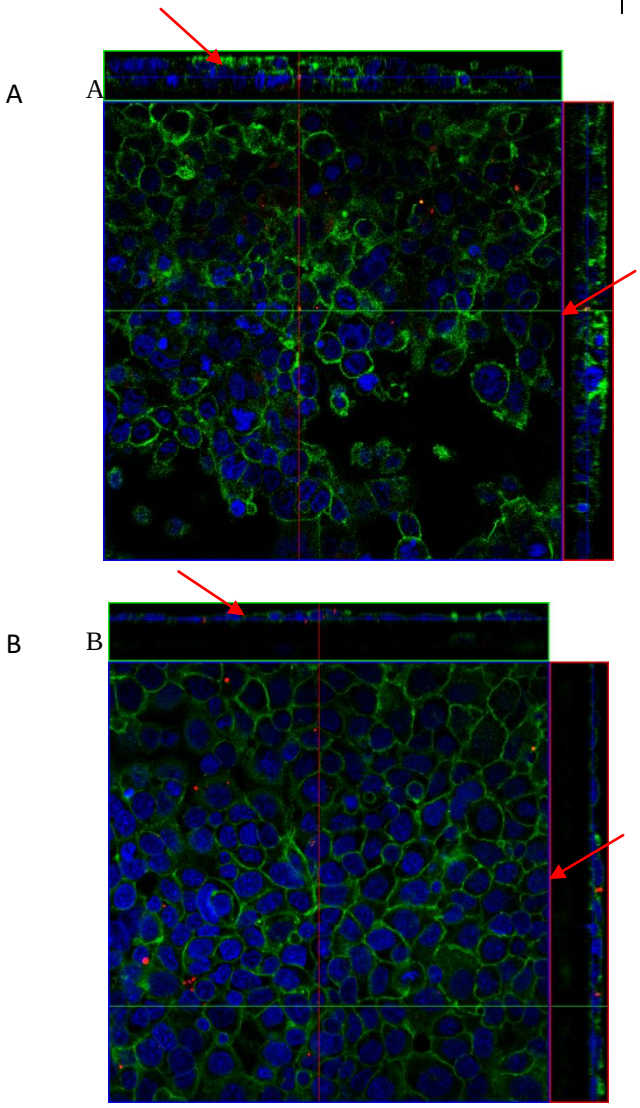

Figure 5.5. CLSM images of TCCC incubated at 37°C in the presence of fluorescently-labelled $DPPC_{Rhod}$ (A) and $PEI/DPPC_{Rhod}$ (B) hNPs deposited after aerosolization. The arrows show hNPs engulfed by the cells.

5.3.5 Effects of aerosolized hNPs on TCCC

At the tested concentrations, the developed hNPs displayed no significant cytotoxicity as compared to both sodium chloride and mannitol solutions aerosolized at the same concentrations of the samples (p>0.5). On the other hand, a significant cytotoxic effect as compared to TCCC exposed to both low and high hNP concentrations (p<0.001) was observed when the co-cultures were challenged with LPS from *P. aeruginosa* as positive control.

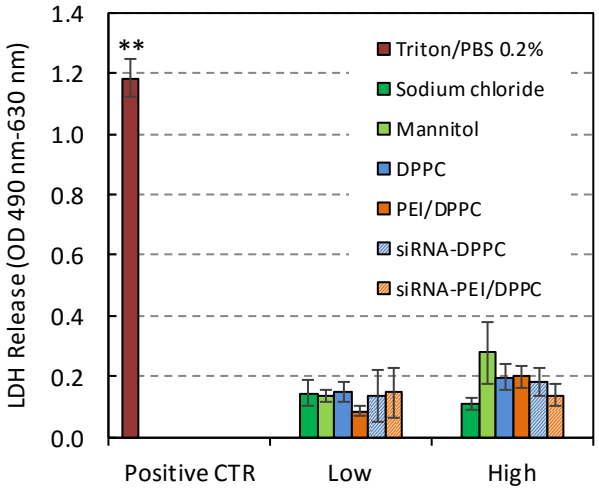

Figure 5.6. LDH release in TCCC upon incubation for 24 h at 37°C after exposure to different amounts (low and high in the graph) of blank and siRNA-loaded PLGA/DPPC hNPs. Triton 0.2.% (w/v) in PBS was used as positive control. Sodium chloride was used as negative control. Mannitol aqueous solutions at the same volume and concentrations used for the hNP samples were also aerosolized. Data are presented as mean OD values ± S.E.M. of samples diluted 1:10 v/v in cell culture medium (n=3) (**p<0.001).

These findings were confirmed by CLSM analysis of all treated samples, since no alteration to cell morphology occurred after TCCC exposure to hNPs as compared to the negative control (data not shown).

The potential pro-inflammatory effect of aerosolized blank and siRNA-loaded hNPs on TCCC was also investigated by evaluating the amount of TNF-α released as

compared to the negative control (i.e., sodium chloride). As can be seen in Fig. 5.7, at all tested concentrations, TCCC exposure to mannitol solutions determined a less than 1-fold increase (0.839 ± 0.116 and 0.530 ± 0.223 for low and high samples, respectively) of TNF-α release relative to the negative control. When exposed to hNPs, a slight increase of TNF-α release was observed as compared to sodium chloride, being more pronounced in case of siRNA-loaded hNPs. Nevertheless, no significant differences in the fold increase of TNF-α release relative to the negative control was observed between hNPs and the mannitol control, at all concentration tested.

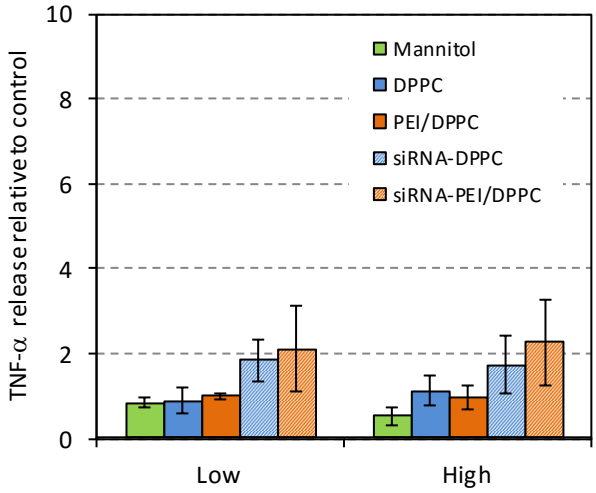

Figure 5.7. TNF-α release in TCCC upon incubation for 24 h at 37°C after exposure to different amounts with blank and siRNA-loaded hybrid PLGA/DPPC hNPs. Mannitol aqueous solutions at the same volume and concentrations used for the hNP samples were also aerosolized as controls. Data are presented as the fold increase relative to the negative control (i.e., sodium chloride) ± S.E.M. of samples.

5.4. DISCUSSION

In the last years, the therapeutic approach based on down-regulation of genes directly involved in the disease pathogenesis (e.g., siRNA administration) has gained tremendous interest to counteract the dehydration, and consequent chronic inflammation and recurrent infections, of CF airways.[16,24,25] Nonetheless, the clinical application of siRNA-based therapies is seriously hindered by siRNA short half-life *in vivo* and its low capability to penetrate cell membranes.[4,5] Furthermore, the typical CF lung environment, i.e thick and viscous mucus layer, may seriously hinder drug interaction with its target at lung, i.e the cells.[11] To overcome these issues, in this work we have designed novel PLGA/DPPC hNPs suitable for pulmonary delivery of siRNA.

The importance of extracellular and cellular barriers imposed by the CF lung in determining the therapeutic efficacy of inhaled drugs is nowadays acknowledged.[11] A current paradigm suggests that only NPs with appropriate size and surface properties may overcome the complex mucus airway barrier and assist NP interactions with human airway epithelial cells.[26,27] This aspect is particularly crucial for siRNA-based therapeutics. The developed PLGA/DPPC hNPs showed a typical core-shell structure,[12] which suggest the presence of a PLGA core surrounded by a lipid shell made by DPPC, independent of the presence of PEI. As demonstrated by mucoadhesion studies, this results in non-mucoadhesive or "muco-inert" hNPs, likely able to easily penetrate across the airway mucus layer.[19,20,26] Furthermore, the adopted formulation conditions allowed the production of hNPs with a hydrodynamic diameter around 150 nm, which are expected to easily diffuse through the gel-like structure of the mucus.[28,29]

Aiming to local delivery of siRNA at lung, another important concern that has been addressed is the transformation of the aqueous hNP dispersion into a solid long-term stable product. Indeed, after optimization of PLGA/DPPC hNP formulation, the most appropriate freeze-drying variables were selected in order to obtain a lyophilizate with good quality, which could be re-dispersed in saline before use without affecting the peculiar NP properties. To avoid common hNP aggregation in

a collapsed cake,[30] different cryoprotectants were added to the aqueous dispersion. Among the most promising, mannitol was selected owing to its established beneficial properties on mucus fluidity in CF[31]. At least in principle, mannitol could work synergistically with DPPC to facilitate hNP transport, and in so doing siRNA diffusion, through mucus.

If DPPC, that is the principal component of the lung lining fluids, is expected to tune hNP interactions with the lung environment, the addition of PEI can play a crucial role for siRNA entrapment inside PLGA/DPPC hNPs. This hypothesis was confirmed by encapsulation studies performed on two siRNA sequences, for α and β ENaC subunits. Indeed, these have been shown to produce a long term reduction of trans-epithelial Na+ currents and of fluid absorption [15], and that the combination of the two siRNA can expand the lung fluid volume *in vitro*.[16] Of note, siRNA was entrapped inside selected hNPs with high efficiency, particularly when PEI was co-encapsulated. This effect could be likely ascribed to the formation of a complex between PEI, employed at the theoretical N/P ratio of 10, and siRNA.

Although an increasing knowledge supports the use of modified PLGA NPs for lung delivery, comprehensive characterization of their biocompatibility and efficacy is a complex task that has not been fulfilled yet. To fill this gap and look to the formulation in a translational perspective, the behaviour of the developed PLGA/DPPC hNPs after deposition on triple cell co-cultures, which realistically mimick human airway epithelium environment, was investigated. Indeed, when primary human bronchial epithelial cells (16HBE14o-) are grown on porous supports at ALI they undergo mucociliary differentiation, reproducing both the *in vivo* morphology and key physiologic processes, sometimes including tight junctions, cilia, basal and mucus cells.[21,32] Furthermore, direct deposition of the aerosolized drug to the apical compartment of the cell culture can be envisaged through systems especially designed for dose-controlled and spatially uniform deposition of liquid aerosols on cells,[33,34] such as the Vitrocell® Cloud here employed.

To attain maximum siRNA availability at lung epithelial cells, where its target is located, the hNPs should: i) deposit on the airway epithelium in their stable form; ii)

penetrate inside the mucus barrier; iii) interact with the lung epithelium, without compromising cell availability. The adopted model was crucial to draw key information on all these points and to establish *a priori* target formulation parameters for siRNA delivery to human airway epithelium (e.g., size, surface modification). Indeed, results demonstrated that the adopted formulation conditions allowed to tune hNP size and surface properties, so as to be aerosolized on lung epithelial cells in their integer form, to penetrate inside extracellular lung lining fluids, to be taken up by lung epithelial cells without exerting neither a cytotoxic effect or a pro-inflammatory response on the treated lung epithelium model.

5.5. CONCLUSION

In this work, we have successfully designed and developed novel PLGA/DPPC hNPs with size and surface properties optimized for siRNA transport and delivery at lung. Stable hNP-based dry powders were produced by freeze-drying with mannitol, an osmotic agent of interest for CF treatment. Optimised formulations allowed entrapment of a combination of siRNA against α and β subunits of the ENaC sodium transepithelial channel with high efficiency, which could be optimized by the addition of PEI inside the formulation. The fate and the effects of hNPs upon *in vitro* deposition on a triple cell co-culture model of the human airway epithelium was thoroughly investigated. Transmission electron microscopy analysis before and after aerosolization demonstrated NP stability towards nebulization on cells. Cell uptake studies confirmed the ability of fluorescently labelled hNPs to be internalized inside the airway epithelial barrier. Finally, hNP hazard assessment demonstrated that the developed system do not exert neither cytotoxic nor acute pro-inflammatory effect towards none of the cell components of the co-culture model. Overall, results demonstrate the great potential of PLGA/DPPC hNPs as carriers for siRNA delivery on the epithelial airway barrier, prompting towards investigation of its therapeutic effectiveness in CF.

References

1. Burnett, J. C.; Rossi, J. J.; Tiemann, K. Current progress of siRNA/shRNA therapeutics in clinical trials. *Biotechnol. J.* 2011, *6* (9), 1130-1146.
2. Lee, S. H.; Kang, Y. Y.; Jang, H. E.; Mok, H. Current preclinical small interfering RNA (siRNA)-based conjugate systems for RNA therapeutics. *Adv. Drug Deliv. Rev.* 2015.
3. Karras, J. G.; Sun, G.; Tay, J.; Jackson, A. L. Reflections on microRNAs in chronic pulmonary disease: looking into the miR-ror and crystal ball. *Inflamm. Allergy Drug Targets* 2013, *12* (2), 88-98.
4. Lam, J. K.; Liang, W.; Chan, H. K. Pulmonary delivery of therapeutic siRNA. *Adv. Drug Deliv. Rev.* 2012, *64* (1), 1-15.
5. Merkel, O. M.; Rubinstein, I.; Kissel, T. siRNA delivery to the lung: what's new? *Adv. Drug Deliv. Rev.* 2014, *75*, 112-128.
6. Singh, Y.; Tomar, S.; Khan, S.; Meher, J. G.; Pawar, V. K.; Raval, K.; Sharma, K.; Singh, P. K.; Chaurasia, M.; Surendar, R. B.; Chourasia, M. K. Bridging small interfering RNA with giant therapeutic outcomes using nanometric liposomes. *J. Control Release* 2015, *220* (Pt A), 368-387.
7. Cipolla, D.; Shekunov, B.; Blanchard, J.; Hickey, A. Lipid-based carriers for pulmonary products: preclinical development and case studies in humans. *Adv. Drug Deliv. Rev.* 2014, *75*, 53-80.
8. Hadinoto, K.; Cheow, W. S. Nano-antibiotics in chronic lung infection therapy against Pseudomonas aeruginosa. *Colloids Surf. B Biointerfaces.* 2014, *116:*772-85.
9. Beck-Broichsitter, M.; Merkel, O. M.; Kissel, T. Controlled pulmonary drug and gene delivery using polymeric nano-carriers. *J. Control Release* 2012, *161* (2), 214-224.
10. Ungaro, F.; d'Angelo, I.; Miro, A.; La Rotonda, M. I.; Quaglia, F. Engineered PLGA nano- and micro-carriers for pulmonary delivery: challenges and promises. *J. Pharm. Pharmacol.* 2012, *64* (9), 1217-1235.
11. d'Angelo, I.; Conte, C.; La Rotonda, M. I.; Miro, A.; Quaglia, F.; Ungaro, F. Improving the efficacy of inhaled drugs in cystic fibrosis: challenges and emerging drug delivery strategies. *Adv. Drug Deliv. Rev.* 2014, *75*, 92-111.
12. Raemdonck, K.; Braeckmans, K.; Demeester, J.; De Smedt, S. C. Merging the best of both worlds: hybrid lipid-enveloped matrix nanocomposites in drug delivery. *Chem. Soc. Rev.* 2014, *43* (1), 444-472.
13. Pandita, D.; Kumar, S.; Lather, V. Hybrid poly(lactic-co-glycolic acid) nanoparticles: design and delivery prospectives. *Drug Discov. Today* 2015, *20* (1), 95-104.
14. Gunther, M.; Lipka, J.; Malek, A.; Gutsch, D.; Kreyling, W.; Aigner, A. Polyethylenimines for RNAi-mediated gene targeting in vivo and siRNA delivery to the lung. *Eur. J. Pharm. Biopharm.* 2011, *77* (3), 438-449.
15. Caci, E.; Melani, R.; Pedemonte, N.; Yueksekdag, G.; Ravazzolo, R.; Rosenecker, J.; Galietta, L. J.; Zegarra-Moran, O. Epithelial sodium channel inhibition in primary human bronchial epithelia by transfected siRNA. *Am. J. Respir. Cell Mol. Biol.* 2009, *40* (2), 211-216.

16. Gianotti, A.; Melani, R.; Caci, E.; Sondo, E.; Ravazzolo, R.; Galietta, L. J.; Zegarra-Moran, O. Epithelial sodium channel silencing as a strategy to correct the airway surface fluid deficit in cystic fibrosis. *Am. J. Respir. Cell Mol. Biol.* 2013, *49* (3), 445-452.

17. Blank, F.; Rothen-Rutishauser, B.; Gehr, P. Dendritic cells and macrophages form a transepithelial network against foreign particulate antigens. *Am. J. Respir. Cell Mol. Biol.* 2007, *36* (6), 669-677.

18. Maiolino, S.; Moret, F.; Conte, C.; Fraix, A.; Tirino, P.; Ungaro, F.; Sortino, S.; Reddi, E.; Quaglia, F. Hyaluronan-decorated polymer nanoparticles targeting the CD44 receptor for the combined photo/chemo-therapy of cancer. *Nanoscale* 2015, *7* (13), 5643-5653.

19. Ungaro, F.; d'Angelo, I.; Coletta, C.; d'Emmanuele, d., V; Sorrentino, R.; Perfetto, B.; Tufano, M. A.; Miro, A.; La Rotonda, M. I.; Quaglia, F. Dry powders based on PLGA nanoparticles for pulmonary delivery of antibiotics: modulation of encapsulation efficiency, release rate and lung deposition pattern by hydrophilic polymers. *J. Control Release* 2012, *157* (1), 149-159.

20. d'Angelo, I.; Casciaro, B.; Miro, A.; Quaglia, F.; Mangoni, M. L.; Ungaro, F. Overcoming barriers in Pseudomonas aeruginosa lung infections: Engineered nanoparticles for local delivery of a cationic antimicrobial peptide. *Colloids Surf. B Biointerfaces* 2015, *135*, 717-725.

21. Lehmann, A. D.; Daum, N.; Bur, M.; Lehr, C. M.; Gehr, P.; Rothen-Rutishauser, B. M. An in vitro triple cell co-culture model with primary cells mimicking the human alveolar epithelial barrier. *Eur. J. Pharm. Biopharm.* 2011, *77* (3), 398-406.

22. Colombo, S.; Cun, D.; Remaut, K.; Bunker, M.; Zhang, J.; Martin-Bertelsen, B.; Yaghmur, A.; Braeckmans, K.; Nielsen, H. M.; Foged, C. Mechanistic profiling of the siRNA delivery dynamics of lipid-polymer hybrid nanoparticles. *J. Control Release* 2015, *201*, 22-31.

23. Hu, Y.; Hoerle, R.; Ehrich, M.; Zhang, C. Engineering the lipid layer of lipid-PLGA hybrid nanoparticles for enhanced in vitro cellular uptake and improved stability. *Acta Biomater.* 2015, *28*, 149-159.

24. Ramachandran, S.; Krishnamurthy, S.; Jacobi, A. M.; Wohlford-Lenane, C.; Behlke, M. A.; Davidson, B. L.; McCray, P. B., Jr. Efficient delivery of RNA interference oligonucleotides to polarized airway epithelia in vitro. *Am. J. Physiol Lung Cell Mol. Physiol.* 2013, *305* (1), L23-L32.

25. Laube, B. L. Aerosolized Medications for Gene and Peptide Therapy. *Respir. Care.* 2015, *60* (6), 806-821.

26. Ensign, L. M.; Tang, B. C.; Wang, Y. Y.; Tse, T. A.; Hoen, T.; Cone, R.; Hanes, J. Mucus-penetrating nanoparticles for vaginal drug delivery protect against herpes simplex virus. *Sci. Transl. Med.* 2012, *4* (138), 138ra79.

27. d'Angelo, I.; Conte, C.; Miro, A.; Quaglia, F.; Ungaro, F. Pulmonary drug delivery: a role for polymeric nanoparticles? *Curr. Top. Med. Chem.* 2015, *15* (4), 386-400.

28. Cone, R. A. Barrier properties of mucus. *Adv. Drug Deliv. Rev.* 2009, *61* (2), 75-85.

29. Lai, S. K.; Wang, Y. Y.; Hida, K.; Cone, R.; Hanes, J. Nanoparticles reveal that human cervicovaginal mucus is riddled with pores larger than viruses. *Proc. Natl. Acad. Sci. U. S. A* 2010, *107* (2), 598-603.

30. Fonte, P.; Reis, S.; Sarmento, B. Facts and evidences on the lyophilization of polymeric nanoparticles for drug delivery. *J. Control Release* 2016, *225*, 75-86.

31. Nolan, S. J.; Thornton, J.; Murray, C. S.; Dwyer, T. Inhaled mannitol for cystic fibrosis. *Cochrane. Database. Syst. Rev.* 2015, *10*, CD008649.

32. Rothen-Rutishauser, B. M.; Kiama, S. G.; Gehr, P. A three-dimensional cellular model of the human respiratory tract to study the interaction with particles. *Am. J. Respir. Cell Mol. Biol.* 2005, *32* (4), 281-289.

33. Endes, C.; Schmid, O.; Kinnear, C.; Mueller, S.; Camarero-Espinosa, S.; Vanhecke, D.; Foster, E. J.; Petri-Fink, A.; Rothen-Rutishauser, B.; Weder, C.; Clift, M. J. An in vitro testing strategy towards mimicking the inhalation of high aspect ratio nanoparticles. *Part Fibre. Toxicol.* 2014, *11*, 40.

34. Endes, C.; Mueller, S.; Kinnear, C.; Vanhecke, D.; Foster, E. J.; Petri-Fink, A.; Weder, C.; Clift, M. J.; Rothen-Rutishauser, B. Fate of cellulose nanocrystal aerosols deposited on the lung cell surface in vitro. *Biomacromolecules.* 2015, *16* (4), 1267-1275.